جامعة سيدي محمد بن عبد الله بفاس
UNIVERSITÉ SIDI MOHAMED BEN ABDELLAH DE FES

كلية العلوم والتقنيات فاس
FACULTÉ DES SCIENCES ET TECHNIQUES DE FÈS

N° d'ordre : 55/2023

Centre des Etudes Doctorales : Sciences et Techniques et Sciences Médicales
Formation Doctorale : Sciences et Génie de la Matière, de la Terre et de la Vie
Discipline : Géologie
Spécialité* : Géotechnique et Ingénierie Géologique
Laboratoire : Ecologie Fonctionnelle et Génie de l'Environnement

Thèse pour l'obtention de DOCTORAT

Landslide Hazard, Inventory, Modelling and Impact Analysis in Fez-Moulay Yacoub Region

Risque de glissements de Terrain, Inventaire, Modélisation et Analyse d'Impact dans la Région de Fès-Moulay Yacoub

Préparée par : Mr Obda Ilias

Soutenue le 18-07-2023 devant le jury :

Pr. Saka Abdel Majid	**PES**	**ENSA-USMBA-FES**	***Président***
Pr. Tabyaoui Hasan	**PES**	**ENSA-USMBA-FES**	***Rapporteur***
Pr. Stitou El Messari Jamal Eddine	**PES**	**FS-UAE-TETOUAN**	***Rapporteur***
Pr. Benmakhlouf Mohamed	**PES**	**FS-UAE-TETOUAN**	***Rapporteur***
Pr. Barkaoui Alae Eddine	**PH**	**EST-UMP-OUJDA**	***Examinateur***
Pr. Amyay Mhamed	**PES**	**FLSH-USMBA-FES**	***Examinateur***
Pr. Azzouzi Nassereddine	**PH**	**FP-USMBA-TAZA**	***Examinateur***
Pr. El Kharim Younes	**PES**	**FS-UAE-TETOUAN**	***Directeur de thèse***
Pr. Lahrach Abderrahim	**PES**	**ENSA-USMBA-FES**	***Directeur de thèse***
Pr. Ahniche Mohamed	**Directeur**	**GEOTECHMED**	***Invité***

Abstract

Slope movements are dangerous geohazards causing serious socio-economic damages on unstable slopes. In the last decade, the number of landslides research studies has increased rapidly because of their complexity, involving multiple parameters varying in time and space, their great potential to hinder the socio-economic development and especially the high budgets invested in risk mitigation interventions worldwide.

In active mountain belts as the Pre-Rif unit, both conditioning and triggering factors are present and human activity is often involved either through land use favouring instability, or the disturbance of hillslopes, and without omitting the vulnerability presented by certain urban and peri-urban extensions.

Nowadays, hazard mapping and its integration into approved land-use planning documents is one of the preliminary and most effective means of mitigating and managing natural hazards. Hence, the public authorities have launched several tenders aimed at producing maps of suitability for urbanization (CAU), particularly regarding the risk of slope movements, in several of the kingdom's provinces. Within the framework of these projects, the present work has been carried out.

Numerous approaches are used in landslide studies, heuristic, deterministic and statistical depending on the geomorphic context, scale, data availability and especially the objectives targeted. In the present research work, three types of approaches are elaborated to investigate landslide hazard in the Fez-Moulay Yacoub region. The deterministic methods developed have proved their effectiveness and complementarity in the study of this hazard in densely urbanized areas and at the scale of detail, providing precise information on the extent and kinematics of landslides affecting the urban center of Moulay Yacoub. As for the heuristic methods, the mapping of the susceptibility to ground movements at a broad scale gave results of high quality and of crucial utility. the analysis and evaluation of the conditioning parameters revealed that the anthropogenic factors are strongly involved, notably the use of land and the proximity to the road network, in addition to the classic factors of predisposition (slope, proximity to the hydro network, etc.).

Several statistical methods have been used in this work to investigate the impact of topographic growth conditioned by active tectonics on the magnitude of ground movements in the southern Riffian front. The results showed the difference in terms of typology and slope dynamics between the southern edge of the Prerif and the hilly landscape dominating the province of Moulay Yacoub. Finally, the analysis of the impact of landslides carried out on several urban extensions showed that human activity is strongly involved in the instability of the slopes, especially because it presents a high vulnerability. Moreover, among the areas investigated, the urban center of Moulay Yacoub as well as the urbanized outskirts of the city of fez proved to be the most vulnerable to slope movements and highly exposed.

Keywords: Landslide Hazard, Conditioning factors, Multidisciplinary analysis, Landslide vulnerability

Résumé

Les mouvements de pente sont des Géorisques dangereux causant de graves dommages socio-économiques sur les pentes instables. Au cours de la dernière décennie, le nombre d'études de recherche sur les glissements de terrain a augmenté rapidement en raison de leur complexité, impliquant de multiples paramètres variant dans le temps et dans l'espace, leur grand potentiel d'entraver le développement socio-économique et surtout les budgets élevés investis dans les interventions d'atténuation des risques dans le monde.

Dans les chaînes montagneuses actives comme l'unité du Pré-Rif, les facteurs de conditionnements et déclencheurs sont présents et l'activité humaine est souvent impliquée soit par l'utilisation des terres favorisant l'instabilité, soit par la perturbation des versants, et sans omettre la vulnérabilité présentée par certaines zones urbaines et périurbaines.

De nos jours, la cartographie des aléas et son intégration dans les documents d'aménagement du territoire homologués est l'un des moyens préliminaires et les plus efficaces d'atténuation et de gestion des aléas naturels. Ainsi, les pouvoirs publics ont lancé plusieurs appels d'offres visant à produire des cartes d'aptitude à l'urbanisation (CAU), notamment au regard des risques de mouvements de pente, dans plusieurs provinces du royaume. Dans le cadre de ces projets, le présent travail a été réalisé.

De nombreuses approches sont utilisées dans l'étude des glissements de terrain, heuristiques, déterministes et statistiques selon le contexte géomorphologique, l'échelle, la disponibilité des données et surtout les objectifs visés. Dans le présent travail de recherche, trois types d'approches sont élaborées pour étudier les risques de glissement de terrain dans la région de Fès-Moulay Yacoub. Les méthodes déterministes développées ont prouvé leur efficacité et leur complémentarité dans l'étude de cet aléa en zone densément urbanisée et à l'échelle du détail, apportant des informations précises sur l'étendue et la cinématique des glissements de terrain affectant le centre urbain de Moulay Yacoub. Quant aux méthodes heuristiques, la cartographie de la susceptibilité aux mouvements de terrain à grande échelle a donné des résultats de haute qualité et d'une utilité cruciale. L'analyse et l'évaluation des paramètres de conditionnements ont révélé que les facteurs anthropiques sont fortement impliqués, notamment l'occupation du sol et la proximité au réseau routier, en plus des facteurs classiques de prédisposition (pente, lithologie, proximité au réseau hydrographique, etc.).

Plusieurs méthodes statistiques ont été utilisées dans ce travail pour étudier l'impact de la croissance topographique conditionnée par la tectonique actives sur l'ampleur des mouvements de terrain dans le front rifain sud. Les résultats ont montré la différence en termes de typologie et de dynamique des pentes entre la bordure sud du Prérif et le paysage

collinaire dominant la province de Moulay Yacoub. Enfin, l'analyse de l'impact des glissements de terrain réalisée sur plusieurs extensions urbaines a montré que l'activité humaine est fortement impliquée dans l'instabilité des versants, notamment parce qu'elle présente une forte vulnérabilité. Par ailleurs, parmi les zones enquêtées, le centre urbain de Moulay Yacoub ainsi que la périphérie urbanisée de la ville de Fès se sont avérés les plus vulnérables aux mouvements de pente et fortement exposés.

Mots clés :

Aléa de glissement de terrain, facteurs de conditionnement, analyse multidisciplinaire, vulnérabilité aux glissements de terrain

Acknowledgement

This long-breath work required the help and collaboration of many people and wouldn't have been possible without their support, and to whom the time has come to express my gratitude and appreciation. My thanks go in the first place to my thesis director, Professor Lahrach Abderrahim (Director of ENSA-Fez, Sidi Mohamed Ben Abdellah University) and my co-director, Professor El Kharim Younes (Professor at the Faculty of Sciences, Abdelmalek Essaadi University, Tetouan), for welcoming me into their laboratories and their research teams in addition to their support, their advice, and their patience which they have shown throughout the period of research.

I would also like to thank all the members of the jury, in particular Professor Saka Abdel Majid, Professor Tabyaoui Hasan, Professor Benmakhlouf Mohamed, Professor Stitou El Messari Jamal Eddine, Professor Barkaoui Alae Eddine, Professor Amyay Mhamed and Professor Azzouzi Nassereddine for agreeing to examine my research work closely and for their comments and recommendations, which will improve the quality of this work.

I am especially indebted to Mr. Ahniche Mohamed (Director of the GEOTECHMED Laboratory design office, Tetouan), who opened wide his laboratory to carry out geotechnical measurements and shared his expertise with me, who incited me to participate in several engineering studies and who putted at my disposal the geophysical material which was used to further pursue my research and expertise.

Special thanks go to Mr Amyay M'hmed, Professor of Physical Geography in the Department of Geography of the Faculty of Letters and Human Sciences, who offered assistance particularly in the field to solve some tasks related to remote sensing and cartography and has always been very supportive and motivating.

I would especially like to thank my brother Oussama who helped me a lot in the field and some crucial issues. My thanks go to my friends and colleagues Ali Bounab, Reda Sahrane, within the Laboratory of the Faculty of Sciences of Tetouan, who shared with me moments of fruitful and pleasant work. I would like to thank my uncle Obda Monaim, Engineer and Director of the Orient Concept Technical Study Office, who helped me with his precious advice related to civil engineering useful in my field of research.

I have also to thank the various administrative technical services, including Doctor Engineer Hamid Rais (Regional Director of Housing and the City, Fez) who provided useful documents for understanding the insalubrious housing of Moulay Yacoub.

Finally, nobody has been more important to me in the pursuit of this research than my parents and my grandmother, whose love and guidance are always with me in whatever I do.

It is clear that contact with all these people from very diverse backgrounds have greatly contributed to strengthening my hard skills (in fundamental geology and applied geology) and my soft skills (skills in 3 languages and communication, in addition to building self-confidence, creativity and cooperative spirit).

I. Table des matières

II. GENERAL INTRODUCTION 5

1. CONTEXT: 5
2. PRINCIPAL STUDY ISSUE 5
3. OBJECTIVE 6
4. GENERAL METHODOLOGY 7
5. THESIS CONTENT: 7

III. CH 1 SETTING OF THE STUDY AREA 9

1. GEOLOGY 9
A. The External domain of the Rif chain 11
2. GEOMORPHOLOGY 25
A. The Saïs plateau 26
B. The Prerif: the hilly-shaped territory of the MY province 28
3. LITHOLOGY 32
4. HYDROCLIMATIC CONTEXT OF THE STUDY AREA 39
A. Climatological context 39
B. Hydrological functioning of the study area 48
C. Conclusion 57

IV. CHAPTER 2 GEOTECHNICAL SETTINGS, VULNERABILITY, AND STACKS 59

1. INTRODUCTION 59
2. GEOTECHNICAL CHARACTERISTICS 59
3. SOCIO-ECONOMIC CONTEXT, VULNERABILITY, AND STAKES IN THE STUDY AREA 62
A. Vulnerability and stakes at Moulay Yacoub scale 63
B. Vulnerability and stakes in the prefecture of Fez 66
C. Conclusion 70

V. CHAPTER 3: SLOPE MOVEMENTS HAZARD IN THE FEZ-MOULAY YACOUB ERRITORY 71

1. INTRODUCTION 71
2. TYPOLOGY 71
3. ANALYSIS OF SLOPE MOVEMENT IN THE STUDY AREA 74
A. Fez prefecture 76
B. Landslide hazard in the territory of Moulay Yacoub 86
4. CONCLUSION 97

VI. CHAPTER 4: LANDSLIDE SUSCEPTIBILITY MAPPING IN THE MARLY CONTEXT OF MOULAY YACOUB REGION 98

1. INTRODUCTION 98
2. SETTINGS OF THE STUDY AREA 100
3. MATERIAL AND METHODS 102

A. Landslide inventory 102
B. Area-Frequency distribution analysis 102
C. Landslide influencing parameters 104
D. Modelling of susceptibility 106
E. Quality control of susceptibility maps 112
4. RESULTS AND DISCUSSION 112
A. Magnitude and distribution of slope movements 112
B. Weight and role of landslide influencing parameters 114
C. Susceptibility maps 119
D. Quality control of the landslide susceptibility maps 124
5. CONCLUSION 125
VII. CHAPTER 5: MULTI CRITERIA ASSESSMENT APPROACH OF SLOW-MOVING URBAN LANDSLIDE HAZARD: THE CASE OF MOULAY YACOUB TOWN (MOROCCO) 127
1. INTRODUCTION 127
2. SETTINGS OF THE STUDY AREA 129
3. METHODS 132
A. Geotechnical Analysis 132
B. Seismic survey 132
C. Field investigations 134
D. Insar Displacement Monitoring 135
4. MATERIAL 136
5. RESULTS 136
A. Marls geotechnical and mineralogical characteristics 138
B. Identification of the depths of landslide rupture surfaces 141
C. Displacement velocities 144
D. Assessment of the impact of slope movements in the urban perimeter 147
6. SYNTHESIS 150
7. CONCLUSION 153
VIII. CHAPTER 6: SYNTHESIS OF THE LANDSLIDE RISK AND ASSOCIATED VULNERABILITY IN MOULAY YACOUB TOWN WITH URBAN PERIMETERS OF SEVERAL NORTHERN CITIES ... 154
1. INTRODUCTION 154
2. LANDSLIDE RISK IN CHEFCHAOUEN TOWN 155
3. LANDSLIDE RISK IN MOULAY YACOUB TOWN 156
4. LANDSLIDE RISK IN FEZ CITY 158
5. LANDSLIDE RISK IN AL HOCEIMA'S URBAN AREA 160
6. SYNTHESIS AND CONCLUSION 161
IX. CHAPTER 7: STATISTICAL EVALUATION OF TECTONIC CONTROL ON LANDSLIDES OVER THE SOUTH RIF BORDER NORTH OF SAIS FEZ 164
1. INTRODUCTION 164
2. GEOLOGICAL AND GEOMORPHOLOGICAL SETTING 166

3. METHODOLOGY 168
A. Choice of the study area 168
B. Inventory of gravitational processes 168
C. Geological data 168
D. Morphometric indices 169
E. Area-Frequency distribution analysis 170
F. Statistical analysis 171
G. Slope instability analysis 171
4. RESULTS 172
A. LIM results 172
B. FR analysis results 173
C. Power law results 174
D. Morphometric analysis results 175
E. ANOVA results 176
F. Factor of safety for marly slopes 178
5. DISCUSSION 179
A. Stability of marls and their erosional landforms 179
B. The effects of active tectonics on landslide distributions 182
6. CONCLUSION 183
X. GENERAL CONCLUSION 184
XI. REFERENCE LIST 187

II. General introduction

1. Context:

The mapping of risks and their integration into approved land use planning documents are one of the preliminary and effective means for natural risks mitigation and management. Today, the public authorities have launched several offers aimed at producing the Urbanization Aptitude Map (CAU). This research project was organized within the framework of the CAU implementation projects, for which the GEOTECHMED study and research office was responsible for the study and mapping of the various natural hazards (floods, landslides, seismic risk, liquefaction, and coastal risks for coastal areas) to which the provinces of Tetouan, Chefchaouen, Ouazzane, Larache, Taounate, Safi and then the territory of the prefecture of Fez and the province of Moulay Yacoub are exposed. This thesis work began before launching the call for tenders which I had the opportunity to participate in the work field, laboratory tests, geotechnical and geophysical field surveys, and monitoring missions in different urban, sub-urban and rural extensions. The resources made available to me by the GEOTECHMED laboratory and by the FST-Fez allowed me to carry out my research work in the best conditions and to develop a rich database in the study area which is the territory of Fez and Moulay Yacoub and which was the basis of research studies and approaches to the hazard of landslides.

Indeed, this research theme is becoming a concern and a topical subject for public authorities wishing to control urbanization and limit natural risks threatening human lives and socio-economic infrastructure. Consequently, the problem of the landslide hazard is an important and operational research and development subject.

2. Principal study issue

The main problem of this research is focused on the realization of a precise diagnosis of the landslide hazard in the Fez and Moulay Yacoub territory. It is a question of making an exhaustive inventory of the slope movements, of investigating the links between these phenomena and the various physical and anthropic factors which generate them, in several scales and various environments imposed by specific site settings. To do so, it is necessary to first perform a good quality landslide inventory, to define the scale for each approach to apply and to identify and investigate the influencing factors in each context. Then it will be possible to obtain the answers sought.

Indeed, the understanding of this hazard begins by analyzing the geological and geomorphological contexts to decipher how its various parameters related to this context intervene and when they become decisive especially during an interaction with other factors. For example, at a detailed scale, it is important to investigate the factors that lead to the modification of the geotechnical characteristics of the original material, and which promotes slope instability. To do so, it is necessary to take rock samples and investigate the physical and mineralogical properties in the laboratory to characterize the

facies delt with and subsequently the phenomena investigated. Then, the geotechnical characteristics of the site materials could then be spatialized with a cartographic illustration at an appropriate scale.

Thus, the main issue is subdivided into several problems and complications requiring treatment and precise analysis from different angles before integrating it as a global view. In fact, it is very complex to approach reality, and it is essential to choose representative cases in terms of the landslide nature and type, in terms of the spatial scale and the degree of vulnerability and socio-economic issues in the study area.

Heuristic methods are known to be tailored for broad scale approaches and are the most effective for proactive projects. For instance, the elaboration of an urban plan or food project planning while relying on a high quality and accurate slope movements susceptibility map can save crucial time, effort, and costs, while preventing serious socio-economic issues.

In a context of interaction between the hazard in question and a fast development of urban and peri-urban extensions where the stakes are highly represented, expert, deterministic and direct approaches are the best. Given the complexity of the phenomena studied and their causes, it is necessary to use a multidisciplinary task to solve the various problems raised by successive stages leading to a global understanding of the issues encountered.

In contexts different from those mentioned above, it is necessary to adopt appropriate approaches that will depend mainly on the objective of the study and the available input data.

3. Objective

This research aims to contribute to a better understanding of the slope movement hazard in the Fez-Moulay Yacoub territory. It is part of both a regional thematic approach that lives to characterize and understand the functioning of slope movements in this region, but also according to a methodology focused on the adaptation of qualitative and quantitative methods of hazard mapping, at small and large scale. This work is focused on three main objectives that structure this research:

1. Characterize the gravitational processes that affect the slopes and develop a time-space database of these phenomena covering the entire study area. Such a data will be the basis for all other approaches used in this research project
2. Perform a heuristic quantitative approach integrated with GIS to study the landslide susceptibility of slopes at a large-scale in the regional context of the study area, identify the influencing parameters and further investigate their implication the landslide hazard.
3. Study and characterize the landslide hazard in a context of complex interaction between the hazard in question and the development of urban and peri-urban areas, by adopting expert and direct approaches
4. Investigate the effects of active and neo-tectonics on the landslide hazard in the south Rif border while adopting a statistical approach.

4. General methodology

The methodology adopted is multidisciplinary, but it boils down to a set of deterministic, heuristic, and statistical physical approaches, each of which is better suited to a certain scale and under certain conditions.

Deterministic methods are based on different techniques for measuring the properties of soils previously affected by landslides. Examples are geotechnical and mineralogical measurements. Furthermore, deterministic methods also include the various techniques relatively recently used in the displacement monitoring and depth measurements of failure surfaces, such as the various geophysical surveys and monitoring techniques using INSAR and UAV.

The heuristic approach designates the evaluation and calculation of physical parameters involved in the observed result, it is based on practical experience and knowledge. This approach also allows the spatialization of phenomena and variables via the use of GIS and subsequently . Its main goal is to narrow down options to guide decision making. The results are summed in landslide susceptibility maps by computing the predisposing factors and the landslide inventory map. These maps show the various levels of predisposition to landslides in the investigated area.

Finally, the statistical approach is used to describe the central values and distribution and especially the decisive parameters and those accessories (size distribution, mean area affected, etc.). This methodology will be further developed and detailed in the next chapters.

5. Thesis content:

This work is carried out in six main sections (according to the number of chapters):

1. The first chapter contains a relatively detailed study and characterization of the physical context of the territory of Fez-Moulay Yacoub

2. The second chapter presents the geotechnical analysis of the various materials encountered in the study area, a socio-economic inventory and an assessment of the vulnerability of the stacks within the territory of Fez and Moulay Yacoub.

3. The third chapter show a detailed inventory of landslides, their type, and their distribution in the study area, and a general statistical analysis of the database.

3. The fourth chapter exposes a work of susceptibility mapping of slope movements by using two methods (GIS-matrix and FR) as well as the evaluation of the controlling factors involved in slopes instability in the area studied

4. The fifth chapter is the subject of the multi-criteria assessing approach to the risk of landslides in the complex urban perimeter of Moulay Yacoub Town

5. The sixth chapter includes a comparison between the stake's vulnerability in MY town with other urban and sub-urban areas investigated during this research work vis-à-vis the risk of landslides

6. Finally, the seventh chapter consists of a statistical evaluation of tectonic control on slope movements over the South Rif border north of Sais Fez

III. Ch 1 Setting of the study area

The entire area subjected to this research includes the entire province of Moulay Yacoub and the prefecture of Fez. The study area is bounded to the north and northeast by the province of Taounate, to the south and southeast by the province of Sefrou, and to the west by the provinces of Sidi Kacem, Meknes and Al Hajeb (fig. 1a). The province of MY alone covers an area of 1621 km ² while the prefecture of Fez extends over 302 km ². Ten communes are included in the territory of the province of MY, the largest are Sbaa Rouadi and Ain Kansara with areas exceeding 200 km ² (fig. 1b).

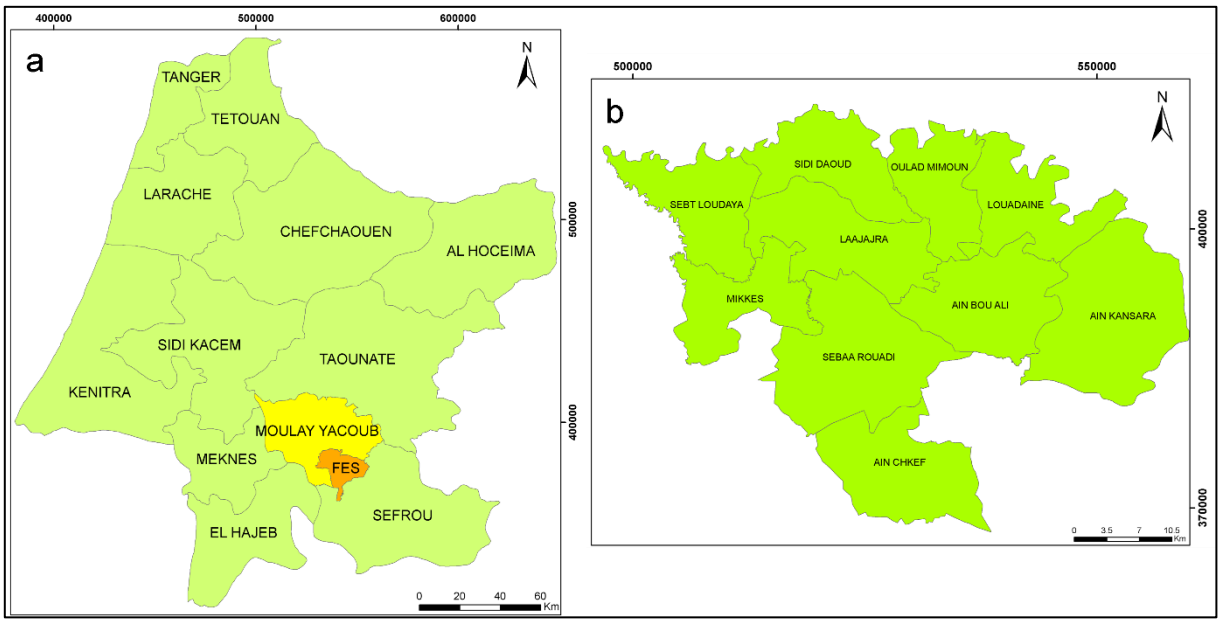

Figure 1 a. Location of the study area among the northern provinces; b. Communes of the Moulay Yacoub province

1. Geology

The entire study area involves two major geological units of northern Morocco, the Saïs basin which is part of the South Rifan Corridor and the Prerif unit, a sub-unit of the External domain of the Rif chain. The Prerif is formed in turn of Prerif nappes and Prerif ridges, which are composed of a long mountainous belt crowned by Mesozoic cornices marking the overlapping contact of the Prerif unit on the South Rifan corridor (fig. 2).

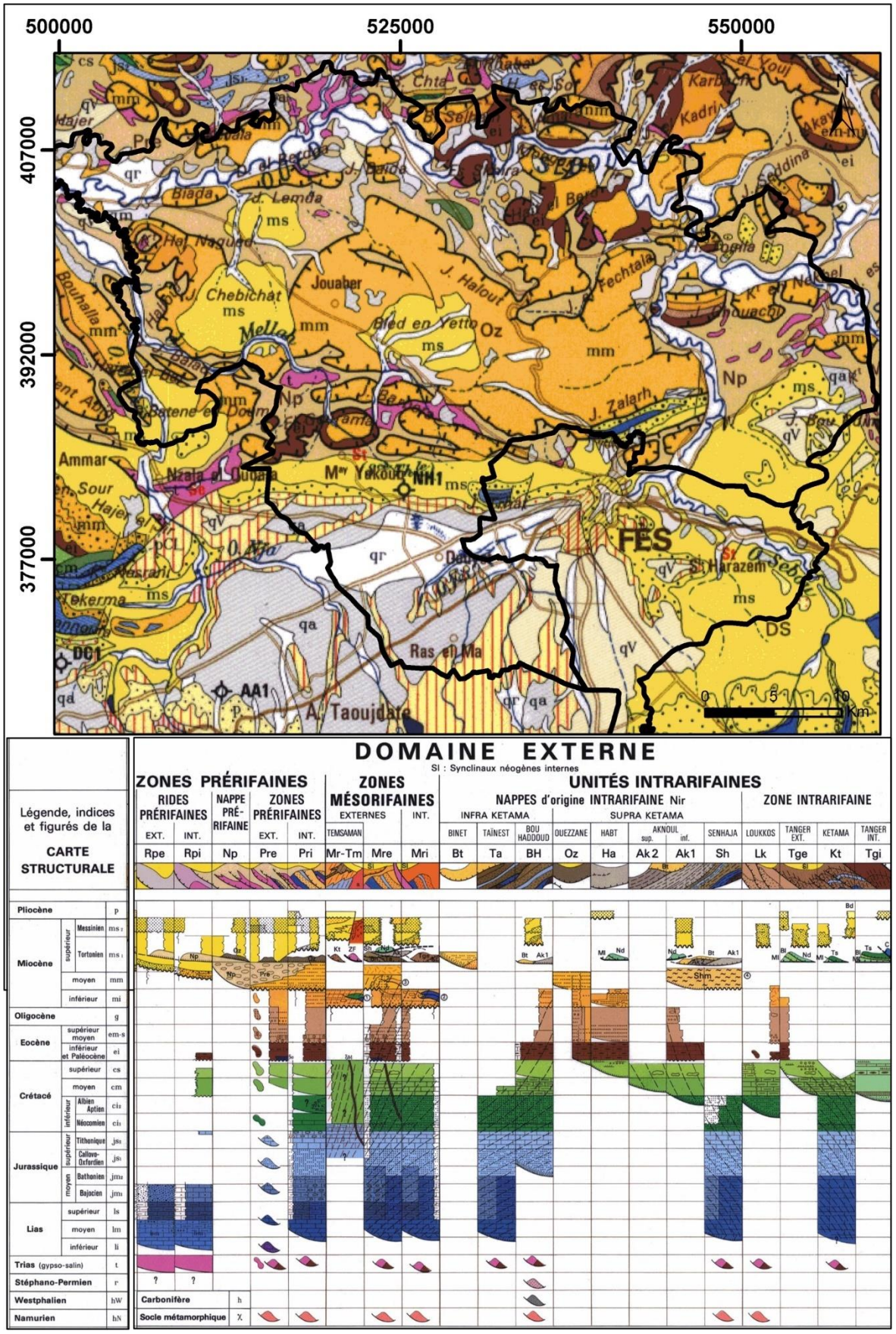

Figure 2 Main structural sub domain of the study area

A. The External domain of the Rif chain

The Rif Mountain belt, located in the North of Morocco, is structurally subdivided into three domains, from the north to the south of the chain, we find the internal domain, the Flysch domain and the external domain which is represented in the study area by terrains of varying lithologies and ages.

The External Domain is subdivided into three units with lithologies of an age ranging from the Triassic to the Miocene (Suter 1980a), which are, from the north to the south of the chain: the Intrarif with units marked by broad stratigraphic series (Tangier, Loukkos and Ketama units), the Mezorif, characterized by variable stratigraphic series with a predominance of Jurassic formations consisting of carbonates followed by series with detrital and calciturbidite facies and the Prérif, which is formed by blocks of several lithologies and ages reworked in a marly or detrital matrix of Middle Miocene or more recent age (Pique 1994; Wildi, 1983).

In the study area, there are only upper parts or the floating units in addition to the Prerif subunits (Prérifan nappes and Prérifan ridges).

a) The sliding nappes (Upper units or floating unites)

These are units completely displaced from their original basins and organized in nappes of peel thrusts and displaced towards the West. Besides, they can cover units from another Riffian domain, as the Prerif formations (from the Triasic to the Miocene) are covered by Miocene Ouazzane nappes north of the Southern Prerif border.

The origin of these thrust nappes is defined as the cover separated from its bedrock during the Cretaceous age. From a large-scale view, an alignment of furrows of average N-S direction is observed, filled by different lithologies. The age of the latter extends from the Upper Eocene to the Middle Miocene (Suter 1986)

In the study area, only the Ouezzane nappe is observed, generally considered as a syn-orogenic basin located at the front of propagation anticlines (Tejera de Leon 1993). From a stratigraphic point of view, the Ouezzane nappe covers a limestone-marls substratum of Senonian age. The essentially limestone-marls stratigraphic series (fig. 3) resting on a Cretaceous bedrock is characterized by the abundance of marly facies (fig. 4,5,6 and 7):

- Light shade marl-limestone from the Lower-Middle Paleocene

- Marls with flint of the upper Paleocene

- Marls with thin sandstone beds from the Eocene

- Marl with sandstone sequences separated from the lower Oligocene Miocene

- Irregular alternations of marls and sandstone series from the Middle Miocene.

b) The Prerif

Located at the limit at the southern border of the the Rif chain and the foreland basins (including the Saïs basin), the Pre-Rif zone includes the allochthonous nappes of the external Rif and is characterized by essentially marly lithologies which predominate from the Cretaceous (Leblanc 1975). Stratigraphically, we quote from bottom to top (Suter 1980a) (fig. 8):

- variegated marls and schistous clays from the Upper Cretaceous,

- variegated marls (Paleocene) and white marls with siliceous nodules (lower Eocene),

- silici-carbonated flysch with shell debris of the Upper Oligocene Aquitanian,

- fine alternation of pelagic marls and yellow friable sandy beds (Aquitanian-Burdigalian).

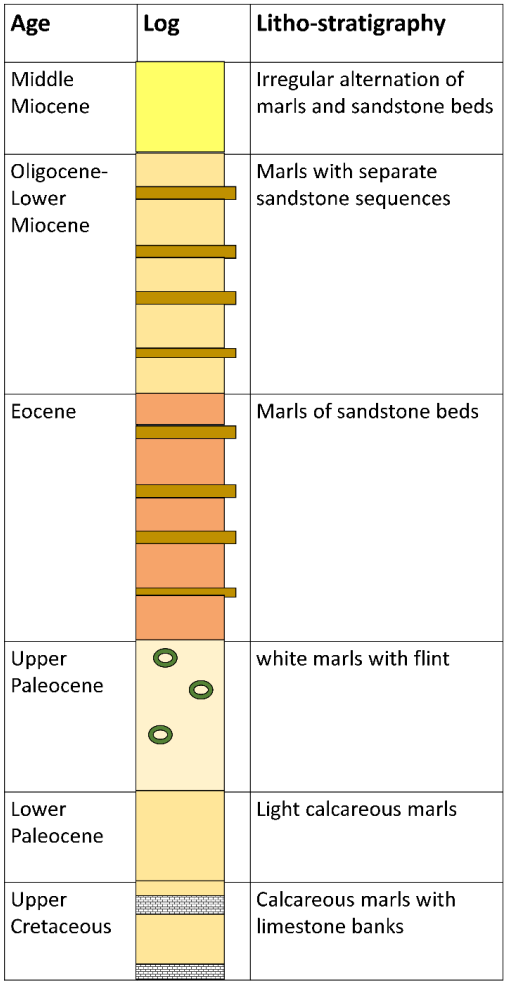

Figure 3 Synthetic stratigraphic log of the Ouezzane nappe (Tejera de Leon 1993)



Figure 4 White marl of the lower Miocene (m4Oz, Ouazzane nappe)



Figure 5 Middle Miocene marl and limestone alternation (Ouazzane nappe)



Figure 6 Marls with decimetric intercalations of Oligocene sandstone with limestone cement (Ouazzane nappe)



Figure 7 Cretaceous marl with limestone banks (Ouazzane nappe)

Some authors, such as Marcais & Suter, 1952 and Wildi, 1983 have distinguished two subunits of the Prerif which, from North to South, are: the internal Prerif and the external Prerif:

- The internal Prerif is made up of peel thrusts rooted under the Mesorif. It contains calcareous lithologies from the Lias and the Dogger with turbiditic layers ("Ferrysch" from the Callovo-Oxfordian) and the platform carbonates from the Kimmeridgian and the Tithonic, which form the "Sofs". These limestone and dolomite massifs, around 700 to 1200 m in altitude, have clay or sandstone intercalations and are oriented East-West, in the form of discontinuous monoclinal crests (Suter 1965; Gartet 1994) (fig. 9).
- The external Prerif is mainly in the form of gravitational nappes with a chaotic structure (Suter 1965; Vidal 1971). These thrust nappes have a marly-sandy matrix of the Upper Miocene containing elements of all sizes resulting from the destruction of the thrust nappes fronts (Ben Yaïch et al. 1991). According to Suter, 1980; Wildi, 1983, we find there the Ouezzane nappe, the Tsoul nappe (Leblanc 1979) and the Habt nappe (Suter and FIECHTER 1966). These are sliding thrust nappes made up of marly facies from the Upper Cretaceous to the Middle Miocene.

Age	Log	Litho-stratigraphy
Middle-Upper Miocene		Chaotic sedimentary complex in a marly matrix
Oligocene-Middle Miocene		Marls with sandy layers and sandstone beds
Oligocene		Marls of rare sandstone beds
Eocene		White marls with flint
Upper Cretaceous		Calcareous marls

Figure 8 Synthetic stratigraphic log of the Prerif nappes (Leblanc 1975 and Suter 1980a)



Figure 9 Sofs of Ain Aicha

(i) The Prerif nappes

The Prerif nappes, corresponding to the external Prerif, have been cited in the literature as allochthonous nappes of the "Prerifain complex" (Leblanc 1977), sometimes as "tectono-sedimentary complex" (Feinberg 1986) and/or as "accretionary-prism" (fig. 10) which progresses towards the external parts of the Rif chain (Flinch 1993).

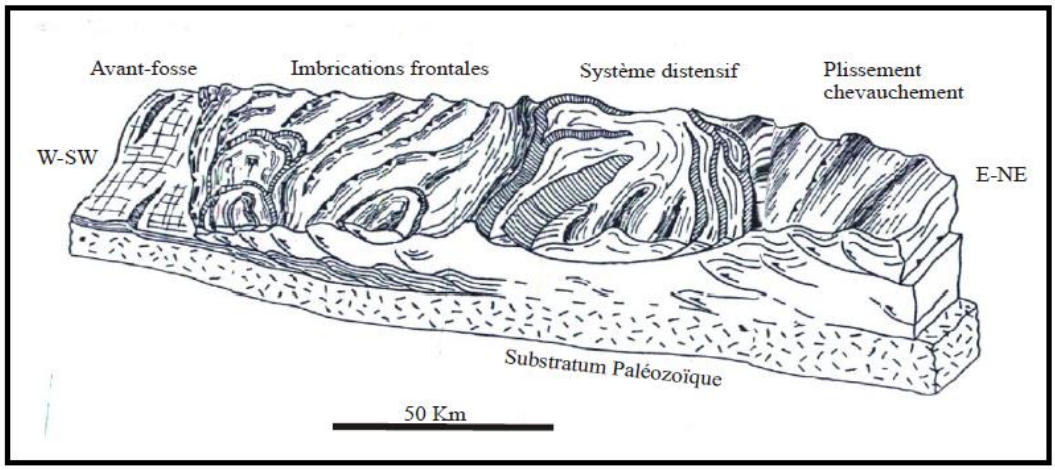

Figure 10 Block diagram of the complex of the Prerif nappe, as an accretionary prism (Flinch 1993)

The Prerif nappes consist mainly of detrital and turbiditic clays and Triassic evaporites. According to Flinch, 1993, the series from the Triassic to the Miocene are distorted, they would have been detached from their substratum and carried over the Mesozoic and Middle Miocene of the foreland. Given the variety and abundance of reworked elements in the Prerif nappes, their exact age is difficult to define.

From a stratigraphic point of view, these nappes bring together a chaotic set of all sizes elements packed in a marly matrix. These elements are interstratified in Miocene marls (fig. 11 and 12). The most frequent elements are made up of a Triassic gypsiferous marls (fig. 13) having as their origin the nappes of the external parts of the Rif chain. In these Triassic clays, the basaltic neck observed results from an alkaline magmatism manifestation.



Figure 11 Upper Miocene white marls Sidi Chahed dam (Prerif nappe)



Figure 12 Upper Miocene white marl (Prerif nappe)

(ii) The Prerif ridges

The Prerif ridges are located in the southern front of the Rif chain (fig 14), at the limit between the latter and the Saïs basin to the south and the Gharb basin to the western border. These reliefs are crowned with Jurassic series and arranged in concentric overlapping arcs with concavities directed towards the NE (Haddaoui et al. 1997). These Jurassic reliefs are separated by depressions of Neogene to Quaternary series (Faugères 1978; Boutakiout 1990). They were uplifted continuously during the Neogene (Faugères 1978). During this period, these ridges provided sediments to the adjacent basins, the case of the Saïs for example. The Ridges are subdivided into two large groups: a western arched group, convex to the west, and an eastern group which forms a less accentuated arc. Further east, in the extension of the second group, there are two other isolated ridges: Jbel Trhat and Jbel Zalagh.

Geologically, the Prerif Ridges have long been interpreted as peel thrusts with Mesozoic material from the Riffian foreland spilled towards the south and west. They result from a compression phase contemporary with the Prerif nappe installation (Daguin 1934; Durand-Delga and Mattauer 1960; Delga et al. 1962; Suter 1965). Thus, an interpretation was proposed by Vidal & Faugeres (1975), according to which the Prerif ridges would constitute a compression zone limited by two systems of conjugate strike-slips to the west and to the south. The tectonic phase which would have structured the ridges would be posterior to the major phase of the Rif responsible for the installation of the nappes, either by compression (Andrieux 1971), or by sliding (Vidal 1971). According to Faugeres (1981), this region belongs to the post-Hercynian basin which borders the margins: African, American and Western European. Its history begins with the first manifestations of the separation of the American and African continents.



Red clays topped by Miocene marls



Gypsum in red clays



Basalt neck piercing the Triassic clays

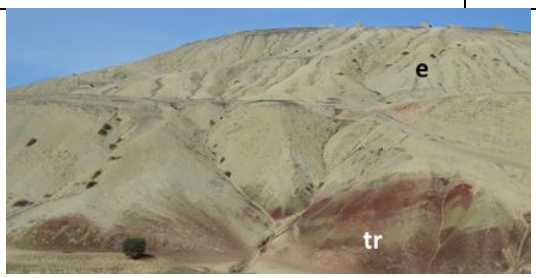

Pre-rifan nappe (Triassic pelites and gypsum clays -tr- and marl with alternating marl-limestone with rare flint nodules of Eocene age



Marl with clayey limestone beds (M1) surmounting Triassic red saliferous clays (tr) in the vicinity of Sbaa Rouadi



White marls of the Prerif nappe with Triassic gypsum north of Jbel Zalagh



Cretaceous brown pelites



Triassic gypsum intercalated in the Prerif nappes (exit from Al Kansera towards Taouante)



Saliferous Triassic exploited to extract salt associated with red saliferous clays



Triassic ophites

Figure 13 Some facies of the Prerif nappe

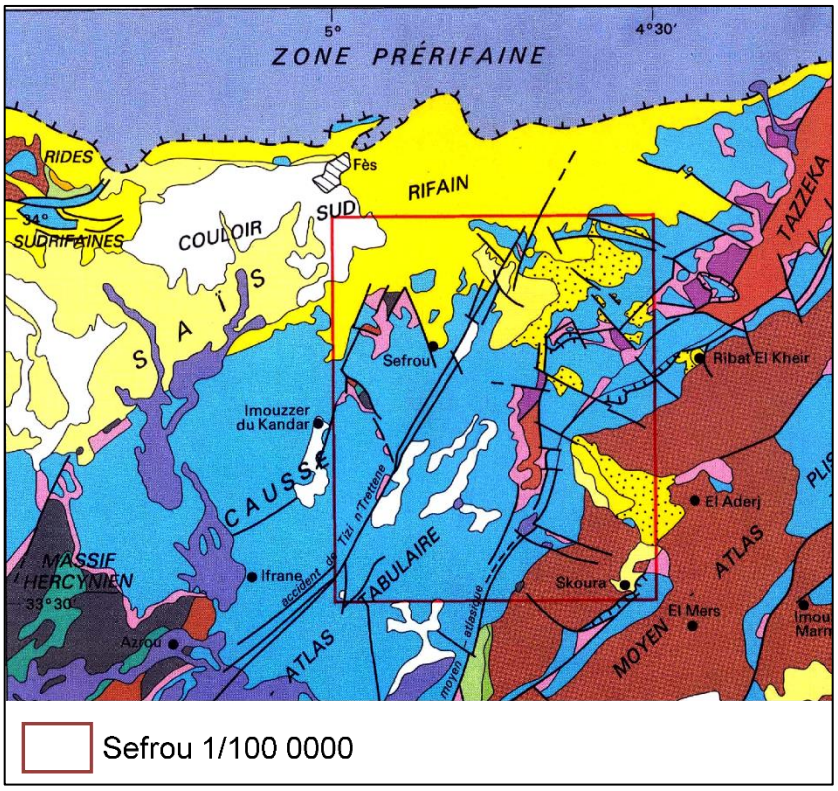

Figure 14 Structural map of the Eastern part of the south Rif foredeep

The lithostratigraphy of these ridges shows the superposition of three sedimentary sequences separated by major unconformities and by long periods of emersion and continental erosion (fig. 15). These series are from bottom to top (Benzeggagh et *al.*, 2016): lower series (corresponding to the Triassic-Bajocian substratum), intermediate series formed of Aptian -Paleocene facies (transgressive and discordant on the silty marls of the lower Bajocian) and upper series (transgressive on the majority of the ridges), starting with molassic limestones of the middle Miocene, discordant on the Jurassic and the Cretaceous.

The sedimentary and stratigraphic history of these ridges can be divided into two phases: the first (Triassic - upper Bajocian), located in a general context in extension and the second (Miocene - Pliocene), takes place in a general compression context.

A. Paleozoic substratum

In the Triassic-lower Lias, lithologies represented by schists and quartzites are affected by faults of NE-SW structural direction which will control the Triassic sedimentation.

B. Triassic

According to the authors, the Triassic volcanic formations are considered as the result of an extensive tectonic phase during the Triassic, with the development of numerous evaporitic basins

trending NE-SW to NNE-SSW. In the ridge's domain, the Triassic is only well represented on its southwestern and eastern edges.

The Triassic outcrops (fig. 16) are either diapirs of deep origin, (Faugères 1978), large masses of salt diapirs in the nappes or injected along faults and thrusts during the Mio-Pliocene tectonic inversion (Zizi 1996).

C. Jurassic

The Jurassic deposits (fig. 17) are grouped into three groups (Faugères 1978; Haddaoui 2000): - reduced series (lower and middle Lias), essentially made up of very varied carbonated facies (with a carbonated series outcropping especially in the Western Ridges and meridionals), - intermediate series, composed of deposits of an internal carbonate platform topped by Toarcian marly and marl-limestone deposits and Bajocian sandstone-deltaic deposits, - thick series, characterized by their deeper marl and marl-limestone facies of the Toarcian and Bajocian.

D. Cretaceous

Transgressive and discordant over the Jurassic, the Cretaceous (fig. 18) is found only in the Oued Debiane depression. It is represented by a base of conglomerates, 40m thick white sandy marl-limestones, covered by oyster marls and limestones, a chalky limestone bar (10m) fossiliferous, thick yellow marls (70m) and by a second bar of crumbly calcareous-marls.

E. Miocene

In general, the Miocene series (fig. 19) is made up of lower molasses (Middle Miocene), beginning with sandstone limestone and surmounted by bioclastic limestone, by red marl-limestone with Helix and by fine red sandstone (continental Miocene), by upper molasses (slightly sandy marly limestone) and by very thick white marls.

During the Neogene, the ripples underwent a progressive and continuous marine evolution. The confinement of the ripple region, following a drop in sea level, was not total, it remained in communication with the Atlantic Ocean.

In the study area, there are only the eastern Prerif ridges, represented by Jbel Trhat and Jbel Zalagh which are isolated ridges, elongated E-W with southern vergence.

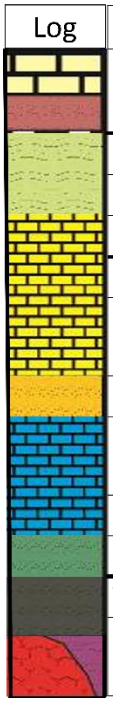

Facies	Age
Lacustrine limestone Fawn sands	Pliocene
Calcareous marls	Tortonian
Sandy marls	
Carbonated rocks	Serravallian
Marl and limestone	Cretaceous
Carbonated and deltaic deposits	Bajocian
Marl and sandstone	Aalenian
Marl-limestone alternation	Toarcian
Carbonated rocks	Domerian
Evaporitic formation	Triasic
Turbidites	Carboniferous
Granite and metamorphic rocks	Cambrian-Ordovician

Figure 15 Synthetic stratigraphic log of the South Rif ridges (Faugères 1978; Zizi 1996)



Figure 16 Saliferous Triassic formations to the North of Jbel Trhat



Figure 17 Marls and sandstones of the upper Jurassic of Jbel Trhat



Figure 18 Marls with carbonate intercalations of the Cretaceous of Jbel Trhat



Figure 19 Miocene molasses of Jbel Boudra Sidi Kacem (South Rif ridges)

- ***Jbel Trhat***

Trhat Mountain, which is in fact an E-W anticline with a Jurassic core and overturned towards the South, outcrops under the Upper Miocene marls of the Prerif (fig. 20 and 21). Its southern slopes rest on Plio-Quaternary conglomerates and lacustrine limestone of the Saïs basin. Jbel Trhat is bounded at both ends by lateral strike slips, sinistral N20–N40 at its eastern end and dexter N160 to N170 at its western end (Chalouan and Michard 2000; Bargach et al. 2004). A fault system cuts through the Bajocian limestones, its northern flank is cut by a large old normal fault EW trending with a north dip which touches the Miocene molasses formations. A blind fault is found at the limited ridge of Trhat and the Saïs basin (Chalouan and Michard 2000; Bargach et al. 2004).

As for the Miocene of the ridge: on the slope of Jbel Trhat, there are sandy microcrystalline limestones of a hundred meters covered by whitish marls. These two facies are of Tortonian age and are crowned by a thick series of yellow/grey marls with local calcarenites beds. Its south-east flank of Upper Pliocene-Quaternary age is made up of conglomerates and lacustrine limestone (fig. 20).

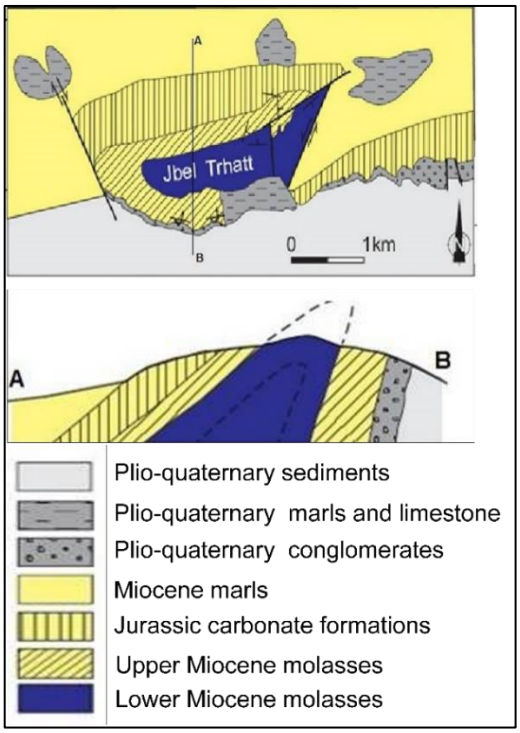

Figure 20 Geological map of Jbel Trhat (according to El Alami & Lahmid, 2016)



Marls with limestone intercalations from the Cretaceous of Jbel Trhat



Upper Jurassic marls and limestones of Jbel Trhat



Marly slopes with benches of limestone on the northern flank of Jbel Thrat (Douar Ain Sikh)



Decimetric to metric limestone benches at Douar Msabih

Figure 21 Some facies of Jbel Traht

- ***Jbel Zalagh***

J. Zalagh is considered in the eastern part of the South Rif ridges (fig. 22). It limits the city of Fez on the north side with an ENE-WSW elongation. In fact, Jbel Zalagh is an anticline overturned towards the south with a N110° axis. Overhanging the slope and the marly plain, it affects the frontal zone of the Prerif nappe and its Upper Miocene cover. It is made up of carbonates (dolomites and banded limestone) from the Lower-Middle Lias, fossiliferous marl-limestone from the Dogger and marls and molasses from the Middle-Upper Miocene (fig 23, 24 and 25), which form a slight unconformity on the carbonate facies (El Alami & Lahmid, 2016).



Figure 22 Panoramic view of Jbel Zalagh and its southern slopes

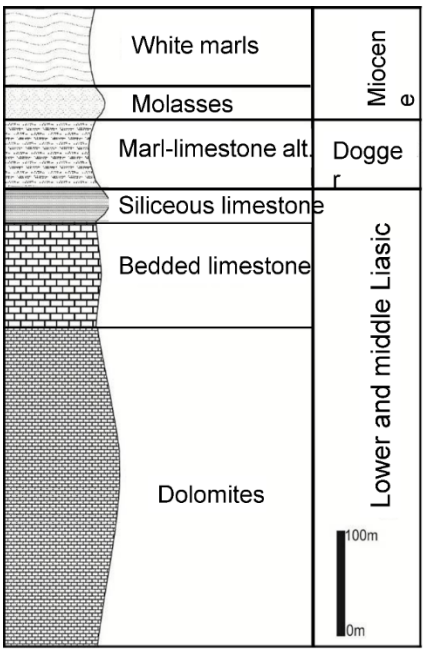

Figure 23 Stratigraphic log of Jbel Zalagh

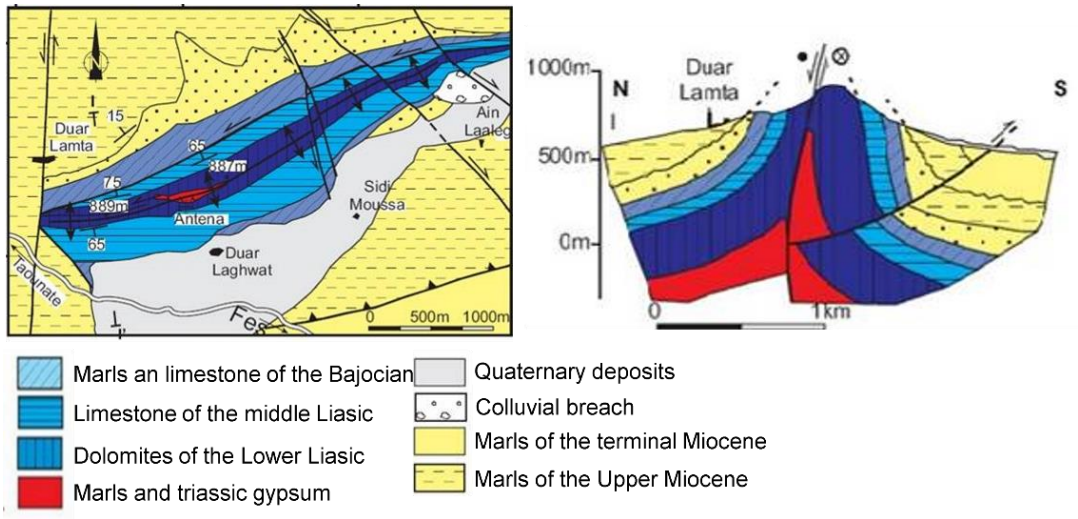

Figure 24 Geological map of Jbel That (El Alami & Lahmid, 2016)



Middle Liassic limestone



Lower Lias dolomites

Figure 25 Some facies of Jbel Zalagh

2. Geomorphology

The variation in relief shapes between the two major units (the prerif and the plain of Saïs), to which the Fez-MY region belongs, is mainly due to a litho-structural contrast (fig. 26). Hence, the study area is part of the following two morpho-structural units:

- The plain of Saïs where the prefecture of Fez is settled
- The hills landscape with marly slopes, covering almost the entire province of MY

The slopes of the study area are quite diversified. Those at the level of the Sais plateau are very low, while the steepest slopes are encountered at the front line of the south -Rifan thrust (exceeding 60 °). Within the province of Moulay Yacoub, the steepest slopes are generated by ledges often armed with sandstone banks (case of Sidi Chahed in the west of the province) or by carbonated formations and semi-rocky alternations. The rest is dominated by a hilly landscape including plains such as those of the communes of Laajajra and Sidi Daoud.

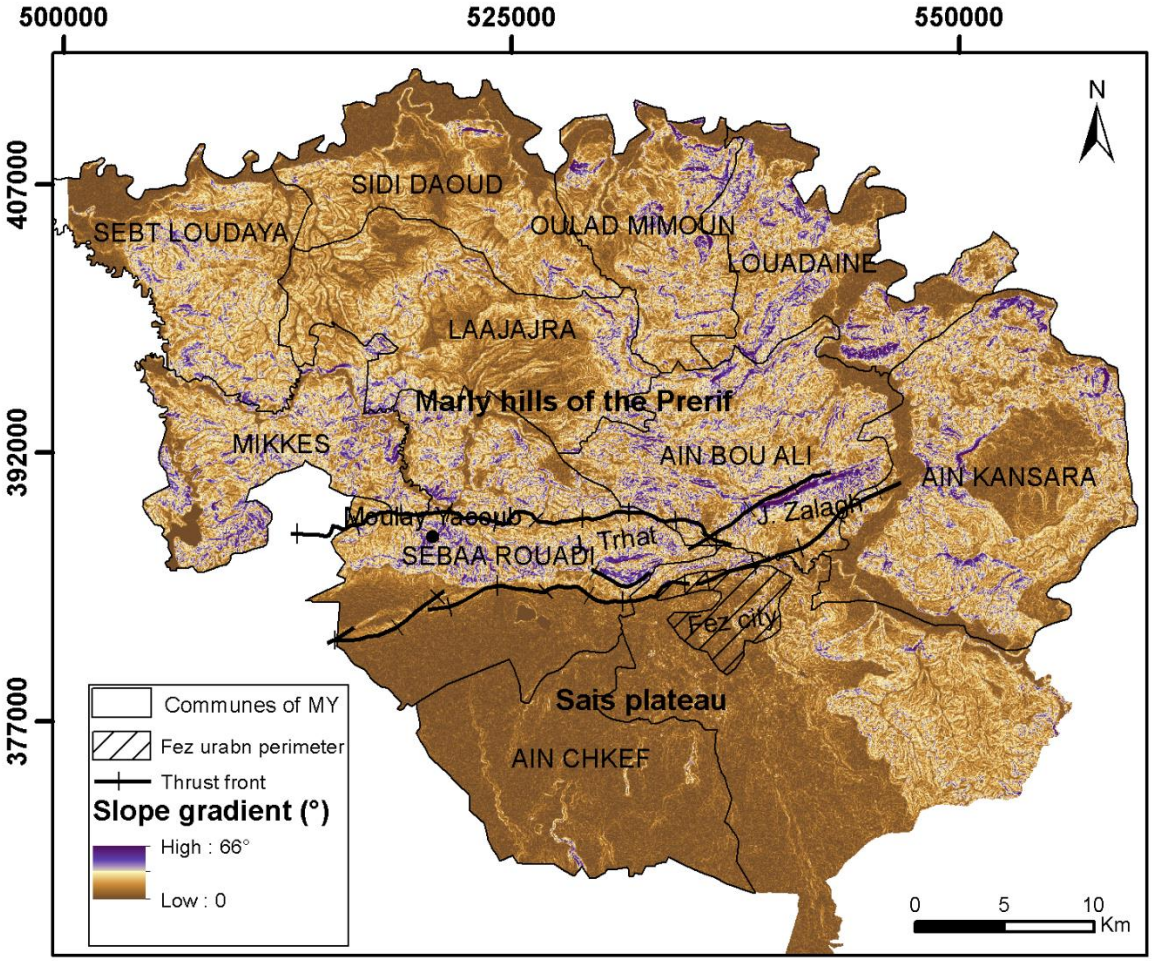

Figure 26 Slope Map of the study area

A. The Saïs plateau

It is the territory where the city of Fez develops (fig. 27). The origin of the flattening of the Saïs plateau is the fact that the latter represented a foreland basin limited by two structural units; the Prerif and the Middle Atlas. The supplying in carbonates by Oued Sebou (having an endorheic system at the time) and its affluents coming from the middle Atlas (dominated by carbonate rocks) allowed the final filling of the basin by the quaternary lacustrine limestones.

The low and poorly drained areas of the Fez-Saïs are at the origin of the marshy areas such as daya of Douiyate to the west of the city. The topography of the plateau slowly increases from 400 m towards the southwest, extends and joins the plateau of Meknes-Saïs from Ain Taoujtate. On the east side of the Fez city, the Saïs plateau is bounded by the Sebou and Fez rivers, where travertines ledges (fig. 28) developed by the lacustrine limestone leaching, follow one another towards the confluence of the mentioned rivers. On the SE side, at the town of Sidi Hrazem, a landscape of marly hills settles in, covered by quaternary benches and terraces (fig. 29). Finally, the topography rises gently to the South-

West, towards the Middle Atlas glacis, called dirs de Sefrou. As for the North, it rises sharply in contact with the Prerif ridges (Jbel Zalagh and Trhat).



Figure 27 The Saïs Fez from the road leading to Moulay Yacoub



Figure 28 Relief anthropized by the exploitation of travertine ledges



Figure 29 Marly slopes terraced at their summits in the region of Sidi Hrazem

B. The Prerif: the hilly-shaped territory of the MY province

The Pre-Rif ridges link the plain of Saïs to the Prerif marly hills. These ridges control the landscape by the two elongated reliefs Jbel Trhat and Zalagh (fig. 30), which culminate respectively at 837 and 900 m.

The territory of the MY province is dominated by low marly hills (less than 200 m height) (fig. 31). However, the latter reach higher altitudes (between 200 and 300m height) with steeper slopes when the hills are covered by marls with intercalations of Eocene or lower Miocene clayey limestones. The predominance of the soft material of the Prerif and Mesorifan nappes is at the origin of the low and spacious reliefs dominating the territory of the study area. In addition, the biodetritic bar cornices of the Miocene afford to the marly hills high elevations exceeding 300m in altitude (the Sidi Chahed edifice: 435m and the elongated crest of Baten Ed Doum: 547m). The ridges line is mostly covered by calcareous marls with flint nodules (line of jbels Halout culminating at 800m and jbel Ben Manama at 620m altitude) (fig. 32).

The alterability of the white calcareous marls forms strongly gullied Badlands (fig. 33). The intense weathering of the whitish marls also develops a thick layer of clayey colluvium downhill, under the effect of sheet-flow erosion of the white marls, a phenomenon relayed by the dynamics of the creeping slopes. Moreover, the marly slopes of these hills are highly affected by various gravitational processes, ranging from widespread shallow solifluctions and earth flows to deep landslides. As for the rock falls, they are mainly located at the foot of the escarpments provided by rocky bars such as the biodetrital Miocene cornices of Sidi Chahed.

The hilly landscape of the My province is interrupted by open valleys filled with clay-silty alluvium, as a leaching of essentially clayey materials from the surrounding hills (whether they are formed of grey or whitish marls, brown pelites or red saliferous clays) (fig. 34). As for the Sebou valley, it is relayed by Quaternary terraces (fig. 35) and generally preserved by coarse alluvium. The Mikkes oued, of less importance, only has remnants of old terraces partially levelling the surrounding marly hills (fig. 36).



Figure 30 The Prerif ridge of jbel Zalagh



Figure 31 Landscape of marly hills in the province of Moulay Yacoub



Figure 32 Line of crests of the middle hills (jbels Halout-Ben Manama), overhanging the low pre-rifan hills (in the foreground)



Figure 33 The ravine reliefs of white marl with a skeleton of centimetric intercalations of clayey limestone (Ouazzane nappe)



Figure 34 Clayey alluvial cone fed by the leaching of white marls, Triassic red clays and Cretaceous Pre-Rifan grey pelites



Figure 35 The current floodplain of Oued Sebou and an old alluvial terrace reinforced by its Pliocene conglomeratic cornice

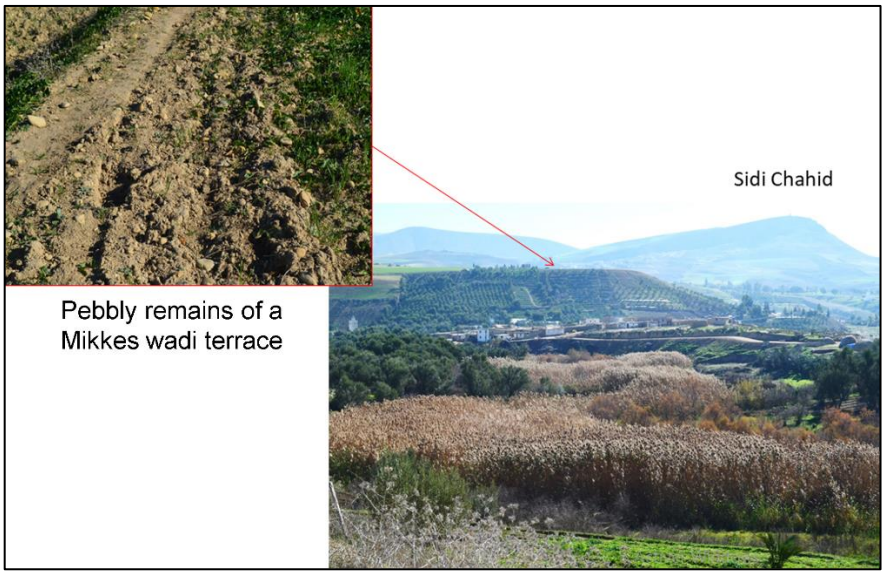

Figure 36 Douar Ketatba installed on the major bed of Oued Mekkes, just behind a terrace shaped in Miocene yellow marls and Jbel Sidi Chahed in the background

3. Lithology

The lithological map of the study area is produced by digitizing the geological maps available for the study area. Subsequently, a reclassification and grouping of geological formations into lithological complexes and lithological units was carried out without considering their structural or stratigraphic affiliation.

There are several lithological classification methods according to different parameters, the most common of which are the spatial extent of the study area and the level of facies diversification. In the present work, despite that the study area is characterized by a large spatial extension, the monotony of the soft rock facies (marly soils) urges them to be differentiated knowing that they have different mechanical characteristics, and consequently, an unequal predisposition to landslide. Thus, the lithological classification used in the present work considered the subdivisions adopted by Millies-Lacroix (1968) in the Rif, while integrating some notions brought by Varnes, (1984) in terms of natural risks and the recommendations proposed by the international association of engineering geologists (AIGI, 1976) about the preparation of lithological maps for geotechnical purposes, without considering their structural or stratigraphic membership. The main lithological classes distinguished in the entire territory of the study area are presented in figure 37 and their surface of outcrop in table 1.

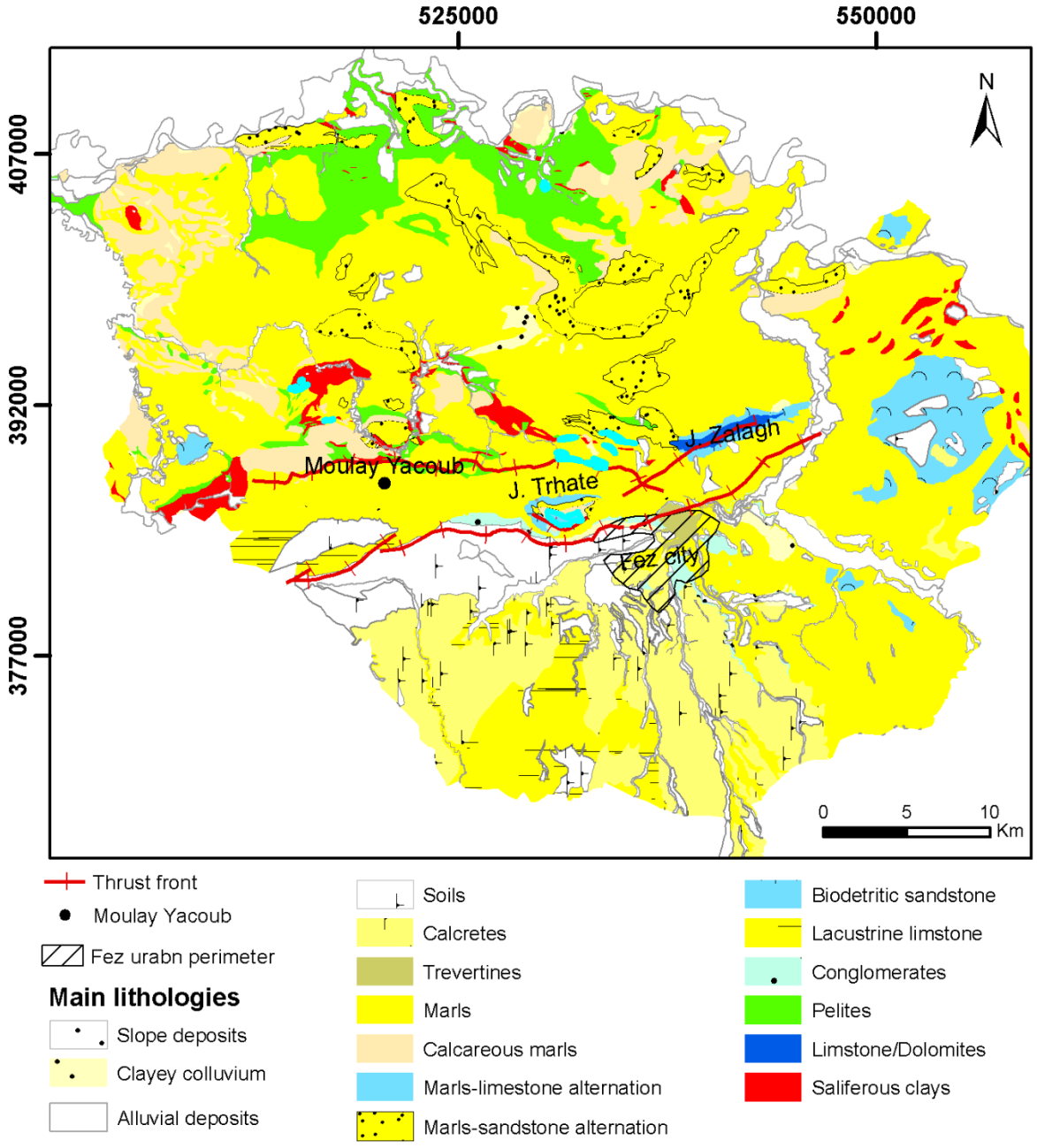

Figure 37 Distribution of main lithological formations in the Fez-Moulay Yacoub territory

Table 1 Area of outcrop for main lithological formations

Lithological formation	Outcrop surface	%		Lithological formation	Outcrop surface	%
Alluvial deposits	184.4	10.4		Marls	778.8	**43.7**
Saliferous clays	28.6	1.6		Calcareous marls	104.1	5.8
Limestone/dolomites	5.3	0.3		Sandy marls	8.3	0.5
Lacustrine limestone	82.3	4.6		Marls-limestone alternation	2	0.1

Calcretes	186	10.4	Marls-sandstone alternation	80.7	4.5
Clayey clolluvium	25.6	1.4	Pelites	105	5.9
Conglomerates	11.6	0.7	Soils	109	6.1
Slope deposits	12	0.7	Travertines	4.3	0.2
Biodetritic sandstone	52.6	3.0			

The spatial distribution of the different classes thus distinguished shows a clear predominance of marly facies (almost 80 km²). Pelites and calcareous marls also show significant outcrop surfaces even if the marly facies are subdivided and detailed more than the other lithological ones. Moreover, the distribution reflects the particularism of the geological substrate of each part of the study area. If in the province of MY almost entirely outcrop marls and pelites (80%); in Fez, it is the superficial formations, in the form of tufted or clayey soils, which predominate with (80%); moreover, most of rocky formations outcrop at the south Rifan contact, on top of the mountainous edifices and high hills along the lineament of the thrust front.

The rocky lithologies

The class of rock masses includes compact, massive, or bedded carbonate formations in the form of limestone and dolomites of the Liasic (fig. 38). Moreover, these formations constitute the Jurassic core of the Prerif ridges, e.g., Jbel Trhat and Jbel Zalagh. The rocky class also includes sandstone banks forming some ridges like the cliff of Sidi Chahed (fig. 39). These sandstone banks of variable thickness constitute in places the terminal Micocene covering few marly hills at the level of the southern Rifan contact, to the west of the Sais basin.



Figure 38 Carbonate rocks on top of Ain Sikh



Figure 39 Sandstone cornices of Sidi Chahed ridge

Semi-rocky lithologies

These are transition materials between the rock masses and the materials of less cohesion. In this class were grouped:

- The Pliocene lacustrine limestones, mainly crumbly at the Saïs plateau. In Adrej, on the other hand, they are progressively more consistent towards the South.

- Quaternary travertines, very widespread at the east of the urban perimeter of Fez which are relatively consistent. They were subject to extraction as building materials.

- The conglomerates, especially Pliocene, encountered in the eastem part of the province of Fez, along Oued Sebou (Commune of Sebt Loudaya, province MY). Some outcrops to the north of Fez city show that they were overturned during the uplift of the Prerif ridges.

- Eruptive rocks (Basalts and ophites). These materials are classified in this category because of their variable consistency. In the province of MY, they are locally associated with the Triassic clays.

Alternating facies

These are transition materials between rocky and marly lithologies by alternating cohesive and incoherent facies (fig. 40 et 41):

- The alternation of limestone beds and Miocene marls of the Ouazzane nappe found only in the province of MY. They form the lines of summits of the hilly reliefs in the province.

- The alternations of sandstone beds with neogene marls which appear in a straighte ned series on the sides of the Prerif ridges (limit of the MY and Fez provinces). To the east of the said provinces, these alternating, essentially sandstone facies cover the Neogene series forming flat areas.



Figure 40 Sandstone-marls alternation



Figure 41 Limestone-marls alternation

Marls and pelites

These are essentially clay soils based on relatively consistent clays depending on their compactions or cementations by carbonates (fig. 42). Their surface friability is obvious. Generally, in this category we quote:

- Neogene marls, post-nappes, with variable carbonate content. The latter is quite weak to the east of the prefecture of Fez where the clay material in question is exploited for brick industry and pottery. In MY town, the compact marls are quite hard due to their high carbonate content (Obda et al. 2022).

- The white marls of the Ouazzane nappe, with their high carbonate content, locally arm and cover hills in the MY province (eg. Douar Byada)

- The Prerif Tortonian marls showing centimetric limestone intercalations in places. However, its main particularity is the presence of Cretaceous pelites and saliferous clays injections. These last two outcrop in large areas in the province of MY.

- Red Triassic gypseous or saliferous clays, with relatively large pockets of salt or gypsum. Some of the large salt pockets constitute real exploitable deposits in the province of Moulay Yacoub.



Neogene marls, post-nappe, with variable carbonate content



Prerif Tortonian marls



White marls of the Ouazzane nappe at Sebt Loudaya

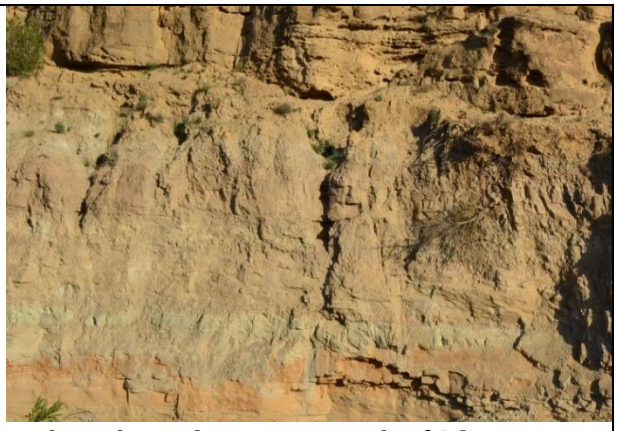

Relatively sandy Neogene marls of Adrej



Red Triassic gypsiferous or saliferous clays near to Moulay Yacoub town



Sample of very compact calcareous marls from the Mikkes center

Figure 42 Marly facies of the Moulay Yacoub territory

Colluvium and slope deposits

They are formed of reworked materials of low cohesion. In this category, we distinguish the scree, which are very localized notably at the feet of the rocky ridges (eg. the scree of Jbel Trhat, Jbel Zalagh and those of Sidi Chahed cliff) and the clayey colluvium which are the most widespread slope deposits in MY province (fig. 43).



Figure 43 Clayey colluvium with sandstone pebbles in Ain Sikh

Alluvial deposits

Ancient terrace

These are ancient alluvial deposits from the Quaternary periods (Villafranchian, Rhegregian, Tensiftian, Soltanian, or undetermined) in terraces at different altitudes above the current levels of the oueds. They are composed of relatively loose formations, based on cobbles with a clayey-silty-loamy matrix, arranged in layers (fig. 44).

Recent alluvial deposits

These are the current alluvial deposits, formed of clayey-sandy silt with pebbles, which form the minor and major flanks of the watercourses, and which are much more frequent in the municipality of Sebt Loudaya (fig. 45).



Ancient terraces of Oued Sebou



Fine silty alluvium at Sebt Loudaya

Figure 44 Examples of ancient alluvium



Current alluvial deposits in douar Sidi Ayyad (Sebt Loudaya)



Recent alluvial deposits in Douar Khribyate (Sebt Loudaya)

Figure 45 Examples of recent alluvial deposits

Developed soils

Given the extent of certain flat areas in the provinces (especially the Fez prefecture), soils (fig. 46) can constitute several shallow cover types: the red soils of decalcification of the various carbonate substrates; the calcretes (calcareous crusts) developed in places on the sloping borders of the Saïs plain (especially towards the south), where clay-tuff soils less carbonated than the first ones as well as brown clay soils have formed.



Figure 46 Brown clay soils in Saïs-Fez

4. Hydroclimatic context of the study area

The hilly relief formed by friable marls and clayey soils, by undergoing wetting and drying out, becomes unstable and generates risks for the socio-economic infrastructures of the Moulay Yacoub territory, especially in the douars and the villages with high population densities. As for the relief of the prefecture of Fez, it is shared between the Saïs plateau with essentially lacustrine formations, where most of this territory extends, and the Prerif margins, which are subject to the same instability problems as Moulay Yacoub province. Thus, the study of the climatic and hydrological context of the study area of these two administrative units helps to better understand their implications in the landslide risk. Furthermore, a precise diagnosis of such key parameters is a basic tool of an action plan containing the various measures necessary in risk mitigation, including measures limiting the wetting process of the sub-soil and the substrate of the built-up area in the Moulay Yacoub town and the peripheral districts of the Fez agglomeration.

A. Climatological context

The Moulay Yacoub province and the prefecture of Fez, whose urban extensions are distanced from each other by about 10 km, belong to the same bioclimatic stage called subarid with hot summer (fig.47) according to the Bioclimate model of Emberger (modified by C. Sauvage, 1963). The main

factor causing field moisture, the runoff on the slopes, the flows in the hydrographic network and the supply of the various hydrological reservoirs is essentially the precipitation which varies spatially from 400mm (in the wide, deep and sheltered valleys around Moulay Yacoub); to 500mm on the Saïs plateau, to 700mm on the high reliefs of the neighbouring Prerif ridges such as J. Zarhoun in the west and the summits of Zalagh in the east, and even to more than 1000mm on the Middle Atlas Causse drained by the tributaries of the Fez and Mikkes oueds.

It is especially the fine and elongated rains that soak the soils and the basements by breaking the balances which can trigger the landslides by jostling these geotechnical characteristics of the materials pushing the slopes outside their stability limits.

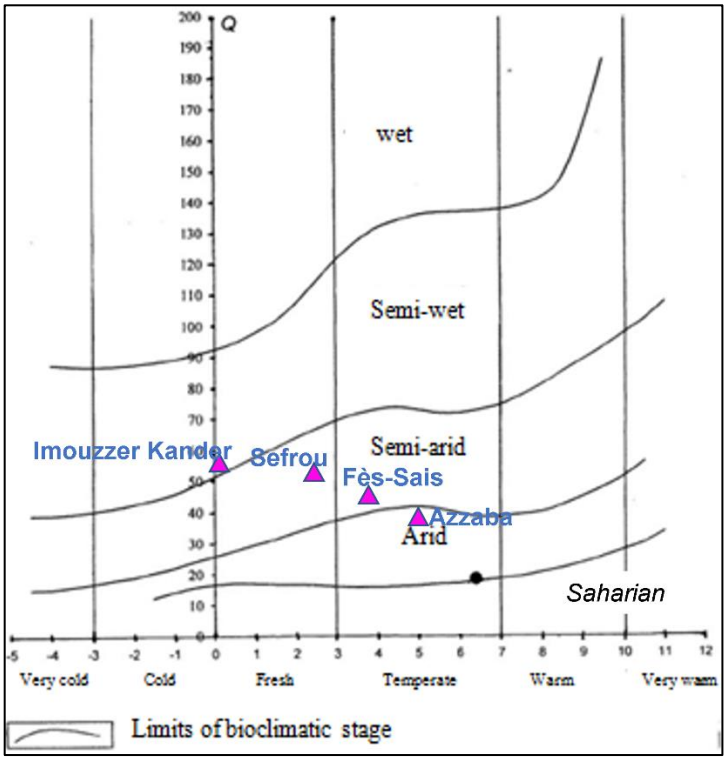

Figure 47 Location of the main hydraulic stations in the Emberger climagram (modified by Sauvage, 1963)

To analyze the temporal rainfall characteristics of the study area, we chose two main climatic stations, Dar El Arsa at 164m above sea level, managed by ABHS, and Fez-Saïs located at Fez Airport at 570m above sea level, managed by the National Meteorology, which have reliable data and a fairly long observation period in addition to the Moulay Yacoub station at an altitude of 450m which has only 5 years of observation (see figs. 48, 49 and 50). To study the spatial variability and draw up the isohyets map of the study area (fig. 51), we used data from a dozen stations available in the Prerif, the Saïs and the middle Atlas border in order to approach the pluviometric reality of the entire study area (ABHS; Meteorology).

The average annual rainfall in Fez-Saïs (570m altitude) is about 516mm calculated over a period of 100 years with a monthly maximum in December (75.3mm) and a minimum in July (1.6mm) (see Table 5 and figure of seasonal and monthly rainfall patterns below). In Dar El Arsa, 164m above sea

level in the Sebou valley, which is not far from the cities of Moulay Yacoub and Fez, the average annual rainfall (over 39 years: 1976 – 2015) amounts to 435mm. In Moulay Yacoub (altitude 450m), the average annual rainfall recorded (for only a few years from 2013 to 2017) is around 322mm while during the same years, Dar el Arsa recorded 360mm and 336mm at Pont de Sebou near Karia Ba Mohamed. The average number of rainy days is 64 per year in Dar El Arsa (1976-2015) (fig. 50).

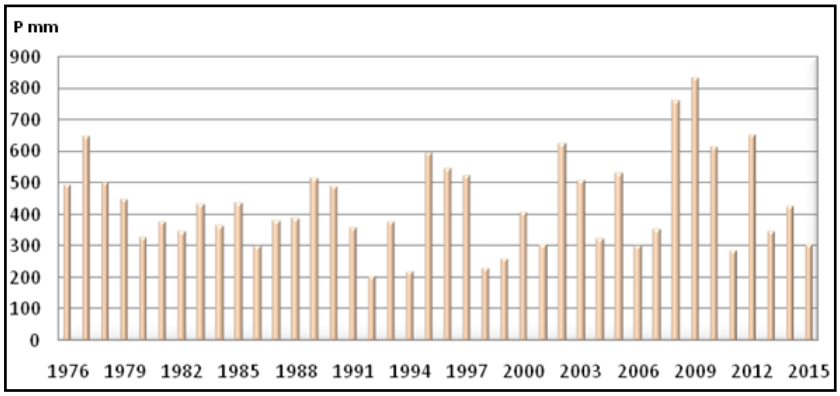

Figure 48 Annual rainfall in Dar El Arsa (1976 – 2015)

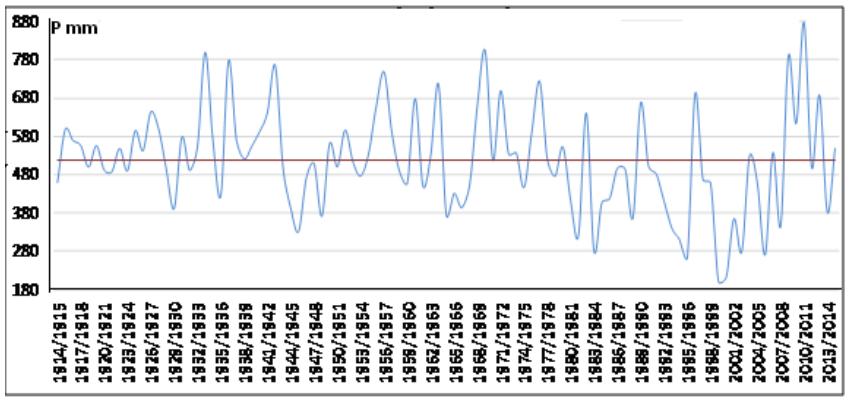

Figure 49 Variability of annual rainfall at Fez-Saïs station (1914/15-2014/15)

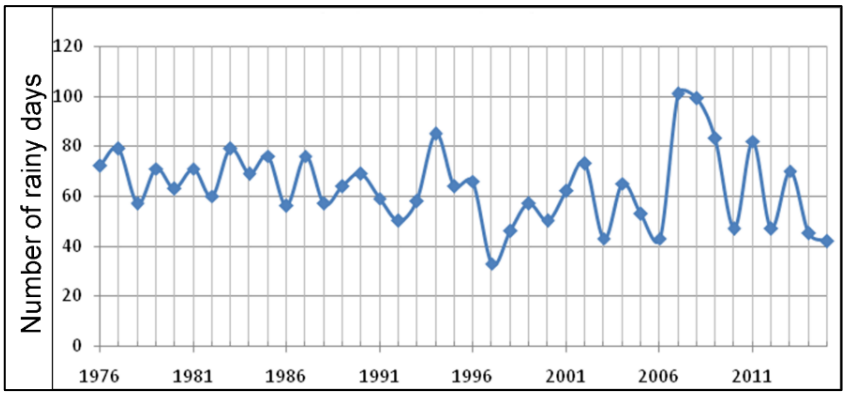

Figure 50 Number of rainy days in Dar El Arsa (1976 – 2015)

To study the spatial variability of precipitation and then calculate the layer of precipitated water in the study area, we based on a dozen stations available in the bordering areas: the Prerif, the Saïs and the middle Atlas border (fig. 51).

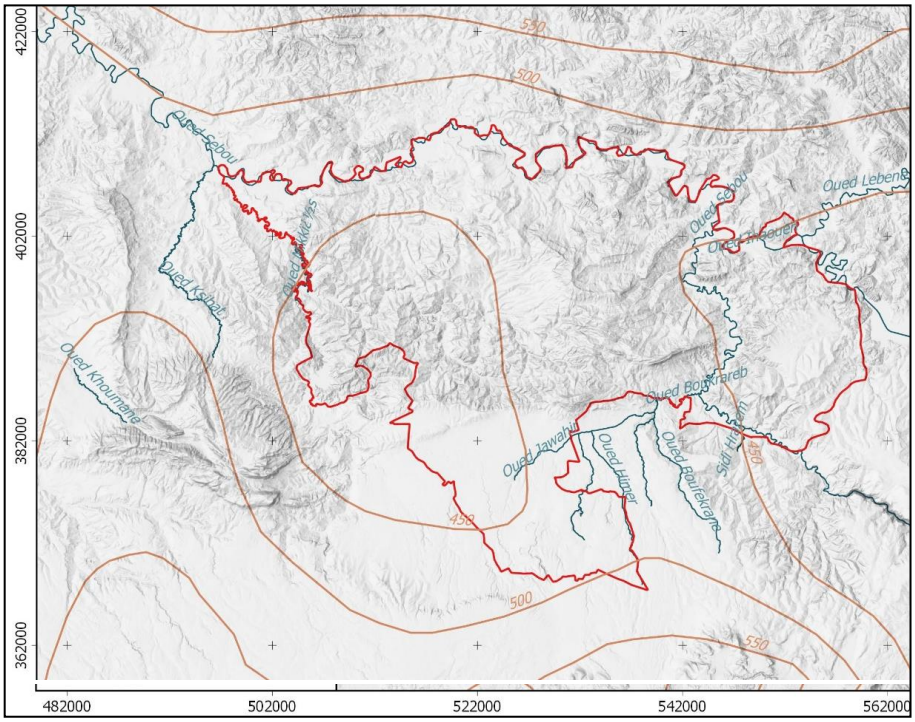

Figure 51 Isohyet map of the study area

The average precipitated water layer that can be calculated by several methods including a simple arithmetic average, the method of Thiessen polygons, the method of isohyets, etc. (fig. 51). We have chosen the last one whose formula is as follows:

$$Pmoy = \frac{\sum_{i=1}^{K} \text{Ai}.\, Pi}{A}$$

Pmoy: average rain on the watershed, with Pi= (hi+hi+1)/2; A is the total area of the watershed and Ai is the area between 2 isohyets i and i+1; k is the total number of isohyets.

The average layer of water precipitated on the watershed of the Moulay Yacoub oued is around 450mm. The spatial variability of precipitation within the territory of the Moulay Yacoub province is very low given the restricted surface and the topographic homogeneity dominated by the hilly relief without significant difference in height. Thanks to the contribution of the higher and exposed upstream part, the average layer of water precipitated on the watersheds of the Mikkes and Fez oueds is 520mm. In the study area and neighboring areas, the amount of precipitation is mainly controlled by topographic factors, in particular the altitude and the exposure of the slopes in relation to the trajectories of rainy cloudy air masses coming mainly from the Atlantic Ocean (West). The following

graph clearly shows this link via the relationship between the average annual rainfall and the altitude of the rainfall stations (fig. 52).

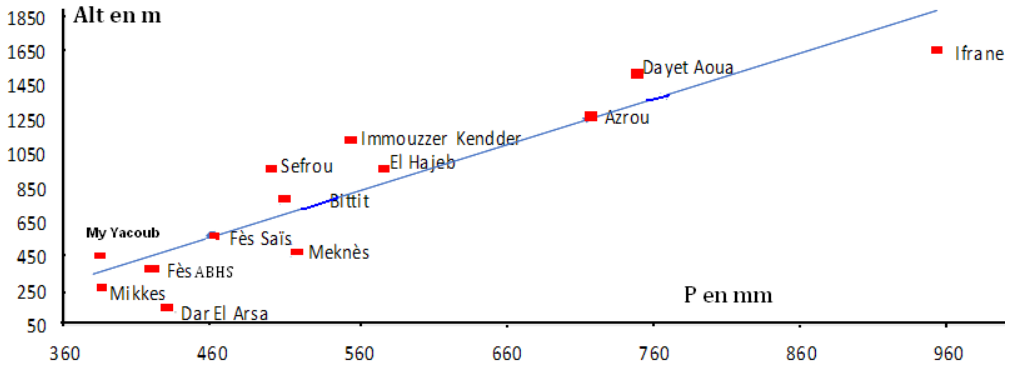

Figure 52 Relationship between average annual rainfall and the altitude of rainfall stations

Morocco is located in a transitional Mediterranean climatic zone with a more arid tendency where climatic fluctuations are frequent and their socio-economic and environmental consequences are decisive. The territory is subject to a double climatic influence, namely a relatively humid climate thanks to the rainy air masses, coming mainly from the Atlantic Ocean, which concern the North of Morocco and another desert influence covering the South of the Upper Atlas, which forms a barrier to its penetration towards the rest of Morocco. This pivotal Mediterranean climate is characterized by mild and wet winters in the North, and dry and hot summers everywhere. Yet, the interior territories like the Saïs and its pre-Rifan surroundings are penalized by a continentality accentuating the climatic austerity.

Indeed, Morocco has frequently suffered droughts periods, some of which are intense when they last for several successive years. Drought, which begins as a weather event, gradually spreads to all water-related activities. This is how we generally distinguish 5 types of droughts: meteorological, agricultural, hydrological, hydrogeological, and socio-economic. They are all linked to the consequences of a rainfall deficit.

Climatic drought is a significant decrease in rainfall compared to the normal situation during a given period. It is quickly followed by agricultural drought, which is a deficit in soil moisture that cannot meet the needs of crops in a given region. The significant decrease in precipitation leads to a hydrological drought manifested by a significant decrease in the flows of the oueds compared to the normal module of the flows calculated over a long period at a given hydrometric station. The persistence of climatic drought leads to hydrogeological drought, which is a significant drop in the level of underground reservoirs. At this stage, the spring flows begin to decrease or even dry up, and all water resources suffer a significant decline. Consequently, the water needs of the populations and their main socio-economic activities are affected. This stage of socio-economic drought necessitates the implementation of a crisis management plan that had to be prepared in advance.

These different aspects of lack of water are all originally generated by climatic drought, so the determination of the latter makes it possible to understand how moisture intervenes in slope movements in general and in landslides especially.

To determine dry and wet periods or relatively homogeneous wet or dry rainfall sequences, the CUSUM method was used (Brunet-Moret, 1971; Lettenmaier, 1976; Nejjari et al., 2001; Obda K., 1998.; Obda, 2004). It is derived from the method of simple accumulations; its formulation is written as follows:

$$CUSUM = (\sum Pi) - \bar{P}j$$

CUSUM value of rainfall is calculated for each year allows plotting the CUSUM curve for a given weather station.

$(\sum Pi)$ the cumulative rainfall for each of the years from 1 to N

$\bar{P}$: the average rainfall of the long series

j: the order of the year Pi.

The CUSUM of annual rainfall at the Fez-Saïs station 1914/15-2014/15 (the longest series in the study area) shows that the period 1914/15/1978/79 is relatively wet with an average of 545 mm (fig. 53), then the average rainfall will decrease to only 410mm during a long dry period from 1979/80 to 2007/08. Yet, a rise of this average to 590mm between 2008/09 and 2014/15 indicates a short recovery of humidity until the year in question.

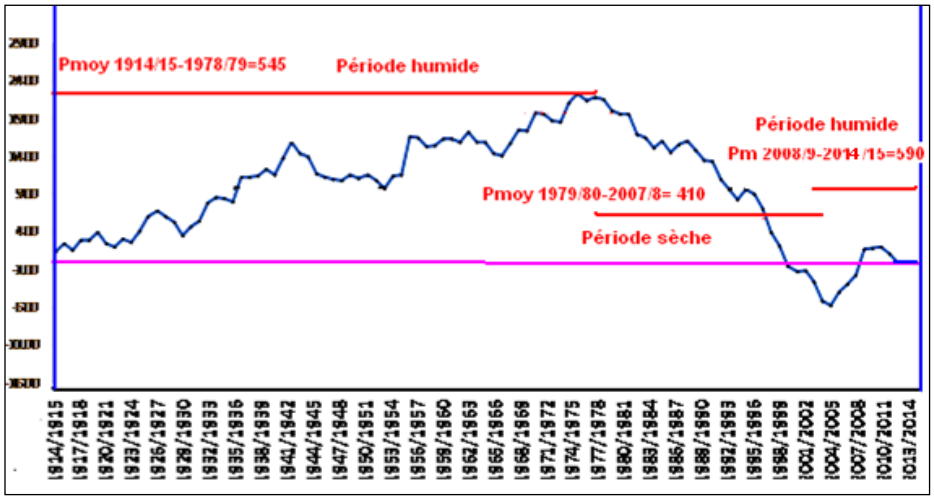

Figure 53 CUSUM of annual rainfall in Fez-Saïs 1914/15- 2014/15

a) Seasonal and monthly precipitation patterns

If the moisture of the soil in relation to its substrate is one of slope instability factors, the analysis of the seasonal and monthly precipitation regime becomes essential for understanding the dynamics of the slope movements which are linked to these regimes. The seasonal and monthly precipitation

regime (2013-2017) in Moulay Yacoub shows a seasonal rhythm of three wet seasons (winter, spring, and autumn) with a maximum in winter and a dry season in summer. This regime is analogous to neighboring rainfall stations with a long series of observations (fig. 54). This seasonal precipitation regime records its maximum in winter with more than 39% followed by spring 32% and autumn 25%. It is an uneven seasonal pattern with 370mm equivalent to almost 72% falling in only two seasons (winter and spring) while the summer season receives only 3.5% in the form of very concentrated thunderstorms in time and space (table 2).

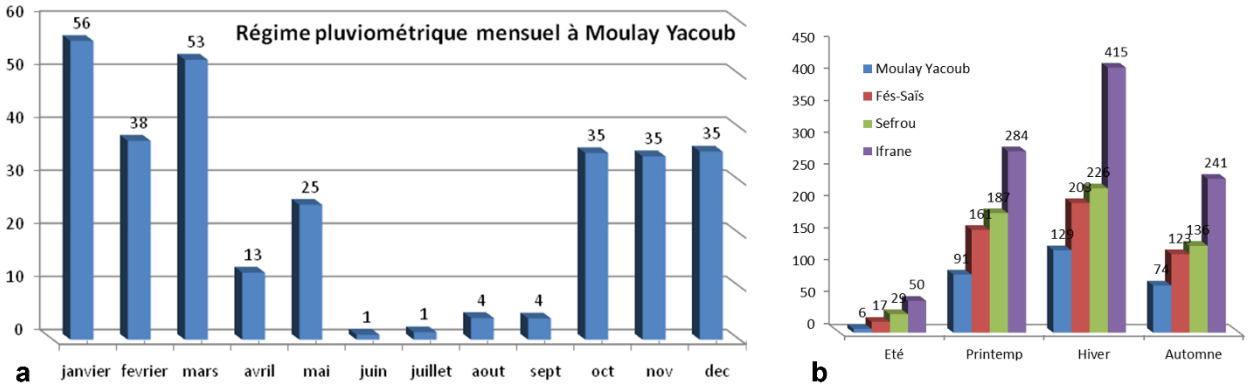

Figure 54 **a.** Average monthly P scheme in My Yacoub (2013-2017); **b.** Ifrane, Sefrou, Fès (1935-2015) and My Yacoub (2013-17)

Table 2 Monthly and Seasonal precipitation regime in Fez-Saïs (1915-2015)

Months	Dec	Jan	Feb	Mar	Apr	May	Jun	Jul	Aug	Sept	Oct	Nov	Annual
Monthly average	75.3	63.4	64.8	67.9	62	36.5	13.9	1.6	2.8	14.1	44.9	69.3	516.5
seasonal average	203.5			166.4			18.3			128.3			516.5
%	39.4			32.2			3.5			24.8			100
Seasons	Winter			Spring			Summer			Autumn			

Indeed, according to the ombrothermic diagram (fig.55), the monthly precipitation regime shows 7 wet months from October to April and 5 dry months during the hot season. As for the seasonal rainfall pattern, it peaks in winter with more than 39%, followed by 32% in spring and 25% in autumn. It is an uneven seasonal pattern with 370mm equivalent to almost 72% falling in only two seasons (winter and spring) while the summer season receives only 3.5% in the form of very concentrated thunderstorms in time and space.

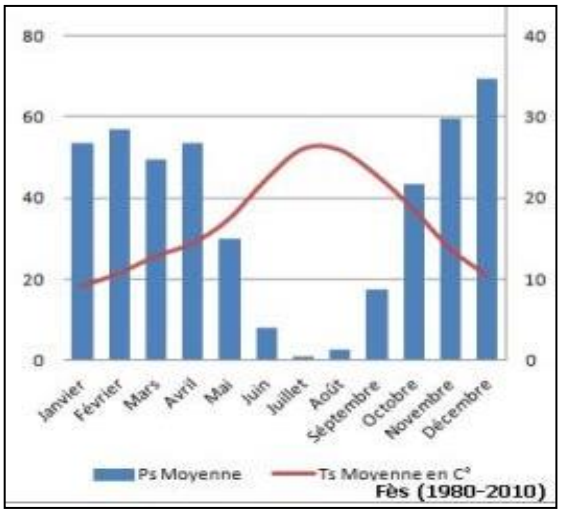

Figure 55 Ombrothermic diagram of Fez (1980-2010)

With more detail, the precipitation intensity on a daily and hourly scale shows a high concentration over time reflecting a high rainfall contrast, which is the culprit agent in soil degradation via splash effect and water erosion of the slopes. The maximum intensities recorded (on 4 tipping bucket rain gauges installed in Fez by the Hydro-sciences of Montpelier and the FST of Fez as part of a Volubilis research project) were in the period 2008 to 2020 varying between 2 and 36.6mm/h (recorded on 5/3/2018) with an average around 10mm/h (Bouizrou Ismail 2021).

The high intensity of precipitation triggers significant runoff on the slopes then a rapid swelling of the flows concentrated in the gullies and then in the ravines by widening their vertical and lateral heights on the slopes. These ravines converge, creating a dense hydrographic network that merges and grows from upstream to downstream, causing strong and violent floods affecting infrastructures along the alluvial valleys with various damage levels. These violent floods also dig and undermine the banks of ravines and oueds which triggers many slides along the hydrographic network.

The figure 56 and the table 3 show some rainfall events of high intensity and a succession of several days of rain that soak the sub soil of the slopes, and more particularly the layer of the weathered marls, especially those with high clay component. The graph also shows the antecedent humidity during the succession of several days of rain that accumulate the humidity in the sub-soil by soaking the slopes which becomes unstable. These climatic conditions increase the probability of landslides hazards occurrence especially when the stakes vulnerability is high, as in the case of the Moulay Yacoub town, and some marginalized districts in the agglomeration of Fez.

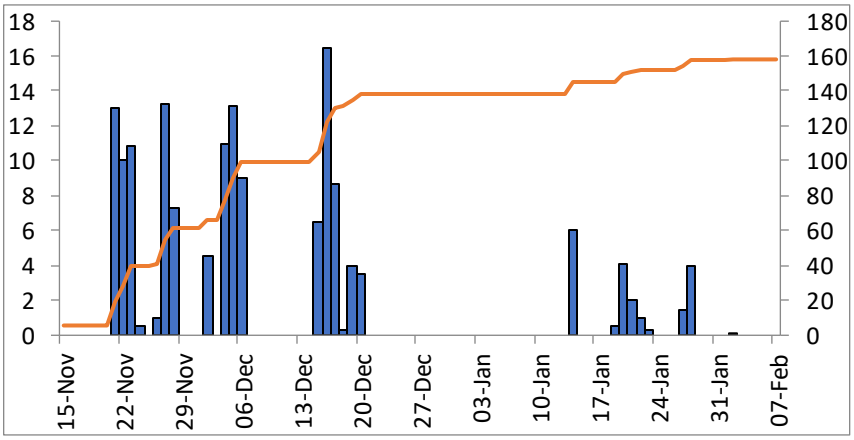

Figure 56 Daily rainfall from Nov. 15, 2016, to Feb. 7, 2017

Table 3 Daily precipitation from Nov. 15, 2016, to Feb. 2, 2017

15/11/16	0	01/12/16	0	17/12/16	8,7	02/01/17	0	18/01/17	0
16/11/16	0	02/12/16	4,5	18/12/16	0,3	03/01/17	0	19/01/17	0,5
17/11/16	0	03/12/16	0	19/12/16	4	04/01/17	0	20/01/17	4,1
18/11/16	0	04/12/16	11	20/12/16	3,5	05/01/17	0	21/01/17	2
19/11/16	0	05/12/16	13,1	21/12/16	0	06/01/17	0	22/01/17	1
20/11/16	0	06/12/16	9	22/12/16	0	07/01/17	0	23/01/17	0,3
21/11/16	13	07/12/16	0	23/12/16	0	08/01/17	0	24/01/17	0
22/11/16	10,1	08/12/16	0	24/12/16	0	09/01/17	0	25/01/17	0
23/11/16	10,8	09/12/16	0	25/12/16	0	10/01/17	0	26/01/17	0
24/11/16	0,5	10/12/16	0	26/12/16	0	11/01/17	0	27/01/17	1,5
25/11/16	0	11/12/16	0	27/12/16	0	12/01/17	0	28/01/17	4
26/11/16	1	12/12/16	0	28/12/16	0	13/01/17	0	29/01/17	0
27/11/16	13,2	13/12/16	0	29/12/16	0	14/01/17	6	30/01/17	0
28/11/16	7,3	14/12/16	0	30/12/16	0	15/01/17	0	31/01/17	0
29/11/16	0	15/12/16	6,5	31/12/16	0	16/01/17	0	01/02/17	0
30/11/16	0	16/12/16	16,5	01/01/17	0	17/01/17	0	02/02/17	0,1

Temperature levels follow an almost regular cyclical variable. The hot season begins in May and ends in October. In the Moulay Yacoub province, the average annual temperature is around 18.3°C. The average maximum temperature of the hottest month is 35°C recorded in August. Yet, the heat record at the station of Fez-Saïs reached 47°C on July 17, 2000. While the January days are the coldest during the year with the lowest monthly average, showing 8.4°C in Fez-Saïs (fig. 57).

The temperature effects are particularly involved in shrinkage and swelling during humidification and drying cycles of clays. Moreover, the succession of these humidification-drying cycles favours the evolution of the weathering in depth of the marly facies, dominating the study area, which predisposes

the weathered shallow layer to the various type of associated slope movements, namely, landslides, earthflows, and solifluctions, thus threatening agricultural land, habitat, and infrastructure (roads and other socio-economic equipment).

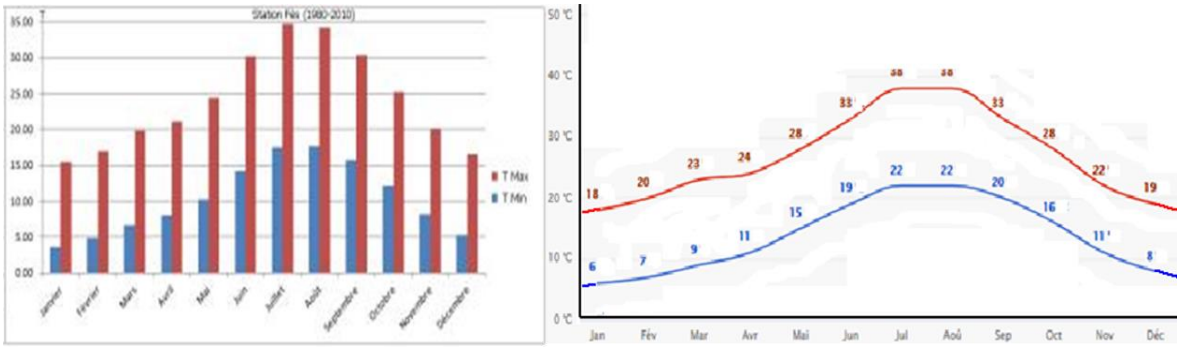

Figure 57 Maximum and minimum average temperatures in Fez-Saïs and Moulay Yacoub

b) Sunshine

The study area is dominated by completely sunny days and partly cloudy ones. The number of sunny days can exceed 300 days; it reaches more than 23 days in July and drops to less than 13 days on average in winter, especially during the months of December and January. Hence, cloudy days are very rare in summer but relatively more frequent in winter (fig. 58).

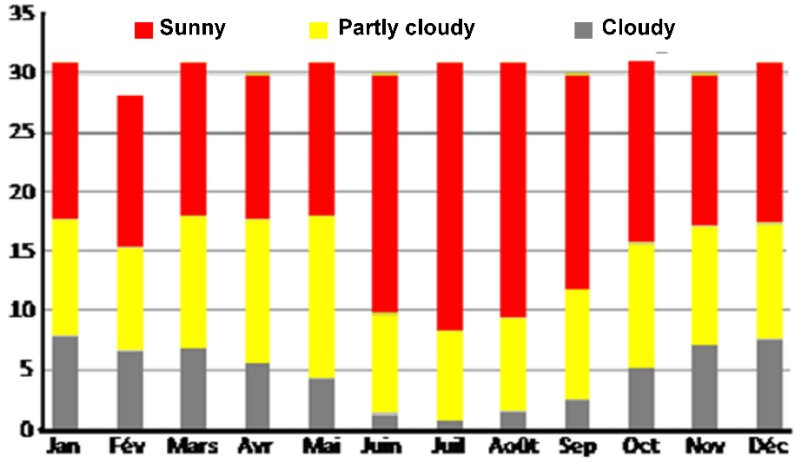

Figure 58 Distribution of the average monthly sunshine during the year in My Yacoub

B. Hydrological functioning of the study area

The study area belongs to the Sebou watershed, which is one of the most important Moroccan rivers, but on the local hydrological view. Hydrographically, it belongs to the middle part travelled by the Sebou river where its tributaries the Fez and Mikkes oueds in turn collect their tributaries (tributaries of Mikkes: Atchane, N'Ja, Ain Taoujdate, Tizguit, Mehdouma, Jdidda, Sbaa Ayoun, and tributaries of Fez oued: Chakou, El Himmer, El Mehraz, Boufekrane and El Malleh) coming from the northern borders of the Middle Atlas causse crossing the Saïs-Fez, in addition to the oueds draining the southern slopes of the Prerif (oued el Mellah and oued Moulay Yacoub). The prefecture of Fez and

the Moulay Yacoub province extend over the watersheds of the Fez, Mikkes and Moulay Yacoub Oueds, which drain the middle part of the Sebou watershed (fig. 59). The latter is spread over more than 40,000 km² where 5,560 Mm³ flows per year, equivalent to 1/3 of Morocco's surface water supply, and it supplies nearly 6 million populations spread over 17 provinces.

The Prerif marly hills, which make up most of the Moulay Yacoub province territory, are devoid of underground water resources. The only underground water resource is limited to thermal springs which are the source of the Moulay Yacoub town's reputation. Only surficial flows drained by intermittent oueds are available and flow exclusively during rainy days. Yet, the northern edges of the middle Atlas causse and the Saïs-Fez are relatively rich in water resources thanks to the large reservoirs available in the causse (water tower of Morocco), the deep Liasic aquifer of the Saïs and the Plio-Quaternary aquifers spreading over the Saïs plateau. The prefecture of Fez extends over the Saïs - Fez and the extreme southern part of the Prerif with essentially hilly and marly relief drained by intermittent oueds.

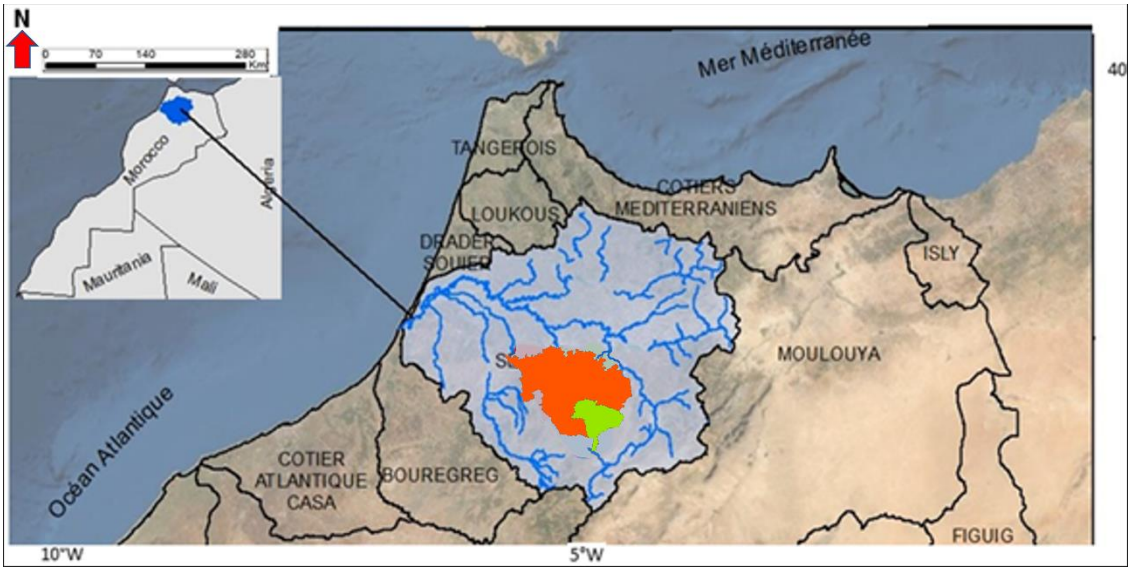

Figure 59 Location of the province of Moulay Yacoub (in red) and the prefecture of Fez (in green) in the the middle part of Sebou watershed (in grey)

a) Hydrology of Moulay Yacoub province

As for the Moulay Yacoub province, it is completely included in the Sebou watershed. At its NW limit, the lowest point of the province converges the Sebou oued with its tributary, the Mikkes oued (fig. 60). The latter constitutes the limit of the province to the west. After piercing the province in its southern part in a wide valley-oriented N-S, the Sebou changes direction after its confluence with the Inaouene oued and heads west. The boundary of the province follows the bottom of the valley to its confluence with the Mikkes oued. Thus, the entire hydrographic network system of the Moulay

Yacoub province is conditioned by the appearance of these two large valleys, Sebou and Mikkes. The entire surface of the province is drained either towards the Sebou (the north) or towards the Mikkes (south). The size of the sub-watersheds is very variable. Apart from a few (such as Al Atchane 302 km^2 which fringes a small area of the Moulay Yacoub province), the majority is a few tens of square kilometres. The northern and western boundaries of the province coincide with the Sebou Valley. Locally, the flows in the valley are conditioned by the upstream Sebou basin in its entirety.

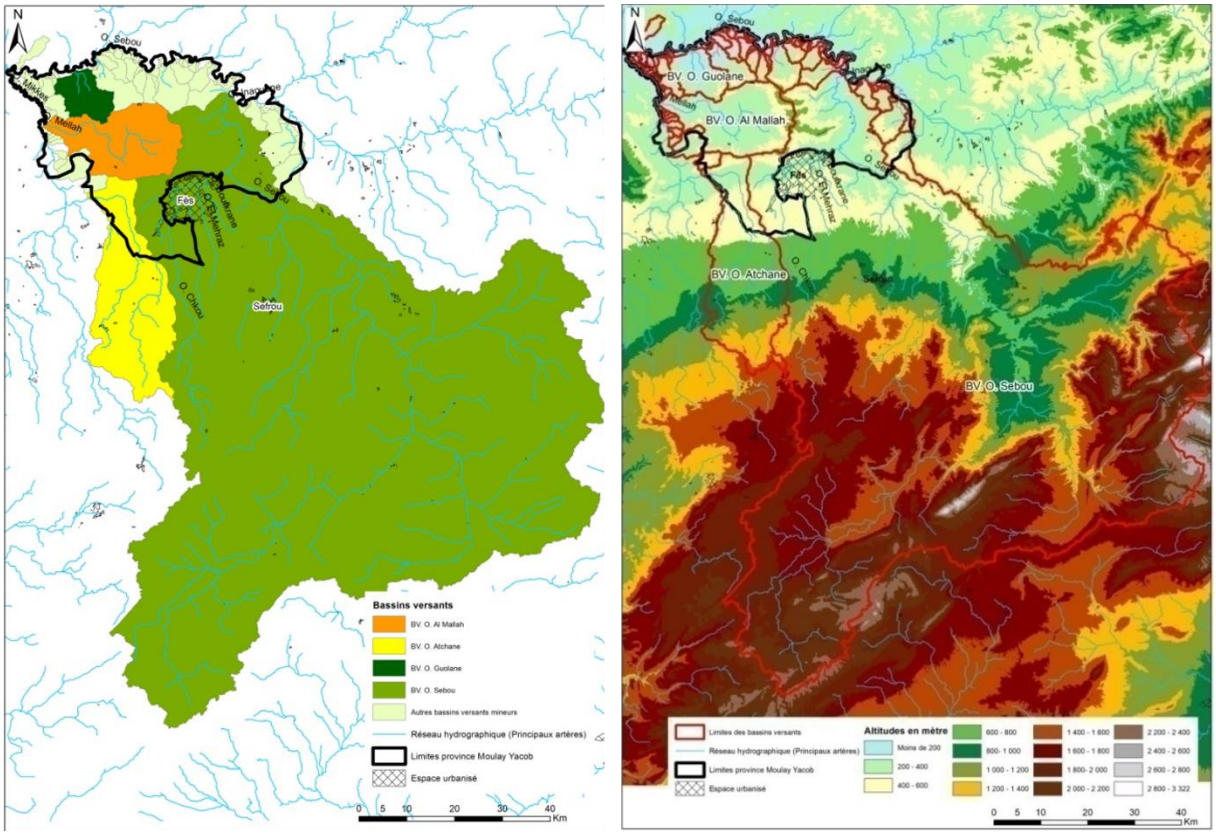

Figure 60 Watershed of the oueds crossing the province of MY and their hypsometry (on the right)

The territory of Moulay Yacoub province also extends over the watersheds of the Mikkes oued and the Fez oued which drain the borders of the middle Atlas causse and the Saïs-Fez via several tributaries (oueds tributaries of Mikkes: Atchane, N 'Ja, Ain Taoujdate, Tizguit, Mehdouma, Jdidda, Sbaa Ayoun and tributaries of Oued Fez: Chkou, El Himmer, El Mehraz, Boufekrane and El Malleh).

The geometric shape of the watershed is deduced from the GRAVELIUS compactness coefficient which is the ratio of the perimeter of the basin to that of a circle of the same area and the same perimeter. The higher the value of the coefficient and the slower the response (Table 4).

The Gravelius compactness coefficient is defined as follows:

$$\mathbf{Kc = 0,28 \,.\, \frac{P}{\sqrt{A}}}$$

Where P = perimeter of watershed (km) and A = area (km²). The following table gives the most common classification in the hydrological bibliography.

Table 4 Correspondence between the value of Kc and the type of hydrological response expected (Roche 1963; Obda 1991; Obda 2004)

Compactness coefficient	**Form**	**Response**
Kc< 1,25	Compact watershed	Rapid response
1,25<Kc< 1,5	Medium form watershed	Average response
Kc> 1,5	Elongated watershed	Slower response

As for the equivalent rectangle, which is a simple geometric transformation allowing the assimilation of the catchment area to a rectangle having the same surface and Kc by calculating its length and its width using the following formula:

$$L = \frac{C\sqrt{S}}{1,12}\left[1 + \left(\sqrt{1 - \left(\frac{1,12}{C}\right)^2}\right)\right]$$

With: S = area (km²) and C = Gravelius shape index or Kc.

The width of this rectangle (l) is obtained as follows: **l =(S/L)** With: S = the area (km²) and L = length of the equivalent rectangle.

Then the other characteristic parameters of the relief are calculated, in particular the following elevations and slopes*:*

Theoretical hight difference (Dt in m): Dt= alt max-alt min.

Useful hight difference (Du in m): Du = alt 5%-alt 95%.

Theoretical slope (Pt in m/Km): Pt = Dt/L.

L: length of the equivalent rectangle.

Useful slope (Pu in m/Km) or overall slope index (Ig in m/Km) =Du/L.

Specific elevation (Ds in m): = Pu√A = Ig√A, A is the watershed area in km².

Then, The specific hight difference (Ds) allows, according to (Dubreuil and Guiscafre 1971), to compare the reliefs of the watersheds and to classify the following relief: R1: Very low relief <10m

R2: Low relief 10<Ds<25m

R3: Fairly low relief 25<Ds<50m

R4: Moderate relief 50<Ds<100m

R5: Quite strong relief 100<Ds<250m

R6: Strong relief 250<Ds<500m

R7: Very strong relief >500m

b) Hydrology of Fez Prefecture

The prefecture of Fez is drained only by the tributaries of Sebou. The Fez oued drains almost the entire extent of the prefecture, but its watershed extends southwards to the middle Atlas causses. Another small sub-basin of the Aarous oued covers a minimal part of the surface of the Fez prefecture. Apart from these two main sub-basins, there are only small ravines developing in micro-sub-basins directly joining the Sebou oued.

(i) Morphometric characteristic of the principal oueds and their watersheds crossing the study area (tables below):

The Fez and Mikkes oueds watersheds have elongated geometric structures (fig. 61), with a shape coefficient of 1.96 for the first and 1.73 for the second indicating a slow hydrological response to rainfall events (table 5). The tributaries of Fez oued and Mikkes all have a shape coefficient around 2 except Oued El Mellah, a tributary of Fez oued and Oued N'Ja, which have a relatively compact shape (respectively 1.33; 1.38) indicating a rapid hydrological response.

The watershed elevations of the Fez oued are between 2030 m in the Middle Atlas and 190m at the outlet (confluence with Sebou oued) and the watershed of the Mikkes oued are between 2091 m and 220m at the entrance of the Sidi Echahed Dam (table 6 and fig. 62). The values of the slopes (theoretical and useful) and the differences in height of the two watersheds of the Fez and Mikkes oueds show a strong relief for the first (Ds equal to 450m) and very strong for the second with a Ds of 584m. It is a structural relief in stepped panels with uneven elevations by ruptures due to tectonics.

Table 5 Geometric shape of the Fez oued watershed and its tributaries

Oued Fez			
Watershed area (km2) =	879	Maximum altitude in m	2050
Watershed perimeter (km)=	206.5	Minimum altitude in m	191
Gravelius coefficient =	1.96		
Equivalent rectangle L =	94.74	Length of the Hydrographic Network Km	1341
Equivalent rectangle l =	9.28	Drainage density km/km2	1,53

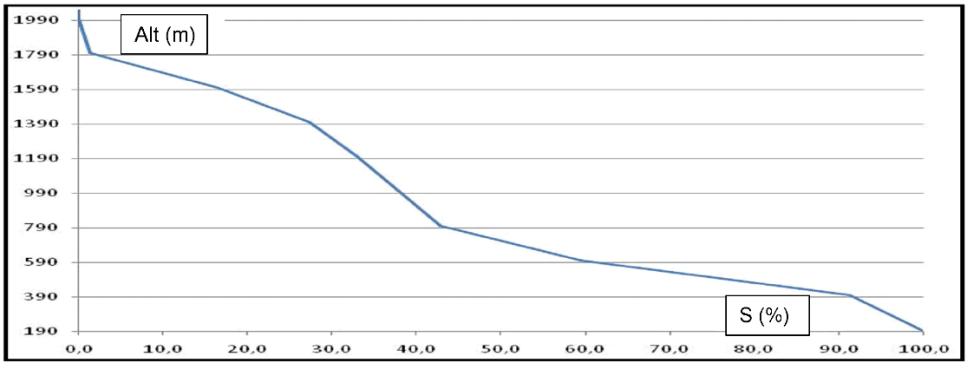

Figure 61 Hypsometric curve of the wtershed of the Fez oued and its tributaries

Table 6 Geometric shape and characteristic altitudes of the Mikkes oued and its tributaries

Geometric shape		altitudes caractéristiques	
Basin area (km2)	1514	Altitude Maxi en m	2091
Basin perimeter (km)	241	Altitude Mini en m	220
Gravelius coefficient	1,73	Altitude moyenne en m	1155
Equivalent rectangle L	106	Altitude médiane	1150
Equivalent rectangle l	14,4	Longueur du réseau Hydrographique Km	1332
Drainage density km/km2	0,88	H5%	1970
Specific height difference (Ds) in m	584	H95%	370

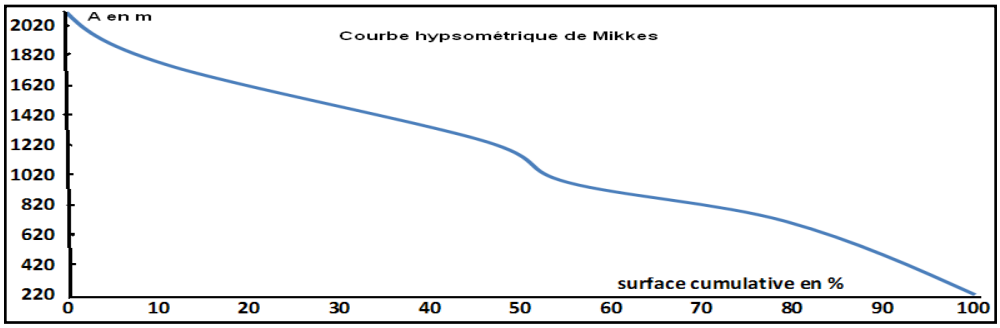

Figure 62 Hypsometric curve of the Mikkes oued watershed

(ii) Morphometry of the Moulay Yacoub oued watershed (Province de Moulay Yacoub)

The urban territory of Moulay Yacoub town is drained by the oued taking the name of the thermal spring, which watershed rises over 500m to the south of the town (fig. 63).

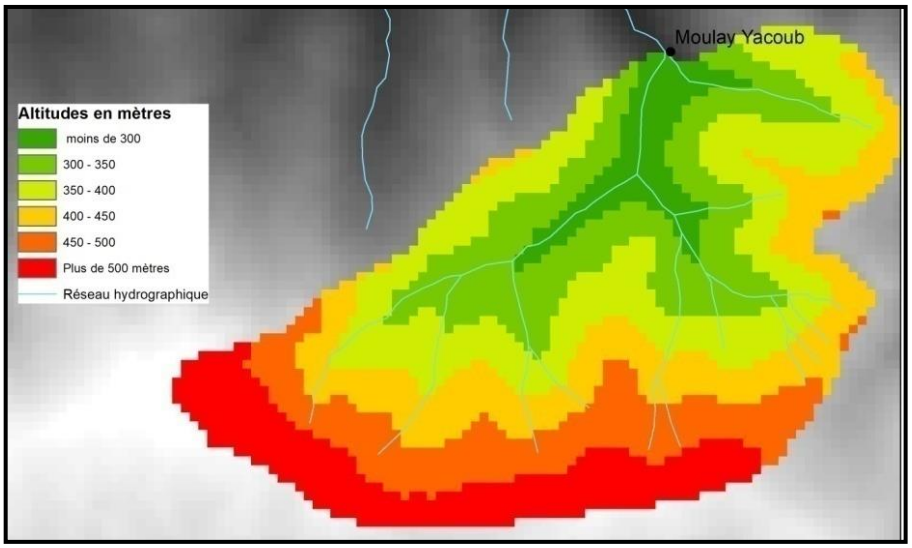

Figure 63 Hypsometry of the Moulay Yacoub watershed

The following table summarizes the morphometric characteristics of the Moulay Yacoub oued watershed.

Table 7 Geometric shape of the Moulay Yacoub oued watershed

Oued M Y at the entrance to the town of Moulay Yacoub			
Basin area (km2)	4.14	Maximum altitude in m	597
Basin perimeter (km)	8.8	Minimum altitude in m	258
Gravelius coefficient	1.22		
Equivalent rectangle L in km	3.10	Length of the hydrographic network	13,1
Equivalent rectangle l in km2/km	1.34	Drainage density	3,16

The area of the watershed overlooking the Moulay Yacoub town is only 4.14 km² and the perimeter is 8.8 km. It has a compact geometric form with a shape coefficient of 1.22 (table 7 and fig. 64). This indicates a violent and rapid hydrological response to the rainfall events even if the watershed size is very small, but the high gradient of the slopes and the impermeable marly outcrops make the oued in the form of a torrent collecting a network of ravines with a strong drainage density 3.16 km/km2. This network has a dendritic geometric shape analogous to tree branches where ravines meet forming acute angles forming V-shaped valleys crossing impermeable and relatively homogeneous outcrops in terms of water erosion resistance. Thus, the outcrops covering the Moulay Yacoub watershed are friable specially the shallow formations.

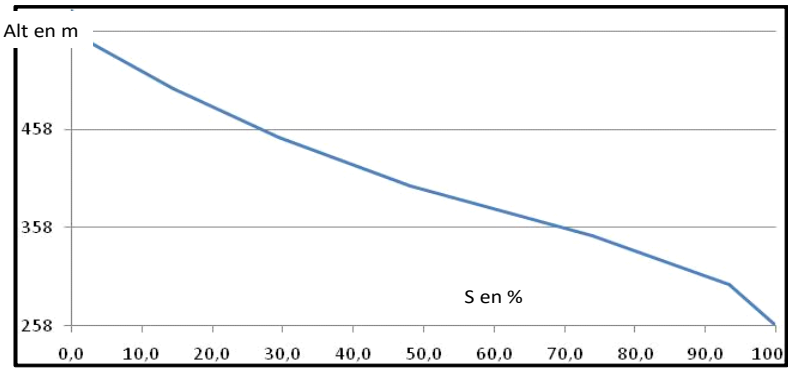

Figure 64 Hypsometric curve of the Moulay Yacoub oued watershed

The slopes values e (theoretical and useful) and watershed elevation differences of the Moulay Yacoub oued calculated above show a fairly strong relief with a specific elevation difference (Ds) of 163m. Therefore, a very short and fast response time to meteorological hazards isexpected.

c) Flow regime and hydro-systems in the study area

The hydrology of Saïs-Fez and its immediate Prerif borders attached to the Moulay Yacoub province is no longer as before. These territories are experiencing deep changes on the hydrological level. The Saïs-Fez, which is hydrologically connected to the middle Atlas causse (water tower of Morocco), remained for a very long time as an environment rich in water resources even in hot water ones thanks to the thermal springs of Sidi Harazem, Aïn Allah in addition to Moulay Yacoub situated on the immediate Prerif borders. These hydro-systems have gone from rich hydrological environments, regular and balanced by underground reservoirs via many springs to disturbed hydrological environments, threatened by extreme forms of flow such as flooding of built-up areas or water deficiency, particularly during the succession of several dry years in addition to a strong anthropogenic stress manifested mainly by overpumping (Obda et al,). As for the Prerif part of Moulay Yacoub province, it is characterized, hydrologically, by the absence of large expanses of reservoir rocks which could perpetuate and regulate the rivers flow. The oueds in this territory have an intermittent or seasonal flow regime during very rainy seasons. Thus, these oueds are in the form of deep ravines which have a violent hydrological behaviour favored by the precipitation concentration, sometimes, and the impermeability of the marly and friable soils where the solid contributions to the liquids are added, all of which amplify the fluvial dynamics of the river. The Moulay Yacoub Oued collects most of this territory. These conditions force the incision and undermining of the ravines banks which disturb slopes instability and trigger mass movements. In the field, we noticed in the tributaries of the Moulay Yacoub Oued, weak flows and seeps probably resulting from drainage of soils and surface formations. However, the profound effects of the hydrographic network are the digging and deepening of the beds and banks undermining which destabilize slopes overhanging the watercourses. It so happens that the town of Moulay Yacoub is located on one of the unstable slopes. This town is threatened by a significant number of slow landslides (Obda et al. 2022).

As for water resources, the site of the Moulay Yacoub town has the specificity of having many thermal springs welding within the Miocene formations of the south Rifan coridor. These sources have a very deep origin as evidenced by the temperature of the waters which exceeds 50°C (Barkaoui et al. 2017). This thermal spring is at the origin of the birth of the town and has made its reputation thanks to the therapeutic virtues of its waters, rich in chloride and sulphide mineralization. The city welcomes nearly one million visitors per year (Ambroggi 1995).

The average flow of the Moulay Yacoub spring is around ten l/s. This thermal spring dropped from 11.3 l/s (1993) to 9.5 l/s in 1996 (Benaabidate 2000) under the over-pumping effect and the succession of dry years since the end of the seventies (see climate component).

As for the Saïs-Fez plateau, it is the one that has undergone the most intense hydrological modification. To understand these changes, it is necessary to recall the palaeogeography of the Saïs which has influenced the current hydrology. In the terminal Pliocene, the Saïs was an endorheic basin fed by the paleo Sebou river. The extent and thickness of the lacustrine formations prove the size of this lake. In the Quaternary, neotectonics reactivates the main regional structures by causing the emersion of the lake basin, the change of the Sebou river course and consequently the conversion from an endorheic regime to an exoreic hydrological one where the Sebou evacuated waters to the east, and its tributary Oued Mikkes to the northwest, towards the Atlantic. Today, the Saïs becomes a median sub-basin of Sebou between the Middle Atlas and the Gharb (Fassi 1999; Charroud et al. 2007). But several vestiges remain witnesses of the endorheic system such as Douyet, Marja etc.

Indeed, the geographical territories of Saïs-Fez and its pre-Rif borders are dotted with rural extensions, most of which take the names of the springs near them. They are also traversed by perennial oueds taking their sources in the causse such as the oued Chakou which drains the karstic environments where the lakes meet (Dayet Hachlaf, Dayet Aoua), today threatened by disappearance due to the succession several dry years and strong anthropogenic pressure. Under the karstic, tectonic and especially anthropogenic (withdrawals) effects, these oueds are unable to reach the surface of the Fez and Mikkes oueds downstream except during periods of high water and high floods.

On the other hand, the Fez and Mikkes oueds and their tributaries can run off high flows during heavy storms even if the oueds slopes and the generally permeable terrain strongly dampen surface runoff. But there are very wet years which cause the rise of the nearby water table in some places such as in the Marja district (swamp) northwest of Fez-Saïs flooded for several days due to the overflow of the Fez oued and the rising of the water table (Fig. 65).

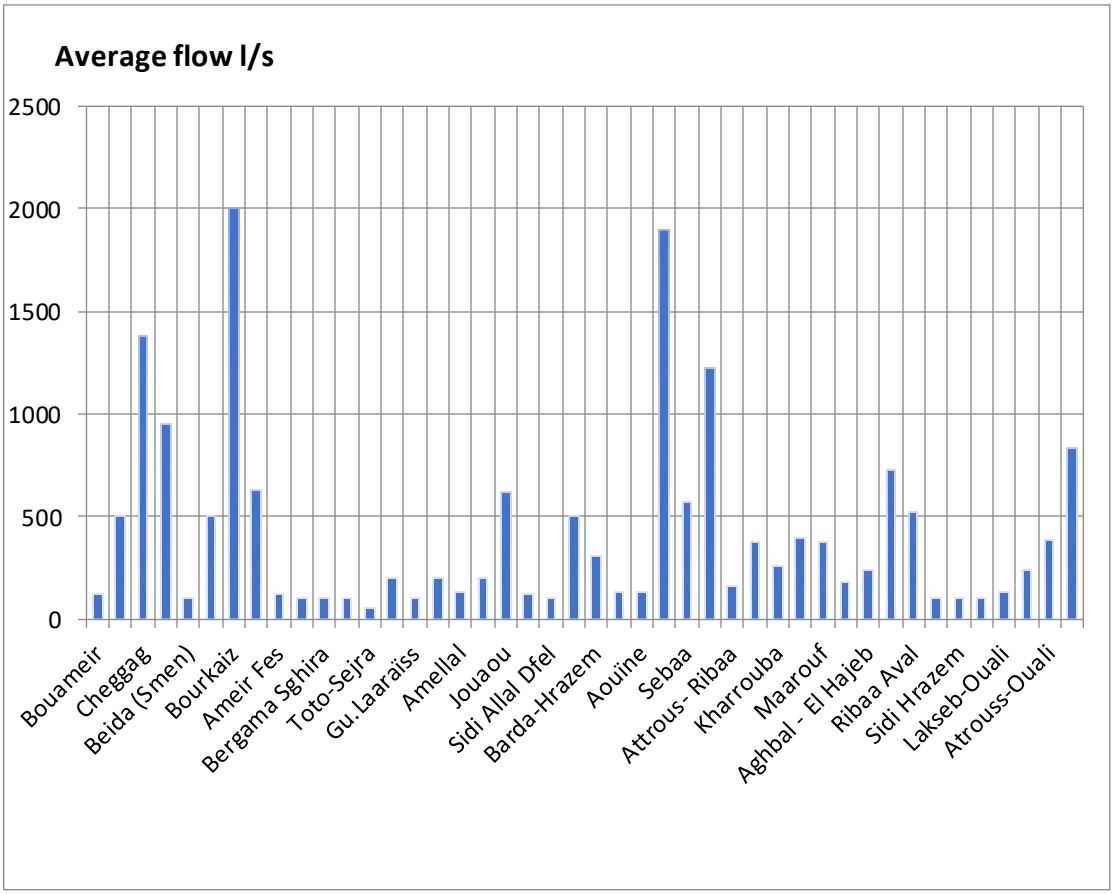

Figure 65 Wealth in water resources: main sources of Saïs-Fez (Obda k. Et al. 2004)

C. Conclusion

This hydroclimatic context of the study area shows a favorable environment to hydro geomorphological hazards which proliferate natural risks where human and socio-economic issues are important. The major bed of the Moulay Yacoub oued is nibbled by the city extension which has become threatened by flooding. The marly slopes, undermined at the base by the oueds and active gullies, ploughed each season, terraced and occupied by vulnerable habitats constitute conditions conducive to landslides and to swelling /shrinkage of the sub-soil. Certain outlying districts in the north of Fez located on the marly slopes or on the old embankments are also threatened by these phenomena.

On the other hand, the floods affecting the city of Fez are not violent but slow, they are often generated by the rise of the water table very close to the surface for the western part of Fez (Hay Lalla Soukayna, al Marja) except the eastern and northern part where the Boufkrane, Mehrez and El Mellah oueds are causing damages. We must also not forget that Saïs-Fez was endorheic and that the current Dayets and Marjas such as Douyet and Marja are the vestiges of this endorheism which began to become exoreic late on the geomorphological level, but it remains unfinished to this day. The major

problem remains the anthropization of riverbanks, poorly designed facilities, and poor urban management.

As for the rest of the oueds crossing the Moulay Yacoub town baying violent floods caused by intense storms, typical of the Mediterranean rim climate, the solutions of the biological developments (reforestation) and especially mechanical (thresholds and dikes) and technical (hill dams of bottom valve to evacuate a flow equivalent to the capacity of the section crossing the city) are easy and bearable by the means of the territorial municipalities. The warning systems are inoperative for the town of Moulay Yacoub given the very short duration of the flow concentration time.

To sum up, the hydroclimatic conditions of the Fez-Moulay Yacoub territory are strongly involved in the predisposition of terrains to slope movements and to the phenomenon of swelling-shrinkage which also causes significant damage to buildings even on flat topography. Indeed, the succession of dry and wet periods causes the alteration of the surface layer (a phenomenon to be detailed later); the latter evolves in depth and forms an altered mantle prone to landslides and shallow movements such as solifluctions and earthflows. Moreover, field visits show that bank undermining by oueds and active gullies is responsible for the triggering of numerous landslides in the study area, knowing that the soil impermeability promotes surface runoff shaping the hilly landscape of the study area. Furthermore, the stormy rain events typical of the Mediterranean climate are considered a triggering factor for slope movements and can also accelerate already active ones.

According to several authors, the inter-annual variability of winter precipitation over the Mediterranean basin is largely modulated by the mode of the North Atlantic Oscillation in southwestern Iberia (Hurrell 1995; Qian et al. 2000; Trigo et al. 2004) which is a weather phenomenon over the North Atlantic Ocean of fluctuations in the difference of atmospheric pressure at sea level (SLP) between the Icelandic Low and the Azores High. Consequently, this phenomenon has a considerable impact on the climate of the northwest of Morocco, and which controls the phenomena of succession of dry and wet periods as well as stormy rain events. The NAO was discovered through several studies in the late 19th and early 20th centuries, and it is one of the most important manifestations of climate fluctuations in the North Atlantic and surrounding humid climates. Moreover, recent studies have correlated this climatic phenomenon and the triggering of various types of slope movements (Trigo et al. 2005; Zêzere et al. 2005; Zêzere and Trigo 2011). The results state that the landslide activity is related to both intense, short duration precipitation events (1–15 days) and long-lasting rainfall episodes (1–3 months). The former events trigger shallow movements while the later episodes are usually associated with deeper and larger slope movements. This explains the abundance of shallow slope moves in the Fez-Moulay Yacoub territory.

IV. Chapter 2 Geotechnical settings, vulnerability, and stacks

1. Introduction

In landslide studies, several parameters must be taken into consideration, most of which have been studied in the previous chapter in the frame of the regional context of the study area. However, apart from the geomorphological, climatic, and hydrological contexts, other physical and qualitative parameters are also key data to characterize the landslide risk.

In this chapter, an investigation of the geotechnical properties of the main formations of the study area is carried out in order to study the veracity of these formations towards the gravitational processes and to the risk of shrink-swelling. Then, a soscio-economical inventory is realized to evaluate the vulnerability of the stakes prone to the risks evoked previously.

2. Geotechnical characteristics

In the study area, two distinctly different groups of geotechnical materials can be distinguished, hard and compact rocks and loose materials. The group of hard rocks includes compact shales, dolomites, sandstone, gypsum and schistose pelites (table 8), while the second includes several encountered marly facies, Triassic clays, mainly clayey colluvium and pelites (Table 9). Regarding the geotechnical laboratory tests, the density and the mechanical resistance were determined rocky materials. On the other hand, an identification and mechanical testing program was carried out for the variety of soft rocks sampled in the study area, knowing that this class dominates and is the most prone to landslides in the geo-morpho-dynamic context implied by the region. Table 8 and 9 presents the geotechnical characteristics of the different formations, making it possible to extrapolate these values for indicative purpose only and not systematically, to the entire area studied. They should, therefore, be considered as representative values of the geological formations encountered and not of a particular site.

Table 8 Geotechnical properties of hard/compact rocks

Lithology	*Density*	*Mechanical resistance (Mpa)*
Compact calcareous marls	1.7-2.2	0.7-2.3
Pelitic shales	1.81-1.93	5.9-11.8
Gypsum rock	1.64-1.72	3.1-6.5
Limestone	2.1-2.4	26.4-62
Alternation limestone	2-2.24	12-15.4
Dolomite	2.3-2.6	41.3-72.2
Sandstone	1.9-2.12	14.3-19.5

For the hard rocks, the higher mechanical resistance values were recorded for dolomites and massif limestone followed by sandstone samples. However, limestone from alternated marly formations displays lower mechanical resistance. In addition, the hard pelitic shales show mediocre resistance values while the lowest mechanical resistance was recorded for gypsum rocks and compact calcareous marls. As for the soft rocks, in addition to gypsum clays, saliferous clays, clayey colluvium and pelites, four marly formations were distinguished based on their stratigraphic affiliation, which seems to differentiate them in terms of colour shade. Furthermore, each of these marly formations exhibits specific geotechnical properties (Table 9), notably for the yellow and the grey marls which need to be individualized even though they belong to the same stratigraphical stage. Their predisposition to landslides is therefore uneven.

After a cross comparison between the soft formations in terms of liquidity limit and plasticity index and according to the Casagrande's abacus for fine soils classification (fig. 66), the Eocene flinty marls and the clayey colluvium show highly plastic soils while the other formations display moderate plasticity, except for grey Tortonian marls which show low plasticity values for most samples. The absorption capacity deduced from the VBS values, and which characterizes the sensitivity to water and, hence, the clay content shows that most of the samples contain clayey soils ($2.5 < VBS < 6$, G.T.R classification) except for Eocene marls, Yellow Tortonian marls and clayey colluvium which contain strongly clayey soils ($VBS \geq 8$). As for the calcium carbonate content, the Triassic saliferous and gypsum clays are noted as non-carbonate soils while pelites, clayey colluvium, yellow marls and Eocene marls show low to moderate carbonate values. On the other hand, the highest contents are recorded for the calcareous marls and the grey Tortonian marls. These values seem to, directly, affect the apparent cohesion obtained by the drained consolidated shear test and which afford to these highly carbonated soils a cohesion no less than 25 Mpa. The other samples show week apparent cohesion except for the pelites whose certain samples presented a cohesion close to that of carbonate soils.

Table 9 Geotechnical properties of soft formations

	Identification tests					**Mechanical tests**			
Soft rocks	*Density*	*VBS*	*WL*	*IP*	*%CaCO3*	*Cc*	*Cs*	*c'*	*Φ'*
-Flinty Eocene marls	1.7	8	62	39	42	0.5	0.08	14	18
-White calcareous marls	1.8	5	35	22	59	0.29	0.04	25	10
-Yellow Tortonian marls	1.6-2.1	5-9	40-49	26-35	42-54	0.32-0.5	0.05-0.17	3-21	17-29
-Grey Tortonian marls	1.8-2.4	3-5	29-37	16-25	63-75	0.1-0.3	0.02-0.04	25-37	4-8
-Gypseous clays	2.2	3	46	22	10	0.2	0.01	23	9
-Saliferous clays	1.65	6	36	27	0	0.7	0.06	14	13
-Clayey colluvium	1.7-1.87	7-11	48-62	32-45	15-53	0.34-0.4	0.07-0.15	12	25
-Pelites	1.84-1.9	2.3-6	33-41	21-27	26-37	0.4-0.6	0.04-0.18	7-28	5-14

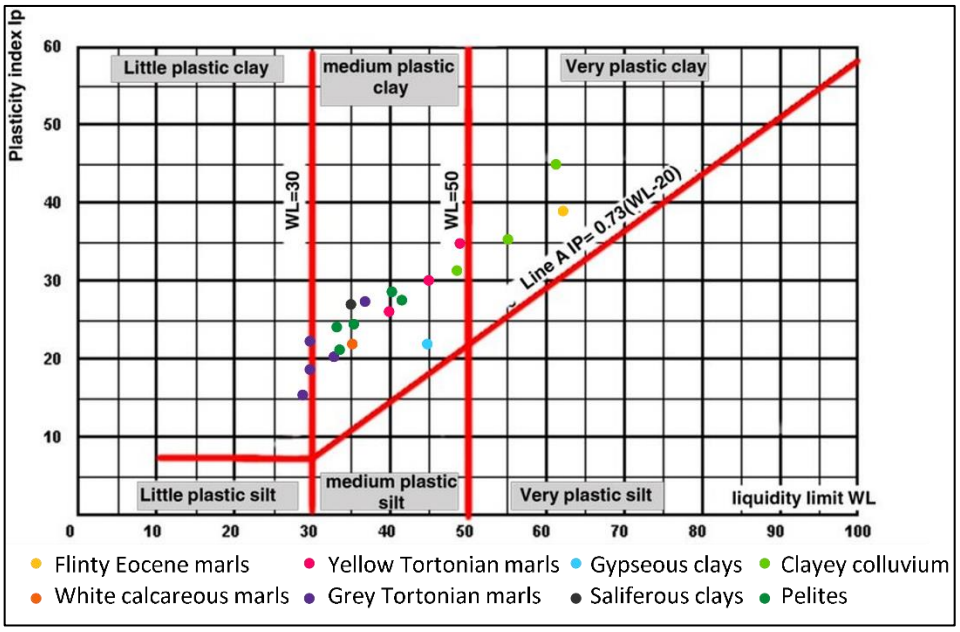

Figure 66 Presentation of fine samples in the Casagrande Abaqus

Furthermore, according to the international classification of laboratory soil testing (ASTM Committee D-18 on Soil and Rock 2010), the results of compression and swelling obtained from oedometer testing curves show high to extremely high swelling potential for pelites and extremely high for the Eocene marls, yellow Tortonian marls and clayey colluvium while white calcareous marls, saliferous clays and grey Tortonian marls indicate moderate to high swelling capacity. The low swelling potential was obtained for gypseous clays. As for settling tendencies, pelites, saliferous clays and Eocene marls show very high to extremely high compressibility while Yellow Tortonian marls and clayey colluvium display very high compressibility levels. The white calcareous marls indicate high settling capacity while the rest of soft formations (grey Tortonian marls and gypseous clays) indicate moderate trends.

3. Socio-economic context, vulnerability, and stakes in the study area

The analysis of the socioeconomic context makes it possible to extract and understand the vulnerability and the stakes of the study area. Natural hazards are when intense natural phenomena interact with human and threaten his activities (Tobin and Montz 1997; Alcántara-Ayala 2002). When addressing the potential losses related to one hazardous event or in other terms, the vulnerability related to one hazardous event, the risk definition appears as the combination of the probability of an event and its negative consequences (UNISDR 2009), that was classically written as the risk equation (e.g. Dauphiné & Provitolo, 2001; Wisner et al., 2012 among others):

$R = H \times V$

where R= risk, H= hazard, and V=vulnerability.

Risk: combination of hazard and vulnerability.

Hazard: Probability of occurrence of a phenomenon and its intensity

The vulnerability of the prefecture of Fez and the province of Moulay Yacoub requires the analysis of their socio-economic context in order to assess the degree of the stakes. It is clear that the choice of the sites of the two cities is related to the physical conditions, which are primarily the richness in thermal springs for Moulay Yacoub and for Fez as well located not far from Moulay Yacoub and Sidi Hrazem. There are also surface water resources (the Fez oued and its tributaries, the Sebou, the Dayets) and the abundance of springs from underground reservoirs (see chapter on hydrology). Given also the continentality and the strong heat in summer, the chosen core site (the Medina) corresponds to the shaded side exposed to the North taking advantage less of the duration of exposure to the sun. It is an inclined slope with an average slope that enables water supply and wastewater treatment under gravity action. The hydraulic energy of these waters is used in water mills or all kinds of artisanal applications such as the hydraulic clock in the Medina of Fez. But the rapid and often anarchic urban development of the two cities (Fez and Moulay Yacoub) and their satellite villages is at the origin of the amplification of vulnerability that has been in the past very negligible, but today, it takes on a worrying and threatening dimension that leads the public authorities to rethink urban management and spatial planning.

Today, Morocco has become aware of the threat of the risks generated by floods and slope movements, especially landslides. This awareness reflects the perception of this risk (a prerequisite for solving the problem) which leads to a change in the attitude of the population and the public authorities. Indeed, land use managers and planners have so far lacked a reliable legal and legislative tools and valid cartographic documents to consider these risks in urban management and land planning. The Urbanization Suitability Map (CAU) is a basic tool in the risk management strategy.

A. Vulnerability and stakes at Moulay Yacoub scale

According to the results of the general census of population and housing RGPH, of 2014, the population of the Moulay Yacoub province extents to 174,079 inhabitants, against 150,422 inhabitants in 2004, equivalent to 4% of the population of the Fez-Meknes region and 0.5% of the national population (Table 10). The population of the province shows an average annual growth rate of 1.47% between 2004 and 2014; but the increase in the urban population is registering a very strong growth compared to the rural one (Table 11). The numbers in the following tables are explanatory of the human phenomena amplifying the vulnerability of the Moulay Yacoub town and most of villages of the province.

Table 10 Population of the Moulay Yacoub province by residence type and average annual growth rate

Type	Pop[1] 2004	Pop 2014	TAAM[2] (%)
Urban	3 153	25 075	23.04
Rural	147 269	149 004	0.12
Total of the province	150 422	174 079	1.47

Source : RGPH 2014, 1: Population, 2- TAAM : Average annual growth rate.

Table 11 Population of the Moulay Yacoub province according to the 2014 RGPH

Area surveyed	Pop Urban	Pop Rural	Total
Province of Moulay Yacoub	25 075	149 004	174 079
Fez-Meknès Region	2 549 791	1 667 166	4 216 957
Morocco	20 432 439	13 415 803	33 848 242
Prefecture /Region	1.0%	8.9%	4.1%
Prefecture / Morocco	0.1%	1.1%	0.5%

Source : RGPH 2014

Thus, the population of the study area, which was 174,079 inhabitants in 2014, reaches 180,746 inhabitants in 2020 and may reach 227,021 inhabitants in 2050 according to the extrapolation of demographic evolution (Table 12).

Table 12 Demographic evolution by 2050

Distribution of population	Population 2014	Population 2020	Population 2050
Urban	25 075	30 114	70 485
Rural	149 004	150 632	156 536
Total population	174 079	180 746	227 021

The populations of province communes have experienced various levels of demographic growth. Indeed, with negative growth rates, the rural communes Mikkes, Sidi Daoud and Oulad Mimoun saw their population decline between 2004 and 2014. While the municipality of Moulay Yacoub, Ain Chkef and other communes such as, Sebt Loudaya, Sebaâ Rouadi, Ain Bou Ali, Ain Kansra, Laâjajra and Louadaine recorded growth rates (table 13 and fig. 67). In addition to the Moulay Yacoub town population, there are visitors who approach an average of one million annually equivalent to 2750 visitors per day. Before 2008, the town was spread over an area of 305 Ha, today its area exceeds 555 ha.

The strong increase in the population and the chaotic extension of the town with a type of generally substandard housing built on unstable sites on the geomorphological and geotechnical level strongly

amplify the vulnerability which, in turn, increases the risk. Indeed, the roads leading to the city, the streets, the drinking water supply, sanitation networks and the buildings are frequently damaged (cracks, slopes, settlements, partial or total collapse) and even collapse after long or intense rainfall events that accelerate the slides displacement velocities. Maintenance and repair works are almost permanent in the areas in question and the townspeople live each day with a high degree of risk.

Table 13 Legal population by communes in 2004 and 2014

Cercle	**Caïdat**	**Municipality / Commune**	**Pop 2004**	**Pop 2014**	**TAAM (%)**
Moulay Yacoub (Mun.)			3 153	4 612	3.88
Moulay Yacoub	Ain Chkef	Ain Chkef	36 368	54 477	4.12
		Centre : Ras El Mae		20 463	-
	Mikkes	Mikkes	6 773	6 089	-1.06
		SebtLoudaya	12 232	12 423	0.16
	SebaâRouadi	SebaâRouadi	20 695	23 519	1.29
Oulad Jemâa Lemta	Ain Bou Ali	Ain Bou Ali	12 269	12 282	0.01
	Ain Kansra	Ain Kansra	11 534	12 291	0.64
	Laâjajra	Laâjajra	13 931	14 476	0.38
		Sidi Daoud	12 791	12 771	-0.02
	Oulad Mimoun	Louadaine	11 283	11 767	0.42
		Oulad Mimoun	9 393	9 372	-0.02
Total de la province de Moulay Yacoub			150 422	174 079	1.47

Source : (RGPH 2004, 2014)

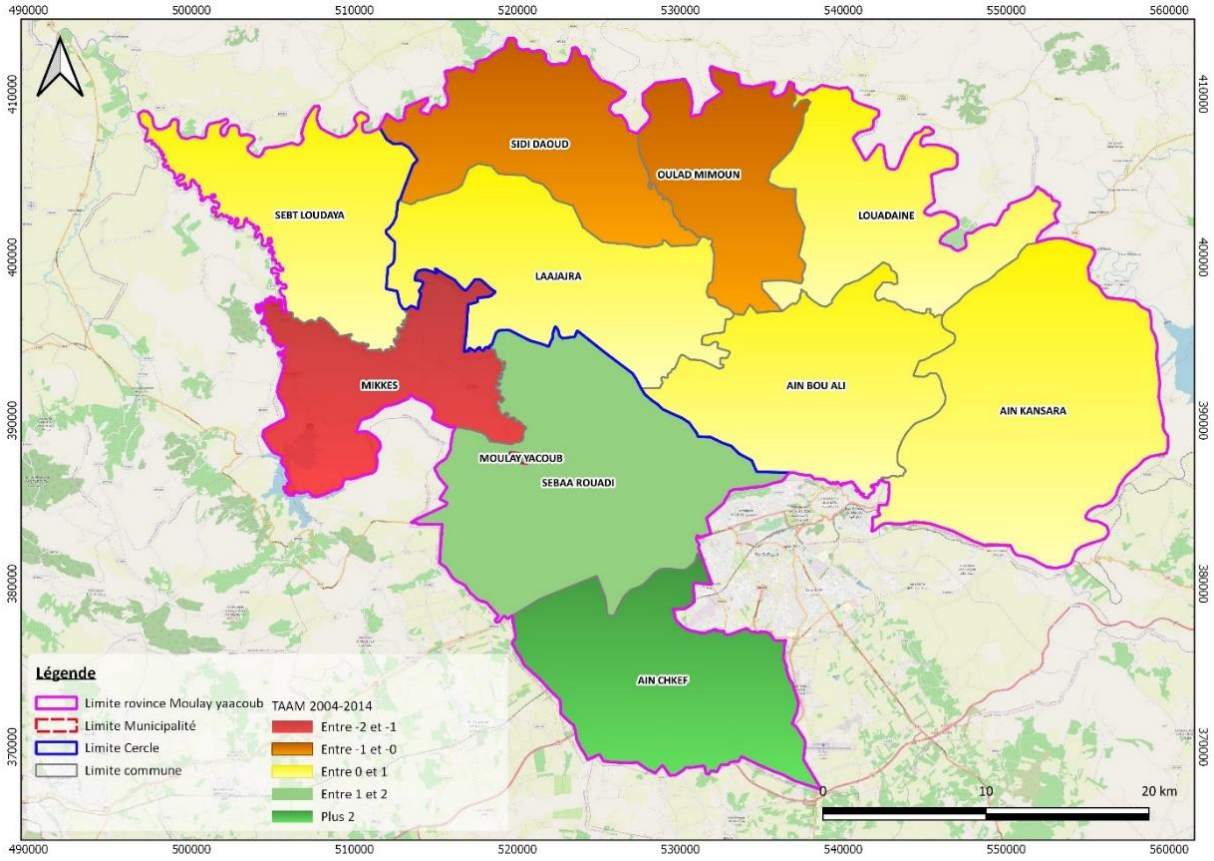

Figure 67 Population growth rate (in %) of the Moulay Yacoub province between 2004 and 2014

B. Vulnerability and stakes in the prefecture of Fez

The birth of Fez city goes back to twelve centuries, since it underwent mutations and variable changes under the authority of the powerful Moroccan dynasties (Idrissids, Almoravids and the Merinids until the last current dynasty the Alaouites (fig. 68) along these 12 centuries when Fez was, for a very long time, the imperial capital of Morocco. Today, Fez is an agglomeration extending over more than 100km² for a population of more than one million inhabitants. (1.15 million 2014). The Fez agglomeration has undergone, during the last decades, a strong demographic evolution due to the natural demographic growth and the massive rural exodus in particular during the acute droughts of the eighties and nineties that led to an uncontrolled urbanization (table 14 and fig. 69). Its population has evolved from 100,000 in 1912 to 1.15 million in 2014.

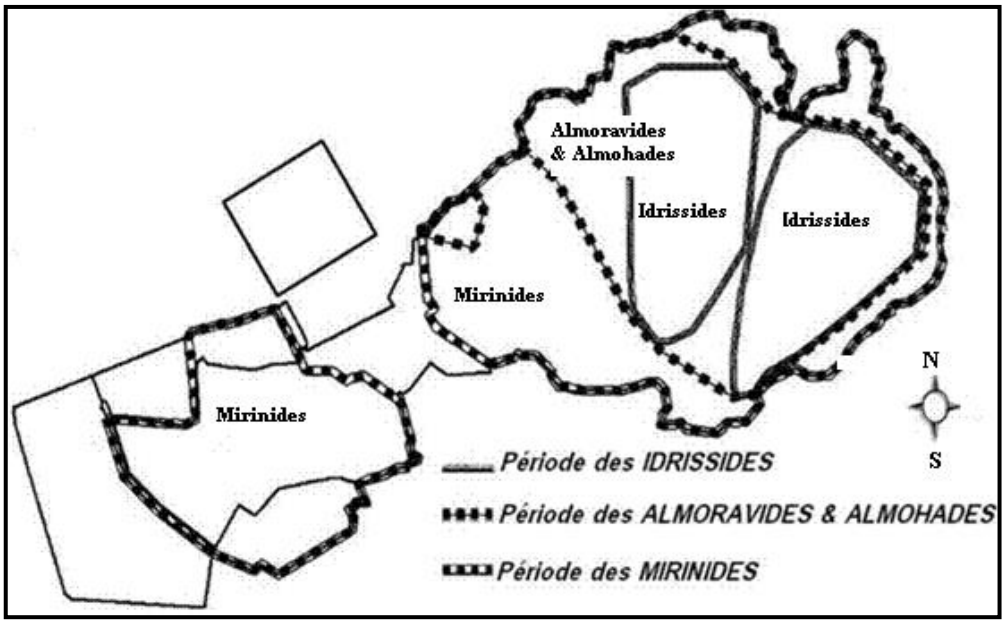

Figure 68 Historical map of the Fez Medina (Ader, FEZ)

Table 14 Evolution of the population of the city of Fez between 1912 and 2014 (RGPH, 2014)

Year	Population
1912	100000
1960	220000
1971	321500
1982	484654
1994	796200
2004	977949
2010	1079000
2014	1139000

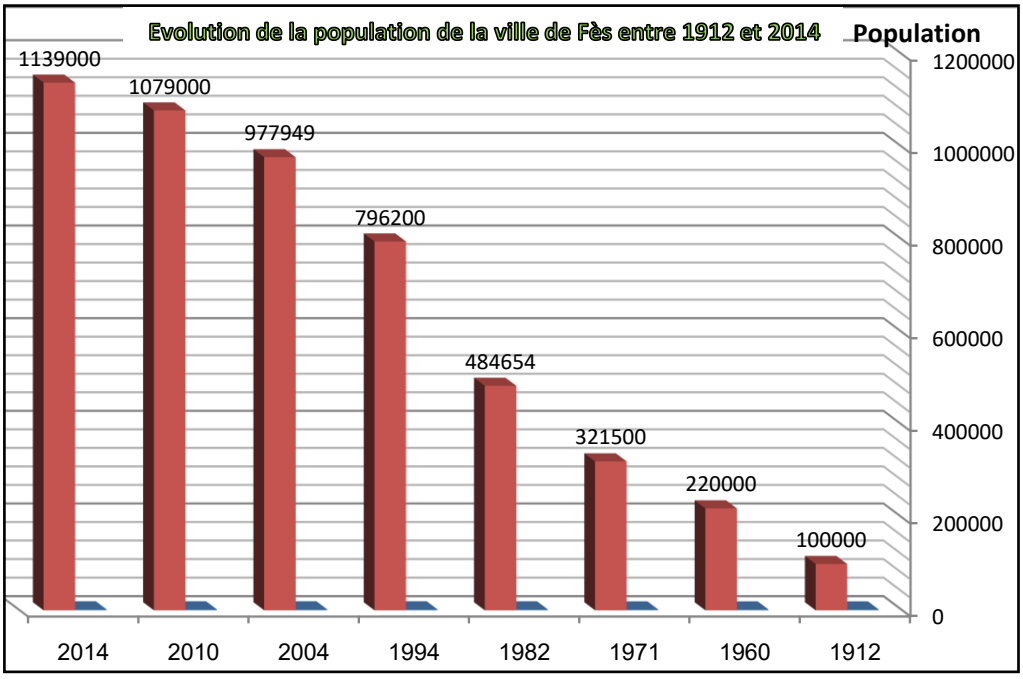

Figure 69 Evolution of the population of the Fez city between 1912 and 2014 (RGPH, 2014)

This strong population growth is accompanied by an extraordinary demand for housing, in particular socio-economic housing in the peripheral perimeter of the city, in addition to the increase in weight and the overloading of old urban units such as the Fez Medina, which has suffered from the density of socio-economic activities and population often of rural origin. For example, the number of households in the districts of Zouagha and Saïss has doubled in ten years (1994 to 2004) (Fig. 70). This phenomenon of disproportionate urbanization has generated substandard habitats condensed in high-risk urban areas threatening ruin at the level of the Medina. The latter also suffers from dilapidated buildings and the degraded old water supply and sanitation networks whose water leaks under the buildings promoting the vulnerability. The anarchic form of urbanization has resulted in the multiplication of habitats and socio-economic infrastructures that do not meet the standards of legal construction or urbanizable land or the choice of sites. The follow-up and the final consequences are the strong aggravation of vulnerability and exposure to the so-called natural risks, and man remains, almost in all cases, the main culprit.

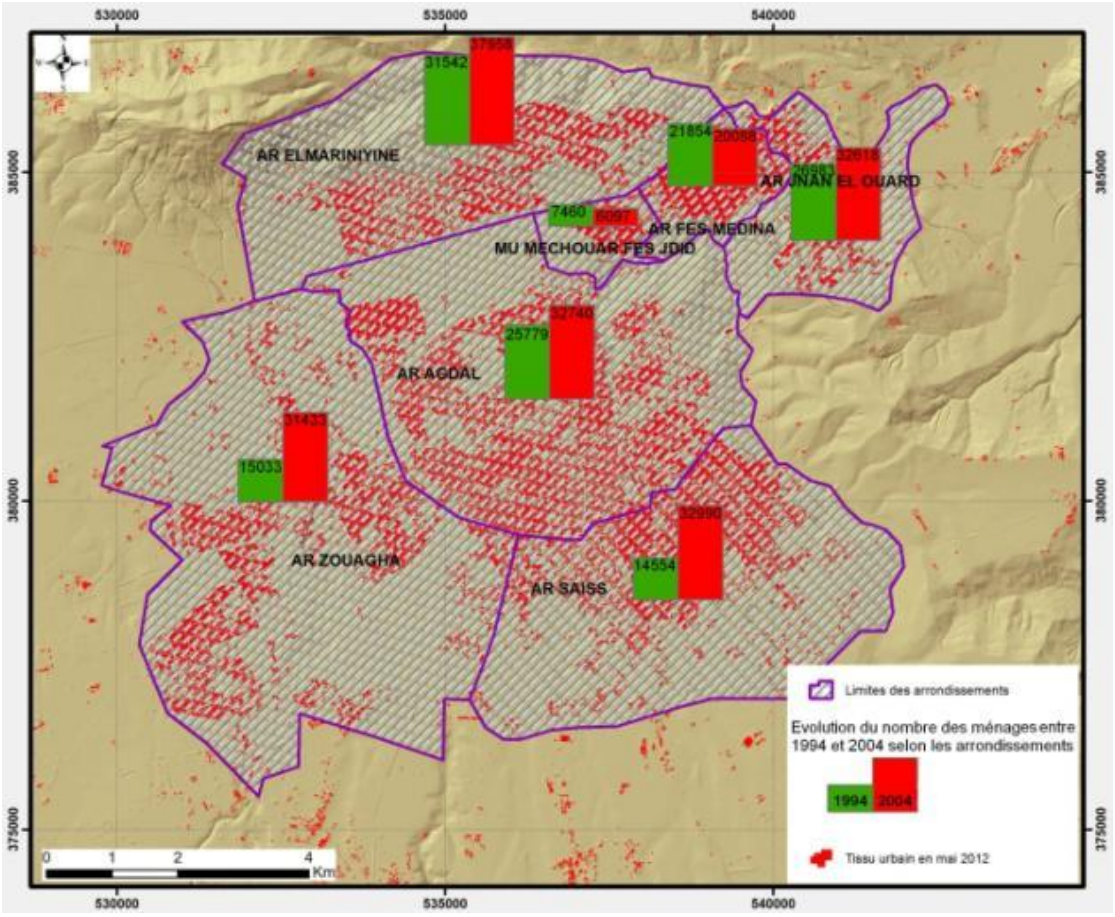

Figure 70 Evolution of the number of households between 1994 and 2004 according to the districts (Regional inspectorate of Fez-Boulemane 2013)

The urban territory of the Fez agglomeration has expanded rapidly in the absence of application in accordance with the urban development plans. This urban sector increased during a century (fig. 71) from 2.5 km² in 1912 to 11 km² in 1962, to 28 km² in 1990, to 80 km² in 2012 and to more than 100 km² currently. The urban area of the city has sometimes extended over land prone to slope movements, such as Trhat district and its neighbouring habitats and the northern districts overlooking the valleys downstream of the Fez oued and its tributary El Mellah oued, and floods as El Marja, Aaouinate Alhajjaj, etc.

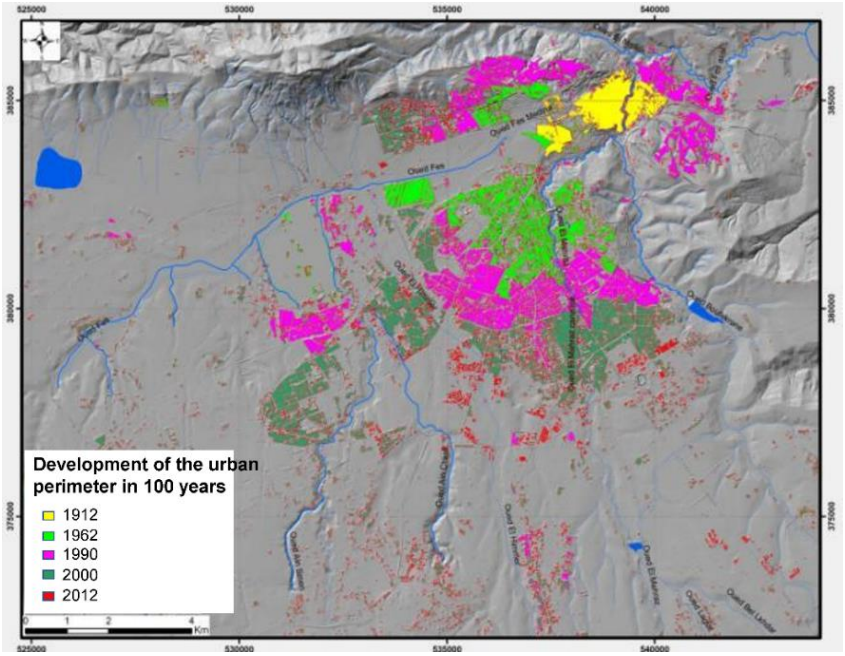

Figure 71 Evolution of the urban area of the Fez city in a century (1912 to 2012), (Lasri 2015)

C. Conclusion

In conclusion, this disproportionate extension of the urban fabric of the Fez agglomeration and the Moulay Yacoub town resulted in the construction of habitats vulnerable to the vagaries of slope movements, especially landslides. Moreover, agricultural activity integrating into food-production, whose terrains constitute the majority of the rural and uninhabited territory of Moulay Yacoub, is also considered as one of the stakes that is devastated by the shallow landslides. In fact, the cereal growing activity dominating the province predisposes the slopes to these shallow phenomena and is one of the factors altering their stability. The repeated land ploughing increases the void ratio of the shallow layer and promotes the rainwater retention capacity. In the presence of impermeable marl substrate, this layer saturated and soaked with water tends to flow, which explains the abundance of surface slope movements affecting the province slopes. For this, it is necessary to adopt certain methods to mitigate the risk by reducing the vulnerability of these lands such as afforestation (the plantation of olive trees which has already started, and which has covered a significant part of the territory is a case in point); and the terraces agriculture which decreases on the one hand the intensity of surface flow and increases on the other, the stability of the terraced sections vis-à-vis the shallow slope movements.

The magnitude of the issues is becoming significant, only a more precise diagnosis of the various factors and aspects of vulnerability makes it possible to have a correct vision and to draw up an action plan staggered over a short, medium, and long-term calendar making it possible to mitigate, as much as possible, the vulnerability degree. This study is one of the basic documents of the diagnosis in question.

V. Chapter 3: Slope movements Hazard in the Fez-Moulay Yacoub territory

1. Introduction

Landslides are a complex natural phenomenon that constitutes a serious natural hazard in many countries (Brabb and Harrod, 1989), with costly impact hindering the social economic development. This urges to promote studies and investigations in this area. However, the inventory of slope movement is a master data for all landslide studies. Such data can be exploited to investigate the distribution, types, pattern, recurrence and statistics of these phenomena (Guzzetti et al. 2012). Therefore, in order to carry out a successful inventory of slope movements in the study area, it is first necessary to classify each event and define its typology.

Several previous studies proposed reference classifications for slope movements (Julian, 1989; Keefer and Johnson, 1983; Varnes, 1978; Varnes and Cruden, 1996 ; etc.), each having some usefulness in emphasizing features pertinent to recognition, avoidance, control, correction, or other purpose for the classification. Among the characteristics that have been used as criteria for slope movements identification and classification: material type, displacement velocity, geometry of the area of failure and the resulting deposit, age, causes, degree of disruption of the displaced mass, relation or lack of relation of slide geometry to geologic structure, degree of development and state of activity (Varnes 1978). The use of these classification parameters differs depending on the purpose of the study and the precision of classifications required. The classification model of D. Varnes (1958, 1978; and 1996) is considered the most widely used classification system. However, an interesting update of the Varnes classification system was established recently by Hungr et al., (2014) and which proposes more typologies and less ambiguity when types grade from one to another, reason why we adopted it in the elaboration of the inventory of slope movements in the territory of the study area.

2. Typology

Slope movements, commonly referred to by the term landslides, include various processes of gravitational movements, more or less brutal, of the subsoil, involving natural (climate, earthquakes, river undermining, etc.) or anthropogenic factors (earthworks, excavation, vibration, deforestation, exploitation of materials or aquifers, etc.). They can manifest as:

- Subsidence, collapse, settling by shrinkage,

- Collapse by landslide or falling blocks,

- Landslide, creep, mudslides or debris, torrential lava,

- Swelling and shrinkage following drying and rehydration of soils

In fact, the chief criteria used in most classifications of landslides are type of material (fig.72, table 15). However, other criteria could be used for the classification of these gravitational processes as the displacement velocity.

In table 15, within the framework of a matrix whose rows represent the type of movement and columns the type of material, are 29 landslide type names or keywords (fig. 72) (based on Varnes 1978). The velocity scale classification was later updated by International Geotechnical Society's UNESCO Working Party on World Landslide Inventory (WP 1995) and Cruden & Varnes, (1996) (Table 16).

Table 15 A summary of Varnes' 1978 classification system

Movement type	Rock	Debris	Earth
Fall	1. Rock fall	2. Debris fall	3. Earth fall
Topple	4. Rock topple	5. Debris topple	6. Earth topple
Rotational sliding	7. Rock slump	8. Debris slump	9. Earth slump
Translational sliding	10. Block slide	11. Debris slide	12. Earth slide
Lateral spreading	13. Rock spread	–	14. Earth spread
Flow	15. Rock creep	16. Talus flow	21. Dry sand flow
		17. Debris flow	22. Wet sand flow
		18. Debris avalanche	23. Quick clay flow
		19. Solifluction	24. Earth flow
		20. Soil creep	25. Rapid earth flow
			26. Loess flow
Complex	27. Rock slide-debris avalanche	28. Cambering, valley bulging	29. Earth slump-earth flow

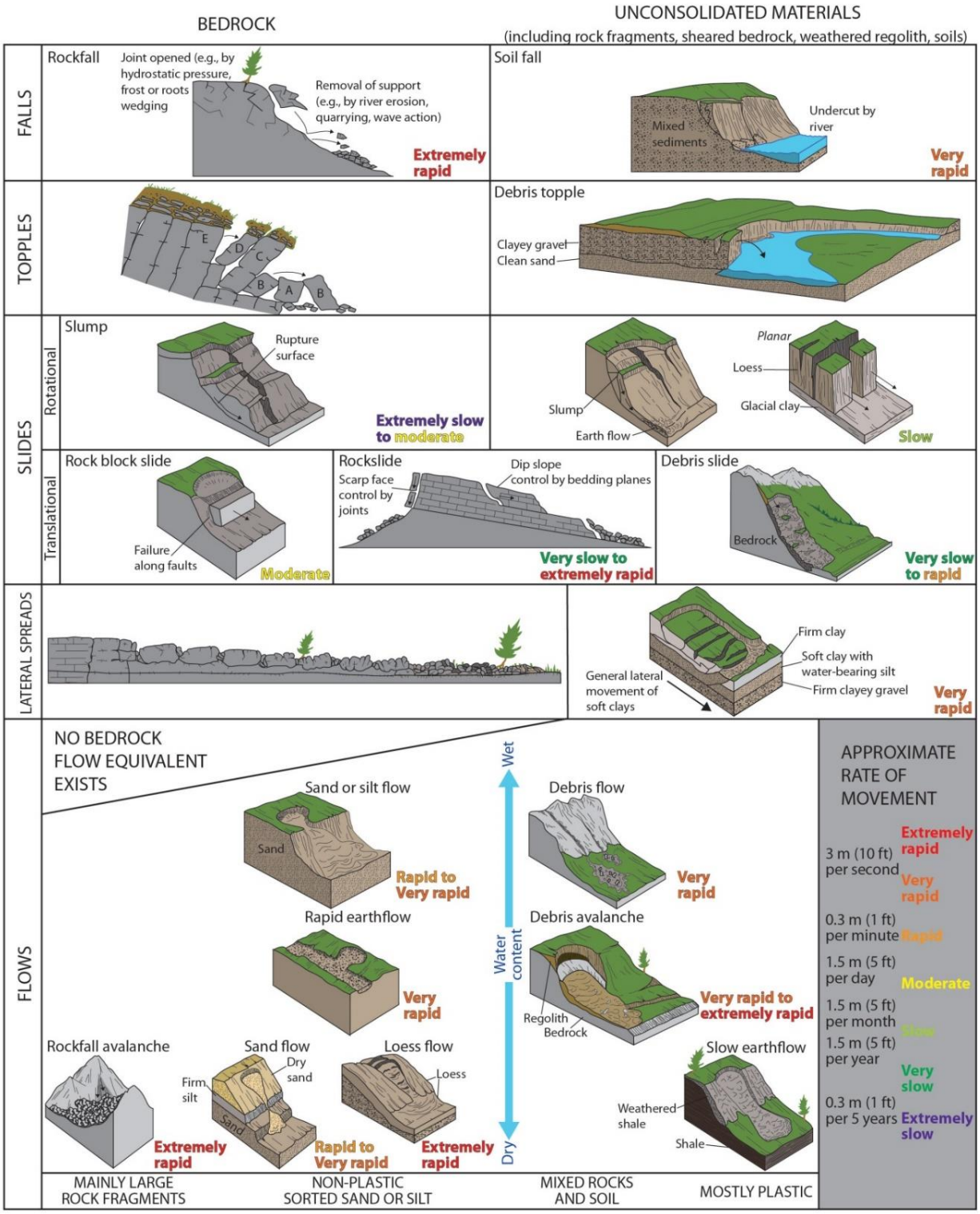

Figure 72 : Types de mouvements de versants (Thornberry-Ehrlich TL 2014)

In fact, the authors' view is that geotechnical material terminology is most useful, as it relates best to the mechanical behavior of the landslide. To describe materials modified by geomorphic processes, including land sliding itself, it is necessary to supplement the geotechnical terms by names of mixed materials, namely "debris" and "mud". The proposed list of material types, compiled by means of a

simplification of existing soil and rock description systems, is summarized in Table 17 (Hungr et al. 2014). The first column of the table lists the material types that can be used directly in forming landslide names. These types: "rock," "clay," "mud," "silt," "sand," "gravel," "boulders," "debris," "peat," and "ice" replace the former threefold material classes used by Varnes (1978). Characteristics listed in the second column of the table can be used as supplementary terms. For example, "sensitive" clay will lose strength on remodeling, while "partially saturated" silt may lose apparent cohesion on wetting.

Table 16 Landslide velocity scale (WP/WLI 1995 and Cruden and Varnes 1996)

Velocity class	Description	Velocity (mm/s)	Typical velocity	Response
7	Extremely rapid	5×103	5 m/s	Nil
6	Very rapid	5×101	3 m/min	Nil
5	Rapid	5×10−1	1.8 m/h	Evacuation
4	Moderate	5×10−3	13 m/month	Evacuation
3	Slow	5×10−5	1.6 m/year	Maintenance
2	Very slow	5×10−7	16 mm/year	Maintenance
1	Extremely Slow		<10 mm/year	Nil

Table 17 Landslide-forming material types (hunger, 2014)

Material name	Character descriptors	Simplified field description for the purposes of classification	Corresponding unified soil classes	Laboratory indices
Rock	Strong	Strong—broken with a hammer		UCS>25 MPa
	Weak	Weak—peeled with a knife		2<UCS<25 MPa
Clay	Stiff Soft Sensitive	Plastic, can be molded into standard thread when moist, has dry strength	GC, SC, CL, MH, CH, OL, and OH	Ip> 0.05
Mud	Liquid	Plastic, unsorted remolded, and close to Liquid Limit	CL, CH, and CM	Ip>0.05 and Il>0.5

3. Analysis of slope movement in the study area

In Fez-Moulay Yacoub territory, 10233 slope movements have been inventoried in the hole study area perimeter (fig. 73), including 16 rock falls, 2073 solifluctions, 3637 slides, 4318 earth flows and

189 complex movements (with most of the cases a sliding component). The landslide inventory map was established according to the classification system of Hungr et al., (2014). The main landslide-mapping step was based on geomorphological field mapping, on visual interpretation of the aerial photos, and on the use of satellite-derived imagery from the Google Earth and Bing databases. Then several field missions were conducted since February 2019 in order to complete the inventory of mass movements and to cover the entire territory of the study area.

The landslide inventory map shows that most slope movements are located in the MY province, with a very high LS density to the South of the province, north of Fez city. On the other hand, the Sais basin displays few landslides to the East and no cases were recorded to its Ouest part. The flat topography is certainly the main reason.

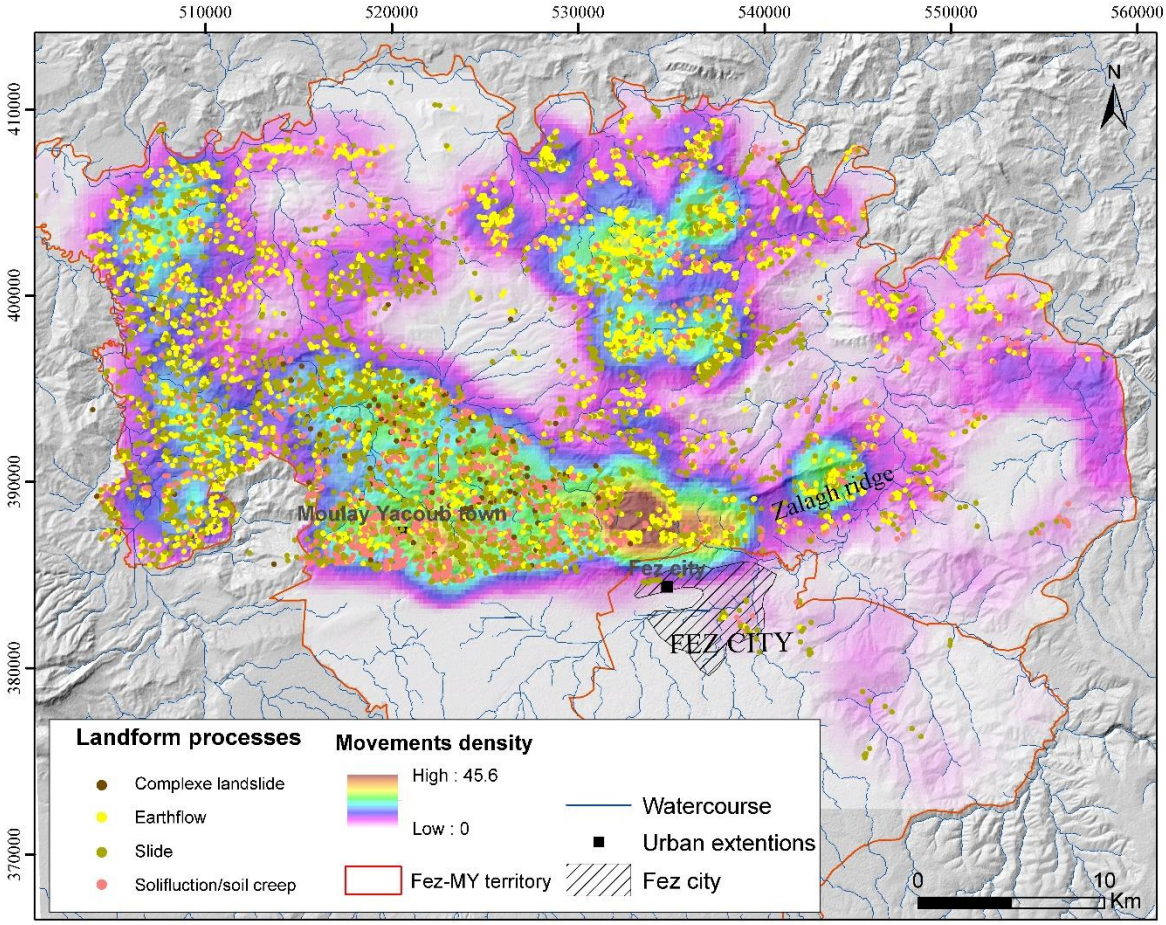

Figure 73 Distribution of slope movements in the Fez and Moulay Yacoub territory

The total area affected by the slope movements is approximately 105 Km². However, despite that earth flows are more numerous than slides, the latter's affected surface is more important, due to the magnitude of certain slide phenomena inventoried in the study area (fig.74). The small cases are generally recent, and their date of activation or reactivation is often in 2010, which recorded

exceptional rainfall which was consequently responsible for the activation and/or reactivation of a large number of landslides over the study area.

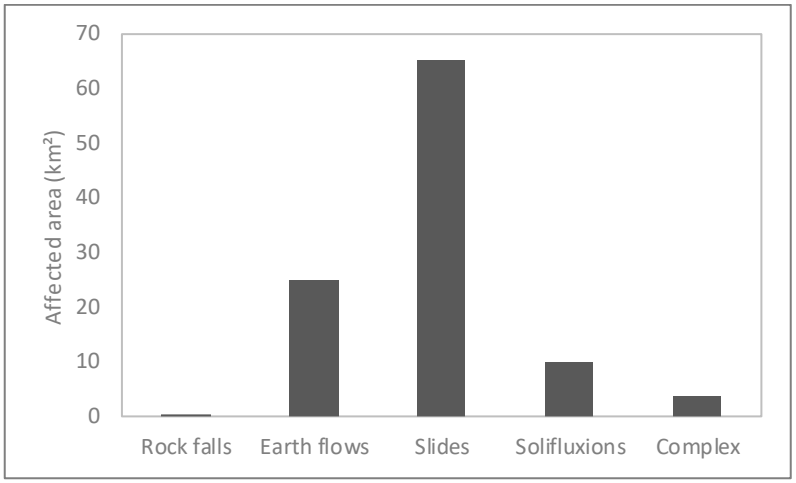

Figure 74 Area affected by landslide type (Km²)

A. Fez prefecture

The territory of the Fez Prefecture is spread over the Rif chain limit. It is formed by essentially marly formations. Despite the absence of steep drops and the litho-structural contrast, conducive to the instability of the slopes and characteristic of the mountainous nature of the relief in the northern provinces (Chefchaouen, Al Hoceima and Taounate), the Fez region is nevertheless susceptible to a varied instability forms according to regional particularities. Moreover, the anthropogenic action has unfortunately induced or exacerbated slope instability in several cases.

In the territory of the study area, previous interesting research studies have investigated the landslide hazard. Nonetheless, they are usually limited to site-specific investigations, while others are based on largely descriptive analysis which does not provide sufficient data and evidence to characterize the multifacets of the landslide hazard at different scales.

a) Previous landslide studies covering Fez prefecture:

Below are cited the main previous studies carried out in the study area:

- Millies-Lacroix, (1968) drew up a map of susceptibility to slope movements of the Rif, at 1/1,000,000° scale (fig. 75). It is a pioneer map on a global scale of landslide hazards. The assessment of susceptibility was carried out analogically, by overlapping layers of the topographic, lithological and spatial distribution of precipitation map. The various classes of these factors were weighted to obtain 9 degrees of spatial hazard. The majority of the territory is classified under medium to low hazard.

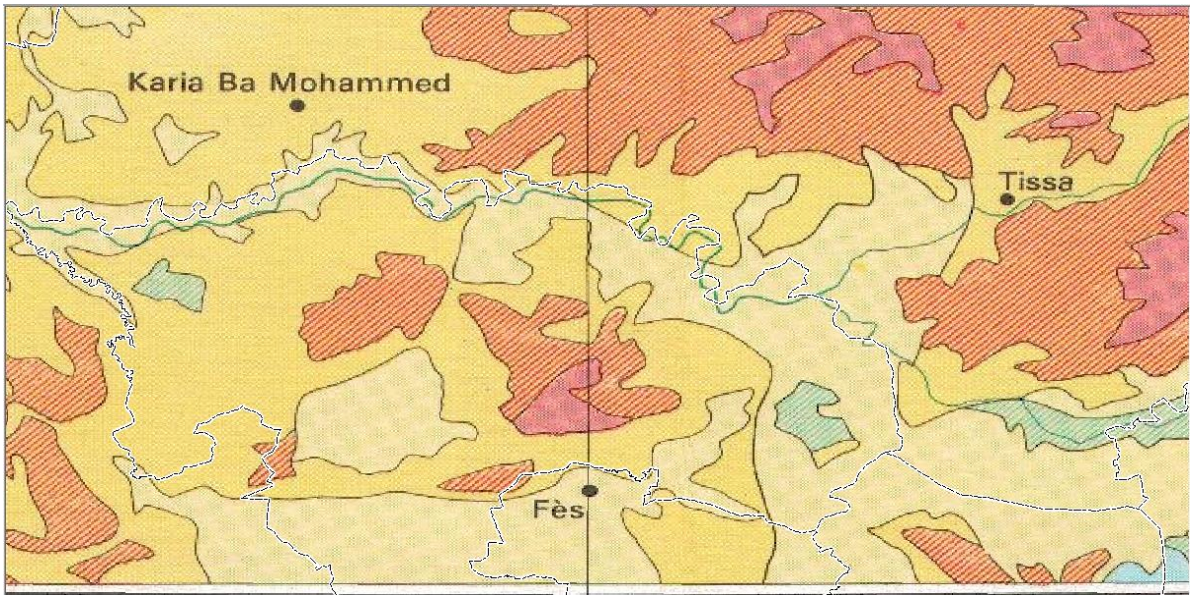

Figure 75 Extract from the provisional map of slope movements in the Rif at 1/1,000,000° (Milliès-Lacroix 1968). The boundaries of the provinces are schematized by drawn lines

- • Gartet (2008, 2011, 2013) carried out a follow-up of the evolution of dozens of gravitational processes (subsidence, cliffs and cavities collapse, landslides, falling blocks, etc.) in the urban perimeter of Fez as it defined the physical and anthropogenic predisposition conditions as the vulnerability of the built environment associated with this terrain's instability. Figure 76 show a cartographic recapitulation of these processes.

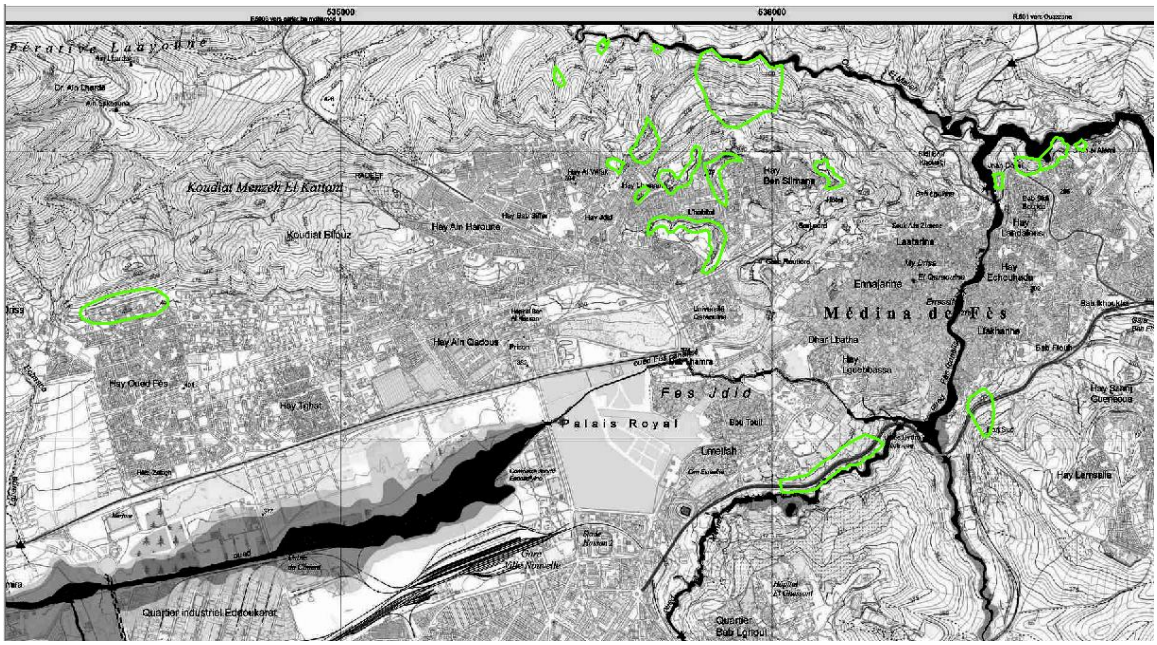

Figure 76 Summary of sites distribution affected by landslides (circled in green) in the urban perimeter of Fez city (Cartographic summary from the collection of sites studied by (A. Gartet, 2008)

- Moreover, Charroud et al., (2007) et Cherai, (2017) proposed a map approach of landslides risk areas in the northern part of the urban domain of the Fez city, based on an inventory of gravitational processes as well as an analysis of causative factors (Fig. 77).

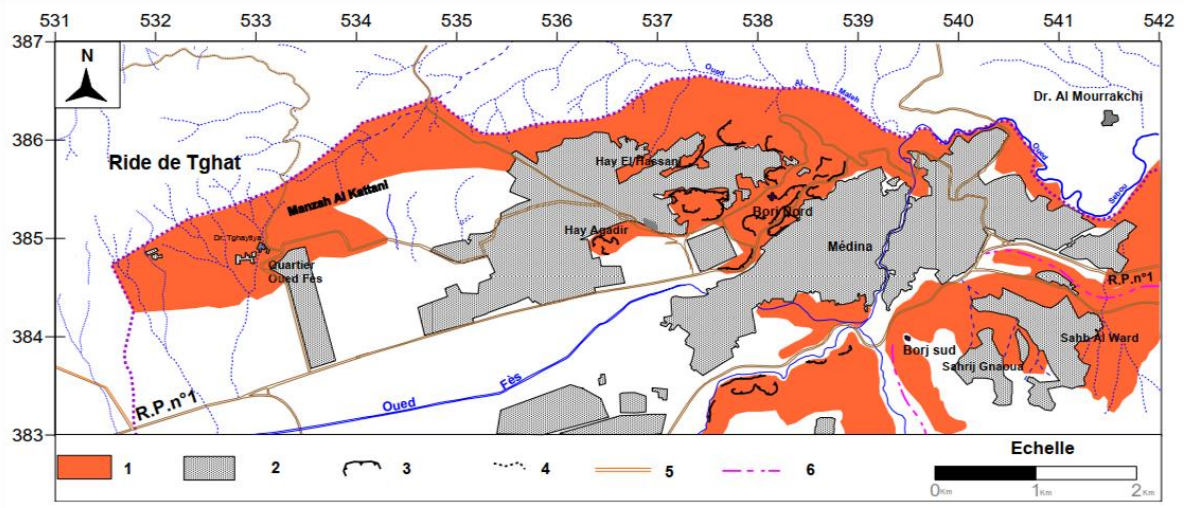

Figure 77 Map of areas at risk of landslides in the northern part of the urban perimeter of Fez city (Cherai et al. 2017). 1: Areas at risk of slope movements, 2: Urban agglomerations of Fez, 3: Cliffs and escarpments of quarries, 4: Limit of the urban plan of Fez, 5: Main roads, 6: The railway

b) Slope movements in the south Rif border (fig. 78)



Figure 78 View of the Sais plain from the Jbel Trhat foothill

It is an area of plains and low slopes on which is built and spreads the city of Fez on the one hand and several rural agglomerations of the MY province. The basin of Saïs is delimited from the east by reliefs of high elongated hills, locally nicknamed Jbel Tghat, Zalagh), whose sides constitute slopes predisposed to landslides and gullies system. These are the Pliocene conglomerates and especially the alluvial deposits of the various Quaternary formations based on clays, silts which, in places, are encrusted with calcretes. Pliocene conglomerates and Quaternary travertines also form cuestas like the Dhar Mehrez Plateau. When the Sebou, Bou Fekrane, Mahrez and Fez wadis enclose these rock formations (Pliocene conglomerates and Quaternary travertines), they release rocky cliffs surmounting marly slopes. The types of geomorphological hazards that can affect this basin are mainly subsidence,

tilting and rock falls from rocky escarpments, landslides, creeping, expansive soils by shrinkage-swelling and liquefaction in loose formations of deep alluvial plains.

c) Slope movements in Saïs Fez plateau:

The main cliffs with instability risk are in the northern areas laying on fissured travertine, travertine/cave, or those of sandy marls in the NE sector (fig. 79 and 80). The average heights are between 15 and 40m, the predisposed sites include Hafet Kaf el Azba, Hafet My Driss, Hafet Benzakour, Hafet Hay Hassani, Benslimane and Cariane El Hajoui laying on cracked travertine or travertine/cave in the North next to Jnane Slaoui, Jnane Mekouar and Jnane El Alami and on sandy marls to the North-East.

Moreover, the lacustrine limestone cover of the Saïs plateau shows collapses in the Zliligh douar (Ain Chkaf commune) (Fig. 81).



Figure 79 : View of Fez city and its cliffs from the northeast



Figure 80 Rock falls at the travertine cliff of Borj Echamal

As for landslides and earthflows, most of them are observed on the marly slopes and associated facies, as at the southern flank of J. Thrat (Figure 82), on the slopes of the hay Hassani, jnanate districts (Fig. 83) and to the East of Sidi Harazem marly slopes (Fig. 84 and Fig. 85).



Figure 81 Collapse of the cemetery of the Zliligh douar resulting from ancient underground cavities caused by the extraction of Pliocene lacustrine sands

Despite the presence of slope-gravitational processes, clay-marly formations, even on gentle slopes, are also prone to differential settlement due to expansive soils, which have a significant material impact on constructions.

As for the slides, they can affect all the backfill and marly slopes, gentle or steep ones, whether in urban or peri-urban areas, and human factors are to blame. The most affected areas are Trhat district

(fig. 82), the Jnanate distrcits (fig. 84 and 85), and the marly slopes surrounding the town of Sidi Harazem (fig. 83).

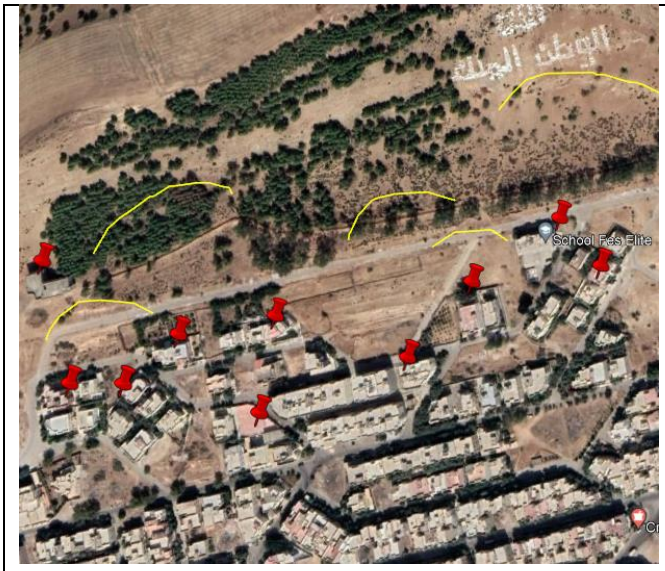

Upstream of the Oued-Fez district where buildings are affected by varying cracking levels (red placemarkets)





Figure 82 Landslides upstream of the Oued Fez district



Figure 83 landslides in Skhounate East of Sidi Harazem (the arrows represent the sliding direction)



Figure 84 Landslides in Sehb El Ouerd (on the right) and in Jnane Eddar districts (on the left) (the arrows represent the sliding direction)



Figure 85 Landslide in Ain Nokbi district (the arrows represent the sliding direction)

d) Impact of slope movements in in Saïs Fez plateau:

Fez has experienced, in the recent past, collapse events in different cliff sites such as hafet Kaf el Azba, Hafet Mly Driss, Hafet Benzakour, Hafet Hay Hassani, causing human loss, injuries and material damage (Le monde 1988; Gartet 2013; Le matin 2016). These events Between 1985 and 1999, 171 dead and 90 injured were recorded, as a result of the 7 accidents involving the collapse of cliffs, the immediate surroundings of which were invaded by substandard constructions, often of several levels. To the North-East of Fez, the landslides of Jnanate give evidence to the complicity of natural and anthropic factors (construction on loose and fractured slopes of watercourses) which has the consequence of altering the installation conditions of several districts (fig. 86 and 87).

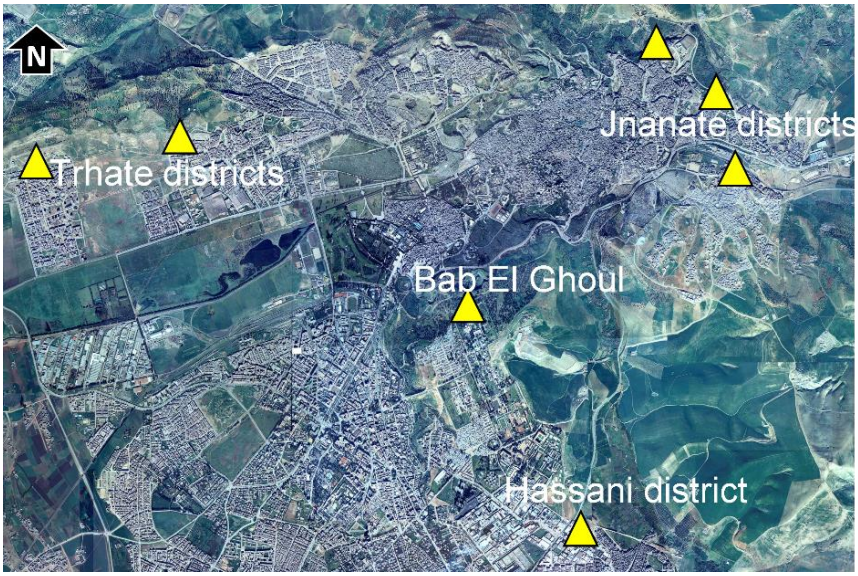

Figure 86 Main affected urban extensions in Fez city



Figure 87 Damaged/evacuated constructions laying on unstable cliffs due to bank undercutting by Oued Fez in Jnanate districts

Moreover, the private school and houses of the new district upper part of Oued Fez (to the east of the district of Trhat) are almost all affected by cracks, due to the active rotational landslides, to the point that the construction of a clinic was aborted under the severity of the damage submitted (fig. 88). Moreover, expansive soils are also the cause of several building pathologies noticed in flat areas.

Effect of expansive soils on a construction at Chaâbat Trhat (right)

Spacing of joints between constructions in Trhat district (bottom left)

Several cracked and repaired buildings in the Bab Al Andalous housing group (bottom right)



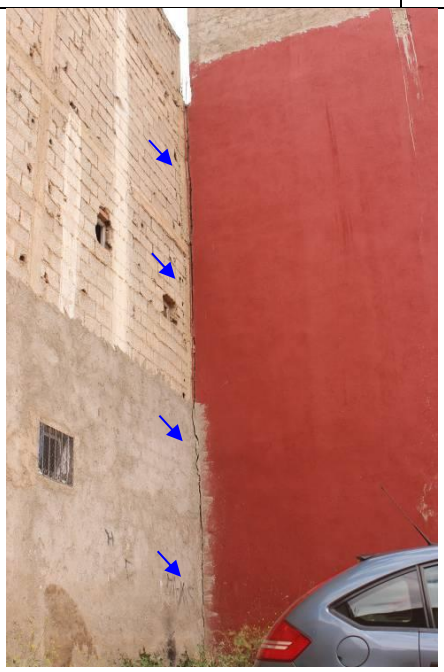



Figure 88 : Gaps between constructions (left) and fixed wall cracks (right) in Annahda Housing group

The road network is also experiencing damages, especially the sections crossing the marls below the travertine cornices or conglomerates. Sections of the RR501 are affected by the scree from the summit part of jbel Zalagh. Furthermore, the road section traversing the town of Sidi Hrazem (fig. 89a) and few rural extensions at the entrance of Fez (fig. 89b and c) are under threat of rock falls from sandstone ledges.

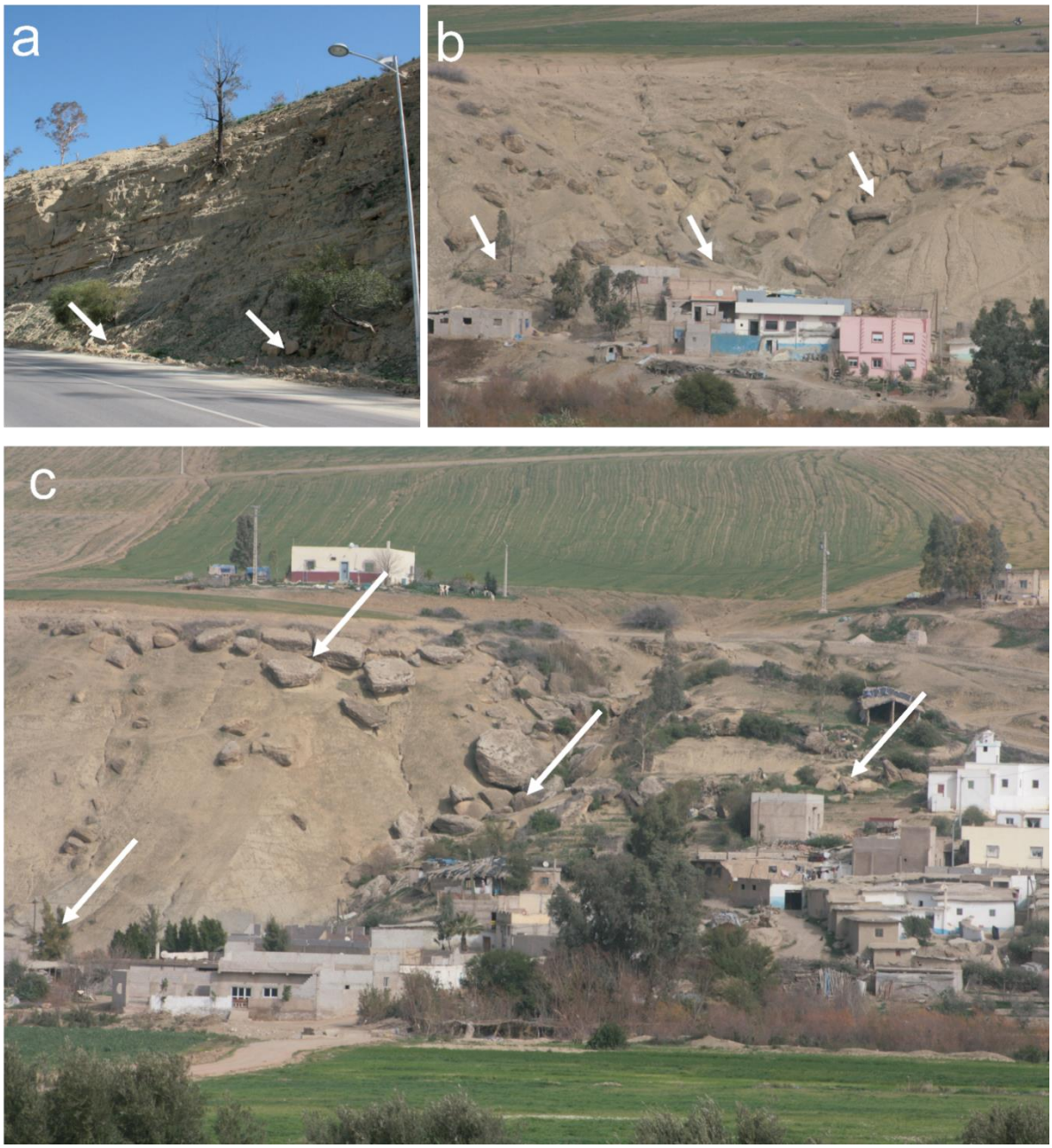

Figure 89 : Topples and rock falls from sandstone ledges at the entrance to Sidi Hrazem (a) and on the left bank of the oued Sebou at the exit of Fez city (b and c)

B. Landslide hazard in the territory of Moulay Yacoub

The territory of the province occupies a portion of the southern limit of the Rif chain dominated by marly formations as well as parts of the Saïs basin. Despite the absence of steep slope gradients and litho-structural contrast, conducive to slope instability, the Moulay Yacoub sector is nevertheless susceptible to a varied instability landforms according to regional and sometimes local particularities (site effects). The province is characterized by its low hills and middle slopes typical of the Prerif landscape.

a) Previous studies in the Moulay Yacoub province

- • Milliés-Lacroix (1968) cited above, and whose study also covered the province of MY, drew up a map of susceptibility to landslides in the Rif, at 1/1,000,000° (Previous map). Most of the territory is classified under medium to low hazard; except for the surroundings of Jbel Fechtala, where the hazard locally affects the middle to relatively strong classes.
- •Faleh & Sadiki, (2002) studied the large-scale complex movement of Dhar El Herrag, which was reactivated at the beginning of the 1960s and which affects the white marls of the Ouazzane nappe overlapping the Prerif substratum, involving the fluvial dynamics of the Sebou wadi meander.
- • Obda et al., (2018) et Obda I, (2017) dealt with landslides and associated building pathologies in the urban perimeter of Moula Yacoub town. The sector of which is dominated by marly slopes and affected both by shallow and deep slope movements and by expansive soils.

Although this territory is located in the Prerif, where the topography is relatively smooth (fig. 90), compared with the high relief of the northern and central Rif, it is heavily affected by gravitational manifestations, although, not many are spectacular as in the northern Rif provinces. The slopes in the Prerif region are generally moderate showing medium and low hills, shaped into marls conducive to solifluctions; to which are added abrupt reliefs which spring between the first (j. Zalagh, j. Trhat, Dhar El Harrag, Bourdime, …). The steepness of their slopes and the geological contrast of their formations make them prone to various slope movements and to intense gully erosion. Moreover, the slopes surrounded by higher order watercourses undergo intense bank undercutting causing slides and flows of variable magnitude. All these instability phenomena are observable in the territory of the Moulay Yacoub province.



Figure 90 : Prerif landscape where middle marly hills marly predominate

The main types of geomorphological hazards that can affect the MY province's territory are:

- Landslides and earth flows in the marls and colluvium that cover them (fig. 91 to fig. 95); This

basin is experiencing several large-scale slope movements, the most spectacular of which are in most cases very old, eroded and intensely ravined (fig. 93). Moreover, several cases were classified as complex movements featuring uphill sliding components and a flow like morphology at the foot (fig. 94). However, most of the processes inventoried are shallow or of low magnitude (fig. 95).

- Rock falls are limited to the reliefs emerging from the sandstones or the Soils (karst reliefs) or from the Prerif ridges (fig. 96);
- Expansive soils due to clays shrinkage/swelling phenomenon, even on flat topography; The Moulay Yacoub region is one of the regions where soils, known for their swelling potential, predominate (Obda et al. 2022). These expansive soils develop on marly bedrock or on plains filled in by the leaching of marly slopes. Both the clayey-silty soils of the plains and the marly slopes in this region are susceptible to shrinkage-swelling phenomena.

- Intense gullying: The abundance of essentially clayey facies in the basin predisposes the slopes of MY territory to advanced water erosion in gullies, very often with several meters of incision, sometimes reaching Mesozoic substratum. This phenomenon occasionally affects the red saliferous clays, the Neogene marls and the white marls of the Ouazzane nappe (fig. 97, 98 and 99).

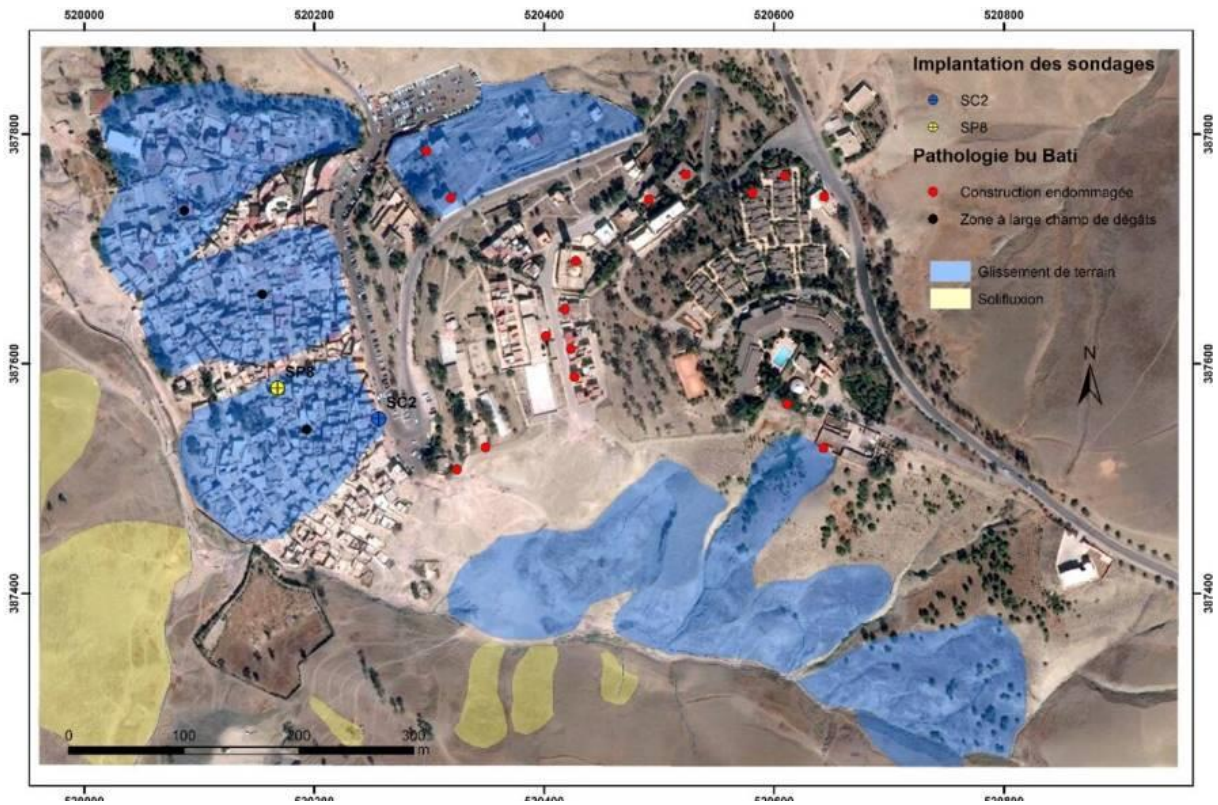

Figure 91 : Slides and earth flows in the urban perimeter of MY (Obda et al., 2018)

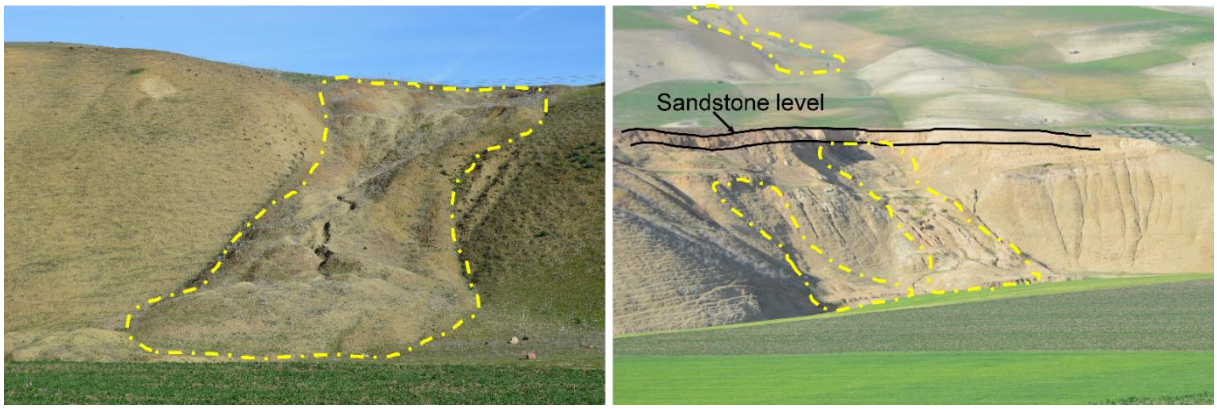

Figure 92 Typical earth flows in the MY province

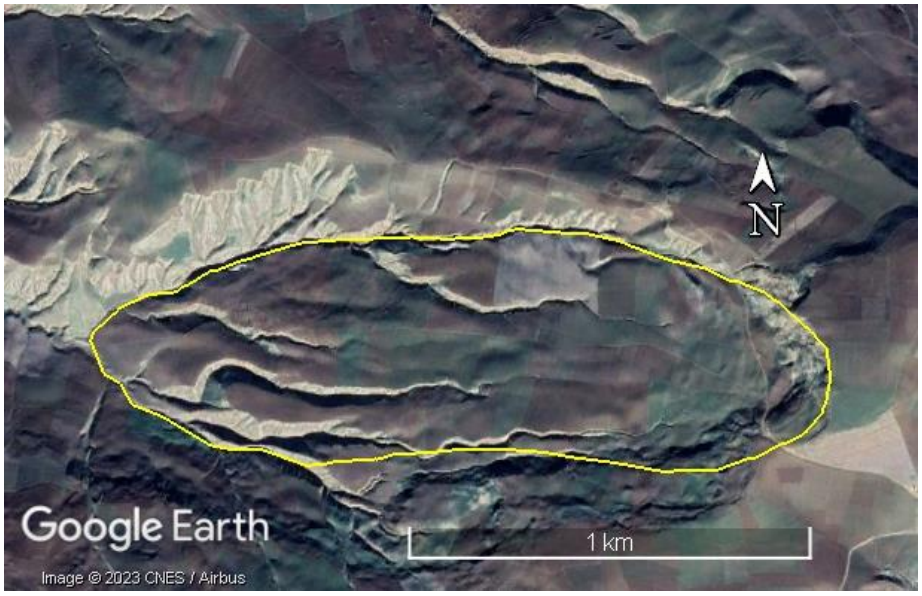

Figure 93 Aerial photo of a spectacular, eroded and ravined slide in the commune of Mikkes



Figure 94 : Complex (slide-flow) movements affecting the slopes of the Sbaa Rouadi commune in the MY province



Figure 95 shallow slope movements (earthflows and solifluctions) affecting Moulay Yacoub region

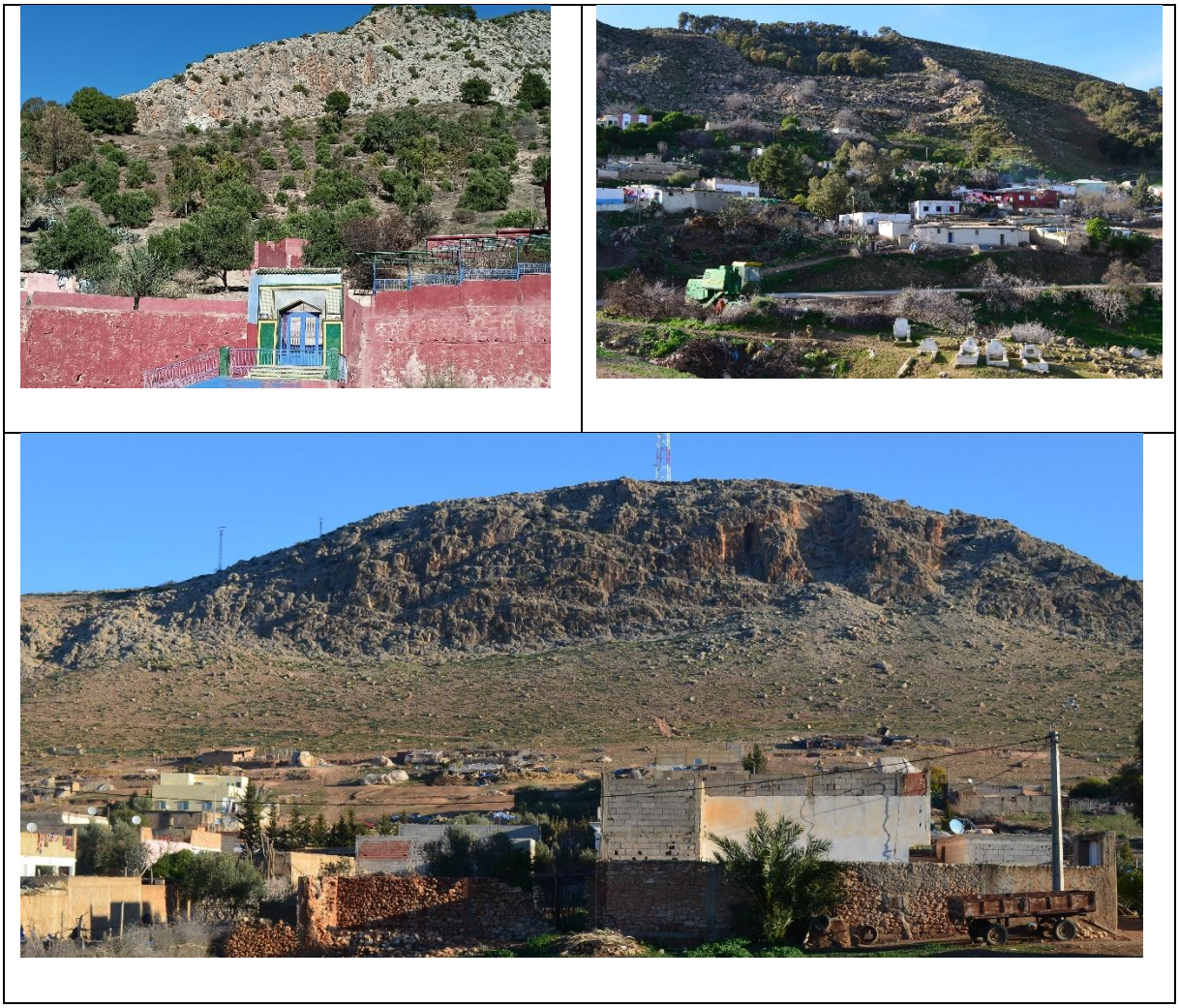

Figure 96 : Jbel Zalarh (left), Jbel Trhat (right) and other rocky cliffs with scree phenomena, signs of recurring rock falls threatening constructions downstream



Figure 97 : Gullying of marly slopes in aerial view



Figure 98 : advanced gullying in Triassic salt clays (left) and Neogene marls (right)



Figure 99 : Ravines deeply incising the white marls of the Ouazzane nappe and reaching the underlying Prerif Cretaceous pelites.

b) Impact of slope movements in the MY province

Our field visits to the town of Moulay Yacoub and to the other urban and rural areas allow us to observe the vulnerability of man-made facilities to slope movements. Many constructions, whether private or public, are affected by various degrees of cracking caused either by slope movements, or by shrinkage-swelling phenomena of expansive clays (figs 100 to 103). The diagonal cracking an cracked-connected doors and windows are usually characteristic of the inadequacy of the structure with the expansive nature of the soil.

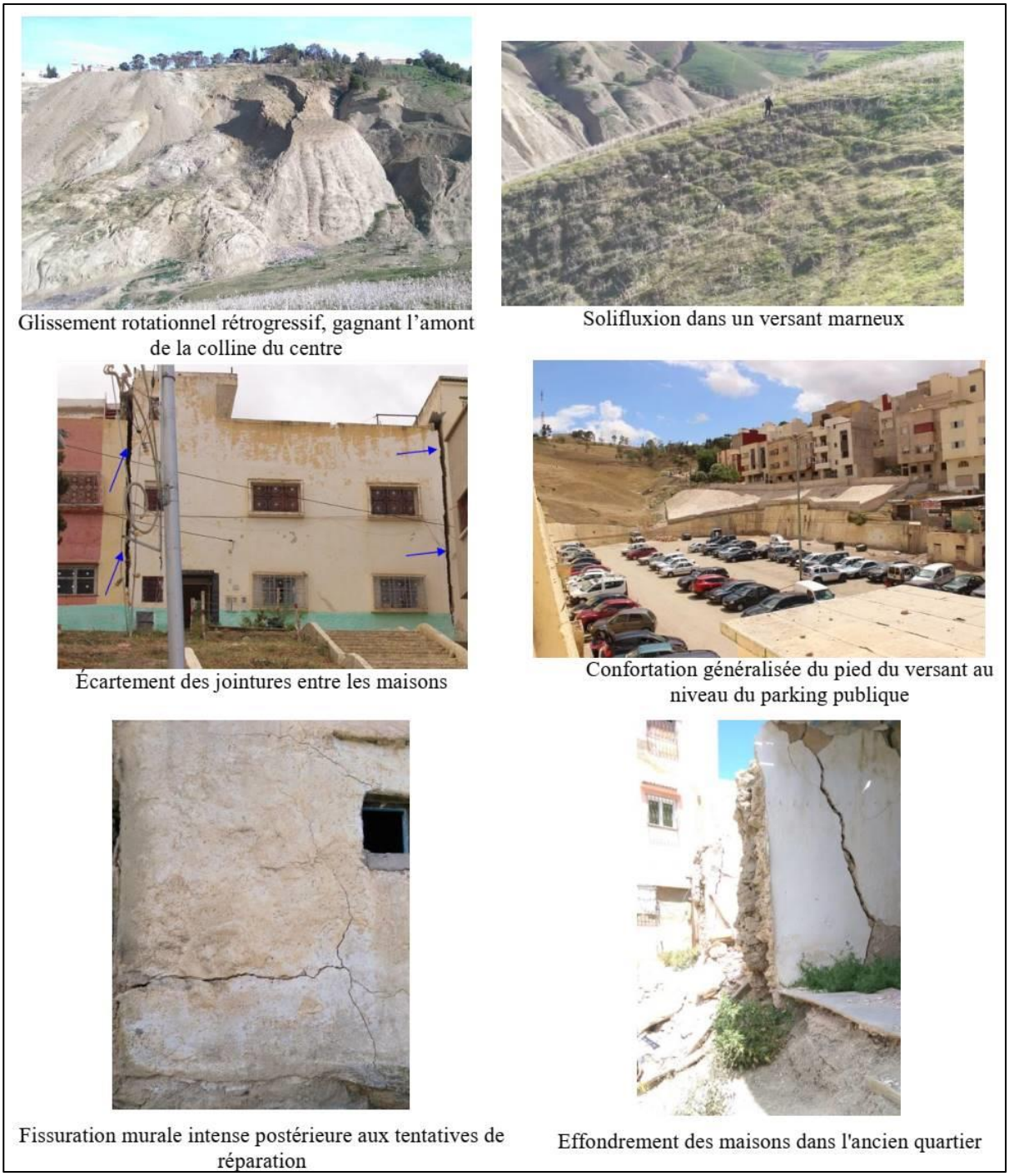

Figure 100 Types of gravitational processes affecting the Moulay Yacoub sector and associated building pathology (Obda et al., 2018)

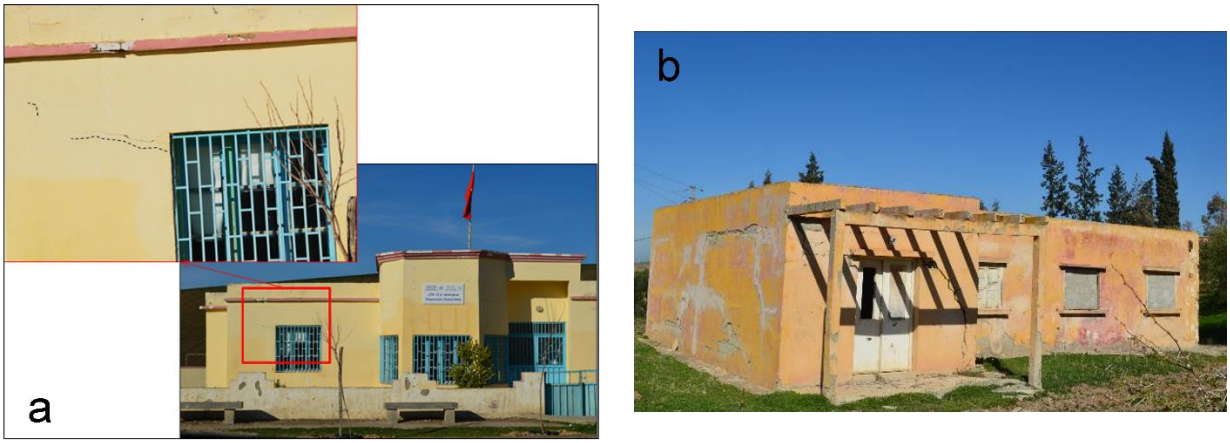

Figure 101 **a**. Diagonal cracking in the dispensary of Sbaa Rouadi built on clay alluvium; **b**. Severe structural pathology affecting constructions of the Department of Equipment, in charge of the Sidi Chahid dam installed on a marly hill



Figure 102 : Cracks affecting most constructions of Ain Bouali commune (Yellow arrows), built on flat topography but on expansive clay soil

The road network in the MY province is frequently damaged by whether slope movements or swelling of the sub-soil (Fig. 104). Despite the works of reinforcement and repair, these gravitational processes are often reactivated by climatic or/and anthropic factors, which makes the task quite complicated and costly for the decision makers.



Figure 103 Intense cracking affecting the rural houses of Sbaâ Rouadi center



Figure 104 Sample photos showing damage caused by slope movements and expansive soils to road infrastructure in the Fez-Moulay Yacoub territory

4. Conclusion

The slope moves inventoried in the territory of the study area come in different types, in different sizes and affecting several lithological formations. Also, these phenomena affect several slope gradients, both low and steep ones, and the human factor has been found to be involved in many cases. The database developed in this research step is fundamental and constitutes the basis of studies and approaches to the risk of slope movements in the different contexts presented by the study area. As observed in the field, the typology of slope movements inventoried in the study area is controlled by certain parameters, regional or local (specific to the sites), which must first be identified, then their degree of involvement should be investigated. Furthermore, the weight of these factors will have to be assessed with the other influencing parameters in order to understand the dynamics of slope movements in each specific context and at different scales in the study area. Thus, any intervention or even anticipatory measures can be able to target and/or reduce the weight of predisposing factors and avoid useless efforts and costs.

VI. Chapter 4: Landslide susceptibility mapping in the marly context of Moulay Yacoub Region

1. Introduction

Landslides represent the most costly geological hazard in word wide (Bao et al. 2020; Petley et al. 2005; Robert L Schuster 1996; Robert L Schuster and Highland 2001), especially in the Mediterranean rim where the environments are known by an erratic distribution of intense rainfall events, and the neo-tectonic activity is coupled with a high-energy relief (van Beek 2002). Sometimes, the interaction between these geo-hazards and the local practice of land use causes serious damages to infrastructures and agricultural lands and threaten local socioeconomic activities (Lee and Choi 2004; Conforti et al. 2014; Del Soldato et al. 2017; Harmouzi et al. 2019; El Kharim et al. 2021; Obda et al. 2022). According to the International Federation of Red Cross and Red Crescent Society, in the last decades, more than 3.2 million people have been affected by landslides with more than 1.700 million dollars losses (Hölbling et al. 2015). The large damaging effects of these phenomena have incited adopting several prediction strategies to identify high-risk areas that are the most vulnerable to future landslides based on local physical parameter, such as the relevant geology, geometry and slope forming processes (Fell et al. 2008). With such information, people and decision makers can foster the prioritization of slopes requiring follow-up actions and take appropriate preventive measures to spare expensive socioeconomic losses and to plan safe future development activities (Pantelidis 2011). Therefore, in the last decades, landslide susceptibility mapping has become an essential subject in international geomorphology, engineering geology and regional/urban territory planning (Bălteanu et al. 2020; Monsieurs et al. 2019; Tien Bui et al. 2019), especially since the development of GIS-aided mapping procedures has enhanced the capability of preparation of landslide susceptibility maps, thus allowing the analysis at a broad scale (Rybar et al. 2002). However, the quality landslide susceptibility mapping (LSM) depends mainly on the completeness and precision of the landslide inventory (Pereira et al. 2012; Gaidzik and Ramírez-Herrera 2021; Bounab et al. 2022) and the quality of causal factors used for modelling (Pereira et al. 2012; Mind'je et al. 2020; Cao et al. 2021).

In fact, the inventory of past occurrences remains the most influential input factor on the calculation of the spatial probability of landslide occurrence (Pereira et al. 2012; Bounab et al. 2022), which makes the landslides mapping a decisive step. Landslide inventory maps are prepared for several objectives, such as defining the location and type of landslides in the study area (Antonini et al. 2002; Cardinali et al. 2001), showing the abundance of slope movements (Degraff 1985; F Guzzetti et al. 2000), determining the frequency-area statistics of slope failures (Hovius et al. 1997, 2000; Guzzetti et al. 2002; Malamud et al. 2004), and providing relevant information to construct landslide susceptibility and hazard models (Soeters and Van Westen 1996; Chung and Fabbri 1999, 2003, 2005; Guzzetti et al. 2005, 2006).

Actually, recent studies proved that a proper computation of landslide frequency-area distributions (FAD) remains an efficient tool for testing the completeness of the landslide inventory (V. Eeckhaut et al., 2007), quantifying the risk and estimating erosion and sediment yields (Malamud and Turcotte 1999; Guzzetti et al. 2002; Hungr et al. 2008; Frattini and Crosta 2013; Fu et al. 2020) as well as comparing different geomorphological contexts in terms of landslide predisposition (Qiu et al. 2020). However, good probability size distribution models can only be obtained from detailed geomorphological inventories (Galli et al. 2008).

As for the conditioning factors, which are considered as the second key parameter in landslide susceptibility modelling, recent studies usually assess about ten variables considered as predisposing factors of slope instability, e.g., Lee et al., 2002 (13 variables); Lee and Choi, 2004 (15 variables); V. Eeckhaut et al., 2010 (9 variables); Sterlacchini et al., 2011 (9 variables); Biou et al., (2021) (11 variables). However, most LSM studies, especially those published before the 2020s, tend to mainly focus on the effects of different statistical techniques used to calculate the landslide susceptibility model and to validate its goodness of fit without assessing the correlation rate between landslides and the variables chosen (e.g. Süzen and Doyuran 2004; Schicker and Moon 2012; Kavzoglu et al. 2015; Othman et al. 2015; Aditian et al. 2018). Moreover, the choice of these parameters (data of influencing factors) could depend on the spatial extent of the study area, where a local spatial scale requires more accurate input data (Zêzere et al. 2017) as compared to a regional scale, where the choice of input is more generalized (Thiery et al. 2007; Holec et al. 2013). However, the selection step of these influencing parameters requires a geomorphologic synthesis by experts of the geomorphological context of the study area to achieve data consistency and to avoid objective evaluation of landslides spatial susceptibility (Bounab et al. 2022; Chung and Fabbri 2005). This could provide physical explanations of the observed statistical correlations and contribute to advancing our understanding of the underlying physical processes controlling the evolution of hillslopes.

In the Rif Mountain belt, the high energy relief and the lithological factor, dominated by loose formations, combined with human practices made landslides very abundant (Mastere et al. 2013; Rouai and Jaaidi 2003; Tribak 1997), especially in the region of Moulay Yacoub-Fez-Taza, where the lithology, represented by weathered clays and marls, combined with steep slopes and water saturation are the main factors involved in slopes instability (Hassan et al. 2015). However, the study of the anthropogenic factors (especially the land use) and their impact on landslide occurrence in the Moroccan territory (especially in the Rif mountain belt) is uncommonly investigated while international studies focusing on this important topic have increased exponentially since the 1960s (Beguería 2006; García-Ruiz et al. 2010; Guns and Vanacker 2013; Notti et al. 2015), with most irrigation-induced landslides occurring in dry climates (Garcia-Chevesich et al. 2021). Following this, recent studies have shown clear evidence of a strong and increasing control of the land use practices, especially the land cover change, agricultural activities and even urban extension, on landslide

occurrence (Guns and Vanacker 2013; Garcia-Chevesich et al. 2021; Obda et al. 2022). Therefore, the integration of this parameter cannot be omitted in the landslide hazard analysis. Furthermore, landslide susceptibility analysis in the Pre-Rif region is still very poorly investigated. Recently, projects of construction of aptitude for urbanization maps launched by the ministry of the national territory planning aim to provide the whole of the Moroccan territory with reference documents making it possible to consider the dimension of the risk of natural disasters, including the landslide hazard, during the urban planning process and particularly, during the development phase of the various urban planning documents. The later cannot be established without basic expertise and analysis of landslide susceptibility in predisposed areas.

The aim of the present chapter is first, to create a landslide database and to identify the characteristics specific to the regional study context and which have a direct impact on the predisposition of slopes to landslides. The second goal is to develop a landslide susceptibility map for the first time in the MY region, whose slopes are widely affected. Thus, future prevention measures could be proactive and efficient. To achieve this, we have chosen two among the most robust and accurate methods used in landslide susceptibility studies. The bivariate statistical Frequency Ratio (FR) method is one of the effective and widely used processes in landslide susceptibility mapping. It provides better understanding of the influence of the factors selected (whether geomorphological, climatic or anthropogenic) on landslide occurrence (Vakhshoori and Zare 2016; Razavizadeh et al. 2017). Moreover, the FR outperformed many other methods in landslide susceptibility mapping (weights of evidence, fuzzy gamma model, support vector machine, Evidence Belief Function, etc.) in terms of accuracy (Ramesh and Anbazhagan 2015; Vakhshoori and Zare 2016; Huang et al. 2018) and the ease of data manipulation in a GIS platform (Shafapour Tehrany et al. 2019; Zhang et al. 2020). Furthermore, the landslide susceptibility results pointed out the quality of the maps drawn by means of the GIS Matrix Method (GMM) in comparison with those made by other bivariate-statistical techniques (Jiménez-Perálvarez et al. 2009) and those made by the multiple-regression method (Irigaray et al. 2007). Its application showed satisfactory results and can be tailored for a broad scale where the same predisposing factors prevail (Irigaray et al. 2007; Boualla et al. 2019) which constitutes a similar context of our study area. In this study, we opted for these two models because in addition to the satisfactory results they provide according to the authors cited above, the FR method is counted among the most frequently used models, vice versa, the matrix method is still very little used in the modelling of landslide susceptibility, which encouraged us to test it and compare its results with the FR method in a specific and highly landslide-prone area as the MY province.

2. Settings of the study area

The study area is located in the west part of Moulay Yacoub province (MY) northern Morocco (Fig. 1), and includes 3 rural municipalities: Mikkes, Sebt Loudaya and Laajajra. The total area

covered is 335 km². MY province occupies the extreme south of the Pre-Rif unit (sub-unit of the Rif belt) and is limited to the south by the South-Rif overlapping front, which separates the Pre-Rif from the plain of Saïs (fig. 105). The Pre-Rif consists of marly overthrust nappes that belong to Cretaceous and Tertiary ages (Sendide 2002; Winckel 2002; Lakhdar et al. 2006; Charroud et al. 2007). The marls domination affords to the region a landscape of hills with 5 to 20% average slopes. The highest hills rarely reach 900m altitude and are usually armed with sandstone or limestone ledge. The observed processes of water erosion (sheet, rill and gully erosion) reveal the relative soils impermeability, their friability and the strong surficial flow (Heusch 1970; Tribak et al. 2009).

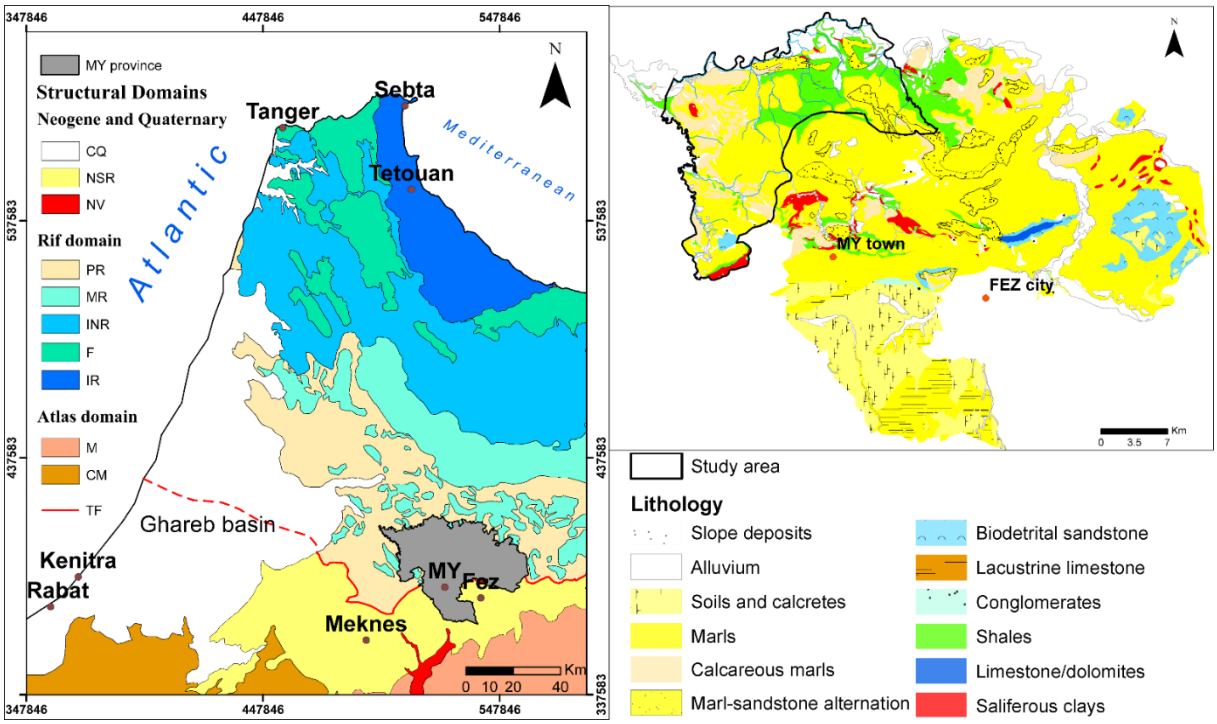

Fig. 105 a Geological map of northwest Morocco: (CQ) continental quaternary, (NSR) Neogene South-Rifan corridor, (NV) Neogene volcanism, (PR) Prérif , (MR) Mesorif , (INR) Intrarif, (F) flysch unit, (IR) Internal Rif, (M) Mesozoic blanket, (CM) Caledonian western Meseta, (TF) Frontal thrust; b Lithological map of the MY province

The drainage pattern is non-perennial and quite dense. Moreover, the study area is known by subarid climatic conditions with an average of 314 mm of annual precipitations. Rainfall data of Fez and MY's hydraulic stations show that most precipitations fall as stormy rain events, sometimes exceeding 50 mm, during very short periods (2 to 10 days), which expresses a severe seasonal contrast (DGM Moulay Yacoub; Obda et al. 2022). For the structural geodynamic of the region, the last studies confirmed recent tectonic activities at this Southern-Rif border (Bargach et al. 2004; Chalouan et al. 2014; Poujol et al. 2017a; Agharroud et al. 2021).

The main activity of the population in MY province, which does not exceed 200 000 residents (RGPH 2014), is the agriculture which is primarily based on cereal farming and olive tree plantation.

The housing regime is mostly rural except for the municipality of MY where the urbanization is closely linked to touristic and commercial activities provided by the existence of the thermal springs.

3. Material and methods

A. Landslide inventory

In the province of Moulay Yacoub, no slope movements data have been developed previously. The inventory map was established according to the classification of Hungr, 2014, who proposed a more detailed update to the Varnes classification. The landslide mapping was based on geomorphological field mapping, on visual interpretation of the aerial photos of the 1991 and 2005 missions at a scale of 40000 and 30000 respectively, and on the use of imageries like Google Earth and Bing maps, where most of landslides were mapped on the December 2018 image. Then, a field investigation was conducted to check and validate concealed processes by land cover (especially brushwood and trees), and relatively eroded ones. Earthflows, slides, and rock falls were observed and inventoried in the study area (fig. 106a). However, since rock falls are fairly localized, particularly at the foot of a few rocky escarpments, they were discarded from this study.

The term earthflows is used to design processes whose materiel is composed of marly soils (fine-grained material), has a flow-like surface morphology (fig. 107), is essentially ductile and does not significantly lose strength during deformation (Hungr et al. 2014; Varnes and Cruden 1996). As a result, earthflows move slowly and intermittently without requiring steep slopes to be triggered (less than 12°) (Schuster et al. 1996). In fact, they have long periods of relative dormancy alternated with more rapid "surges", allowing infrastructure and man-made projects to be built on them (Hungr et al. Picarelli 2014; Picarelli et al. 2005).

B. Area-Frequency distribution analysis

Nowadays, modelling landslide size distribution is considered as essential in quantitative hazard and risk assessment because of the assessment dependency on the relationship between landslide size and frequency distribution (Malamud et al. 2004; Corominas and Moya 2008). Moreover, several studies in the last decades have shown that landslide populations exhibit some power-law scaling across a portion of their size distribution (Brunetti et al. 2014; Jafarimet al. 2018; Malamud et al. 2004b; Qiu et al. 2020; Stark and Hovius 2001). In fact, the tail of landslide size probability distribution for medium and large landslides is a power law where α controls the power law decays for medium and large landslide sizes, while β controls the maximum probability density of landslide distribution in square kilometers, and γ controls the rate of decay for small landslide areas in square kilometers.

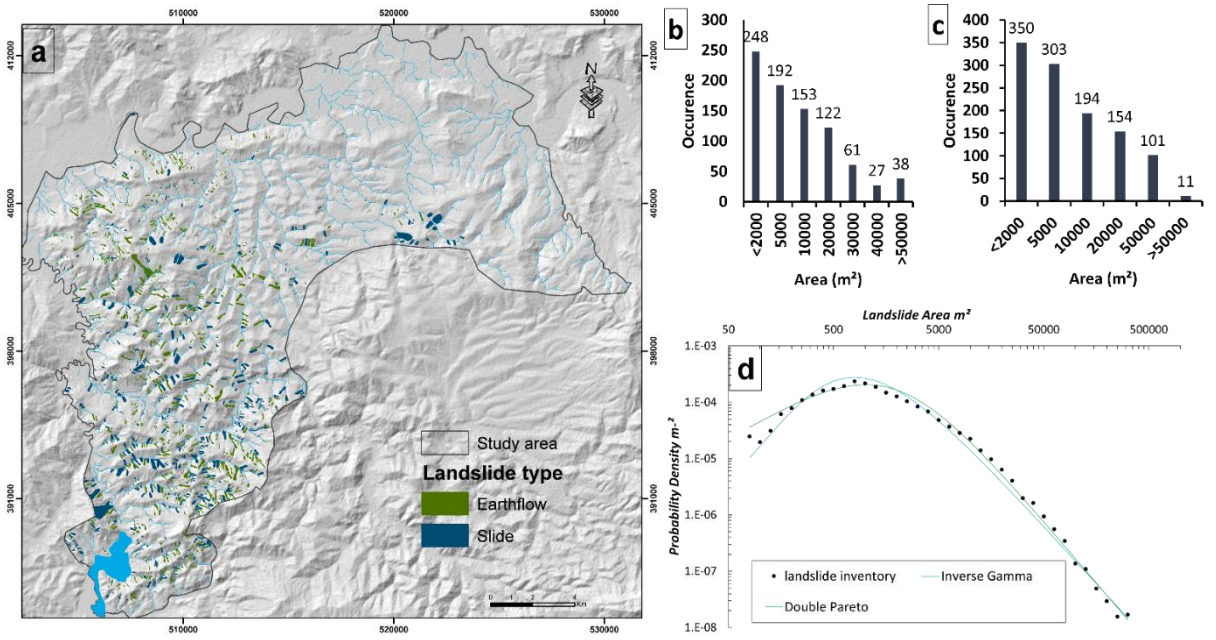

Fig. 106 a. Landslide inventory map and its statistical analysis. a. landslide inventory map; b. occurrences of earth flows by area of the movements; c. occurrences of slide by area of movements; d. Double Pareto, and Inverse Gamma models with frequency area distribution of the landslide inventory

In addition to its ability to characterize the size distribution of the landslides affecting the slopes of the study area, the probability size distribution also helps to assess the completeness of the landslide inventory carried out (V. Eeckhaut et al. 2007; Fausto Guzzetti et al. 2002; Li et al. 2016). In the present work, an Area-Frequency distribution analysis will be carried out to check the completeness of the landslide inventory but also to investigate further how the land use practices affect the size of landslides in the study area. This will give us a better understanding of the role of vegetation types in landslide occurrence (Guns and Vanacker 2014), which is essential to integrate the land use practices in the protection programs against the landslide risk in the region.

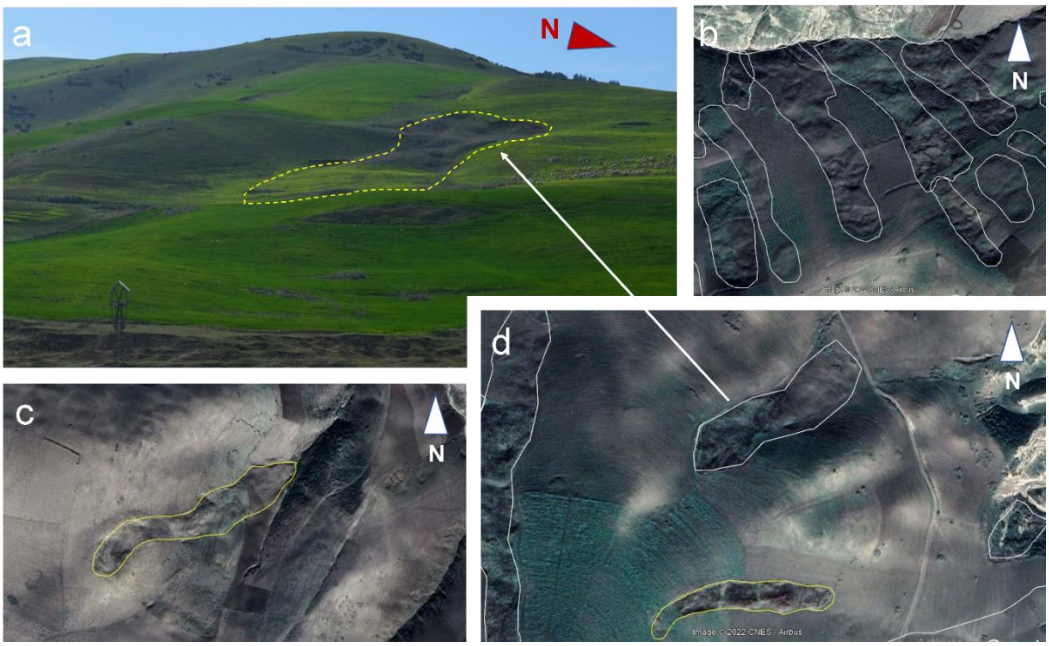

Figure 107 Image board showing earthflows and their flow-like/ductile appearance in the study area; a field mission photo where the earth flow was concealed by cereal farming (b, c, and d earth flows mapped on google earth 2018's image)

C. Landslide influencing parameters

Many factors have been used to establish landslide susceptibility maps (Catani et al. 2005; Wang et al. 2012). There are two types of involved factors in the occurrence of landslides, intrinsic and extrinsic factors. The first type is directly connected to slope instability, as the types of terrain, the presence of discontinuities, to the morphology of the slopes and to the hydrological conditions. The second type includes rather triggering factors such as intense rainfall, earthquakes and anthropic activities (railway or road constructions, mining, deforestation, drilling, different uses of lands, etc.) (Crozier 1984; Hansen 1984). For this study, the factors taken into consideration were those where data and maps were available. In the first step, slope, aspect, elevation, curvature, surface roughness, topographic wetness index (TWI), proximity to drainage network, proximity to roads, proximity to faults, lithology and land use were selected by as the involved parameters of landslide influence in this study (fig. 108). The first six factors have been calculated from the 12 meters DEM downloaded from ALOS-PALSAR platform, using GIS software. Lithology and faults were digitised from the FES-Ouest geological map. As for the land use, roads, and the hydrographic network, they were extracted from the topographic maps and have been detailed on google earth imagery. The aspect has an impact on hydrological phenomenon, evapo-transpiration, it governs soil moisture, vegetation and grass, and root penetration. Therefore, slope aspect has an indirect link on landslide occurrence and its degree of susceptibility (Neuhäuser et al. 2012; Pourghasemi and Rahmati 2018). Moreover, recent susceptibility mapping studies have shown that surface roughness proves to be an important parameter with a strong influence on the landslides occurrence (Abidi et al. 2019; Komac 2006).

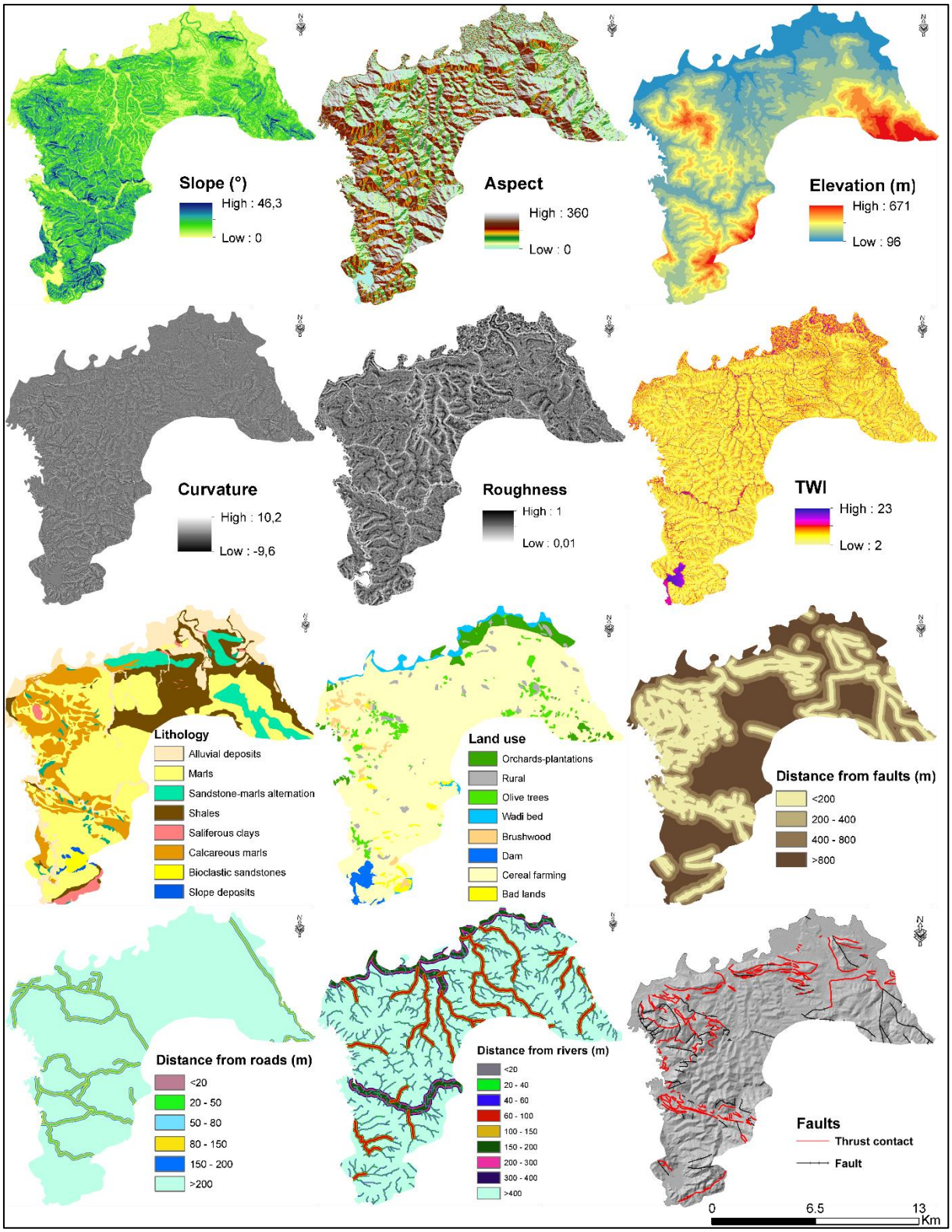

Fig. 108 Landslide influencing parameters in the study area

As for the TWI, it is usually used to study the on-going hydrological processes of the sub soils. The topographical character of the terrain directly affects the soil moisture, which is considered as a conditioning parameter of shallow gravitational processes, and is recently used for their forecasting

(Marino et al. 2020). To calculate the values of the index of the topographic moisture index we can use spatial data, namely the digital terrain model (Krivoguz and Bespalova 2017). This prompted us to evaluate the correlation of these parameter with landslide occurrence. Table 20 summarizes the class range chosen for each parameter.

After selecting the influencing parameters in slope instability, a geostatistical connection between these parameters and each landslide type was estimated by analyzing the association coefficients of contingency tables (Table 20). Then, a cross-tabulating of each factor grid layer and the landslide vector layer was analyzed using SPSS statistical software to quantify the relative correlation. This step allows, on the one hand, to select from the factors previously considered as those which most contribute to each movement type giving rise to the landslides inventoried, and to square parameters that faintly influence the instability on the other. Good-man-Krustal's Gamma (G-K) and Pearson's R were the two correlation coefficients calculated (Davis 1973; Goodman and Kruskal 1979). The predictor variables are classified as "effective" (EFF) if the condition G-K index > 0.5 and R > 0.4 applies, and as "not effective" if it doesn't (Fernández et al. 1996, 2003; Costanzo et al. 2012).

Despite that the cross-correlation were carried out for each landslide type, the G-K and R coefficients showed close values for earthflows and slides (Table 18). Therefore, the susceptibility maps were developed for the two landslide types combined.

D. Modelling of susceptibility

Two types of approaches are commonly used to perform the landslide susceptibility maps, qualitative and quantitative methods. Each of the latter has both advantages and drawbacks (Li et al. 2017). Qualitative approaches are based on the expert point of view (Akgun 2012; Bourenane et al. 2015; Chabok et al. 2019; Demir et al. 2013; Feizizadeh et al. 2014; Hasekioğulları and Ercanoglu 2012; Lazzari et al. 2012; Osna, et al. 2014; Park et al. 2013; Pourghasemi et al. 2012; S. Zhou et al. 2016), who should have enough knowledge about the local conditioning factors involved in landslides manifestations. Quantitative methods are based on the analysis of the functional relations between the factors of instability and the distribution of landslides and can be categorized into bivariate and multivariate methods. In the bivariate ones, each factor is combined with the landslide distribution map. As for the multivariate approaches, they are usually more adapted to irregular data distribution (Kavzoglu et al. 2014).

In the present chapiter, the two susceptibility methods used are the Gis Matrix Method and the Frequency Ratio.

a) GIS Matrix method (GMM)

The GMM is based on the construction of three matrixes in which the following data are recorded (Degraff and Romersburg 1980; Irigaray 1995; Chacón et al. 2006):

- The first matrix TSM (Total Surface Matrix): was calculated by computing the selected factors as effective parameters, making all possible combinations among the selected factors, and then calculating the area occupied by each combination.
- The second matrix LM (Landslide Matrix): was calculated by cross tabulating the reclassified landslide inventory binary map with the first resulting matrix TSM, this step allows us to calculate the area affected by landslides for each unique combination. (Irigaray et al. 2007),
- The third Matrix SM (Susceptibility Matrix): is the result of dividing the LM by the TSM, the results can be calculated by a percentage that represent an assessment of relative susceptibility levels (0<LSM<100).

Table 18 G-k and R values showing the correlation degree of the pre-selected conditioning factors with landslide types

Earth flows			**Slides**		
Factor	R	G-K	Factor	R	G-K
Land use	0,7	0,4	Land use	0,7	0,43
Dist roads	0,68	0,57	Dist roads	0,68	0,6
Dist rivers	0,68	0,4	Dist rivers	0,68	0,46
TWI	0,66	0,55	TWI	0,66	0,55
S. Rough.	0,65	0,6	S.Rough.	0,65	0,65
Lithology	0,63	0,39	Lithology	0,63	0,42
Slope	0,61	0,64	Slope	0,61	0,68
Elevation	0,5	0,37	Elevation	0,5	0,39
Dist. faults	0,4	0,45	Dist faults	0,4	0,45
Aspect	0,31	0,4	Aspect	0,31	0,46
Curvature	0,11	0,33	Curvature	0,11	0,33

Then, the matrix of susceptibility (SM) is established from these data where the percentage of each of the combinations occupied by rupture zones for each type of movement is recorded (Table 19). The higher the percentage, the more susceptible is the corresponding combination of factors to landslide phenomena (Fernández et al. 2003).

Finally, the values obtained are visualized showing 5 susceptibility levels (very low, low, moderate, high, very high). Moreover, it should be noted that there are no statistical rules for

automatically categorizing continuous data (Ayalew et al. 2004). So, most researchers use their own expert opinion to develop class boundaries (Chaudhary et al. 2016). In our case, the landslide susceptibility levels of the GMM map were categorized using the Quantile method (groups that contain an equal number of values).

Table 19 Sample of the landslide-susceptibility matrix considering all the slope movements in the study area: Cm: combine number whose line shows the numbers of each class factor, Lith: lithology, Ele: elevation, Ds-ri: distance from river, Lu: land use, Sl: slope, Ds-ro: distance from roads, Twi, topographic wetness index, Rgh: slope roughness, LSM%: percentage of landslide susceptibility matrix, LS: landslide susceptibility

	Effective factors									
Cm	Lith	Ele	Ds-ri	Lu	Sl	Ds-ro	Twi	Rgh	LSM %	LS
1	8	4	9	8	6	6	1	3	100	very high
4	4	6	9	9	3	6	1	4	25	high
10	4	4	9	9	3	6	1	2	10	moderate
13	5	4	2	8	3	6	3	2	61	very high
14	1	3	8	8	4	6	1	2	36	very high
15	9	1	4	8	2	5	2	2	67	very high
15	1	5	3	8	3	6	1	2	20	high
20	6	8	9	8	3	6	1	3	10	moderate
29	7	8	9	8	5	6	2	3	65	very high
196	9	1	6	4	3	6	2	2	10	moderate
…	…	…	…	…	…	…	…	…	…	…
32346	3	3	9	8	2	6	2	3	1	very low

b) Frequency ratio method (FR)

In order to investigate landslide susceptibility at medium and small scales, statistical methods are the most frequently adopted approaches (Van Westen 2000; Cascini 2008; Yalcin et al. 2011). Frequency ratio is one of the statistical methods frequently used (Lee and Sambath 2006; Yalcin et al. 2011; Pourghasemi et al. 2018). The FR method estimates the area correlation of landslide occurrence with each of the landslide-inducing parameters (Kannan et al. 2013). The reclassified factor maps were combined with the inventory map to calculate the frequency ratio of each factor class according to the equation below (Youssef et al. 2015). The higher it is the more it represents a positive correlation and high landslide susceptibility. In other words, if the FR is greater than 1, it means that a high association exists between slide locations and different classes, and a value lower than 1 means lower correlation.

$$FR = \frac{\frac{Np(LXi)}{\sum_{i=1}^{m} Np(LXi)}}{\frac{Np(LXj)}{\sum_{j=1}^{m} Np(LXj)}}$$

With FR = frequency ratio of class i of factor j, Np (LXi) = number of pixels with landslides within class i of factor variable X, Np (Xj) = number of pixels within factor variable Xj, m = number of classes in the factor variable Xi, n = number of factors in the study area.

The Landslide Susceptibility Index (LSI) represents the relative susceptibility or hazard to landslide occurrence. To obtain the sliding susceptibility index, each factor's frequency ratio values were summed to the training area as in the equation below (Yalcin et al. 2011; Hong et al. 2017; Sun et al. 2018). The higher LSI value indicates higher susceptibility to landslide. As or the landslide susceptibility levels of the FR map, they were categorized using Natural bricks method

$$LSI_i = \sum_{j=1}^{m} FR_i^{(j)}$$

Table 20 Contingency tables showing the total surface (class pixels), the affected surface by landslides (L. pixels) and the percentage of the latter (% L. pixels) of each class factor

	Factor classes	Class pixels	% Classes pixels	L. pixels	% L. pixels	Factors	Factor class	Class pixels	% Classes pixels	L. pixels	% L. pixels
Slope (°)	0 - 5	570343	26.6	4946	4,8		>200	1894140	88.4	93765	91,2
	5 - 10	726226	33.9	29528	28,7	Land use	orchards-plantations	100337	3.8	46	0
	10 - 15	559019	26.1	42434	41,3		rural	47332	2.2	678	0,7
	15 - 20	222766	10.4	20314	19,8		olive trees	72081	3.4	4361	4,2
	20 - 25	53523	2.5	4641	4,5		wadi bed	53458	2.5	553	0,5
	25 - 30	9605	0.4	818	0,8		brushwood	35239	1.6	863	0,8
	30 - 35	1465	0.07	63	0,1		dam	29993	1.4	52	0,1
	>35	256	0.01	17	0		cereal farming	1769794	82.5	94635	92,1
Elevation (m)	<150	261236	12.2	1282	1,2		bad lands	32592	1.5	1587	1,5
	150 - 200	405838	18.9	9121	8,9	Lithology	marls	920465	43	65662	64
	200 - 250	512825	23.9	23251	22,6		sandstone-marls alternation	145047	6.8	347	0,3
	250 - 300	362016	16.9	27498	26,8		shales	343627	16	5432	5,3
	300 - 350	254866	11.9	21922	21,3		saliferous clays	34453	1.6	640	0,6
	350 - 400	151753	7.1	12558	12,2		calcareous marls	320690	15	24095	23,5
	400 - 450	100548	4.7	5282	5,1		bioclastic sandstone	17211	0.8	402	0,4
	450 - 500	47019	2.2	1585	1,5		slope deposits	38403	1.4	5123	5

	>500	47102	2.2	262	0,3
Slope Roughness	<0,2	9501	0.4	68	0,1
	0,2 - 0,4	338084	15.5	13106	12,7
	0,4 - 0,6	1582055	72.5	86284	83,9
	0,6 - 0,8	246361	11.3	3338	3,2
	>0,8	6072	0.3	1	0
Witness index	<4	64354	3	5013	4,9
	4 - 8	1714058	80	82761	80,5
	8 - 12	302654	14.1	13407	13
	12 - 16	54486	2.5	1454	1,4
	>16	7651	0.4	126	0,1
Road proximity	<20	26498	1.2	706	0,7
	20 - 50	39100	1.8	1102	1,1
	50 - 80	38494	1.8	1139	1,1
	80 - 150	86277	4	3418	3,3
	150 - 200	59318	2.8	2645	2,6

	alluvial deposits	323134	15.1	950	0,9
Dist. Faults	<200	651196	30.4	31293	30,4
	200 - 400	368053	17.2	14545	14,2
	400 - 600	249774	11.7	11203	10,9
	600 - 800	195712	9.1	10189	9,9
	>800	679092	31.7	35545	34,6
River proximity	<20	88716	4.1	5534	5,4
	20 - 40	95906	4.5	5777	5,6
	40 - 60	84243	3.9	4925	4,8
	60 - 100	126899	5.9	4571	4,4
	100 - 150	63834	3	2642	2,6
	150 - 200	132137	6.2	4633	4,5
	200 - 300	36576	1.7	1352	1,3
	300 - 400	36136	1.7	1221	1,2
	>400	1479380	69	72120	70,2

E. Quality control of susceptibility maps

The results quality assessment is an essential step in any mapping of susceptibility and/or hazard. In this research, the quality-control of the landslide susceptibility maps were assessed through the cross correlation between these maps and a previous inventory composed of 200 instability movements. In each case, two robust validation methods were used:

(i) In the first method, the degree of fit or concordance (DF) was determined (Goodchild 1986; Jiménez-Perálvarez et al. 2009). This statistical method has been used and judged valid by several researchers studying instability movements (Fernández et al. 2003; Chacón et al. 2006; Mathew et al. 2009; Romer and Ferentinou 2016; Zieher et al. 2016; Boualla et al. 2019). The degree of fit was obtained according to the following equation:

$$DF_i = \frac{Z_i/S_i}{\sum Z_i/S_i}$$

Where Zi is the area occupied by the landslide at each susceptibility level and Si is the area of the i class of susceptibility.

For DF results, the lower the values in the low and very low susceptibility classes and the higher the values in the high or very high susceptibility classes, the higher the quality of the susceptibility map (Fernández et al. 2003; Irigaray et al. 2007; Boualla et al. 2019).

(ii) The Area Under the ROC Curve (AUC) was the second validation approach. it is used to assess the performance of the statistical model, and larger AUC is considered better (Zhou et al. 2018). The AUC estimates the quality of the statistical model by describing its power to predict the occurrence or non-occurrence of landslide events (Feizizadeh and Blaschke 2013). Values close to 1 (100%) show excellent prediction, conversely if it is around 0.5 (random fit).

4. Results and discussion

A. Magnitude and distribution of slope movements

In the study area, 1113 earthflows and 843 slides were identified (fig. 106), which expresses a total sliding surface of 17,74 km². Panels a and b of the same figure shows that for both landslide types, earthflows and slides, small size and therefore shallow movements (<10000m²) are much more common. This is undoubtedly controlled by the predisposing factors specific to the regional context of the study area.

The statistical analysis of the landslide inventory shows that the most affected slope gradient is the range of 10-15° with 1003 movement which represents 51% of the total occurrences, followed by the

ranges 15-20° and 10-15°, which represent about 20% each (fig. 109a). As for the material affected, about 1250 movements affects marly slopes and 484 and calcareous marls, equivalent to respectively 63% and 25% of total occurrences (fig. 109c). Furthermore, earthflows represent 57 % of the total sliding area and most of them occur in cereal farming slopes (fig. 109b). The later alone represents 92% of the area affected by all the landslides (Table 20), although the seasonal agricultural activity has erased morphological features of several gravitational processes, especially the shallow ones. However, earthflows could be instantly reactivated after heavy rain events (Bertolini and Pizziolo 2008; Bardi et al. 2017).

As for the slides, they represent 43% of the landslides mapped. Field visits show that many slides affect the road network. In fact, the latter is suspected to be a significant influencing parameter in slides triggering. Moreover, several cases of compound slides were inventoried in the field and by photo interpretation. The multiple scarps along the sliding area attest that the these movements occur along multiple rupture surfaces, which is commonly encountered in soft lithologies (Hungr et al. 2014; El Kharim et al. 2021; Obda et al. 2022). Furthermore, few large and eroded slides are observed in the region, the oldest ones are not included in the present study presuming that the parameters involved in their activity are not the same as today (Guns and Vanacker 2013). The case study of slides investigated in MY town (east of the study area) develop with rotational components (circular rupture surface), showing prominent main scarp and back-tilted landslide head (Hungr et al. 2014). They are usually very to extremely slow (few mm per year) with short acceleration events (El Kharim et al. 2021; Obda et al. 2022).

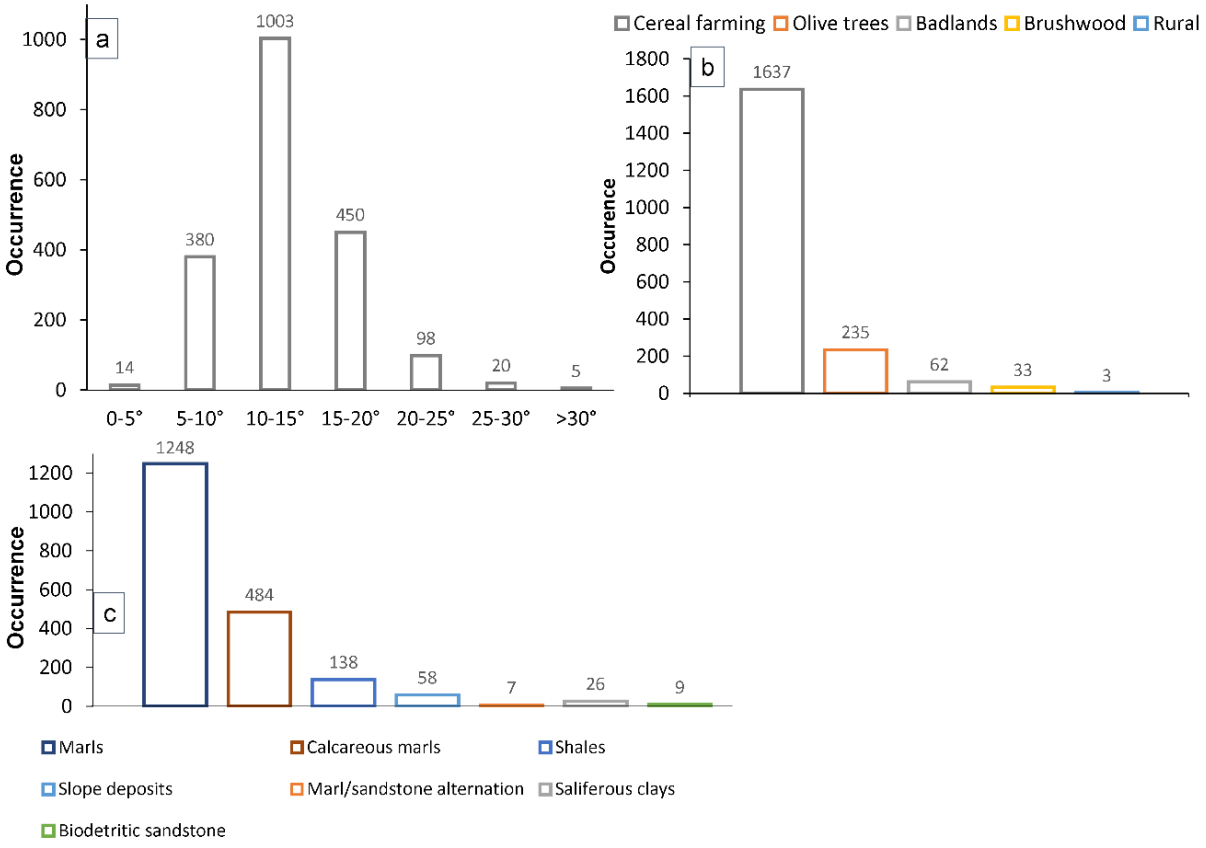

Fig. 109 Diagrams revealing the landslide occurrences by slope ranges (panel a), land use sub-classes (panel b) and by material involved (c)

As for the assessment of the quality and the completeness of the landslide inventory, the probability size distribution of the landslides seems to be well fitted with the double pareto and the three-parameter inverse-gamma models (fig 106d). the rollover is well presented, and the power law does not exhibit a heavy tailed behavior, which means that landslide inventory is quite complete for both ranges, small size/shallow ($<10^4$ m²) and large/deep landslides ($>10^4$ m²) (Qiu et al., 2020; Sahrane et al., 2022) . These quality of the results is quite comparable to the completeness assessing of landslide inventories in V. Eeckhaut et al. (2007); Fausto Guzzetti et al. (2002), and Tanyaş et al. (2019). Furthermore, the landslide size ranges are between 80 and 316,200 m². As for the rollover effect (representing the most frequent landslide range), it is observed at 800 m², which show that the small size landslides are much more frequent. This could be related to differing environmental conditions such as lithology, slope, aspect, and land use practices.

B. Weight and role of landslide influencing parameters

After relating each factor class to slope movements distribution in the contingency tables, the correlation assessment between the factors and the landslides has been performed. Table 18 shows the correlation coefficients (G-K and R) for each factor previously selected. The two factors that have

been discarded are the aspect and the curvature, whose correlation coefficients are not high enough to say that these parameters play a determining role in the landslide hazard (G-K<0.5 and R<0.4). The influencing parameters are listed according to a decreasing order of the R of Pearson absolute value, which does not vary too much showing a moderate to high correlation for all the effective factors. Unlike that, the G-K values indicate a weak to medium correlation for some factors (land use, lithology, dist. from rivers, elevation) and a medium to strong correlation for others.

Slope angle is among the more effective instability factors for all the 3 landslide typologies, having a fairly high G-K and R values (G-K ≥ 0.6). In fact, slope gradient, faults-proximity, elevation, and distance from rivers are strongly connected parameters. In active mountain belts, such as the southern border of the Rif unit (as mentioned before), elevated hillslopes respond to an intense fluvial incision and slope adjustment which generates landslides to compensate for the oversteepening who increases the vertical component of gravity (Burbank 2002; Donati and Turrini 2002; Korup et al. 2010). This domino-effect results in the fact that these 4 parameters usually appear as controlling factors especially in the context of collision belt as the Rif. In the study area, the correlation values of the elevation and the distance to faults are not that high. However, the landslide affected area of the last factor shows that most landslides occur in the first 200 meters from the faults (Table 20). As for the slope and the proximity to rivers, the correlation values clearly express their effective role in the landslide occurrence. Moreover, the landslide affected area of the river proximity factor suggest that most these gravitational processes occur uphill, at the furthest part from watercourses (Table 20).

Surface roughness and TWI are also among the main causative factors in our case showing medium G-K values (0.5<G-K<0.6) and slightly high R values (R >0.6). Surface roughness is considered as a significant conditioning factor in LSM (Abdulwahid and Pradhan 2017). In the specific case of landslides, the study of V. Eeckhaut et al. (2005) have shown that surface roughness can be used to identify landslides shape and estimate their relative age or create an assets landslide map. As for the TWI, it is used to quantify the effect of local topography on hydrological processes and modelling the spatial distribution of soil moisture and surface saturation (Qin et al. 2011). It could also be used for potential debris flow analysis (Chen and Yu 2011; Chen and Chang 2016). In several landslide susceptibility studies, the TWI appears among the main causative factors (Costanzo et al. 2012; Sun et al. 2021), which highlights the effect of soil moisture and surface saturation on landslide occurrence. This, in turn, may be the result of other influencing parameters as the land use.

In fact, the road proximity and the land use are considered as anthropogenic controlling factors that promotes landslides occurrence in this study. The effects of roads and/or trails on slope stability can be summarized as (i) alteration of the natural hydrologic pathways, (ii) undercutting of unstable slopes, and (iii) overloading and oversteepening of the hillslopes (Sidle and Ochiai 2006; Guns and Vanacker 2013). Moreover, field investigations showed that landslides are often associated with bad road

drainage and slope oversteepening, which explains the high R values for road proximity. For the land use, the G-K values are slightly weak, but the R values are the highest. Land cover change induced by human activities significantly controls landslide patterns as vegetation influences slope stability. Vegetation modifies the hydrology of the subsurface (unsaturated zone) by controlling the impact of precipitation and evapotranspiration which affect the amount of water stored in the subsoil. Moreover, roots increase water infiltration and soil hydraulic conductivity (Beguería 2006). Vegetation also has a mechanical effect on the subsoil as roots create an apparent cohesion via root fiber reinforcement that promotes slope stability (Roering et al. 2003; Schwarz et al. 2010). Consequently, the conversion from forest to pastures and agriculture lands results in a rapid decline of the sub soil cohesion. According to Rogers and Selby (1980) study, forms of instability begin to manifest after 3 to 5 years, which corresponds to the time it takes for roots to decay. Furthermore, recent study of Belle et al. (2018) via a hydrological multi-disciplinary approach has shown the importance of maintaining the natural vegetation cover over landslide surface in order to limit aquifer recharge and thus displacements. In the study area, the field investigation shows that significantly fewer landslides are observed in forests, arboriculture zones and brushwood compared with cereal farming areas (fig. 110), knowing that the latter are much more dominant (83% of the total surface). In a recent study (Guns and Vanacker 2013), the analyses of soil physical properties in natural forest soils showed that the saturated hydraulic conductivity is very high (estimated to be 500 mm/h) and the bulk density is very low (0.35 ± 0.13 g/cm3). Also, the observation of high porosity in the forest soils (87 ± 5 %) indicates that water can easily infiltrate and percolate through the solum, which reduces the soil wetness and the landslide activity. Thus, in the study area, the practice of cereal farming to the detriment of forests and brushwood constitutes an effective role in the exposure of slopes to landslides by promoting water infiltration in the sub-surface, which after stormy rain events, triggers shallow landslides.



Fig. 110 Active shallow landslides (a) affecting several cereal farming slopes

The statistical analysis of the influence of the dominant vegetation on landslide occurrence using the probability size distribution have shown that, for both the DP and the IG models, the cereal farming activity promotes more the small size landslides than the olive growing (fig. 111). On the other hand, landslide events occurring in slopes with olive trees, as the main vegetation type, are significantly larger. This finding is statistically attested by:

1. The small size landslides occurring in cereal farming slopes have an area of about 80 m² while for the olive tree slopes, the smallest landslides have an area of about 250 m²
2. The rollover-effect, representing the area of the highest occurrence density, occur at 630 m² in cereal farming slopes and at 1000 m² at olive growing slopes
3. The power law decay of landslide distribution decreases earlier for the cereal farming compared to olive growing, which decreases at a larger landslide size. Moreover, the first decreases more rapidly with an α (angle controlling the power law decay for medium and large landslides) equal to 1.2, while the second decreases with an α of about 1 allowing the power law decay toward larger landslides.

As for the lithology, which is represented by weathered formations, despite the low G-K value, the R ones are slightly high. This parameter is considered among the main controlling factors in landslide susceptibility. Moreover, the low G-K values obtained for lithology do not reflect the real weight of this factor and may even lead to it being underestimated. In the present case, most of the slopes are covered by marls and calcareous marls (equivalent to more than 50%) which reveals the monotony of the lithological factor in the study area. Moreover, 64% of the affected area is part of the marls class and 23% of the calcareous marls class. Which means that these two marly formations represent 87% of the landslide affected area. This leads us to believe that the lithological factor has a very effective role in landslide occurrence. Therefore, to estimate the real weight of this parameter, it is necessary to take into consideration the old, inactive, and eroded landslides that affected the slopes, which are difficult to identify, especially when the weathering and the agricultural practices concealed the topographic features of these mass movements. Furthermore, most of these large and eroded landslides are very old and the factors (except the lithology) involved during their period of activity are not the same as today (especially the faults activity), for the reason that the landslide controlling factors are not fixed in time. Guns 2013 showed in his research that the slope gradient decreases from a predictive power of MPI = 4.395 in 1973 to MPI = 2.558 in 2010. The MPI : measures the parameter importance, evaluates the potential influence of the variable on the probability of event occurrence (Vanwalleghem et al. 2008). However, if some factors are losing weight, the importance of other anthropogenic landslide controlling factors is increasing strongly and cannot be omitted in landslide hazard analysis. Which is the case of the current study where the installation of the road network and the land cover conversion from forests and brushwood to cereal crops are among the most influencing parameters in landslide occurrence.

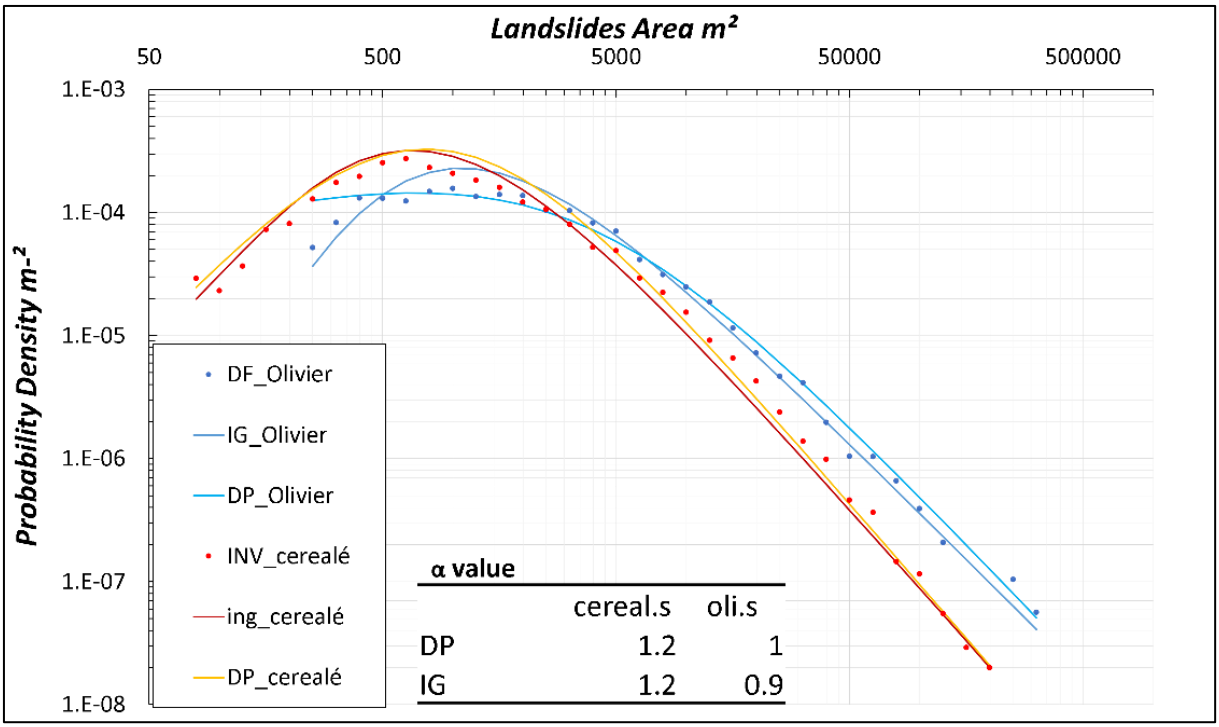

Fig. 111 Double Pareto, Inverse Gamma, and frequency area distribution of landslide inventory in cereal farming and olive trees slopes

C. Susceptibility maps

The landslide susceptibility maps for both GMM and FR methods are presented in figures112 and 113. From a general comparison, the map resulting from the GMM method shows that very low susceptibility levels cover much more areas compared to the map of the FR method Table 21. On the other hand, areas of low and moderate susceptibility levels cover more areas in the FR map. As for the high and very high levels, they cover comparable surfaces.

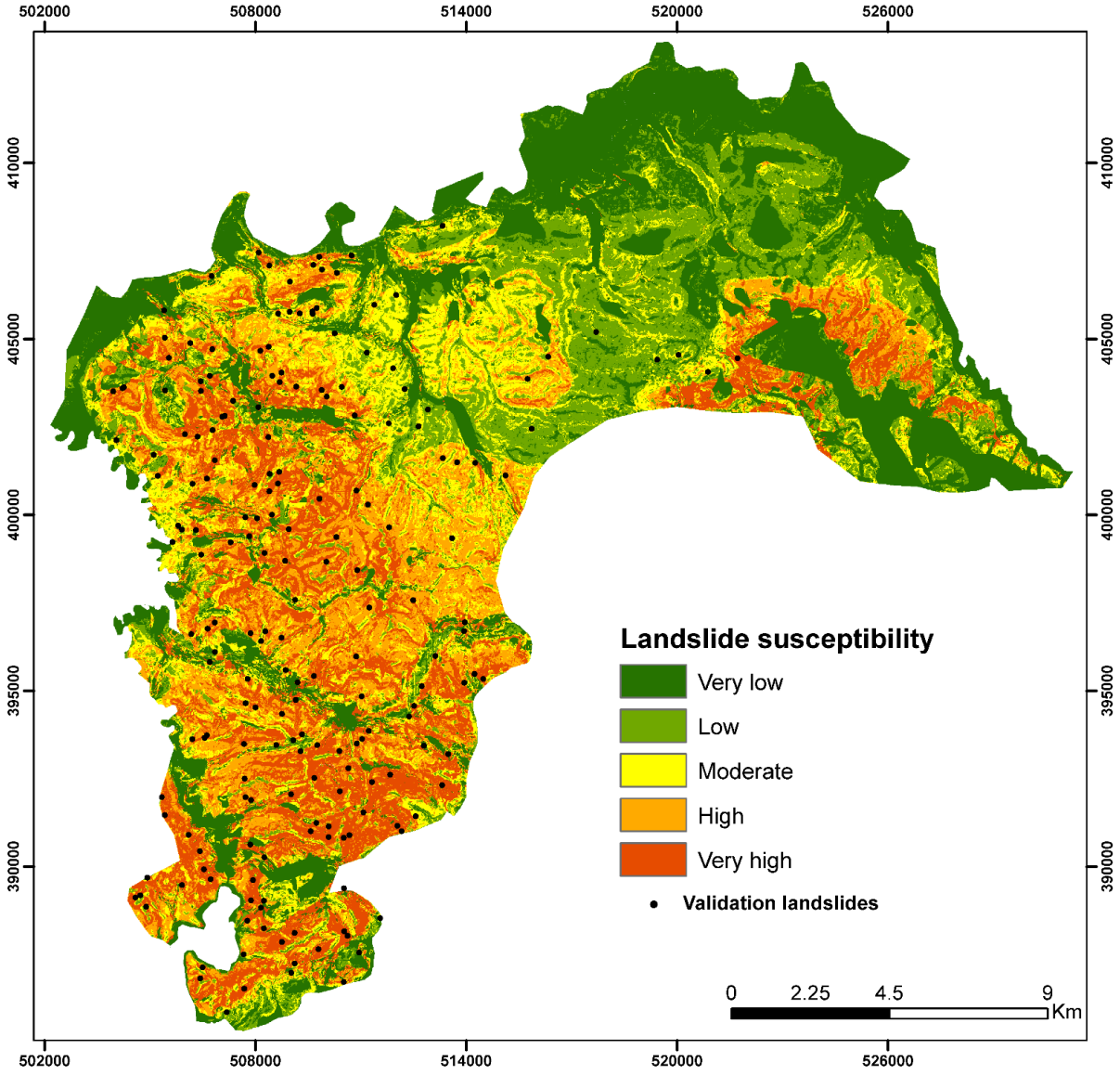

Fig. 112 Landslide susceptibility map drawn using GIS Matrix Method

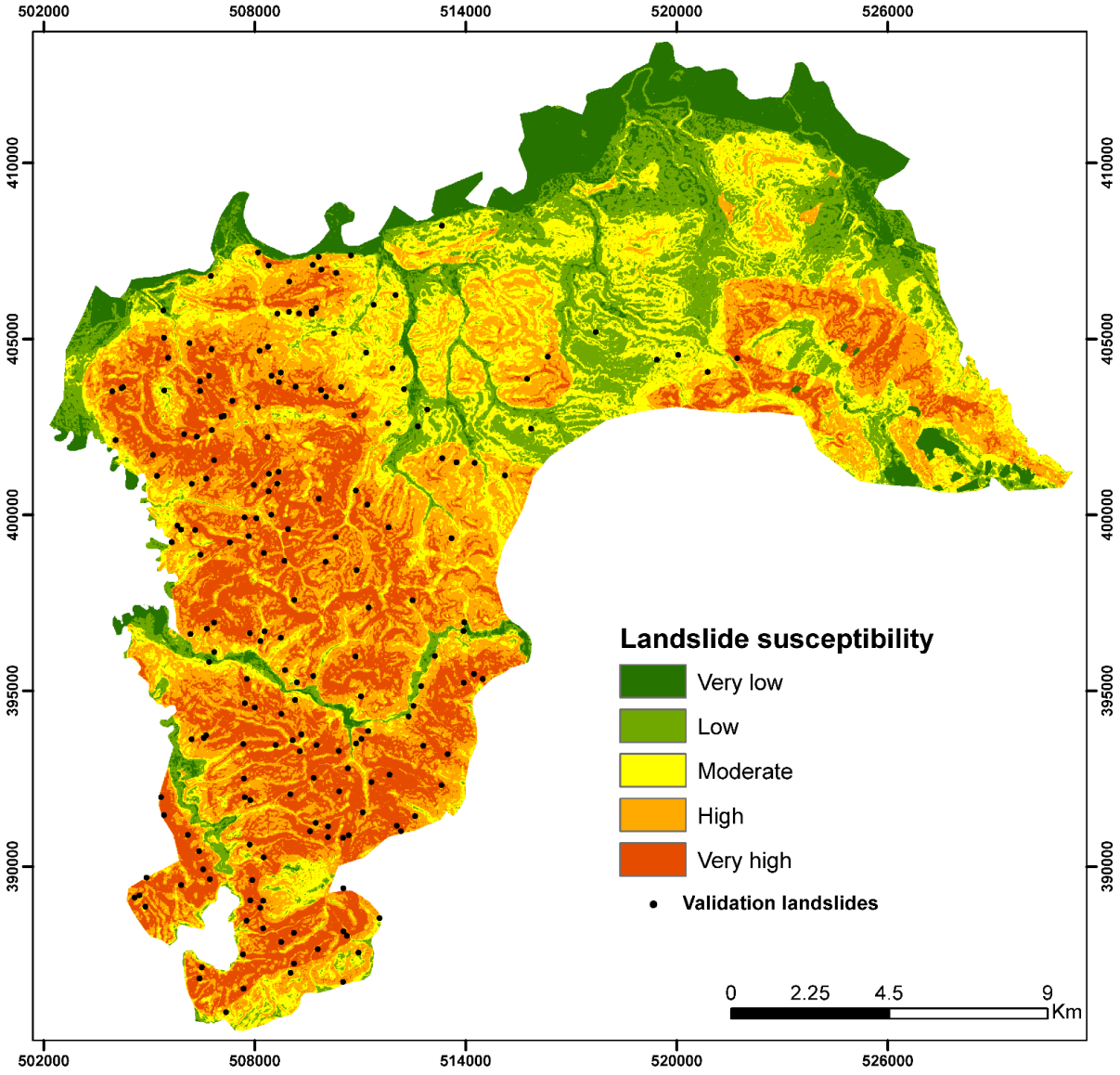

Figure 113 Landslide susceptibility map drawn by FR Method

Table 21 Covering area for each landslide susceptibility class presented by the FR and GMM maps

FR		GMM	
LS	Area covered (%)	LS	Area covered (%)
very low	10	very low	33
low	18	low	9
moderate	23	moderate	13
high	28	high	27
very high	21	very high	18

A cross-comparison between the causative factor maps and those of the landslide susceptibility at a detailed scale have yielded some interesting conclusions about the direct impact of some factor classes on landslide susceptibility. A first observation shows that the valleys and the beds of the wadis have a very low susceptibility to landslides, especially in the GMM map. On the other hand, areas with high susceptibility are featured in the moderate and steep slopes which explains the strong correlation of the slope parameter. Regarding the lithology, the slopes dominated by marls and calcareous marls show high susceptibility levels while shales, saliferous clays and sandstone-marl alternation outcrops seem to significantly increase the slope stability (fig. 115). Moreover, for the land use, the orchards and the brushwood seem to directly reduce the susceptibility level of the areas they cover, especially in the GMM map (fig. 114). Unlike that, most terrains of high and very high landslide susceptibility are dominated by cereal farming. This corroborates what was previously mentioned about the consequences of land cover conversion from natural forests, orchards and brushwood to pastures and cereal farming on the exposure of slopes to landslides in the study area.

Another interesting observation shows that badlands also reduce the landslides susceptibility level of the slopes (fig. 114). Badlands are landform processes that consist in the mobilization of the parent rock downslope by water erosion. They are characterized by steep slopes, minimal vegetation, and high drainage density. Moreover, they inhibit the agricultural use and are devoid of shrubs and grasses that prevent water erosion and infiltrated run-on water during rainfalls (Howard 1994, 2009; Clarke and Rendell 2006), which promotes surface water erosion more than other instability phenomena such as landslides. The latter require water infiltration and moisture storage of the sub surface to be triggered (Garcia-Chevesich et al. 2021).

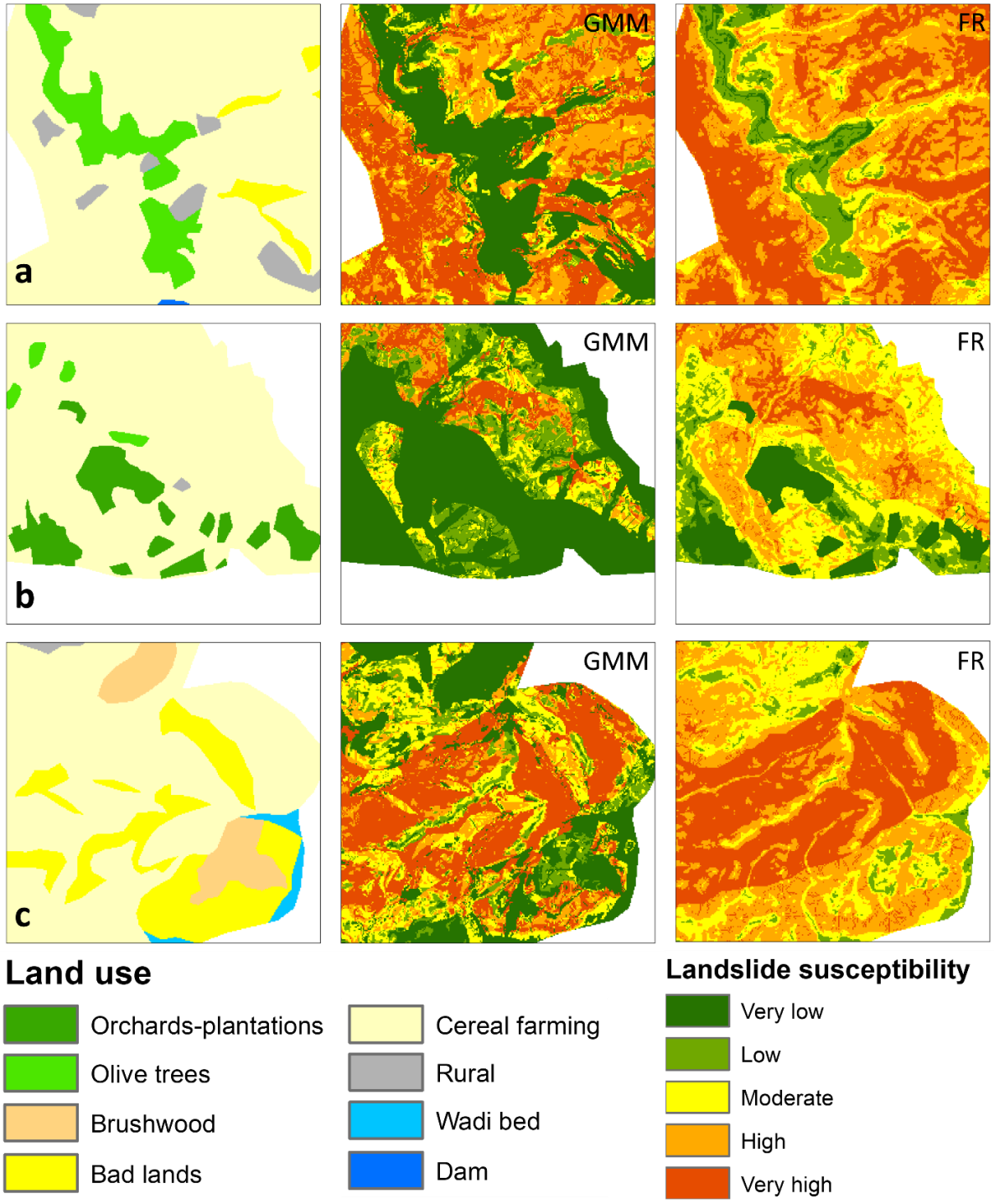

Fig. 114 Noticeable impact of land use sub-classes in mitigating landslide susceptibility level of both maps FR and GMM; a effect of brushwood, b effect of orchards, c effect of Badlands and brushwood

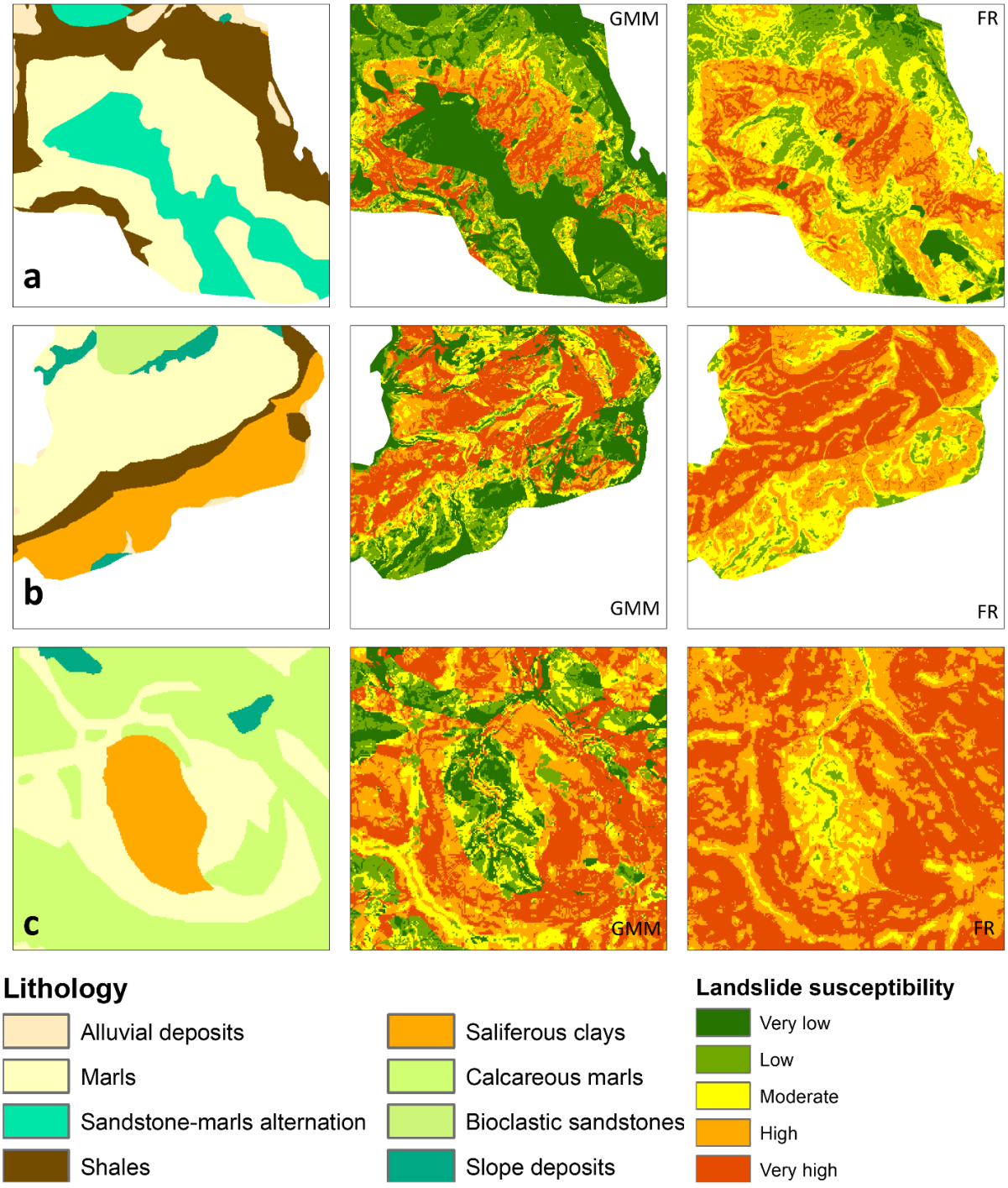

Figure 115 Noticeable impact of lithology sub-classes in mitigating landslide susceptibility level; a. impact of sandstone-marl alternation; b and c. impact of saliferous clays

D. Quality control of the landslide susceptibility maps

The DF values for the very low and low susceptibility classes are 2% and 11% respectively for FR and GMM maps while the values for the high and very high susceptibility classes are 87,3% and 68% respectively (fig. 116). In fact, the quality of these landslide susceptibility maps tested by the degree of

fit method shows good values for each landslide susceptibility map, with a slight advantage for the FR method.

As for the AUC curves, they were plotted based on the number of correctly classified pixels (true-positive) and the number of the incorrectly identified pixels (false-positive). The AUC values for FR and GMM methods were estimated as 0,743 and 0,752 respectively (fig. 116). These comparable results show effective landslide susceptibility modelling, knowing that AUC values between 0.7 and 0.9 indicate good discrimination ability (Swets 1988).

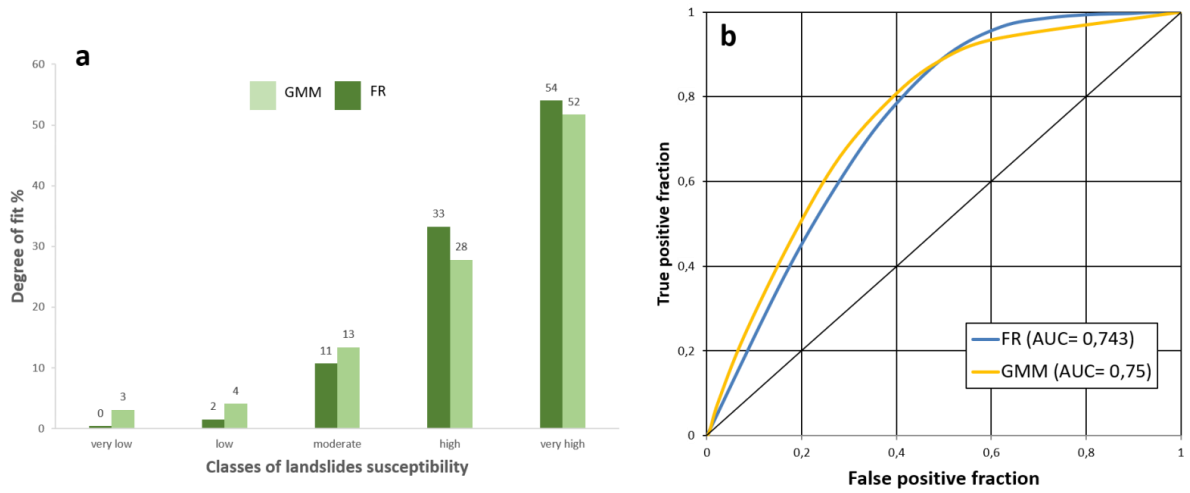

Fig. 116 Quality control results of the two susceptibility maps; a Degree of Fit method, b Area Under the ROC curve of the landslide susceptibility maps generated by FR and GMM models

5. Conclusion

The morphological analysis (interpretation of aerial photos, satellite images, and fieldwork), GIS and statistical analyses allowed to prepare a necessary database to assess the landslide susceptibility using two different methods, the GIS Matrix Method and the Frequency Ratio. The method allows the selected factors to be evaluated classifying them as "effective" or "non-effective" and discarding the non-effective ones. The option of organizing the controlling factors according to a statistical correlational could save both economical and time resources in risk prevention strategies. Also, the exclusion of poorly related predictive variables allows to reduce the complexity of the susceptibility model, which in turn becomes easier to be interpreted from a geological point of view.

In fact, in the present study, the anthropogenic factors seem to be among the most effective influencing parameters in the study area, which highlights the impact of human practices such as land cover conversion from forest, arboriculture areas and brushwood to cereal farming lands. Apart from that, TWI, slope roughness, lithology, slope gradient, elevation and faults proximity are all effective parameters promoting landslide occurrence in the study area. Moreover, we tried to map the susceptibility to landslides in a geomorphologically homogeneous context, where influencing factors

are monotonously repeated over almost the entire study area. In this case, the most efficient method is the one that is less influenced by this homogeneity and gives liberating results with a little detail, this is recently asserted in Sahrane et al. , (2022; a and b). Thus, according to the results of the susceptibility maps produced (fig. 112, 113 and table 21), the FR model seems to amplify the level of susceptibility and is less influenced by the variation of factors such as the land use and the lithology (Table 21, fig. 114 and 115). On the other hand, the cartographic comparison shows that the classes which, according to the statistical results of the landslide affected area (Table 20), are supposed to reduce the susceptibility to landslides, reduce it more in the GMM map than in the FR map (e.g., brushwood, olive trees and orchards, badlands) even in detailed scale, despite the homogeneity of these classes at a broad scale. This confirms that the GMM model gives more liberative results.

This type of map constitutes an essential database to guide urban planning and food production plans in the region. However, the use of these data must seriously consider the influencing parameters identified in this study. Thus, in areas with high susceptibility levels, the risk mitigation could be well oriented and effective while saving time and costs. Furthermore, the models can trustfully be applied in other regions with similar geomorphological and geological contexts, especially in the Pre-Rif region.

Based on the results of these two accurate and practical methods, the future research could be directed towards improving the accuracy of these models by testing different combination of influencing parameters and comparing the results at a regional scale. This method will allow to find the most effective combination for accurate susceptibility results and then, be reliably applied in similar regional contexts.

VII. Chapter 5: Multi criteria assessment approach of slow-moving urban landslide hazard: the case of Moulay Yacoub town (Morocco)

1. INTRODUCTION

Slope mass movements are among the most widespread geological hazards in the world (Schuster, 1996; Schuster and Highland, 2001). In urban extensions worldwide, the local construction and land use practices on hillslopes prone to instability cause an increase in landslide occurrences in the last few decades, sometimes with heavy social and economic impacts (Glade, 2005; Schuster and Highland, 2007; Antronico et al. 2014; GAR. 2009, 2019). Despite this, the true consequences of such phenomena are still poorly quantified (Petley 2012).

In Northern Morocco, not far from Moulay Yaacoub (MY), a cliff collapse in an abandoned stone quarry killed 52 people in 1989 at Fez city. In addition, constructions at the suburban neighbourhoods of Tetouan and Chefchaouen cities also suffer from landslide induced damage caused by the persistent instability of the fine-grained sedimentary rocks outcropping in these areas (El Kharim et al. 2001; El Kharim, 2002; El Kharim et al. 2021). However, the landslide hazard is shown to be higher in the presence of expansive and dispersive marls (Fall & Sarr, 2007; Jiang et al., 2013, Medjnoune et al, 2014). Although the Swelling-shrinkage behaviour of the natural expansive clays does not cause loss of life, it generally constitutes a significant georisk because of the extensive material damage that it causes to buildings and infrastructures (Al-Rawas & Goosen, 2006; Ejjaaouani, 2008). In this regard, it is estimated that billions of dollars in damage worldwide are the direct consequence of soil deformation caused by expansive clays and clay-shales, more than all other natural hazards combined (Jones and Holtz, 1973). For instance, more than 4 million houses in France are potentially highly exposed to such risk (Antoni et al. 2017). In MY, the series of collapse events continue to threaten the buildings and residents of the city.

Of the numerous past events in this region, we cite only the most recent occurrences which caused the collapse of a house in May 14th, 2018; the collapse of a roof in one of the spas in December 11th, 2019 thus injuring many tourists; and the collapse of a retaining wall in April 18th, 2021 at the old district which alerted the authorities and caused terror among residents. In order to prevent similar future occurrences, the state has invested more than 20 million MAD (approximately 2 M$) in the reinforcement of the potentially instable eastern slope and the stabilization and reconstruction of more than 35 severely damaged buildings.

From a geological standpoint, the marly soils of the peri-mediterranean Neogene formations that dominate the hillslopes of MY district, are known by: i) their propensity to swelling-shrinkage and dispersion, ii) the damage that they cause to constructions and iii) their persistent instability (El Amrani N. et al 1998; Lamas et al. 2011; Mazo et al. 2009, Faulkner et al 2003; Faulkner 2013;

Medjnoun 2014; Medjnoun et al. 2014; Abolmasov et al. 2015; Alonso et al. 2015; Lainas et al 2016). Such behaviour is attributable to the mineralogy of this material, which is characterized by the presence of smectites (montmorillonite group) and irregular mixed-layer clays. In fact, such minerals owe their origin to the leaching processes that have affected paleosoils developed under the subarid-temperate paleoclimate of the Upper Miocene epoch (Chamely 1989, El Kharim 1991; John et al. 2003).

Several techniques are commonly used to characterize these geomorphic processes depending on the aims of the study (body morphometry and affected areas; kinematic and activity aspects, controlling factors, hazard mapping, associated vulnerability, dating and historical evolution …). In effect, at the exception of a few unidisciplinary studies, most current researchers opt for multi-disciplinary approaches, which allow for a more holistic understanding of these complex phenomena. For site-specific case studies, such investigations combine geological, geotechnical, and geophysical data in order to analyse all aspects of the slope instability phenomenon (Chacón et al., 2006; Friedel et al. 2006; Fell et al., 2008; Jongmans et al. 2009; Malehmir et al. 2013; Merritt et al. 2014; Malehmir et al. 2014; Solberg et al. 2016; Crawford et al. 2018; Rezaei et al. 2018; El Kharim et al, 2021; Bounab et al 2021).

Geophysical surveys as rapid, inexpensive and non-destructive tools allow to obtain valuable information about the sub-soil structure in the form of vertical and horizontal variations of physical parameters, which can be used to determine the depth of the rupture surface and its geometry, as well as the thickness of the landslide body (Jongmans et al. 2009, Rezaei and Choobbasti 2014, Rezaei and Choobbasti 2017b). However, contrary to the borehole and inclinometric surveys, which constitute so far, the most reliable method for the detection of a landslide's slip surface, geophysical in-situ analysis can only be accurately used in cases where a clear geophysical contrast exists between the landslide body and the underlying non-displaced layers (Jongmans et al 2009, Pilz et al 2014).

Regarding the activity of landslides, researchers nowadays deploy several monitoring techniques to measure the activity of landslides by means of remote sensing methods, such as LiDAR and InSAR (Jaboyedoff et al. 2012, Antronico et al. 2013; Calò et al. 2014, Castaldo R. et al., 2014; Crosetto et al. 2016; Del Soldato et al. 2018; Infante et al. 2018; Peduto et al. 2021), and GNSS measurements and products resulting from UAV data processing which are also commonly used as of late (Lindner et al., 2016; Rossi et al., 2018; Aggeliki et al., 2021). These techniques proved their capacity to accurately document and monitor landslides with accuracies lower than 10 cm. These new techniques are low-cost and have proved to be very effective for studying deformation patterns in slow-moving landslides, especially in areas where man made facilities are present, which can be used as an indicator to support the results.

In the Fez and MY surrounding, where marly formations dominate the hilly topography of the region, few studies have dealt with landslides and the techniques described above were never used. In fact, the studies performed in the region are limited to a description of the observed phenomena or simply dealing with certain aspects of these multifaceted processes (Avenard 1965, Faleh and Sadiki 2002, Gartet 2010, Cherai et al, 2017). Given the abundance of landslides and the damages they induced to constructions at the town of MY (Obda, 2017; Obda et al, 2018), this work aims to characterize landslide processes in this area using the state-of-the-art techniques described above. The multi-disciplinary approach followed in this study is tailored for the investigation of such instability phenomena in densely built areas. It is based on a cross-analysis of field investigations, geotechnical and mineralogical characterization results, inclinometer and PS-INSAR (Persistent Scatterer Interferometry Synthetic Aperture Radar) displacement monitoring data, seismic noise surveys and building damage assessment results. The findings of this study would surely help to bridge the knowledge gap in similar contexts of the region and to establish an instability model for the Neogene marly formations, based on a large set of data.

2. Settings of the study area

The MY town is geologically sited at the southern part of the Rif Mountain chain, a subsiding area dominated by thick Neogene marl formations of the Upper Miocene epoch. Geological maps, 2D sections and borehole data show the presence of underlying Triassic and Cretaceous material, comprised respectively by red clays embedded in doleritic basalts and marls, which outcrop to the north of MY (Lakhdar et al. 2006) (fig. 117). This so called, Rif foreland basin occupies an intermediate position between two major structural units, the Prerif to its north and the Middle Atlas to its south (Sendide 2000; Winckel 2002; Lakhdar et al. 2004; Charroud et al. 2007) (Fig. 117). The former unit is made of the Prerif marly overthrust nappes mainly comprised of Cretaceous and Tertiary material. As for the Middle Atlas, it consists of a set of plateaus that overlook the Saïs basin. Their origin is contributed to a SW-NE flexure mechanism (Termier 1936; Martin 1981; Piqué et al. 2000). Neotectonic studies, regional GPS network data, and seismicity records corroborate recent and active tectonic mechanisms at the region, manifested in a SW to SSW verging displacement of about 1 to 5 mm/year with an average of about 2mm/year (Bargach et al. 2004; Chalouan et al. 2014, Poujol et al. 2017, Agharroud et al 2021). In addition, the tectonic structure at this region is characterized by a remarkable alignment of thermal springs with tectonic fractures, including hot springs of MY town which constitute a great touristic attraction (Rimi, et al. 1998; Winckel et al. 2002; Barkaoui et al. 2014, 2015; Sabri et al. 2019).

From a geomorphological point of view, the abundance of Miocene marl outcrops near MY contributes to the formation of a gentle hills landscape. On the field, one can clearly see the impact of

various surface water erosion processes (sheet, rill and gully erosion) indicating the relative impermeability of the subsoil layers, their friability as well as the strong action of surface runoff processes. The drainage pattern is non-perennial and quite dense.

Regarding the climate, MY is part of the subarid bioclimate level with an average annual precipitation value of 314 mm. In fact, the MY rainfall distribution is bimodal with a first maximum in March and a second in November. Rainfall data of Fez and MY meteorological stations show that most precipitation events come in the form of thunderstorms characterized by high intensities and short durations (2 to 10 days), which expresses the severe seasonal contrast of the study area.

In regard to the socio-economic situation of MY, a population increase has been recorded during the last two decades (Table 22). This demographic development is related to the on-going urbanization of MY, mainly fueled by the tourism and commercial activities related to the previously mentioned hydrothermal springs. Moreover, the urban expansion of this small town is mainly in the shape of unregulated, dense construction (especially in the west flank of the MY hill), where several types of construction practices co-exist (cement, masonry … etc.) (Table 22). In the old town, where most houses are self-built, the clandestine character of the houses is more evident. The reason for this situation is the fact that construction according to the appropriate standards proves to be unaffordable for most residents of the town. In this regard, the Public Utilities Committee reveals the fact that most of the ramshackle homes in the town of MY are a time bomb threatening the safety of the local population. Moreover, the sewage network doesn't cover the entire urban perimeter knowing that 20% of households still use septic tanks (RGPH 2014) and the local authorities declare that more than 20% of the sewerage network is damaged.

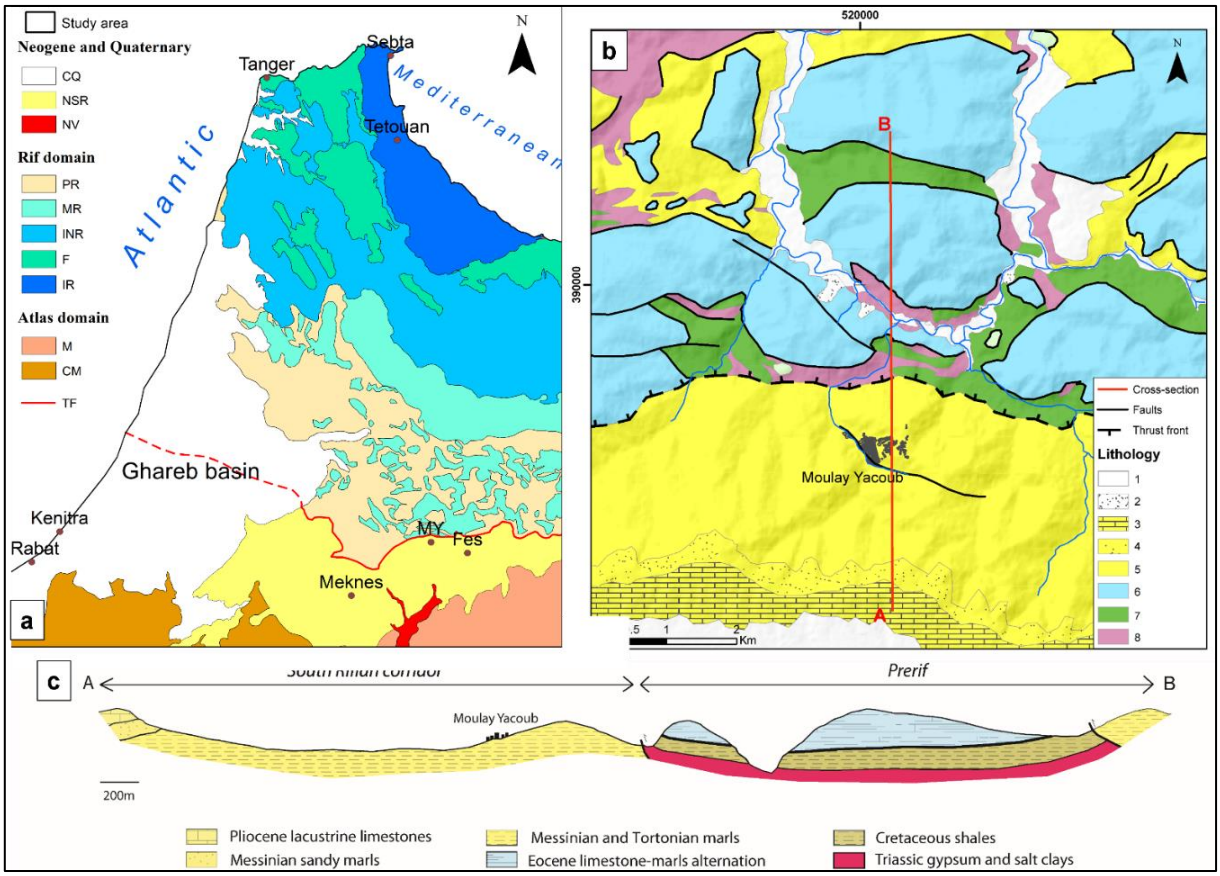

Fig. 117 a. Structural domains of northern Morocco (Base map from Suter G. 1980): (CQ) continental quaternary, (NSR) Neogenic South-Rifian corridor, (NV) Neogenic volcanism, (PR) Prerif, (MR) Mesorif , (INR) Intrarif, (F) flysch unit, (IR) Internal Rif, (M) Mesosoic blanket, (CM) Caledonian western Meseta; b. Lithological map of the MY region (Base map from Fès-Ouest geological map; SGA, 1942): (1) Soils and alluvial quaternary deposits; (2) colluvium; (3) Pliocene lacustrine limestone; (4) Messinian sandy marls; (5) Tortonian and Messinian marls; (6) limestone-marls alternation of Ouazzane unit (7) Cretaceous shales; (8) salty red clays of the Prerif unit ; **c** Simplified geological cross-section of MY's region

Table 22 Urban population and housing type of MY

Municipal population (by number of inhabitants) each census year	
2726 in 1994 / 3153 in 2004 / 4548 in 2014	
Housing Type in 2014	
Moroccan Modern Houses 1 to 2-storey	76 %
Basic housing and rural-type	19.3%
Villa or villa floor	3.6%
Apartment in a building	0.1%
Public establishments and other	0.9%

Housing age in 2014	
Under 10 years	9.1%
10 to under 20 years	17%
20 to under 50 years	45%
50 and over	29%

RGPH, 2014.

3. Methods

A. Geotechnical Analysis

To obtain samples for laboratory tests and gather geotechnical data about subsoil layers at the MY town, three core drillings and pressuremeter tests (Sp2, Sp4 and Sp6) were carried and equipped with borehole inclinometers (i1, i2 and i3) that were monitored during the period 2016-2017 (Fig. 119) (LPEE 2017, Obda 2017). Then, three core samples were extracted from the geotechnical boreholes, and used for conducting several laboratory tests, which include soil-identification tests (grain-size distribution by sieve analysis and sedimentation, Atterberg limits testing, degradability analysis, methylene-blue absorption, calcium carbonate analysis). Additional direct shear and oedometer testing were performed on saturated samples in the aim of obtaining their mechanical properties.

The samples C1, C2 and C3 were taken from the SC2 core at three different depths 1.5-3m; 3.5-4.5m and 8-9m respectively. Five other samples (X1, X2, X3, X4 and X5) were extracted from bedrock outcrops. In fact, the samples X3 and X4 were taken from grey compacted marls outcropping in the perimeter of the study area, while X1, X2 and X5 were excavated from weathered yellow marls. For comparison purposes, the X1 sample was taken from reworked marl material, X2 from undisturbed weathered marls and X5 from marly material outcropping in the depletion zone of a rotational landslide (Fig. 119). This sampling strategy allows comparing the geotechnical parameters of marly material under different geomorphological and erosional circumstances (weathered unsaturated marls, shallow creeping marls, marly landslide material and deep compacted grey marls). In addition, these five samples (X1, X2, X3, X4 and X5) were subjected to standard X-ray diffraction as a natural powder pattern as well as clay thin sections. This mineralogical characterization of marl formations allows to see if the material is more prone to swelling-shrinkage or landslides hazard (Medjnoun et al. 2014; Faleh et al. 2002; Jian et al. 2009; Djerbal et al. 2012; Regmi et al. 2012; etc.).

B. Seismic survey

Knowing that most of the study area is built, which hinders our ability to conduct field investigations or use other remote sensing techniques (interpretation of aerial photographs) to

understand the subsoil structure, we opted for an investigation technique that is adapted to the reality of the terrain. The technique chosen is the H/V ratio technique (Nakamura et al 1989), which allows completing borehole data and understanding the spatial distribution and geometry of weathered layers. In fact, the core drilling (SC) and pressuremeter tests campaign (Sp) did not cover the entire urban area. Consequently, the use of 26 seismic noise stations was deemed important to support the borehole data results in the old town area and to also define the geometry of colluvium and weathered clayey marls as well as the potential landslide slip surfaces in the rest of the study area. H/V measurements were also conducted in two cases of surficial soil creep located to the north and the south of the study area, so as to determine the depth of the involved material. The seismic velocity (Vs) of the first layers is obtained by the MASW method and the thickness (H) is calculated by modelling.

Seismic noise measurement by the H/V method (proposed by Nogoshi and Igarashi (1971) and diffused by Nakamura in (1989)) is generally used to estimate the seismic response of sedimentary layers on rocky substratum (Field et Jacob 1995; Guéguen et al. 2000; Bonnefoy-Claudet 2004; Guillier et al. 2008, etc.). It is based on the numerical recording of ambient seismic noise generated by natural or anthropogenic sources (waves, wind, traffic, etc.) using a three-component seismometer. Then, a spectral ratio between the horizontal and vertical components is calculated. When the impedance contrast is high enough, the spectral ratio H/V exhibits a peak (Bonnefoy, 2004) on the f_0 resonance frequency, where:

$$\boldsymbol{f_0} = \frac{V_S}{4\mathrm{H}}$$ (in the case of a single flexible and homogeneous layer)

On the other hand, Gallipoli (2000), Méric (2007), Jongmans (2009), Hellel (2011), Pilz (2014) and Harba (2017) applied this technique, assuming a constant V_S value, to estimate the depth of landslide slip surfaces, knowing that the latter corresponds to a frequency contrast. All the resulting peaks were then modelled in order to map the geometry of the landslide body. Following this approach, we used six measurements of the multichannel analysis of surface wave method (MASW) (Gang Tian 2003), to obtain the surface seismic velocity value (V_S), which is necessary to model the peaks in areas where no data is available regarding the depth of the soil-bedrock boundary (Fig. 118).

The active MASW method was introduced in surface geophysics in the late 1990s by Choon B. Park. It adopts the conventional survey mode using an active seismic source (e.g., a hammer) and a network of linear receivers, collecting data in a "roll-along" mode (Park et al. 2007). The method uses surface waves that propagate horizontally along the measuring surface directly from the impact point to the receptors. It provides V_s information in 1D (depth) or 2D (interface depth and location) in a cost-effective and fast way. The maximum depth of the investigation (z max) is usually between 10 and 30 m, but it may vary depending on the site and the type of the active source used. According to Bonnefoy (2007), Marc (2007) and Méric (2007), shear wave velocities inferior to 300 m/s or ranging

from 120 to 300 m/s, are due to the presence of shallow weathered clay materials. This physical property of landslide deposits is exploited by Jongmans (2009) who used this V_s contrast to map the geometry of a landslide body in the Trièves area (French Alps).

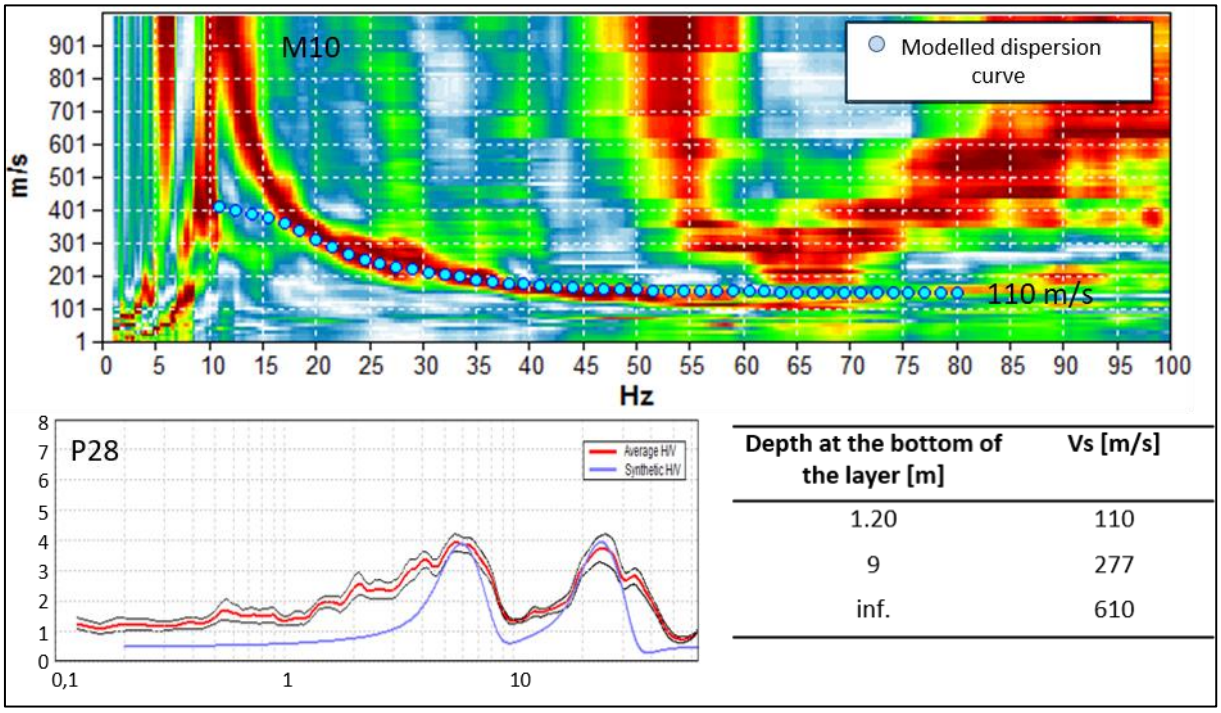

Depth at the bottom of the layer [m]	Vs [m/s]
1.20	110
9	277
inf.	610

Fig. 118 Example of modelled H/V peaks using MASW surface VS, case of the P28 and M10 measurements of the MASW and H/V surveys respectively

C. Field investigations

Landslide geomorphological features (scarps, tension cracks … etc) at the study area were identified and localised during several field surveys. Damage to buildings caused by landslides was also assessed in MY town during the same field trips. Particular attention was paid to the cracks that are characteristic of buildings constructed on unstable slopes. Such types of damage are manifested in the form of wall bursts and oblique cracks (about 45 degrees) from corners to adjacent openings and connecting doors and windows (Ransom 1981; Mika and Desch 1988; Zumraoui et al. 2017). Then, buildings of the MY town were classified into 6 severity classes according to the classification of Burland (1977) also used by Peduto et al. (2017) for the same purposes. This classification system discriminates between buildings based on the width of cracks affecting building facades, their distribution as well as the ease of restoration (Table 23). Other criteria presented by Del Soldato (2019) were also taken into consideration in the present work in order to update this somewhat simple effective method. Therefore, we have adopted the 6 classes of the so-called classification to which we have added the In and Cb, corresponding respectively to intact buildings, usually recent and unaffected, and collapsed ones (Table 23). For the assessment of each individual building, a degree of damage severity is added if one of the three, above mentioned circumstances manifest. We quote the

fissures that affect building structures and foundations, a differential settlement manifestation and the opening of joints between constructions. The spatial distribution of the damage is reported on a building damage map.

Table 23 Damage severity levels along with their description

In	Intact building
D0 (Negligible)	Hairline cracks are mainly caused by shrinkage and thermal gradients. Typical widths are less than 0.1 mm
D1 (Very slight)	Cracks are fine and rarely visible; they can be easily treated via normal decoration. Typical crack widths are up to 1 mm.
D2 (Slight)	Visible cracks can be masked by suitable linings or easily filled. Doors and windows might stick slightly. Typical crack widths are up to 5 mm.
D3 (Moderate)	Cracks are quite visible; they require some opening up and can be patched by a mason. Doors and windows might stick, whereas service pipes might fracture. Typical crack widths are 5-15 mm.
D4 (Severe)	Widespread cracks and extensive damage that requires breaking out and replacing sections of walls, especially over doors and windows. Settlement might cause slight tilt to walls and onset of fractures to structural elements. Typical crack widths are 15-25 mm, but also the number of cracks is to be taken into account.
D5 (Very severe)	Extensive cracking with structural damage that requires a major repair job involving partial or complete rebuilding. Settlements might cause tilt to walls and instabilities requiring the building evacuation. Typical cracks widths are greater than 25 mm, but also the number of cracks is to be taken into account.
Dc	Collapsed building

Burland 1977 and Peduto 2017.

D. Insar Displacement Monitoring

Ground displacement velocities over MY urban and sub-urban area are obtained using the Persistent Scatter SAR Interferometry technique (PSInSAR; Ferretti et al 2001). To do so, 21 Sentinel1 images (from 30.09.2016 to 09.06.2017) acquired on descending orbit, were used. This acquisition geometry was picked due to the fact that MY is built on an East facing slope, which means that displacement along the satellite Line Of Sight (LOS) and the maximum slope azimuth are nearly parallel. The survey period is chosen to support the inclinometers monitoring and to provide a better overview of the sliding kinematics. To obtain coherent interferograms and to avoid noisy results, the

SAR pairs used have a temporal baseline of 10 to 15 days maximum and a vertical baseline smaller than 150 meters. In addition, the high density of man-made facilities on the MY hillslope, which act as stable scatters (Sousa et al 2011), results in coherent interferograms. Thus, a good Permanent Scatter density is expected. The data preparation and processing is performed using the SNAP-Stamps processing chain (Hooper et al 2012; Foumelis et al 2018). The topographic data used for co-registration and interferogram formation is the high resolution (12.5 meters) ALOS PALSAR Digital Elevation Model. Finally, the displacement velocities and the building damages maps are cross-analyzed to get an insight into the kinematics of the study area.

4. Material

Regarding the geophysical characterization, the H/V and MASW surveys were carried out using the "TROMINO" device, which is a three-component digital tomograph designed for recording and processing ambient noise (Castellaro and Mulargia, 2009) and vibrations. The modelling process of the frequency peaks (for the H/V technique) and the MASW spectrum was executed using GRILLA software.

Moreover, the field visual interpretation and the landslide inventory were obtained according to an update of the Varnes classification (Hungr et al., 2014) and using free satellite and aerial images like Google Earth (GE) and similar (e.g., Bing Maps 3- D, MY aerial photos). The latter were chosen because of the respectable spatial resolution as well as their easy access to updated cartography and of the possibility to dynamically manage the slope angles.

5. Results

MY urban center is constructed on the western flank of a Miocene marly hill. Its total elevation contrast reaches 400 meters with moderate to steep slopes (between 20 and 25 degrees). On the surface, desiccation cracks affect the yellowish hued marls which are relatively friable due to surficial weathering action. In areas impacted by deep water incisions or large human excavations, compact grey marls (substratum facies) outcrop.

Stratigraphic logs extracted from the core drillings and pressuremeter results show that the substratum material is reached at various depths, with a maximum of 20 meters (Fig. 119 and 120) (Obda 2017). Similar thicknesses of the weathered layers are also recorded by H/V tests across the study area (Table 24/ Fig. 129). In all H/V ratio profile, a peak is observed around the 3.1 Hz frequency, which corresponds to a fairly deep separation surface (up to 17m) between the weathered layers and the marl bedrock. In addition, a secondary peak (f_0 = 1.5Hz) is observed, the modelling of which reveals a depth of approximately 34m which probably corresponds to a deeper geological boundary. In fact, lithostratigraphic logs presented by Lakhdar et al. (2004) and Charroud et al. (2007) showed that around MY, sandstone layers are found, which may explain our observations.

Regarding V_s values used for constructing the H/V model, the fundamental spectrum of the MASW measurements yield low V_S values (V_S <200 m/s), especially for the M10 measurement where the V_S starts at 110 m/s (Fig. 118), which characterizes the weathered and saturated marls found near the surface.

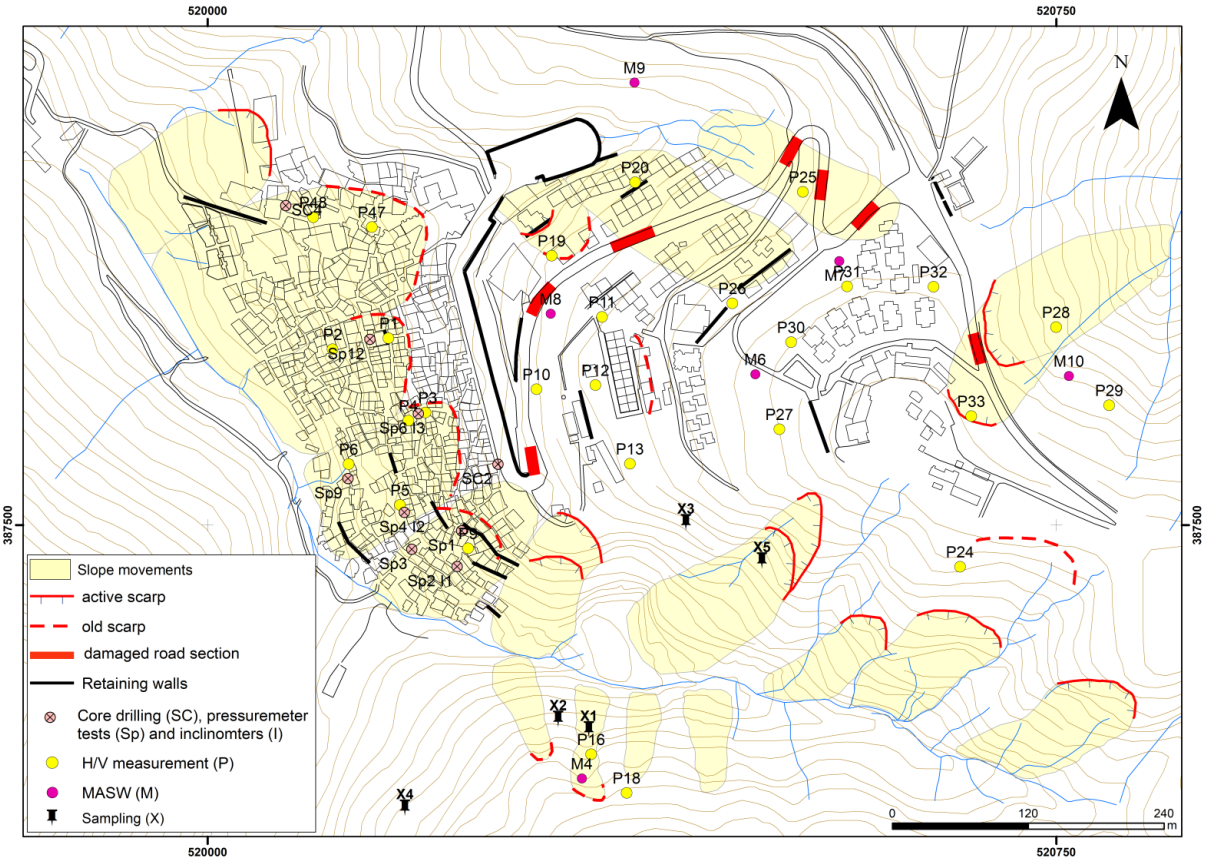

Fig. 119: Slope movements, boreholes, MASW and H/V distribution and sampling locations (road network, building basic data from Moulay Yacoub google earth images; topographic data from Moulay Yacoub topographic map 1/25 000; ANCFCC 2007)

Table 24 Seismic noise measurements, peak frequency, interface depths (modelled) and VS-velocity of the surface layer

Measurement	Peak frequency (Hz)	Interface depth (m)	VS-velocity of surface layer (m/s)		Measurement	Peak frequency (Hz)	Interface depth (m)	VS-velocity of surface layer (m/s)
P1	9 to 7.5	5 to 7	180		**P20**	23 and 5.8	2 and 9.5	180
P2	10	5	200		**P24**	7.6	6	180
P3	9.2 and 3.6	5.5 and 14.5	200		**P25**	4.3	13	190
P4	11.5 and 3.4	4.6 and 15	200		**P26**	11.5 et 3.8	3.7 and 13	190

P5	8 and 3.8	6.4 and 14	200		**P27**	4.4	12	200
P6	10.3	5.2	200		**P28**	23 and 5.9	1.2 and 9	110
P10	3.5	15	195		**P29**	29.5 and 6.8	0.8 and 7	110
P11	18.5 and 3.8	2.5 and 14	200		**P30**	3.2	16	190
P12	4	13.5	200		**P31**	13.5 and 4	3.3 and 13.5	190
P13	3.1	17	220		**P32**	4.75	11.8	190
P16	12 and 7.9	3.8 and 6	185		**P33**	32 and 5.6	0.7 and 10	190
P18	6.1	7.5	190		**P48**	9.3	5.5	200
P19	11.5 and 4.5	4.3 and 11.5	200					

A. Marls geotechnical and mineralogical characteristics

Laboratory test results show that grey marls (C3, E8 and X3 samples) are lean (according to USCS), clayey (50% of particles less than 2 μm) and have a low plasticity (A3-type soil according to GTR classification) with an absorption capacity and water content in the range of 4g and less than 8%, respectively (Table 25). These characteristics are likely due to their relatively high rates of $CaCO^3$ (>60%) which provides a cohesion of no less than 29 kpa, a friction angle around 20° and an average degradability index. Their compression and swelling rates are below 0.23 and 0.046, respectively. Nevertheless, samples taken from shallow marls (C1, C2, E9, X1 and X2) are plastic to very plastic (A2 according to the GTR classification), of fat clays type (USCS classification) and relatively more loamy than deep marls. Their absorption capacity and natural water content are much more important (about 6g and above 10% respectively). These surficial marls are easily deteriorated, with cohesion values less than 20 kpa and a friction angle higher than 23°. Their compression and swelling rates are respectively greater than 0.2 and 0.05, makes this surficial material quite strongly susceptible to compressibility and swelling. According to the classification of Philipponnat (1978) and Chassagneux et al. (1996), such high-volume change values would constitute a very high risk of swelling shrinkage to human facilities. Moreover, the liquid limit and the plasticity index prove that all samples are characterized by a high expansive potential according to Holtz and Gibbs (1956), Chen (1975) and IS (1977).

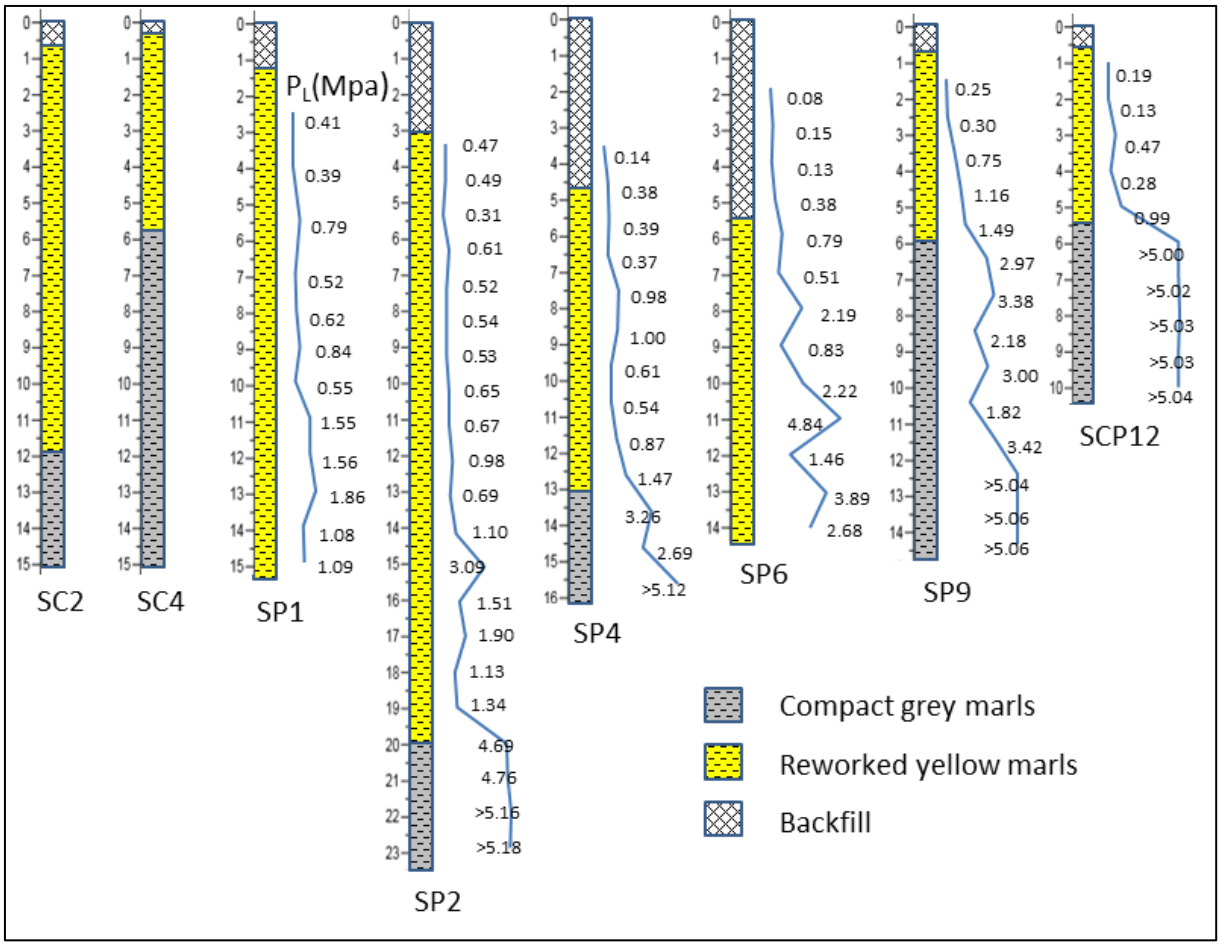

Fig. 120: Lithological characteristics obtained by core drilling and pressuremeter surveys (based on LPEE 2017 borehole data)

The X-Ray Diffraction analysis on the raw powder pattern revealed the abundance of clays, quartz and calcite in all marl samples with slight contents of gypsum and dolomite. Concerning the finer clay fraction (thin section of clays), it consists mainly of Kaolinite (K), chlorite (Ch), illites (I) and irregular mixed-layer of illite/smectite (I/S) (Fig. 121). In fact, the latter minerals are more abundant in the shallow weathered marls (X1, X2 and X5) than the substratum material (grey marls; X3 and X4). Similar findings are reported in Charente, France, where the surficial weathering of the marls observed in the Roumazières profile manifests mineralogically by the dissolution of the carbonate cement, which explains the friable aspect of the shallow marls (Bufalo 1989), and by the transformation of illites into irregular mixed-layers illite/smectite (I/S) (Laffon and Meunier 1982; Velde and Meunier 2008). Besides, this transformation process is responsible for the expansive behavior of the surficial marls. Moreover, the propensity of MY's Neogene marls to swelling-shrinkage and associated damages is not unusual as it was aforementioned. The dispersive behavior of altered surface marls of MY is controlled by a seasonal climate contrast, and thus, its expansive behavior can also be attributed to irregular mixed-layer (I/S). In fact, Al-Mhaidib (2006) reports severe and widespread damages in residential buildings, sidewalks, and pavements caused by the development of heave and swelling

pressure in expansive shales. However, their mineralogical analysis does not show smectites or vermiculites (minerals famous for their swelling potential), but only an irregular mixed-layer (I/S) associated with kaolinites and illites. Furthermore, a high incidence of damage caused by expansive bedrock formations in the Front Range area, the Pierre Shale (Colorado, USA), is caused not only to bentonite layers but also by shales containing such irregular mixed-layer (I/S), and albeit with less swelling potential (Gill 1996).

Table 25: Geotechnical characteristics of MY's marls

Characteristics	C1 1.5-3m	C2 3.5-4.5m	C3 8-9m	X1	X2	X3	X4	X5
% Grain size: >2mm	1	1	0	0	0	0	0	0
2 to 0.08mm	1	3	2	3	3	2	1	5
80 to 20 μm	30	29	20	32	32	18	18	39
20 to 2 μm	28	31	29	28	26	32	31	25
<2 μm	40	36	49	37	39	48	50	31
Natural water content (%)	9.6	10.1	6.1	16.67	12.86	7.75	2.17	18.65
dry density γ_d (kg/m^3)	2149	2108	2094	1850	1879	2186	2405	1674
VBS (g/100g of soil)	6	6	5	7	5	3	4	6
WL (%)	52	50	56	51	53	51	43	50
IP (%)	28	28	24	27	28	25	25	29
$CaCO_3$ rate (%)	42	45	63	47	53	65	75	54
Compression index Cc	0.20	0.12	0.10	0.49	0.33	0.23	0.18	0.32
Preconsolidation pressure σc (kg/cm^2)	1.57	1.90	1.34					
swelling index Cg	0.069	0.082	0.046	0.067	0.050	0.030	0.020	0.052
Cohesion (kpa)	11	20	33	7	13	29	37	9
Friction angle ϕ (°)	24	23	21	24	24	20	19	27

Degradability index				61	34	21	18	24
USCS classification	CH	CH	CL	CH	CH	CL	CL	CH
GTR classification	A_3	A_3	A_2	A_3	A_3	A_2	A_2	A_3

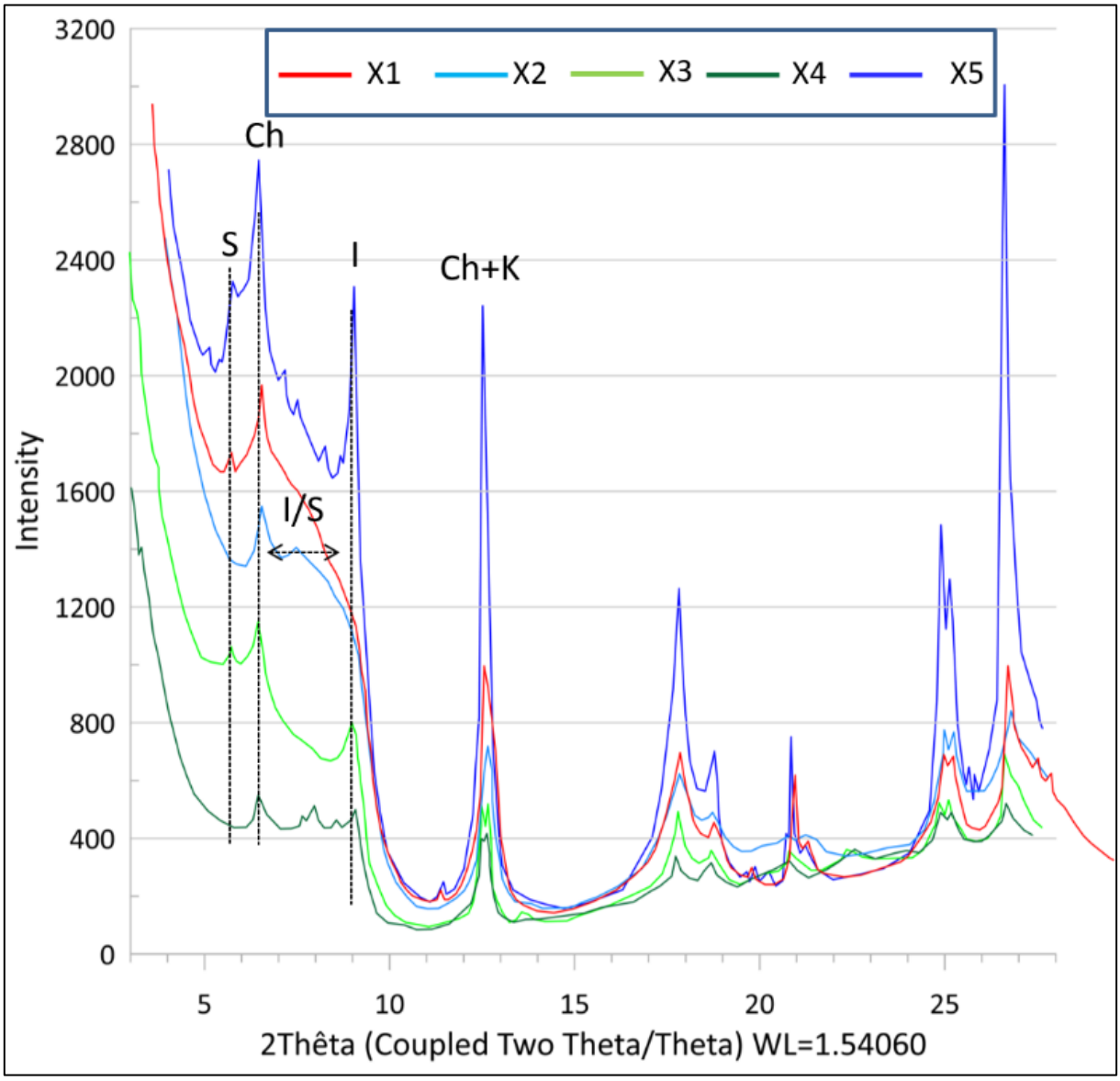

Fig. 121: X-ray diffraction results on of the clay fraction of MY's marl samples; S: smectite, Ch: chlorite, I/S: irregular mixed-layer (illite/smectite), I: illites, K: kaolinite

B. Identification of the depths of landslide rupture surfaces

Despite the expansive behavior of these marls, MY's urban area is greatly affected by deep (rotational landslides) and shallow (soil creep) gravitational processes; the traces of which are clearly perceptible in non-built areas (Fig. 122). Such landslide features appear in the form of decimetric to

metric scarps and fissures and cracks affecting mainly reworked marls and seem to be eroded by surface water runoff. An example of a deep slide was uncovered during field investigations surveys where a deep rotational slide was triggered in 2006 by a football field construction work (Fig. 122a).

The interpretation of H/V peak values allows establishing a link between bedrock-soil interface and the landslide processes described above. In fact, potential slip surfaces at depths of about 10 meters are obtained inside landslides boundary (Table 24/ Fig. 129; P19, P20, P26, P28). Close to these boundaries, the depth of the seismic interfaces is less important which further establishes a geometric relationship between rotational slide processes and the H/V interfaces.

Regarding surficial soil creep, it is geomorphologically characterized by an embossed appearance without apparent fractures on the surface (Fig. 122c and d). The material affected by these processes is mainly weathered marl which seems to be fairly porous on the surface and saturated in depth (Table 25). At frequencies greater than 23Hz, H/V peaks suggest a thickness of about 2 m for the creeping material (P16, P28 and P29 in Table 24 and Fig. 129). However, on the western flank, the instability indicators are completely concealed by the dense unregulated urbanization, where the mapping of slow creep process is only possible through interpreting the aspect of alleys and analyzing the spatial distribution of damaged buildings (Fig. 128). Their very slow but perennial activity is manifested by the severe building damages, distinguishes these unstable zones (Fig. 123 and 128). The core drilling carried out, with the aim of reinforcing the district, and the seismic noise measurements (Fig. 119 and 120) define several potential rupture-surfaces: i) between the anthropogenic layers and the reworked marls, (Sp4 and Sp6) at a maximum 5m depth; ii) between the weathered clayey marls and the compact grey marls. Despite this geotechnical contrast, this interface is clearly noticeable both on the variations of limit pressure in the pressuremeter surveys as well as the H/V frequency values and their peak amplitude.

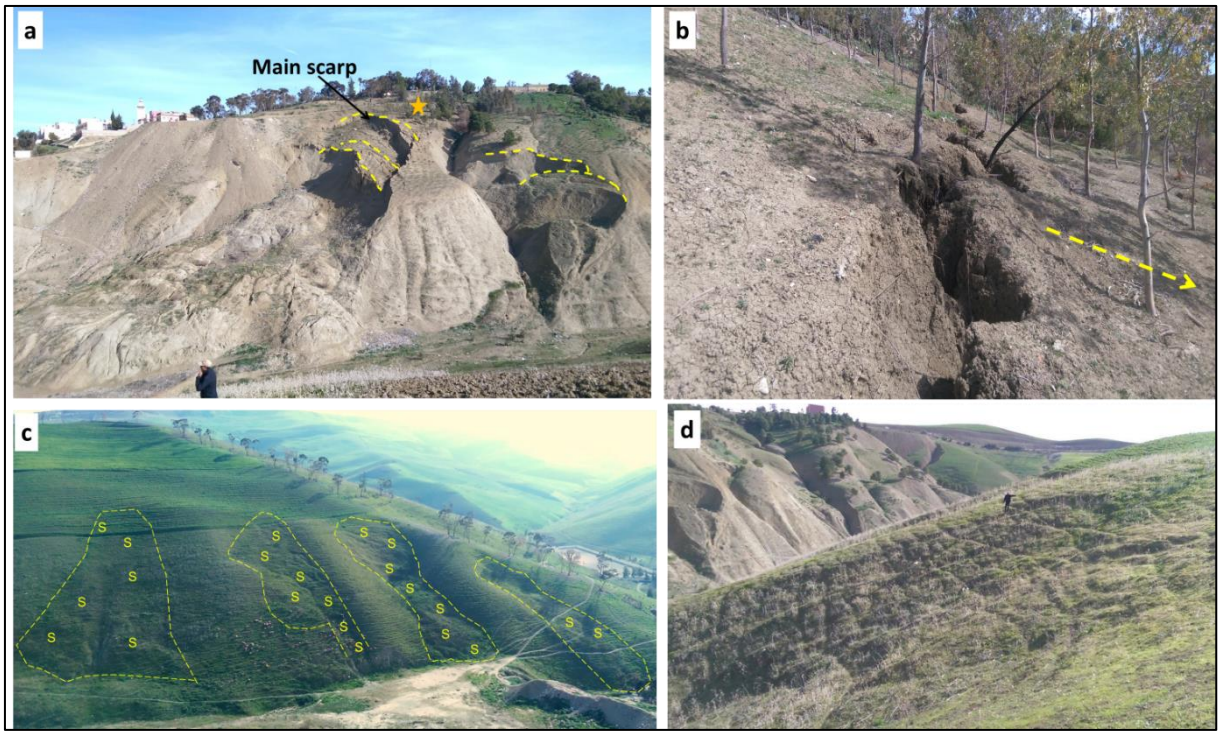

Fig. 122:Samples of slope movements in MY. a rotational slide; b active head cracks; c Soil creep and creeping mass of old landslides (s); d Detail view of a soil creep

Indeed, the retaining wall carried out northward, in order to reinforce the public car park, has managed to minimize building damages upstream the slope (Fig. 119). Notwithstanding, the low to moderate damages affecting newly built constructions imply that the landslide (reinforced downstream) is still active, at least through soil creep. Seismic noise surveys have shown that the rupture surface may develop whether between the anthropogenic material and the reworked marls at 4m depth or between the later and the compacted grey marls at about 13m depth (Table 24, Fig.5; P19, P20 and P26). Moreover, despite the fortuitous reinforcements made beforehand in the rest of the old district and its extensions, landslides are still active at this level, especially to the south where the damages degrees are moderate to severe in several recent constructions (D2 to D4) (Fig. 128).

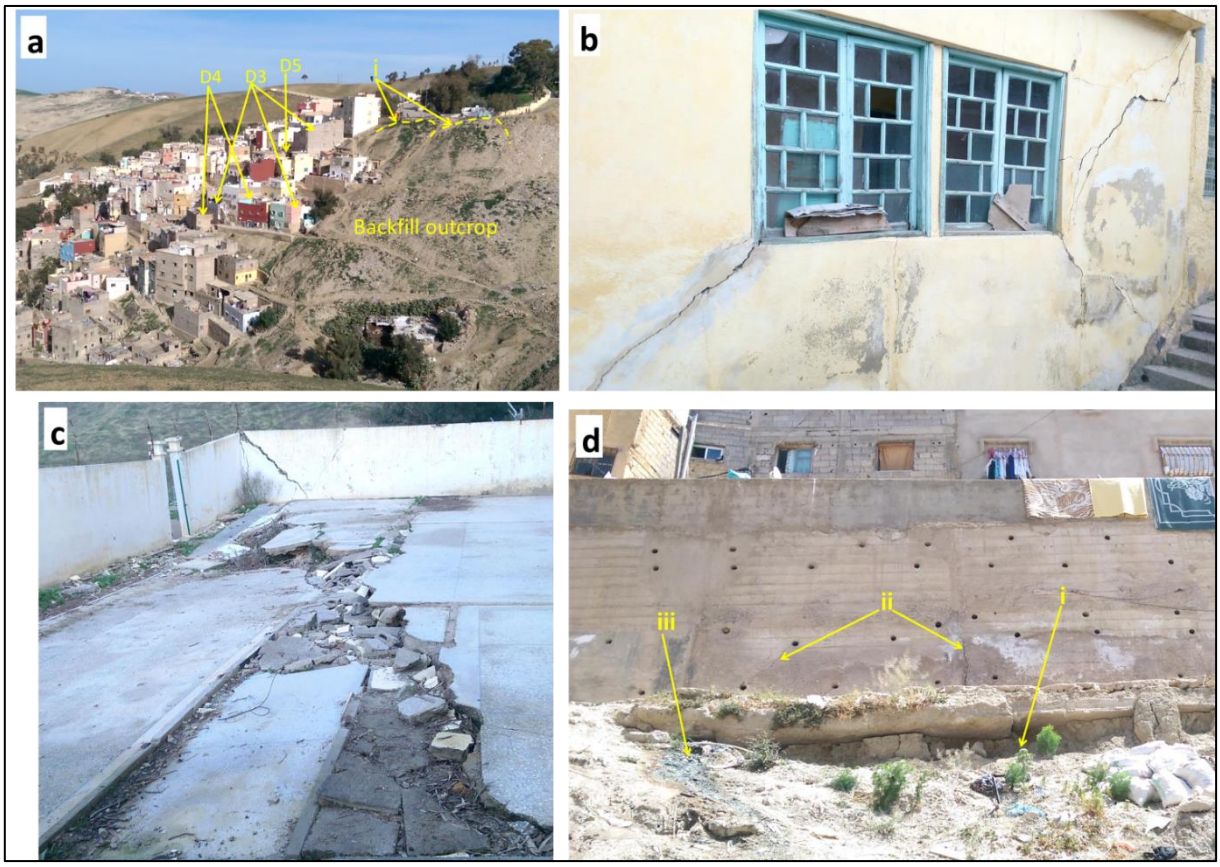

Fig. 123: Observed pathological manifestations at instable slopes of the western district; a recent scarps of a not yet individualised landslide (i), backfill outcrop (ii); b severe wall cracking (D5); c recent scarp affecting urbanized area; d retaining wall whose foundations have been uncovered by the head scarp of the landslide (i), cracks in the retaining wall (ii), waste water leak due to damaged sewerage network by the landslide (iii).

C. Displacement velocities

The inclinometric surveys carried out in 2016-2017 recorded a slight activity for the monitored landslides located in the old district (Fig. 124). The inclinometer "i1" indicates a rupture surface at a depth of 19 m, which corresponds to the weathered marl-bedrock boundary, reached by the borehole SP2 (Fig. 120). The inclinometer i2 shows two rupture-surfaces for the monitored landslide, with the deepest out of the two found at 13.5 m deep and the shallower one at 5 to 7m. This corresponds to the change in the limit pressure of the SP4 borehole and to the pic of the P5 H/V measurement of which f_0= 3.8 Hz (Table 24, Fig. 120 and 129). For i3, the borehole hasn't reached the basal rupture surface and thus found to be of little use since it only indicates that the material involved by the monitored landslide is deeper than 14 meters. However, the good correspondence between inclinometer and H/V allows estimating the depth of the rupture surface at approximately 15m.

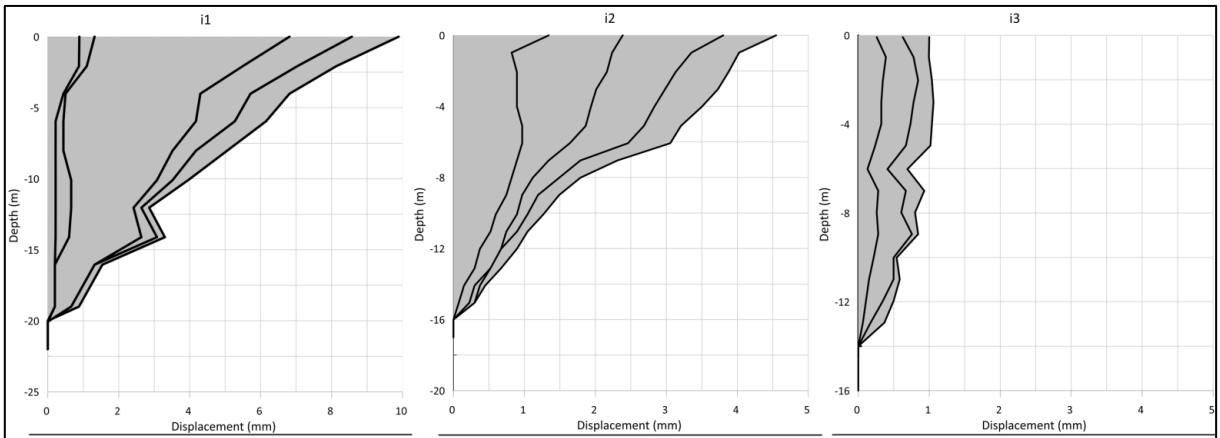

i1	Date of measurement	Day difference
	13/10/2016 -29/12/2016	77
	19/01/2017	98
	31/01/2017	110
	07/02/2017	117
	18/02/2017	128

i2	Date of measurement	Day difference
	12/11/2016 -10/01/2017	59
	07/02/2017	87
	18/02/2017	98
	04/03/2017	112

i3	Date of measurement	Day difference
	23/01/2017 -31/01/2017	8
	18/02/2017	26
	04/03/2017	40

Fig. 124: Inclinometer monitoring (modified from LPEE 2017)

Even though inclinometer monitoring covers a limited period of time, and the displacement of the sliding mass is found to be composite, with the existence of several rupture surfaces (especially in i1 and i2) this technique can still be considered very useful for studying landslides in MY district. The interpretation of relative cumulative displacement curves, which shows a substantial increase in the rate of displacement, perceptible in i1 (measurement of 31/01/2017) demonstrated that the landslide was accelerated by a previous rainfall event (Fig. 125). In fact, data from the MY meteorological station unveil that the study area received more than 77 mm rain (24% of annual precipitation) in less than 10 days during the month of December 2016, which explains the i1 results.

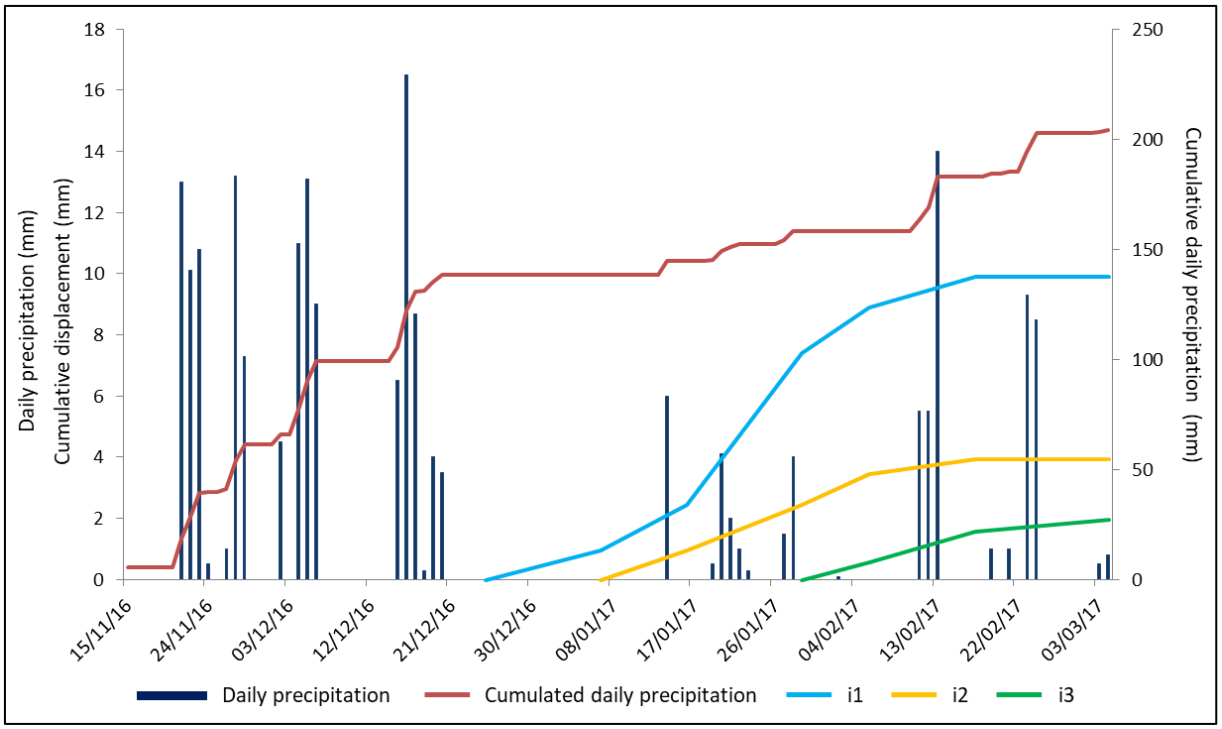

Fig. 125: Daily precipitations of MY rainfall station, from 06/11/16 to 28/02/17; i1, i2 and i3: inclinometer displacements

Regarding PS-INSAR results, a good Persistent Scatter (PS) density was obtained in the urban areas due to the presence of stable SAR reflectors. In the surveyed area, the displacement rate ranges from -50 mm/y to 40 mm/y, with PSs showing relatively strong subsidence mainly located inside the L2 and L3 boundaries. In fact, many PSs with displacement velocities exceeding 4 cm/y are located close to the head scarp area. Compared to the displacements recorded by the inclinometers (about 3 cm/y I1, 1.5 cm/y for I2 and 1 cm/y for I3), the PSINSAR monitoring results showed higher velocities (exceeding 2.5 cm/y). However, these rates were recorded in the head scarp area, while velocities between 0.5 and 2.5 cm/y were obtained in the depletion zone which further confirms the inclinometer results and the robustness of the PSinSAR technique.

Downhill, few positive velocity values (towards the sensor) are obtained, which are associated with the accumulation of the sliding material or with the uplift of the landslides toe due to the rotational components. Such displacement velocities are obtained in the urban perimeter of Barberà de la Conca in Catalonia (Peduto et al 2021) and in the Pianello landslide (Bovino, Southern Italy) (Refice et al. 2019), with velocities exceeding 20 mm near to the main scarp of the surveyed landslide. Therefore, even though the landslide prone area for L1 landslide is densely built, which should provide good data coherence, the results obtained do not show PSs in the head scarp area which doesn't allow for a good comparison with L2 and L3 (fig 126). In fact, we believe that such results are due to the bumpy topography of L1 which created a shadowing effect, common to cause an absence of PS in the shadowed areas (Colesanti and Wasowski 2006, Notti et al 2014).

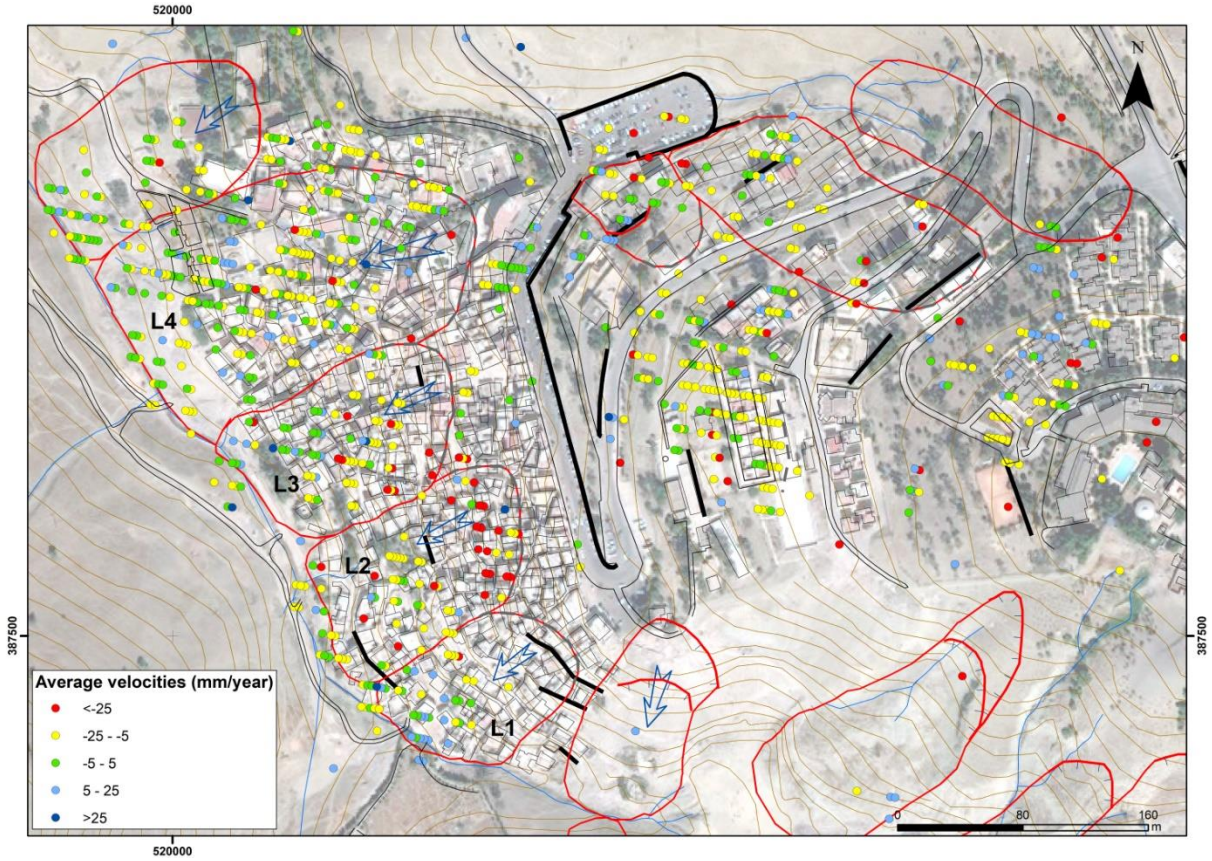

Fig. 126: Average annual velocities obtained by PS-INSAR monitoring in the urban perimeter of Moulay Yacoub town

D. Assessment of the impact of slope movements in the urban perimeter

During the damage assessment surveys realized within the MY urban perimeter, 748 constructions were inspected. 14.7% of the buildings are affected by negligible damage (D0), 44% showed signs for minor damage (D1 and D2), 14.8% are attributable to the moderate damage category (D3) while 7.6% of buildings showed severe damage levels (D4, D5 and EF), 5.7% of which are in the western district (Fig. 128).

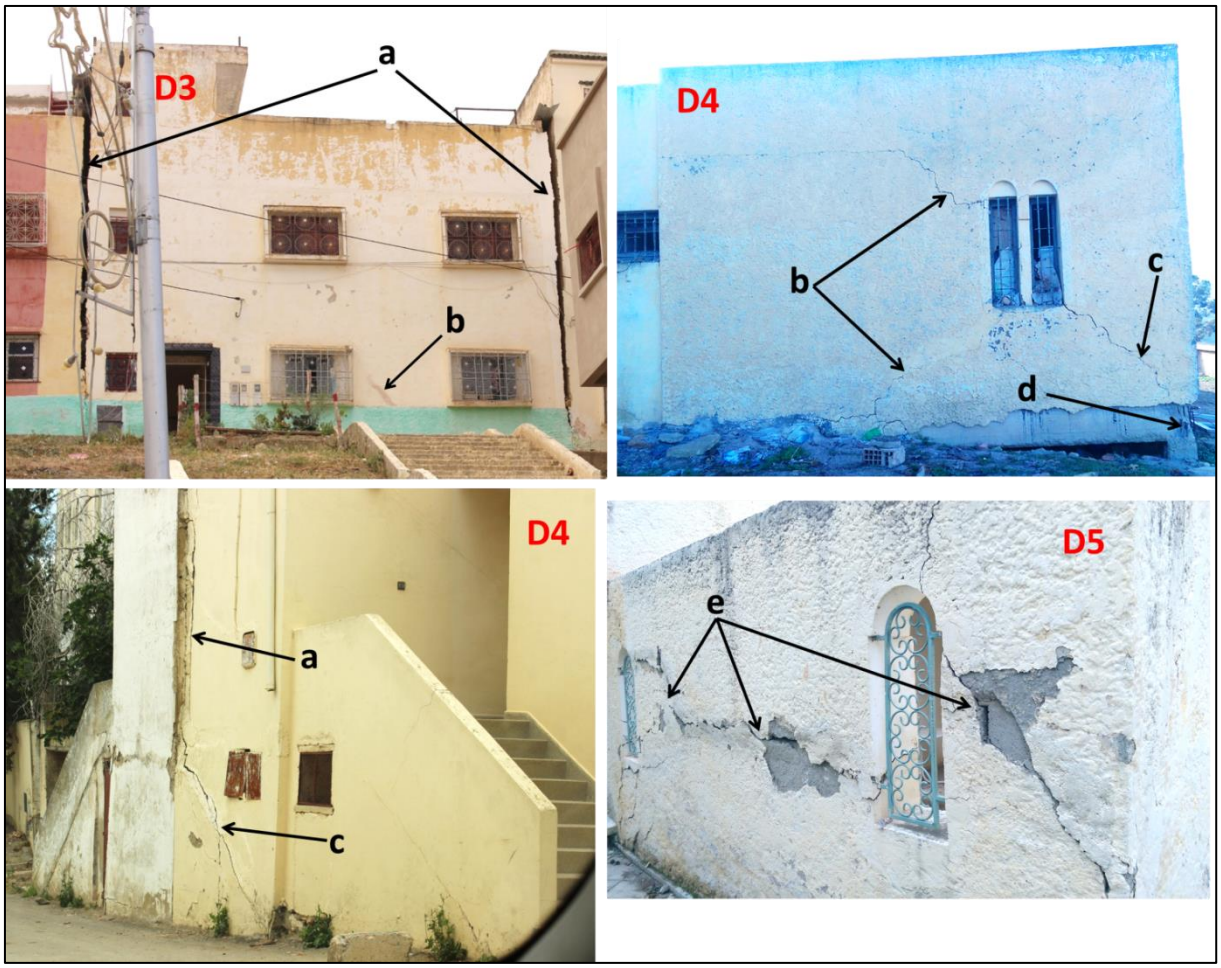

Fig. 127: Pathological manifestations induced by expansive soils; a: Expansion of the building's joints; b: Diagonal cracks connecting windows to building structure; c: Cracks at the corner of the building affecting its structure; d: Differential settlement affecting steel bars; e: Random cracks in all directions involving external facades, which requires building evacuation, Di: level of damage

Moreover, field investigations asserted that many buildings have been subject to major repairs and reinforcement interventions, especially in the western flank. The analysis of the damages and slope movements distribution maps shows that the most severely damaged constructions are located near to the head scarps of the landslides, particularly for those affecting the western district, where four landslides were individualized (Fig. 128). The damage severity decreases gradually towards the bottom of the slope.

In consequence, one could say that the origin of the damage affecting man-made facilities (oblique cracks, spacing of the annexes or opened joints between constructions, tilted buildings and warped facades) is due to vertical displacement of the expansive subsoil layers in areas where no clear landslide features are observed (no field scarps, flat fields or gently inclined) and to downhill displacement inside the landslide boundaries (Fig. 127)

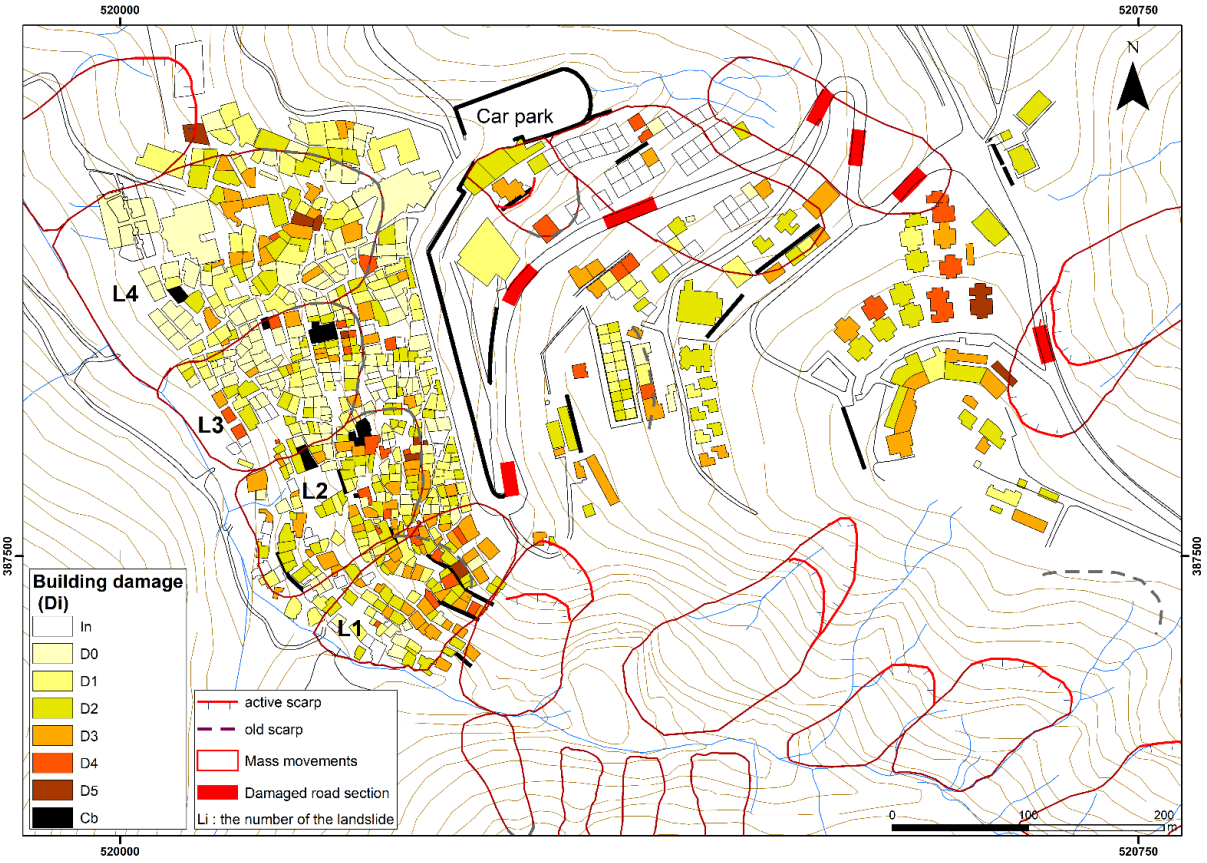

Fig. 128: Buildings damage distribution and instability signs (road network, building basic data from Moulay Yacoub google earth images; topographic data from Moulay Yacoub topographic map 1/25 000; ANCFCC 2007)

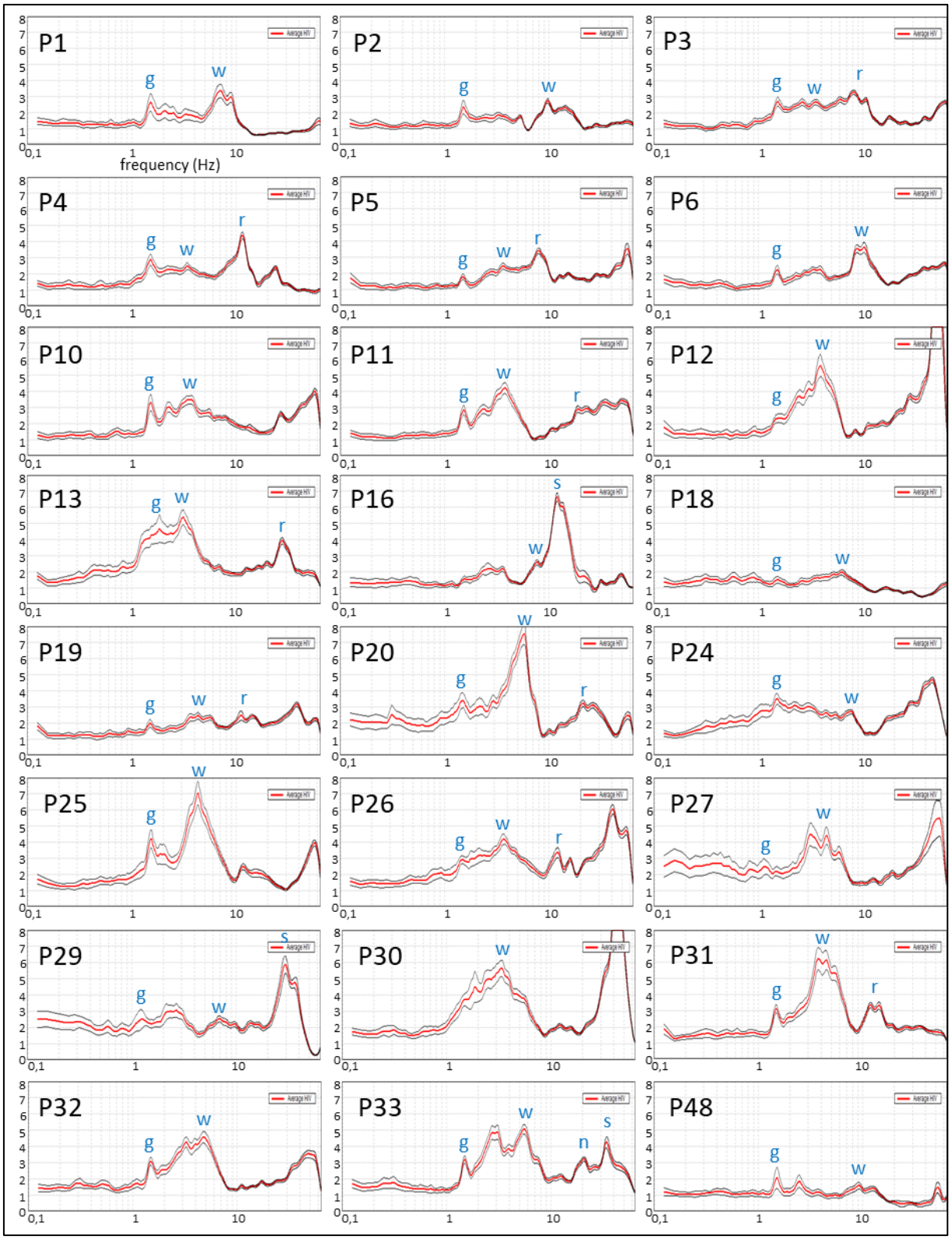

Figure 129 Curves of the Seismic noise measurements

6. Synthesis

This study brings a multifaceted and somewhat complement vision on the mechanism controlling slow the slow-moving urban landslides affecting Neogene marls in MY. Despite the gentle topography

and the sub arid climate of the study area, these urban landslides have proven to be capable of causing severe damage to constructions and spa chambers at the study area. In fact, these geomorphic processes could have gone unnoticed if it wasn't for the presence of constructions which reveal their slow activity.

The analysis of the diverse instability phenomena in the town of MY shows that the damages affecting the constructions are the result of interaction between geomorphological, geotechnical/ mineralogical, and anthropogenic factors. In fact, the urban centre lays on a marly hill exposed to weathering processes typical of the Mediterranean regions, caused by the succession of extreme rainfall events and extremely arid periods. Despite the low precipitation rates in the region, the weathering processes affecting marls consist of the dissolution of calcium carbonates cement, which reduces the cohesion of surficial marls. Consequently, the development of an expansive-compressive soil increases the porosity of marl and promotes water retention (the vacuum indices used to calculate compression and swelling coefficients are higher in shallow samples). Moreover, the succession of dry and wet periods allows the weathering action to reach deep strata and the development of a thick weathered and saturated layer. Similar instability cases have been investigated by Malet (2003) and Abolmasov (2015) where the shift from deep compact grey marls to weathered and reworked yellow ones coincide with the landslides rupture surface.

Furthermore, the expansive behaviour of the shallow marls of MY is attributed to irregular mixed-layer (I/S). Similarly, Al-Mhaidib (2006) reports severe and widespread damages in residential buildings, sidewalks, and pavements caused by the development of heave and swelling pressure in expansive shales. Nevertheless, their mineralogical composition does not prove the existence of smectites or vermiculites (minerals famous for their swelling potential), but only an irregular mixed-layer (I/S) associated with kaolinites and illites. Moreover, a high incidence of damage by the expansive bedrock formations in the Front Range area, the Pierre Shale (Colorado, USA), is caused not only to bentonite layers but also shales containing Irregular Mixed-layer (I/S) and albeit with less swelling potential (Gill 1996). Nevertheless, the swelling potential in MY marls is not the result of the sole presence of expansive clays in MY marls, but also of gypsum (sulphates de calcium hydrates) crystals identified in raw powder samples. Previous studies concluded that this chemical swelling potential is the consequence of gypsum precipitation in rock discontinuities (Alonso et al. 2013). Its precipitation requires necessarily the presence of water. In MY, the presence of gypsum in the samples attests that the chemical conditions were suitable for its precipitation, either by super-saturation of the water or due to evaporation. In reality, water in urban areas, comes from septic tanks and/or from the damaged sanitation network consequential to active landslides.

The Inclinometer and PS-INSAR monitoring show that the landslides affecting the urban perimeter of MY are extremely/very slow (5mm to 5cm annually) (Cruden and Varnes 1996). The comparison

between the displacements recorded by the inclinometers and the daily precipitations reveals seasonal activity of the landslides with periods of acceleration and deceleration. Moreover, The PS-INSAR results reveal not only the displacement velocities across MY urban perimeter but also show that these velocities are more significant at the head scarp area of the inventoried slides. Inversely, the displacement velocities are slower downhill and show sometimes positive values (fig 10) due to the accumulation of the landslide's material or to their rotational component. Likewise, these findings explain the spatial distribution of building damage and reveal why the most severely affected cases are located at the crown area of landslides in MY. As For the L1 landslide in the old district, the lack of monitoring data does not mean that the area is stable considering the high levels of building damage observed.

In addition to the climate conditions and the other factors mentioned above, changes to the topography and hydrography, caused by human activities, proved to have a great influence on the stability of hillslopes at MY. This is clearly perceptible both in the western part of the study area where water coming from the damaged sewage network (damaged sanitation network and water leaking from septic tanks) saturates the weathered layers, and to its south where the earth moving works weakened the slope stability thus inducing a rotational landslide (Fig. 6a). Despite the presence of buildings, infrastructures and other human activities that conceal the landslides morphological features, a case-by-case analysis of their effect on the manmade structures proved to be useful in mapping active landslides of in the area. In fact, the numerous damaged buildings at MY, which show in some cases signs for severe damage, share in common the fact that these constructions aren't adapted to the geotechnical characteristics of shallow marls. Of the various construction malpractices observed at the study area, we cite the fact that some constructions have inadequate foundations (shallow and/or vulnerable to expansive soils), while others are built on a backfill with thickness exceeding three meters in some locations. Besides, the high demand on houses is pushing the population to explore areas prone to landslides. This is the case for the old district located to the south of the study area on a steep slope covered by thick backfill material (Fig. 12 and Fig. 7a). Hence, one can note the complex relationship between landslides activity and the double role of manmade structures as both a determining factor and an element at risk. This relation is also reported in a similar context where construction practices at Chefchaouen city seem to be under the same cause and effect relationship (El Kharim et al 2021). If the slow activity recorded by the PS-INSAR technique and the inclinometer monitoring is shown to have considerable and perceptible impacts on the stability and state of constructions, one has to wonder what the outcome will be if an event similar to that of 2006 (Fig. 6a) were to occur in the densely populated areas of the MY urban town.

Indeed, the seismic noise survey has proven its effectiveness in detecting the depth of the weathered body and potential rupture surfaces in the urban and sub-urban area of the town without having to resort to core drilling and pressuremeter tests. The results obtained could be effortlessly

exploited to determine the adequate depth for future foundations as well as the dimension of retaining walls. Besides, the combination of seismic noise technique and geotechnical characterizations with high-resolution SAR data (as PS-INSAR results) affords a precise structural monitoring system to investigate the urbanized slow landslides despite the complex patterns of displacements and the lack of surface features (Massey et al. 2013; Carey et al. 2015). Moreover, the monitoring campaigns carried out in the urban centre of MY allow to locate the most active areas of the landslides and give an important insight into the average velocities and cumulative displacements to be expected during similar cases of urbanized slow landslide activities.

7. Conclusion

The results obtained in this complex context, constitute a step forward towards completing previous work carried out in the MY town. Results highlight the complementarity of the techniques used in this multi-disciplinary approach, where a combination of field investigations, geotechnical and geophysical tests and remote-sensing techniques give a complete understanding of the slope dynamics at the study area. However, one should stress the fact that these methods allowed reaching such conclusions in a poorly documented region. In this respect, the production of any type of new data in the future could prove to be fruitful for completing the results of this study. Future landslide investigations to be conducted in the region, could also use the method proposed in this study as a blueprint, which would provide a more holistic understanding of landslides on a regional scale, through comparing results across case studies. Finally, several improvements could be proposed for similar future case studies such as:

i) The use of the ERT could give a better characterization of the subsurface in areas where urbanization is not very dense

ii) The use of ground-based SAR in precautionary monitoring of the extremely slow displacements

ii) Cross comparison between temporal sequences of SAR data and daily rainfall, which could give a better understanding of the triggering processes for this type of landslides.

VIII. Chapter 6: Synthesis of the landslide risk and associated vulnerability in Moulay Yacoub town with urban perimeters of several northern cities

1. Introduction

In mountainous urbanized regions, the anthropogenic disturbance of hill slopes causes severe landslide damage (Glade 2003; Soini 2005). In the case of non-controlled suburban extensions, clandestine construction practices increase the predisposition of slopes and multiplies the landslide risk (Smyth and Royle 2000; Schuster and Highland 2007; Chisty 2014). Many old and recent landslides affect the Rif region in Northern Morocco. This natural hazard constitutes a major obstacle for the development of the cities and their suburban districts. In the urban perimeters investigated, Moulay Yacoub, Chefchaouen, Boujibar (Al Hoceima) and several districts in Fez (Trhate, Oued Fez, Jnanate, etc.), the risk of landslides involves both anthropogenic, geological, geomorphological and/or even tectonic/seismic parameters, which are in most cases linked together by the domino effect. The rate of influence of each of these parameters varies for each urban extension according to certain site effects belonging to the structural and geographical context of its immediate surroundings. However, the way of human contribution in amplifying the vulnerability of these urban areas against the risk of slope movements displays several similarities and which will be enumerated in this chapter.

In the last decades, the environmental crises linked to the recurrent droughts that have characterized the Moroccan countryside have been fatal to the stability of rural populations in Morocco. Climatic and, consequently, hydrological droughts have been the cause of a flagrant lack of water resources in the rural world. Which is behind the massive exodus of rural populations to cities (TRIBAK et al. 2019). Consequently, urban agglomerations have experienced a considerable extension resulting mainly from these emigration masses coming from the rural hinterland (Rif, Pre-Rif and Middle Atlas). These massive flows of migrants have largely contributed to the vulnerability of peripheral areas. The latter are currently experiencing the negative impacts of over-density and habitat expansion on risky areas, including slopes prone to landslides. Despite the many state interventions, the development of non-regulatory housing areas remains one of the major challenges for the public authorities.

Subsequently, in these urban perimeters, the study of the risk and the associated physical vulnerability, which defines the damage level to critical infrastructures and buildings, is considered as a key parameter in risk assessment (Del Soldato et al. 2019). Some specific classifications of damage levels, in areas affected by landslides, have been previously developed or updated (Burland et al. 1978; Alexander 1986; Lee and Moore 1991; Chiocchio et al. 1997). Despite small differences in the used criteria, strong similarities were concluded between all classifications. In many examples (Peduto

et al. 2017; Borrelli et al. 2018), the combination of landslide inventory mapping with building damage classifications produces good results. However, building damage can also be caused by the weak geotechnical characteristics of the subsoil or due to differential settlement on expansive soils, irrespective to the gravitational processes (Tokimatsu et al. 1996). Thus, it is necessary to study the geotechnical parameters of the subsoil layers in order to distinguish landslide induced damage from swelling/shrinkage induced building pathologies.

In this chapter, the landslide risk investigated previously in MY town is cross compared with the risk in other northern urban perimeters, and which are known among the most visited tourist destinations in Morocco. The aim of the current step is mainly to compare the parameters involved in the instability, to identify and discuss the dissimilarities obtained in the results and specially to find the common factors, either at the level of the kinematic of the slope movements affecting these urban extensions, or at the level of the vulnerability of these affected areas.

Despite the international tourist reputation of these northern cities,

- Chefchaouen for its special geographical position in the Rif, originally built as a fortress in the 15th century. For its unique landscape afforded by the cliffs of the limestone ridge overlooking the city and which offers several water springs in contact with the basal pelites. For the architecture of its blue buildings of Jewish inspiration, its octagonal mosque, and its Spanish ruins.
- Al Hoceima for its blue waters of the Mediterranean, its light waves and the coastline that outlines the contours of one of Morocco's most beautiful bays. Also, its rating introduces several ancient monuments testifying to the historical aspects of its cost.
- And finally, the town of Moulay Yacoub, visited throughout the year for its hot hydrothermal sulfur springs which spring from the depths via the faults affecting the southern edge of the Prerif domain.

These three tourist cities, as well as the other urban extensions investigated in Fez, suffers from many impediments that hinder its development, among which we retain the non-structured urban extensions resulting from multiphase rural exodus periods and the landslide-induced damages (PCD 2016).

2. Landslide risk in Chefchaouen town

In the town of Chefchaouen, northern Morocco, urban and sub-urban sectors are constantly faced with landslides whose manifestation is only the reactivation of old and relic landslides, which is the case of a large number of landslides affecting the slopes of the Rif chain (El Kharim et al. 2021). in fact, the colluvium and landslide deposits downhill materialize this old multigenerational activity and the fattened surfaces of landslide bodies in this morphology suggest the inactivity of old ones. Nevertheless, the landslide-remodeled slopes of those apparently relict bodies can be partially or

totally reactivated (Millies-Lacroix 1968; Mansour 1998; Darraz et al. 2003; Mastere 2011; Harmouzi et al. 2018). Moreover, old landslide fattened bodies can dissimulate a slow activity, which can be uncovered by surficial fissures and offsets in the buildings.

Where analyze the landslide inventory map and geological setting of the study area, we observed that most of the landslides affect the clayey slopes of Tangier unit. However, rockfalls and debris flows, most of which old to very old, are abundant in the SE and affect the rocky limestone formations. Although limestone scarps are relatively stable, some limestone/ dolostone blocks could be mobilized from scree deposits especially when subjected to road cuts.

As for geotechnical parameters of the affected lithologies, except for the scree matrix, the weathered layers are mainly composed of clay particles which explains their high plasticity. These layers with a relative low density indicate the presence of a high void ratio inside the soil, which causes differential settlement of the sub soil. The vertical displacement in the soil can also be caused by the swelling clays, attested by oedometer test results. Also, the low cohesion values of the weathered layers (6–16 kPa) expose their predisposition to rupture. Still, the most important influencing parameter in Chefchaouen is rainfall since the landslide-induced damage observed has resulted from the reactivation of an old landslide during the exceptionally rainy winter of 2009–2010 (2035 mm of rain from December 2009 to March 2010 with three periods of 10, 11 and 16 consecutive rainy days, while the average annual value is 899 mm) (El Kharim et al. 2021). Furethermore, the inclinometers installed on the landslide affecting Ain Haouzi district showed that this landslide remained active until May 2017 and the analysis of relative displacement curves reveals the strong correlation between displacement and precipitation events. Moreover, the four inclinometers and the ERT profiles demonstrate that the slip surface developed at 7–12 m deep. It is therefore located at the boundary between scree deposits and reworked clay material. The interpretation of the results in the physical context of the case study shows that this deep landslide (>5 m) was caused by the infiltration of precipitation through the permeable scree deposits and its circulation in the contact area (materialized by near 0 resistivity). This situation was aggravated by the lack of a proper sewage network and the leaks in drinking water pipes damaged by previous acceleration events, which injected more water into the sliding body.

3. Landslide risk in Moulay Yacoub town

Although the monotony of the marly lithology reigns over the region, the shallow marls provide the necessary contrast which is exploited by the deep landslides affecting the urban center. On the other hand, the depth of this weathering mantle varies and the processes allowing its formation are slow and complex.

In fact, the weathering of shallow soils and subsoils by the succession of wetting and drying cycles alters the clayey structure of the original marls, (which is not necessarily swelling), (Robert and Tessier 1992), and reduces calcium carbonates in the case of compact marls, thus reducing their cohesion. In fact, the weathering of illites, that exist abundantly in the parent rock (deep gray marls) due to its exposition to meteorological agents, causes on the one hand, interfoliar bonds breaking which frees potassium, and on the other hand, iron oxidation. These two weathering phases provide to the irregular interlayered clays the same smectite's expansive properties, and a great plastic potential (Velde 1995). This leads to the formation of an altered and strongly swelling soil layer inducing damage to constructions even on flat topography. On average and steep slopes, this altered layer can undergo creep after the rain events damaging the sewerage network and which begins to supply the weathered body with water (case of the urban perimeters of the three study areas). Thus, the lower limit of this weathering mantle evolves into a generally slow landslide rupture surface which records periods of acceleration following significant precipitation events. The landslide failure surface was well mapped using several subsoil exploration techniques in the urban center of Moulay Yacoub and found to have a geometry typical of rotational slides. Such information is extremely important in the case of slope retaining and foundation reinforcement measures. In Moulay Yacoub, the depth of the landslide rupture surface affecting the western district of the urban area exceeds 15m in depth. The latter was obtained by inclinometer measurements and corroborated by seismic background noise measurements. Thus, such a depth of the landslide body complicates the reinforcement measures in terms of cost and feasibility. The responsible authorities have asserted that the only way to prevent the catastrophic outcomes in this extreme case is to move the inhabitants of the areas affected by the fairly deep landslides to other more stable sectors (DHP, Fez), a decision which remains very expensive and which shows the need to establish anticipatory studies in areas prone to landslides before any urban planning.

Furthermore, although the dynamics of these monitored landslides are weak and difficult to perceive in urban areas which tend to conceal superficial signs of displacement. Variable displacement velocities were recorded by inclinometers and PS-INSAR in the cities, and the damage is well noticeable on the manmade facilities even if the displacement rate is relatively slow.

As for the building damages in Moulay Yacoub, the non-adaptation of habitats to the hazards of landslides and shrinkage/swelling increases their vulnerability. The shallow foundations observed on several buildings explain the severity of the damage (fig. 130). The latter varies from simple wall cracks to serious damages to construction's structures (cracked foundations, pillars and slabs). The mapping of damage to constructions shows that the most seriously affected cases are near to the main scarps of the slides and that the severity of the damage decreases downhill knowing that the movement speeds recorded at the level of main scarps are the highest.



Fig. 130: Vulnerability of the former MY district to the risk of landslides; a shallow foundation, b Shallow foundations and overstoriying, c extension of the district towards steep slopes and on backfill

4. Landslide risk in Fez city

The urban extensions affected by landslides in the city of Fez are listed in chapter 2. In fact, the interaction of anthropogenic activity with predisposing geological factors is clearly perceptible in several districts of the city. For example, the extension of habitats towards the escarpment shaped by Oued Fez to the north of the Jnanate districts increases their vulnerability to landslides and cliff collapses, the main factor of which is bank undermining. However, the overweight of the buildings, the evacuation of water towards the wadi as well as the uncontrolled discharge observed on the right side of the wadi are all predisposing parameters which increase the vulnerability of the area. Moreover, the damage to the buildings observed in the field are quite catastrophic, which explains the evacuation of many buildings along the cliff (fig. 131).

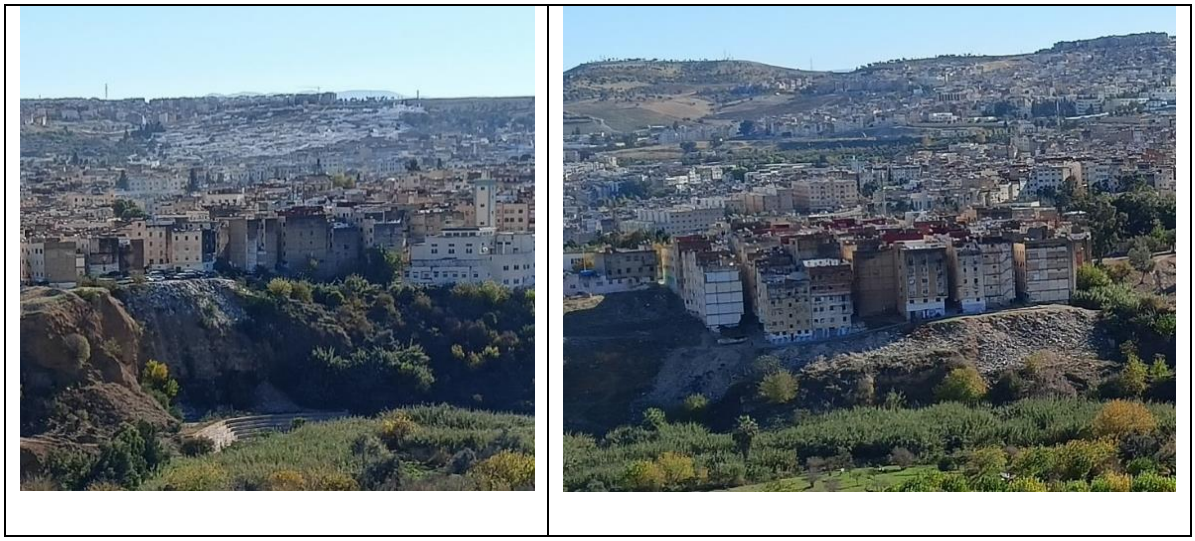

Fig. 131: Habitats of the Jnanate district at high risk of collapse sliding

Moreover, the extension of the neighborhoods towards the NW of the city of Fez on strongly swelling marly terrain (attested by the swelling and settlement coefficients obtained during the oedometric tests) and to the detriment of the slopes affected by large landslides affecting the southern slope of Jbel Trhat, have caused severe damage to the buildings, especially to those built without adequate foundations and non-adapted to the creeping of the basements and to differential settlements (case of the housing estates of Hay Nahda) (fig. 132). These landslides of large spatial extent are relatively old, and their partial or total activation is mainly linked to rain events but also to the topographic growth of the wrinkle zone (Poujol et al. 2017a), in particular that of Trhat, afforded by a recent and active blind overlapping along the toe of the wrinkle (Agharroud et al. 2021).

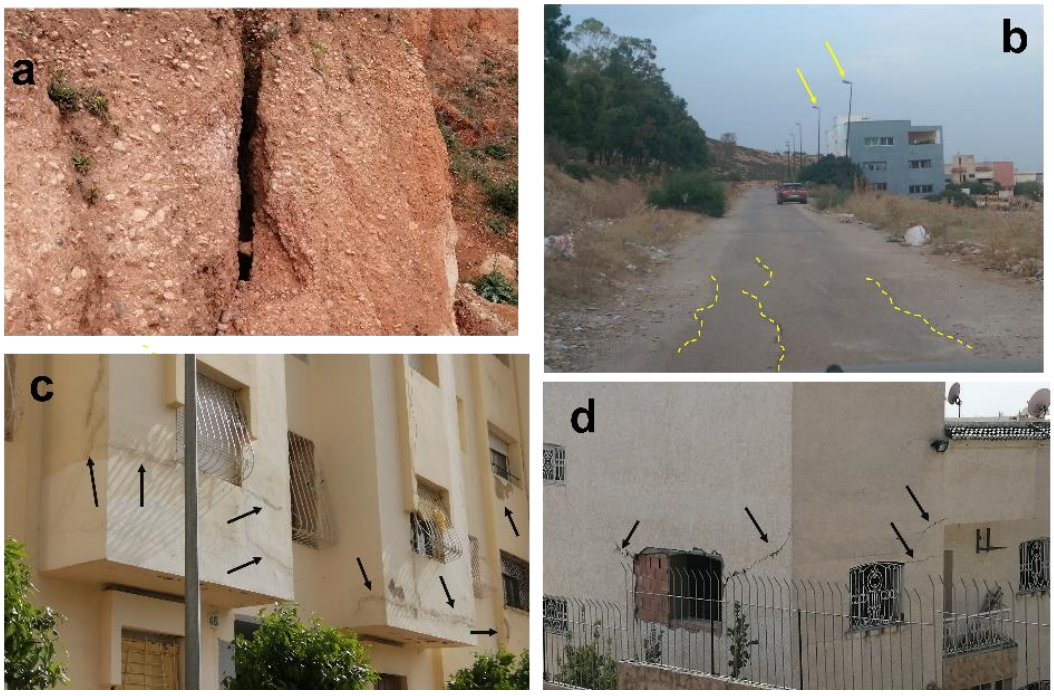

Fig. 132:Rrisk of landslides north of the Trhat district; a reworked marly colluvium testifying to the multigenerational activity of the old large landslides affecting the Trhat district, b landslide activity signs: Tilted streetlamps and damaged road section, c and d obvious cracks affecting houses despite repair attempts

5. Landslide risk in Al Hoceima's urban area

The city of Al Hoceima and its outskirts is located in the eastern part of the Bokkoya massif in northern Morocco and covers an area of 42 km². The main urban extensions affected by landslides are the northern slopes overlooking the beaches of Sabadia, the high embankments of Talla-Youssef to the east of the city and the Boujibar district. The main predisposition factor in the 3 sectors is the lithological nature. In fact, the Silurian shales of the Al Hoceima nappe are quite altered. In fact, the construction of the coastal road along the beaches of this formation has considerably disturbed the stability of the northern slopes. Also, the springs gushing at the foot of these slopes testify to the feeding of the masses of landslides which repeatedly damaged the sections of the coastal road following multiple triggering events. As for the Boujibar district, the Eo-Oligocene marls outcropping in the area are affected by a large old landslide which damaged the buildings in the district following the triggering of its foot. The active ravines which circumvent it can also be involved in this reactivation (fig. 133), the intense undermining of the latter also testifies to a topographic growth of the region, and which can be at the origin of the reactivation of the large old landslides.

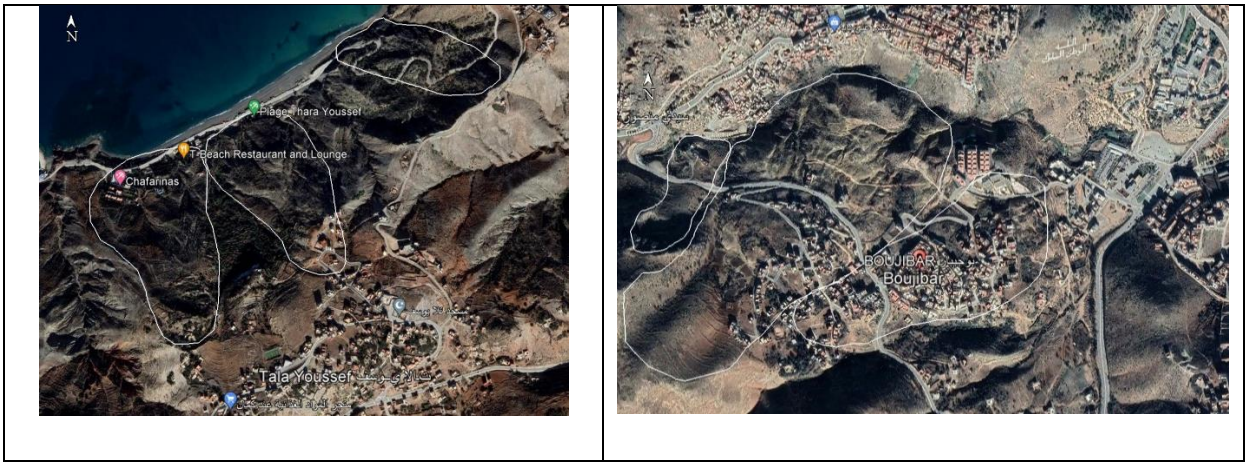

Fig. 133: Landslide affecting urban areas TallaYoussef and Boujibar

In the case of al hoceima, the mapping of susceptibility to landslides carried out showed that the vulnerability of the listed urban extensions is expressed in the fact that these neighborhoods are built on areas with very high susceptibility (fig. 134), given by geomorphological and lithological factors, but also by old and relic landslides on which certain neighborhoods are built. The result of the map remains important data to be exploited during future urban planning in order to avoid the costly consequences and the complexity of intervention which results from the interaction of the risk of landslides with the urban extensions which are generally quite vulnerable.

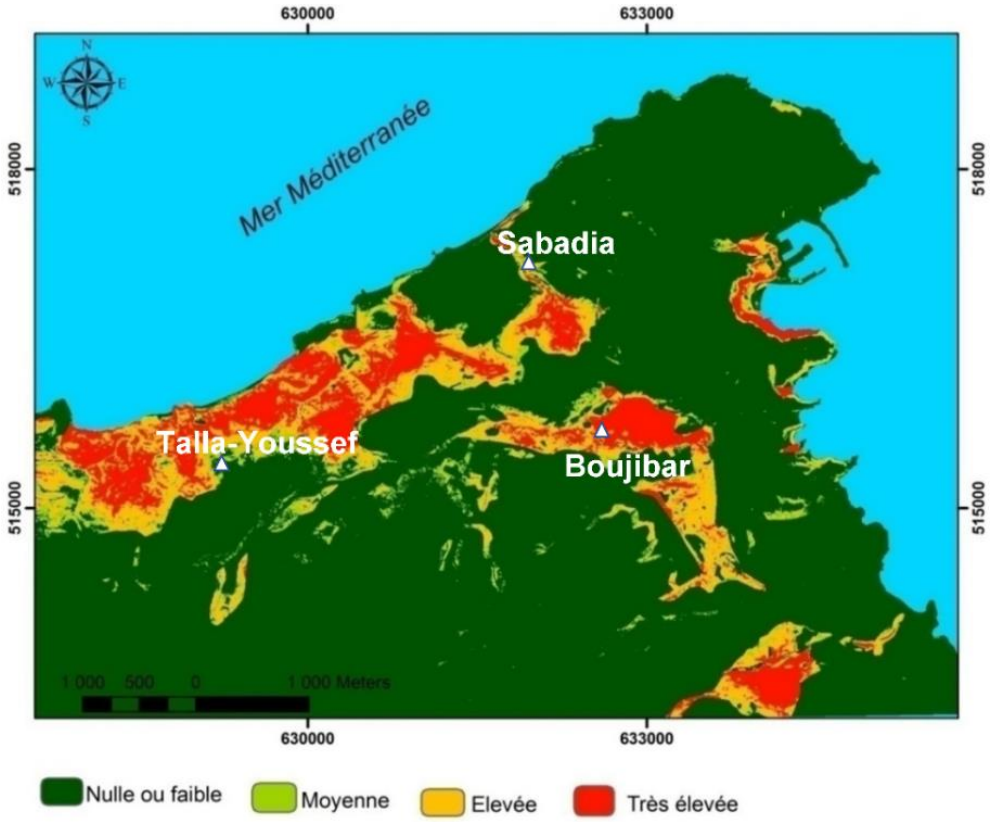

Fig. 134: The landslide susceptibility map obtained by logistic regression analysis (Byou et al. 2020)

6. Synthesis and conclusion

In urban perimeter prone to landslides, it is true that deterministic approaches such as geotechnical methods provide the most accurate results of physical soil properties and landslides dimensions allowing us to understand landslides kinematics affecting these urban extensions. However, the significant cost and time consumed by these techniques complicates their feasibility, especially since many peripheral urban agglomerations have experienced a considerable extension on unstable slopes. For that, and till today, geotechnical studies are not a prerequisite for all construction projects in these areas. Moreover, even when such studies are performed, they are limited to basic geotechnical surveys, which aim to estimate the bearing capacity of the ground and/or to reinforce the slopes and damaged foundations. Hence, these practices cannot prevent future acceleration events nor prevent landslide-induced damage to buildings and infrastructures on hillslopes marked by the legacy of old triggered gravitational processes. Besides, these techniques aren't tailored for broad scale given the cost of laboratory tests, displacement monitoring and expertise. For this, it is necessary to adopt different approaches from deterministic methods, usually performed, to mitigate such serious socioeconomic loss. In Chefchaouen and Moulay Yacoub, the cross-disciplinary analysis performed to characterize the multifaceted landslide risk in the cities, have shown that this risk seems to be comprised in a vicious circle involving both geological and anthropic factors. The geophysical surveys employed have proven to be robust and reliable in addition to the simplicity and speed of production

of data where no geotechnical borehole data have been obtained. Moreover, the PSINSAR technique has proven to be effective in monitoring landslide displacement velocities and can provide multiple speed-data while covering a large unstable area. This relieves us from the complexity involved in the inclinometric monitoring method which requires the drilling of a borehole for the installation of the tubes (a complex task in neighborhoods with narrow alleys such as certain areas of Moulay Yacoub and Chefchaouen) and the monitoring by technicians over relatively long periods to obtain a speed of movement. However, the method followed by the inclinometer remains more precise while giving the depth of the rupture. For this it is considered the best method used for case studies requiring intervention to reinforce a slope affected by a landslide. As for a broad scale (on the scale of a province or region), it is necessary to predict the intensity of the risk before any urbanization plan. For that, landslide susceptibility mapping methods remain the best choice to identify high-risk areas and impose security measures for urban plans covering unstable areas. However, obtaining reliable and satisfactory results requires good quality of the input data which are influencing parameters. For this, a thorough knowledge of the predisposing factors in the studied context is necessary.

For Moulay Yacoub, Chefchaouen, the urbanized sectors of the area studied in Al hoceima, as well as for the marginalized urban areas of Fez (as Annahda Housing complex at the NE of the city) the problem of the risk of landslide is not limited only to the interaction of human activity and geological factors. In fact, urban sprawl in these zones prone to landslides remains a problem whose solution is more complex than it appears. In most of the investigated urban extensions, the urbanized landslide prone areas keep expanding because of the low purchasing power of the population, who cannot appropriate pre-equipped land plots or rent a house in a suitably urbanized area, as noted (Le Tellier 2006) in the city of Tetouan. Hence, these predisposed and non-equipped lands are the least expensive which urges people with low incomes to get them. Consequently, housing in these urban extensions does not respect the construction standards for slopes prone to landslide and expansive soils.

Finally, according to this cross comparison between affected urban extensions, the risk in Moulay Yacoub is clearly of the greatest magnitude (Table 26). The Moulay Yacoub town is characterized by steep slopes (especially the western and southern slopes), although it is located in the Prerif, a territory dominated by medium hills. Moreover, among the subsoil formations encountered in the urban areas investigated, the shallow marls of MY are clearly the least coherent in addition to their high swelling potential, compared with the flysches/pelites encountered in Boujibar and Haouzi districts, or with the marl of Trhate district armed with colluvial pebbles or the alluvial terraces locally armed with pebbles of different sizes. As for buildings, the seismic standards imposed in Al Hoceima and the rocky material used in the old house in Chefchaouen increase the resistance of the constructions towards the displacement of the subsoil, whereas in MY, most of the old constructions are built of silt and marls. Moreover, although the sewage system is frequently damaged in most areas affected by landslides (MY, Haouzi, Boujibar and several neighborhoods in Fez), many houses in MY still have septic tanks,

which further feeds the landslide bodies. On the socioeconomic level, the population of the province of Moulay Yacoub is quite underdeveloped compared to the northern provinces. The substandard housing is quite frequent in the urban center and continues to extend on steep slopes (to the Southwest). Knowing that the consequences are already severe in MY town, they can at any time become catastrophic considering the high vulnerability level of the urban extension, especially at the western district.

Table 26 Comparison of parameters relating to the risk of landslide between the MY town with other investigated urban extensions

	Moulay Yacoub town	Fez city	Haouzi (Chefchaouen)	Boujibar (Al Hoceima)
Slope steepness	+++	+	+++	++
Sub-soil quality	+	++	+	+
Solidity of buildings	+	++	+++	+++
Condition of the sanitation network	+	++	++	++
Socio-economic vulnerability	+++	++	+	+
Substandard housing	+++	+	++	+

IX. Chapter 7: Statistical evaluation of tectonic control on landslides over the South Rif border north of Sais Fez

1. Introduction

Landslides are widely distributed landforms that both influence and are affected by the overall landscape evolution trends and processes (Cendrero and Dramis 1996; Ayalew and Yamagishi 2004). Along with tectonic activity, water stream erosion and base-level fall, landslides constitute an important control factor of geomorphological processes in most mountainous regions (Lomoschitz et al. 2002; Korup 2009; Booth et al. 2013). In most cases, the spatial distribution of mass movements is statistically associated with that of major tectonic structures. The latter play either a passive or an active role in determining the spatial distribution and geometry of landslide-prone areas (Roering et al. 2005; Revellino et al. 2010; Carlini et al. 2016, 2017; Bounab 2022). In the former case, major geological fractures predetermine the geometry of landslides (e.g. Bounab et al., 2021; Mateos et al., 2018; Notti et al., 2015), while in the latter, the topographic growth pushes hillslopes near their stability thresholds (Carlini et al. 2016). In addition to tectonic control, hydric erosion of hillslopes in the form of deeply-incised gullies or stream undercutting, is also genetically tied to landslides and can either be exacerbated by slope instability processes or cause the triggering of landslides (Kukemilks and Saks 2013; Okeke and Wang 2016; Nwankwoala 2019; Reed and Kite 2020; Šilhán 2022).

In the Pre-Rif ridges, Northern Morocco (Faugères 1978), where evidences in favor of active tectonic deformation have being revealed by geomorphic studies (Morel 1987, 1989) and GPS measurements (Vernant et al. 2010; Chalouan et al. 2014), important neotectonic and active tectonic effects on the topography are reported in relation to the ongoing southward crustal motion of the central Rif block. This oblique NE-SW shortening is manifested in the Pre-Rif Ridge by left-lateral transpressive and reverse faults that characterize this area, considered the deformational front of the Southern Rif chain. Geomorphic and seismo-tectonic data recently published by Agharroud et al.,(2021) strongly suggest that such structures were active as late as Quaternary times especially to the immediate North of Fes (X=-5.024106°, Y=34.023377°) and Meknes (X=-5.566023, Y=33.909725°) cities. The uplift along tectonic fractures is responsible for the development of asymmetrical ridge-like morphologies, which greatly influences the surface hydrology processes at the area. In addition, these tectonic structures are also believed to be responsible for historic seismic events such as the Fes-Meknes earthquake of 1755, the origin of which is still highly contested amongst researchers (El Mrabet 2005; Chalouan et al. 2014; Poujol et al. 2017b; Agharroud 2022). Currently, a moderate seismic activity is reported at the area, which is largely due to the ongoing tectonic activity with an annual rate of around 4mm/yr.

To the North of the frontal deformation areas, the effects of the above-mentioned tectonic activity are less expressed, with Miocene deposits being largely undisturbed. Tectonic ridges are also absent, which offers the possibility of evaluating the impact of the latter structures on the evolution of the landscape through comparing the tectonically affected area to the non-affected area. In fact, to the exception of surface hydrology processes, a comprehensive study on the matter has not been conducted yet. In previous research (Morel 1987; Poujol et al. 2017b; Agharroud et al. 2021), efforts were mainly focused on determining the topographic expressions of tectonic activity, without studying the effects of the latter on the stability of hillslopes and the evolution of slope dynamics. Hence the need for further investigations in order to complete findings of previous research and establish a morpho-structural model that explains the evolution of landslides along with that of streams and tectonic landforms.

To understand the underlying landslides geomorphic processes on a regional scale, the establishment of a landslide inventory map (LIM) is necessary since it provides relevant information about the spatial and statistical distributions of landslides parameters (Wieczorek 1984; Rickli and Graf 2000; Galli et al. 2008; Guzzetti et al. 2012). Such parameters include the typology, relative age, location, density, area, volume, width to length ratio and mean slope of the inventoried slope instability processes (Van Westen 1997; Hattanji and Moriwaki 2009; El Kharim 2012; NiculiţĂ 2016; Conforti and Ietto 2020; Bounab et al. 2022). Area-frequency distributions are also characteristic of certain geomorphological contexts and can thus be used for landslide characterization purposes through comparing the statistical distribution parameters of different inventories that represent divers and sometimes contrasted geomorphological settings (Guzzetti et al. 2002; Malamud et al. 2004; Tanyaş et al. 2019; Qiu et al. 2020). To establish statistical association between landslides and their potential causative factors, explanatory statistics and artificial neural network methods are deployed (Ermini et al. 2005; Budetta et al. 2008; Schicker and Moon 2012; Sabokbar et al. 2014; Bounab et al. 2022). However, in the study area, previous research is limited to site-specific investigations that mainly focus on the landslide hazard and vulnerability assessments (e.g. Obda et al., 2022), to landslide susceptibility mapping efforts or to research that is largely descriptive (e.g. Benzougagh et al., 2020), which does not provide sufficient data and evidence to characterize the current and past (Pliocene to present) tectono-geomorphological dynamics.

In this respect, we conducted regional-scale investigations with the aim of characterizing the geomorphological dynamics of the Southern Rif front. First, a landslide inventory was conducted; on which statistical analyses were performed to compare the landslide characteristics of three selected areas marked by different levels of tectonic deformation. Then explanatory statistics are performed in order to assess the effects of lithology and to understand which facies is more prone to the occurrence of slope instability. Since association does not always mean causation, geotechnical data was used to calculate the safety factor in each of the investigated geomorphological settings, for the most unstable

lithological materials. Finally, the results are compared to one another, to findings of previous research and are subsequently summarized to construct a geomorphological evolution model for the Southern Rif front region.

2. Geological and geomorphological setting

The Rif Corridor was a marine channel that connected the Atlantic Ocean to the Mediterranean Sea during the Miocene age (Krijgsman et al. 1999). During this period, a thick post-orogenic marine sedimentation (over 2500 meters thick) (Sani et al. 2007) took place, which corresponds to a major unconformity that separates Neogene material from the underlying Rif thrust system (Feinberg 1986; Wernli 1988). In the southern front of the Rif Mountains, this sedimentary sequence is well preserved in the Gharb, Saïss and Taza-Guercif basins constituting the current manifestation of the South Rif Corridor (Krijgsman et al. 1999) (Fig 135). In terms of lithology, this material generally corresponds to blue marls (Sani et al. 2007), which constitutes the Neogene sedimentary cover of the Pre-Rif nappes (Capella et al. 2017).

The origin of this material is tied to the late Rif orogenic phase, which ended in the Late Tortonian (8Myr) (Van Hinsbergen et al. 2014). The deformation in the inner arc and the subsidence in its outer segment allowed the sedimentation of the said blue marls that are onset and largely undeformed (e.g. Achalhi et al., 2016). The resulting sediments formed the late Miocene, Rif Corridor formations, as part of shallow late-orogenic fill sedimentation in foreland basins (Sani et al. 2007).

In relation to tectonic deformation, the Rif chain is an area of moderate tectonic activity. Its location in the convergence zone between the Nubian and Iberian plates implies an oblique NW-SE shortening with an average rate of around 4 mm/yr (e.g. DeMets et al., 2010), itself associated with the extensional deformation of the Alboran Sea (Vernant et al. 2010). However, the mantle processes observed in the central Rif propose southward crustal movements that are perpendicular to the movement of the Nubian and Iberian plates (Fadil et al. 2006; Pérouse et al. 2010; Vernant et al. 2010). This divergence highlights a complex relationship between crustal tectonics and mantle processes through models such as the retreat of the dipping slab of the oceanic lithosphere or the detachment of a part of the subducting continental lithosphere (e.g. Bezada et al., 2013). These models, coupled with recent data (Faccenna et al. 2004; Bezada et al. 2013; Baratin et al. 2016), indicate that the kinematics of the Rif cannot be simply related to convergence between two plates, but rather to mantle processes beneath the betico-Rif chain (Fadil et al. 2006; Vernant et al. 2010).

Evidences for this crustal deformation are manifested in the southern front of the Rif Range since Quaternary times; due to the reactivation of the Pre-Rif thrust ridges where most of the deformation is manifested (Meghraoui et al. 1996; Bernini et al. 2000; Moratti et al. 2003; Bargach et al. 2004; Chalouan et al. 2006). The latter processes continue in the present with a slip rate of around 0.7 to 4

mm/yr (Chalouan et al. 2014; Poujol et al. 2017b; Agharroud et al. 2021) and an uplift rate of around 0.6-2 mm/yr. Currently, active tectonics are reasonably well-characterized along the Fez-Meknes reverse-senestral fault segments (Poujol et al. 2017b; Agharroud et al. 2021), which is controlled by the interaction between deformation in the Pre-Rif thrust ridges and NE-trending basement faults affecting the Mesozoic cover (Agharroud et al. 2021). Such faults induce a thickening of the Mesozoic material due to compressive deformation (Sani et al. 2007).

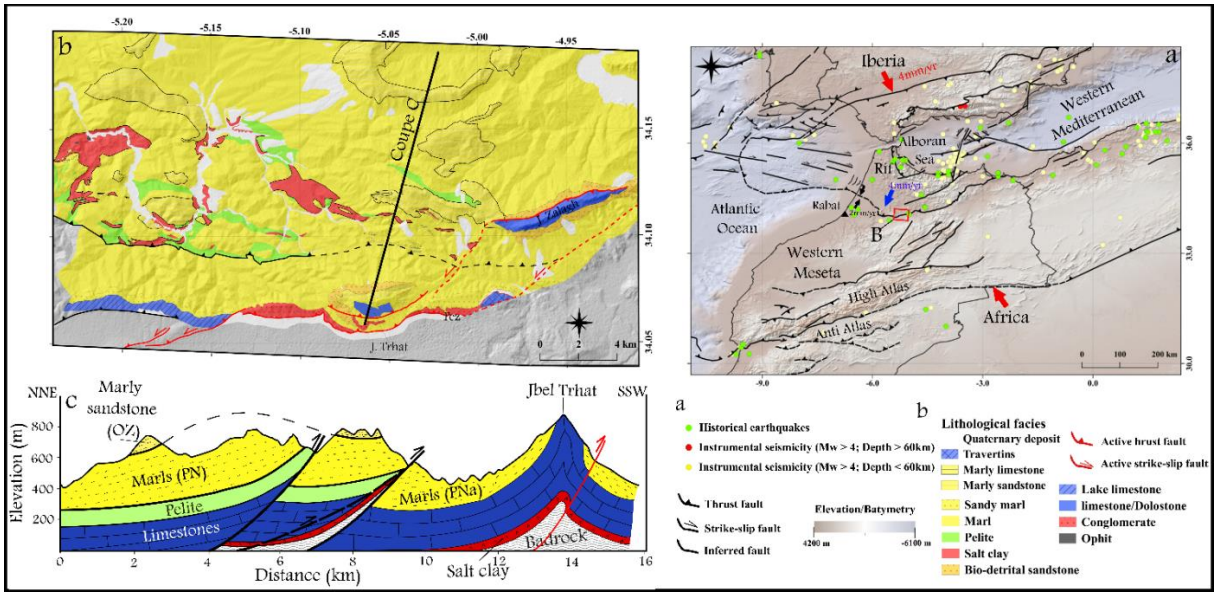

Fig.135 Geological map of the study area. a Seismological and tectonic map of Northern Morocco. b Geological map of the Pre-Rif ridges. c 2D Cross section exposing the structure of the Pre-Rif ridges Morphotectonic unit.

Geomorphologically speaking, the Pre-Rif ridges (Daguin 1934) are two distinct compressive deformation structures that affect the Neogene basins where the Mesozoic and early Cenozoic substratum outcrop (Jurassic, Cretaceous, and Neogene sedimentary sequences) (Fig 135). The Mesozoic formations are detached from the Paleozoic basement and are affected by fold-related faults caused by compressive deformation associated with tectonic convergence (Chalouan et al. 2006; Roldán Garcia et al. 2009). Subsequently, a NE-SW oriented compressional phase of the Late Tortonian forms complex overlapping structures associated with lateral ramps creating thus the outcrop of Pre-Rif ridges that suffer from N-S compressive phase during the Pliocene (Sani et al. 2007). From the Pliocene to the Quaternary era, the direction of compression applied to the Pre-Rif ridges is oriented N-S to NNE-SSW, following the regional geodynamic tendencies (Bargach et al. 2004; Michard et al. 2006). These processes are responsible for the current structuring of the Pre-Rif ridges that dominate the landscape. With regards to active tectonics, these structures are deforming and being translated towards the SSW with an annual rate of 2 mm (Chalouan et al. 2014). However, the rate of deformation can be higher as shown by Chalouan et al (2014) who reported an annual rate of 4-5 mm/yr in the Trhat ridge (Chalouan et al. 2014). Consequently, recent evidence have surfaced

regarding the tectonic reactivation the Pre-Rif (Meghraoui et al. 1996; Bernini et al. 2000; Moratti et al. 2003; Poujol et al. 2017b), with the lest being the in an important seismic event that struck the region in 1755 (Moratti et al. 2003; Poujol et al. 2017b).

3. Methodology

A. Choice of the study area

As stated in section 2, the study area is part of the deformational front of the Rif cordillera, where the current compressive stress is concentrated and manifested. Thus, it was chosen to quantitively evaluate the effects of the latter on the evolution of surface processes, mainly those in relation to mass movements and slope instability mechanisms. However, tectonic deformation is not evenly distributed across the region. In fact, in the South Rif Ridges (SRR) morhostructural unit, where Mesozoic material outcrops, the deformation and uplift are relatively more intense compared to terrains located to their immediate North. Consequently, the impact of tectonic deformation is expected to have more pronounced effects on surface processes especially given the high erosion rates at the area.

Taking this into consideration, we decided to split the study area into three main zones, noted zones 1, 2 and 3 (Fig 136). The latter involves the South Rif tectonically active ridges, while the former is mainly formed by Miocene marly terrains that are moderately affected by neotectonic deformation. Zone 2 is located in an intermediate geographic position and is characterized by neotectonic deformation structures that were not demonstrated to be affected by current tectonic processes. In such a manner, the contrast between the three investigated zones should reveal the amount by which the recent tectonic activity at the area impacts slope dynamics.

B. Inventory of gravitational processes

In the Southern Rif front, no reliable inventory of slope mass movements has been previously developed. Thus, we established an inventory map according to the classification of Hungr et al., (2014) who proposed a more detailed update of the Cruden and Varnes, (1996) system. The main landslide-mapping step was based on geomorphological field mapping, on visual interpretation of the aerial photos, and on the use of satellite-derived imagery from the Google Earth and Bing databases. Although easily accessible, such satellite imagery platforms provide reasonably accurate data that can be exploited by geologists and geomorphologists alike (Qiu et al. 2017a, b). To complete the remotely sensed inventory, seven field investigation surveys were conducted in February 2020, July 2021, and October 2021 in order to check and validate the identified slope instability cases.

C. Geological data

The geological data used in the current study are the lithology and active neotectonic faults. While the former factor was used for conducting explanatory statistics, the latter was used to subdivide the study area into the three zones described above (Fig 136) and integrated later into the geomorphological model. This data was extracted from geological maps covering Moulay Yacoub province: Fez West 1/100 000 (S.G.A 1942) and Rif chain 1/500 000 (Suter 1980b), that we improved and rectified according to field observations, especially regarding lithology. As for active faults, we completed and filtered the data through synthesizing the findings of recent studies on active tectonics at the southern Rif front (Poujol et al. 2017b; Agharroud et al. 2021), which allowed defining active and recent segments that helped distinguish between tectonically shortened areas and those unaffected in comparison.

D. Morphometric indices

a) Landslides morphometry and density

Morphometric analysis of landslides is a useful tool for characterizing slope dynamics in a given region. Although area and length constitute good metrics for studying the size of mass movements, they do not define the shape of landslides and thus are not sufficient for characterizing the morphology of such phenomena. To overcome the limitations of such simple landslide metrics, other indices are used such as the length to width ration (L/W) (Niculită 2016) and the height to length ratio (H/L) (Hattanji and Moriwaki 2009), which provide information about the shape and geometry of slope instability cases as opposed to only relying on size indices. Although acquiring information to calculate such indices is laborious and time consuming, Geographic Information Systems (GIS) allow to estimate the length, width and Height difference for a large number of landslides in a very short time. For the first two parameters, the Bounding Box can be used which yields a good estimation of a landslides general shape (Taylor and Malamud 2012), with its major axis representing the length and its minor one being equivalent to the width of a given mass movement. Regarding elevation height, it can be obtained subtracting the minimum elevation value from the maximum elevation value for an area delimited by the landslide's geometry. In our case, the digital elevation model (DEM) used for this purpose is the 12.5 meters Alos Palsar DEM downloaded from Alaska Satellite Facility platform.

Although the indices described above are good for studying the shape of a given landslides, they give information about its spatial distribution which could also be used to characterize the severity of landsliding phenomena in the study area. To achieve this, Kernel Density (KD) is commonly used in landslides research as a way to measure slope instability abundance in the area of interest (Rossi et al. 2012; Conforti and Ietto 2020). A good inventory is crucial for obtaining reliable values that reflect the reality of the terrain. Hence, the landslide inventory map (LIM) prepared in this study was used to produce KD maps for the three zones of the study area with the help of GIS tool. Then the KD raster files were converted to table in order to be used for comparison purposes.

b) Ravine density

Deeply incised gullies and ravines are often associated with landslides especially in the case of fine-grained sedimentary rocks where they tend to be responsible for triggering a significant portion of landslide processes (Vandaele et al. 1996; Roering et al. 2015; Hsieh et al. 2016). For this reason, we attempt to compare ravine density distributions across all three investigated zones. The deep ravines and gullies are derived from an expert-based inventory of surface erosion processes realized in this study, where ravine affected areas are mapped and represented by single polygons in a GIS platform (Fig 136). For spatial density assessment, the KD method was used.

E. Area-Frequency distribution analysis

Several studies in the last decades have shown that landslide populations exhibit some power-law scaling across a portion of their size distribution in earth and even in Mars (Brunetti et al. 2014). Such distributions seem to be well-fitted to the double Pareto model and the three-parameter inverse gamma probability distributions (Stark and Hovius 2001; Guzzetti et al. 2002; Malamud et al. 2004; Li et al. 2016; Jafarimanesh et al. 2018). The tail of landslide size probability distribution for medium and large landslides is a power law where α controls the power law decays for medium and large landslide sizes, while β controls the maximum probability density of landslide distribution in square kilometers, and γ controls the rate of decay for small landslide areas in square kilometers.

$$f(x) = \frac{\beta}{A_p} \frac{\left[1 + \left(\frac{A_{max}}{A_p}\right)^{-\alpha}\right]^{\frac{\beta}{\alpha}}}{\left[1 + \left(\frac{x}{A_p}\right)^{-\alpha}\right]^{1+\frac{\beta}{\alpha}}} \times \left(\frac{x}{A_p}\right)^{-\alpha-1}$$

Where x is landslide area, A_{max} is the largest landslide area in the data; A_p is the area of the rollover; α and β are exponents of power law scaling related to slope. The probability density distribution for medium and large landslide sizes decays rapidly along a power law with an increasing α.

$$f(x) = \frac{1}{\beta\Gamma(\alpha)}\left(\frac{\beta}{x-\gamma}\right)^{\alpha+1} exp\left(\frac{\beta}{x-\gamma}\right)$$

Where α is a continuous shape parameter (α>0), β continuous scale parameter (β>0) and γ is continuous location parameter. Γ is the gamma function given by:

$$\Gamma(\alpha) = \int_0^\infty t^{\alpha-1} e^{-t} dt \qquad (\alpha > 0)$$

In our case study, we used logarithmic binning to obtain the landslide area-frequency distributions for the three selected areas. This allows to characterize the size distribution as well as the maturity of landslide processes through comparing the power law parameters for medium to large-scale landslides, and rollover locations for smaller ones (Guns and Vanacker 2014; Tanyaş et al. 2019; Qiu et al. 2020).

F. Statistical analysis

a) Analysis of variance (ANOVA)

The difference between the samples and groups can be obvious through comparing their mean and standard deviations. However, the difference is not always statistically significant since sample size and sampling errors may induce differences that are not due to a real variation between the groups. Consequently, statistical tests are needed to assess whether the difference observed is significant enough to reflect true variance across sampling groups. One of the most famous statistical tests is the two-sample Student test which allows to compare the statistical significance of inter-group variation for two samples (Student 1908; Zabell 2008). However, since the study area is divided into three zones (samples), this test cannot be used. The other test which is more appropriate for such application is the one-way ANOVA test which allows to quantitatively assess the homogeneity between various groups and samples for one or more variables. This test can be supplemented by Pos-Hoc tests that show which groups are different and which are similar; In this stuy, the ANOVA technique (Fisher, 1921; Williams 1986; McKillup and Dyar 2010) and the Post-Hoc Tuckey's range test (Tukey 1949) were conducted using R-studio statistical software. The input data used is exported using a GIS tool and is introduced as a data table with each line corresponding to a landslide and each column corresponding to a morphometric variable.

b) Frequency Ratio

Frequency ratio (FR) analysis is a widely used explanatory statistics technique that allows to assess the relative proneness to landslide activity for categorical determining factors. It is widely used in landslides susceptibility research and is considered a simple, time-saving and reasonably accurate method for landslides susceptibility mapping (e.g. Aditian et al., 2018; Chen et al., 2020; Mohammady et al., 2012; Othman et al., 2018; Pradhan and Lee, 2009; Xiao et al., 2020). In addition, this bivariate technique can also be used in geomorphological characterization studies to quantitatively evaluate the cause and effect relationship between landslide occurrence and their potential determining factors (Conforti and Ietto 2020; Bounab et al. 2022). In this study, the correlation between landslides and lithology is analyzed using the FR technique. Although previous case studies suggest Miocene marls to be the most unstable material in the area (e.g. Obda et al., 2022), we want to confirm this conclusion using statistical tools, to see if this fine-grained sedimentary rock is more prone to landslides. The source of lithological data is shown in (section 3.2.).

G. Slope instability analysis

The factor of safety (FS) analysis is a deterministic method to quantitatively assess the stability of hillslopes. Although originally used by civil engineers to simulate the stability of hillslopes especially when topographic and loading conditions are modified (Tsiampousi et al. 2013; Jamsawang et al.

2015), it has been increasingly used by geologist and geomorphologists alike in the last two decades. Of the various applications, the slope instability back analysis can be used to link relict and very old landslides to possible historical triggers such earthquakes (e.g. Claessens et al., 2006; Rodríguez-Peces et al., 2011) or to establish deterministic predictive model for future occurrences (Liao et al. 2010; Jeong et al. 2018; Jiang et al. 2022). In this study, the factor of safety (FS) is used as a tool to define stability thresholds, and thus, to provide good insight on the effects of topography on the stability of materials that promote landslides. The geotechnical characteristics of the geological materials are obtained from laboratory tests conducted on samples that we collected during field surveys in January 2020, and are compared to values reported by (Obda et al. 2022).

4. Results

A. LIM results

In total, 1291 solifluxions, 1766 earthflows, 1968 slides and 170 complex movements were identified in the study area (Fig 2), which corresponds to a total landslide-affected surface of 55.77 km². Most of the inventoried landslides occur in the marly slopes of Moulay Yacoub region. As for landslide types, slides represent 66% of the affected area and are mostly rotational in nature. An example of this situation is presented in a recently published case studies in the region (El Kharim et al. 2021; Obda et al. 2022). Our field surveys and the LIM map presented in Fig 136 show that the largest slope instability cases occur near the Pre-Rif ridges (Jbel Zalagh and Jbel Trhat) and along thrust fault lines, sometimes affecting the road network and man-made facilities (case of Trhat, Oued Fez districts and Moulay Yacoub town). This observation was corroborated by the statistical distribution of each landslide type in the three selected zones (Fig 136), where slides largely dominate in zone 1 and 2 showing a frequency of up to 80% compared to less than 20% for all other landslide types in zone 1 and 45% in zone 2. As for zone 3, earth flows and slides have almost the same frequency of occurrence (~40%). Complex landslides and solifluctions are less significant for all three investigated areas.

With regards to the spatial distribution of landslides, the visual interpretation of the LIM suggests the existence of a significant difference between the three investigated segments of the study area in terms of mass movement density. In fact, to the North, zone 1 seems to house less landslides by comparison to zone 2 and zone 3 with most landslides been spatially associated with the steeper topography and the deep ravines and gullies of the Pre-Rif ridges (Fig 136).

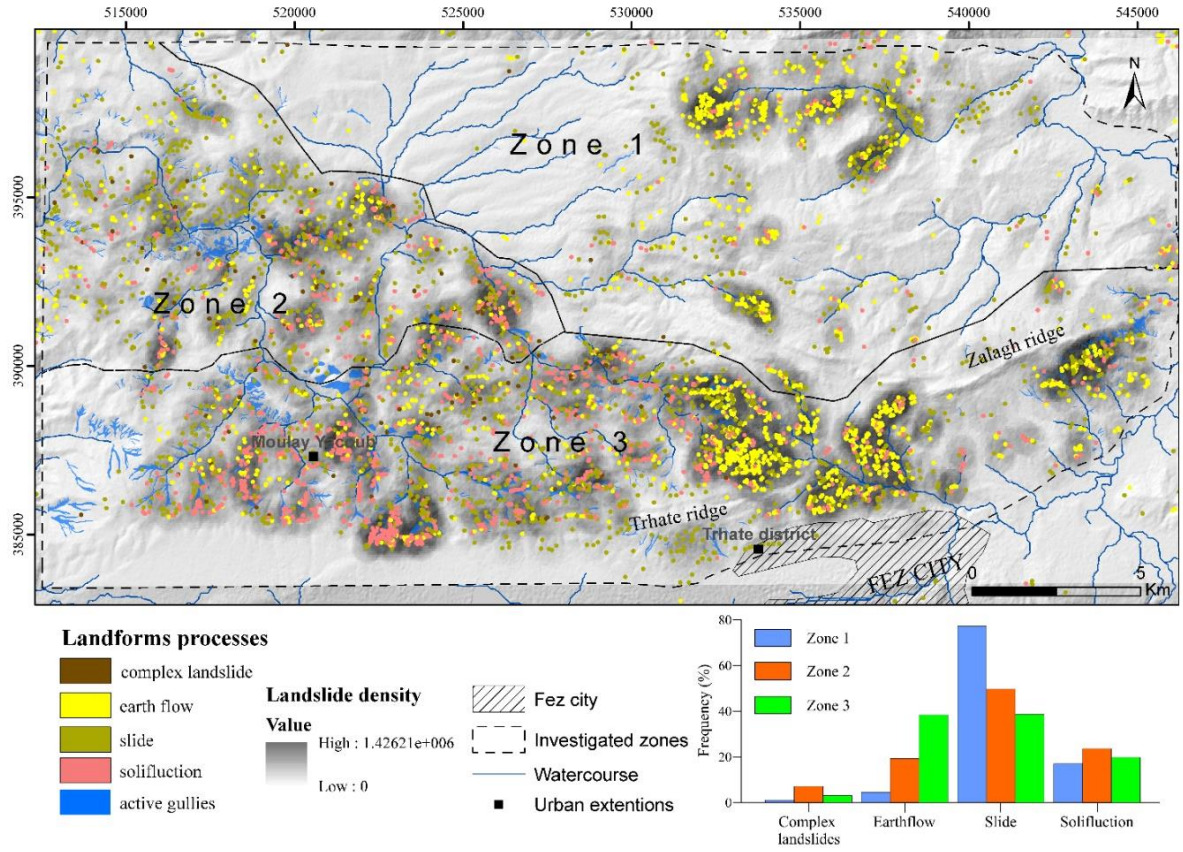

Fig.136 Landslides and active gully inventory with the frequency-type distribution of landslides in the right bottom corner

B. FR analysis results

The FR analysis results show that all lithological formations of zone 1 score low in comparison to the mean frequency of the study area (FR<1), with calcareous marls and clayey colluvium having the highest FR values (Table 27). This further confirms visual interpretation results with regards to the low density of landslides in zone 1. For zone 2, marls and calcareous marls show high FR values (FR>1), especially for marls which exhibit the highest FR value (FR= 1.8) of all lithological formations outcropping at the study area. The large spatial extension of marly outcrops by comparison to other types of lithological formation further increases our confidence in this statistical association, especially given that large spatial extensions in addition to the monotony of marly formations in the pre-Rif region tend to yield conservative FR values in most cases (Sahrane et al. 2022). As for zone 3, fine-grained materials (marls, calcareous marls, pelites, clayey colluvium and sandy marls) are all marked by relatively higher FR values (1.05<FR<1.5), which also suggests the existence of a correlation between marls and landslides in the region. However, it is worth mentioning that Marls in zone 1 have a low FR value of 0.54, which indicates that such geological materials are only correlated with slope instability under certain geomorphological conditions. The latter are discussed in section 5.

Table 27 FR values for each lithological facies within the study area

Lithology	**Zone 1**	**Zone 2**	**Zone 3**
Soils	-	0.11	-
Recent alluvial deposits	0.00	0.73	0.75
Old alluvial deposits	0.01	0.98	0.04
Clayey colluvium	0.84	-	**1.14**
Marls	0.54	**1.80**	**1.50**
Calcareous marls	0.80	**1.19**	**1.05**
Sandy marls	-	-	**1.12**
Marl/sandstone alternation	0.55	0.82	0.17
Marl/limestone alternation	0.70	-	0.63
Lacustrine limestone	-	-	0.04
Conglomerates	-	-	0.88
Pelites	0.71	0.72	**1.43**
Dolomites	-	-	0.58
Saliferous clays	0.15	0.69	0.55

C. Power law results

For the three investigated zones, the results of the landslide frequency-size distribution analysis are generally well-fitted to double Pareto and inverse gamma models (especially for zone 3), with a slight heavy-tailed behavior for large landslides in zones 1 and 2 (Fig 137). In effect, Guzzetti et al., (2002); Sahrane et al., (2022), Tanyaş et al., (2019) propose the degree of fit of a given landslides distribution to the above-described statistical models as a reliable quantitative tool for assessing the completeness of LIMs. Consequently, the LIM of zone 3 can be considered the most complete of the bunch since it fits better to the theoretical size-frequency distributions of landslides. Conversely, zone 2 LIM deviates from the mathematical model at the rollover position, thus indicating a lack of small and medium size processes in the inventory. Such results indicate that slope dynamics in zone 3 are more recent and active by comparison to zone 2 since smaller landslides are not yet erased by erosion processes and cereal farming activity in the former area.

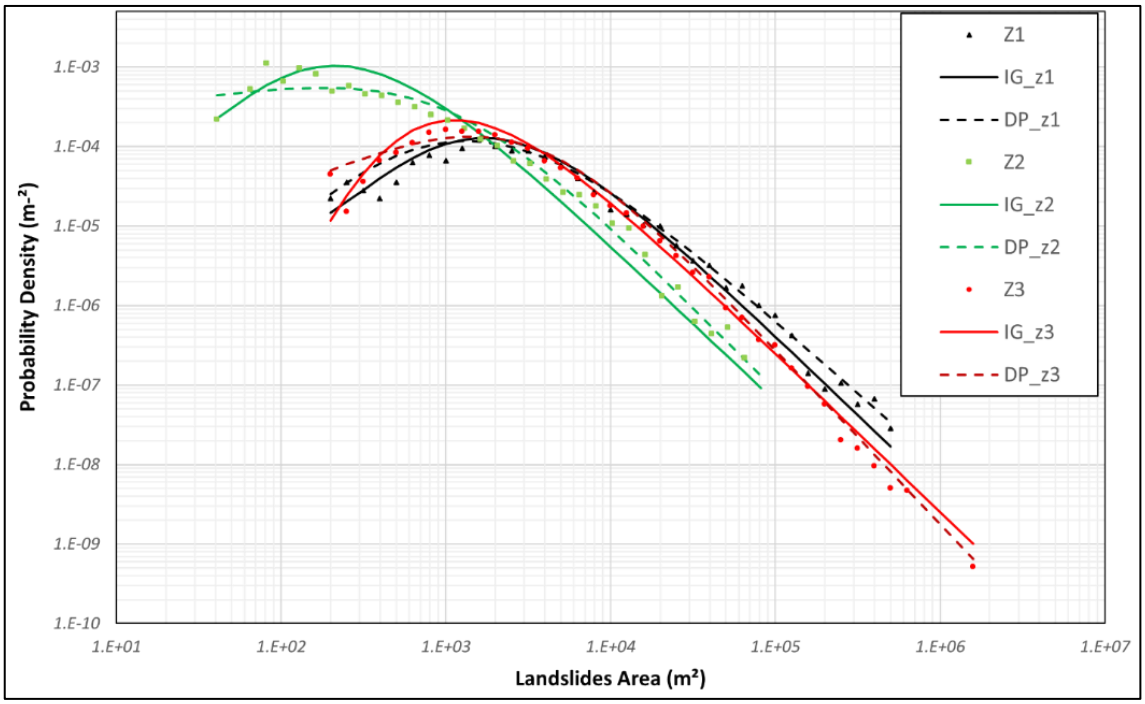

Fig.137 Frequency area distribution for all three investigated zones. IG: Inverse -Gamma, DP: Double-Pareto

D. Morphometric analysis results

The morphometric analysis results show that the kernel density for zone 2 and 3 is much higher than that of zone 1 (3.44) (Fig 139). This is expected given the absence of recent tectonic deformation on the latter and its presence in zone 3 (Chalouan et al. 2014; Agharroud et al. 2021). Although significant tectonic deformation is observed in zone 2, no evidence of recent or active tectonic processes were identified in this segment of the study area.

As for the mean area of landslides, our findings suggest that the highest value can be attributed to zone 1 while the lowest is characteristic of zone 3, which further supports the results of power law analysis. The low average area for zone 3 can be explained by the presence of more frequent small-scale processes that can still be mapped and clearly identified. However, erosion processes have eliminated most small-size mass movements especially in zone 2 where the terrain is steep, and the density of landslides is high, but the mean area is relatively low.

As for the mean slope, the values are quite comparable with a maximum for zone 1 (21.48°) and a minimum for zone 2 (18.08°). This can be attributed to the absence of landslides in the gentle marly terrain in zone 1, hence their low FR values (Table 27), due to the slow tectonic deformation compared with denudational erosion and seasonal plowing activity. However, in zone 2 marls have already reached their stability threshold and were consequently involved in landslides, thus dropping down the mean slope value. For zone 3, marly terrains are still affected by topographic growth given the ongoing tectonic deformation processes which in turn attributes to a higher average landslides slope.

As for the mean ratio values, they are close with a minimum for zone 1 (0.42) and a maximum for zone 3 (0.46). The statistical significance of the difference is revealed in the following section.

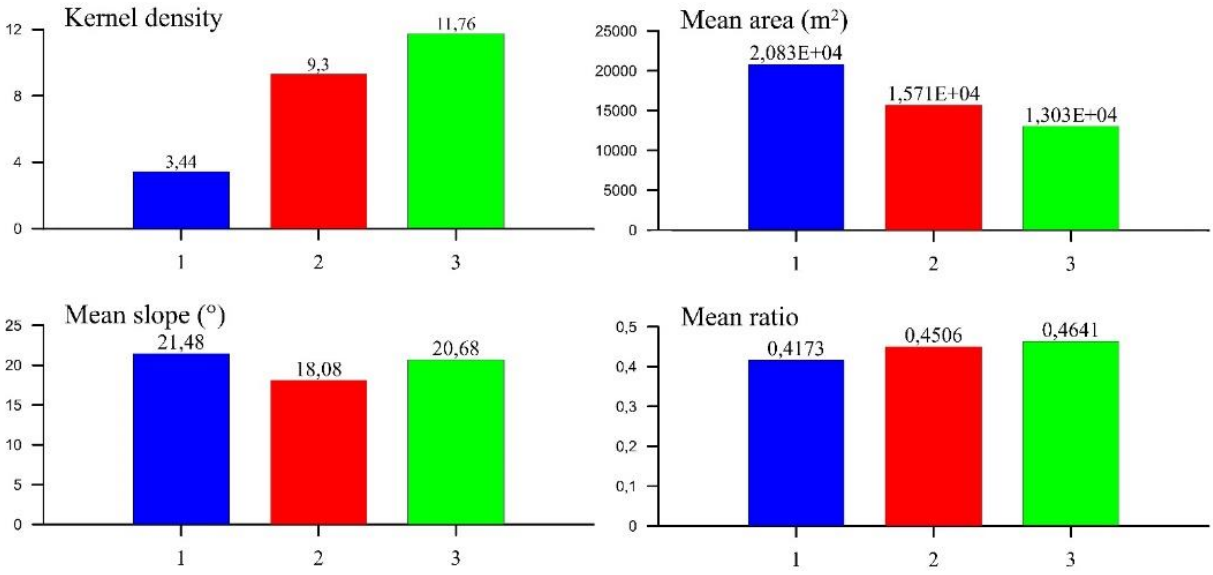

Fig.138 Mean values of the morphometric indices used to characterize the landslide affected area for each zone (zone1 in blue, zone 2 in red and zone 3 in green).

E. ANOVA results

To compare different groups, the ANOVA test/analysis is performed, which allows differentiating between statistically significant variances and those that are due to sample size or hazard (Table 28 and 29). In our case study, we use the 1 factor ANOVA technique to compare the three investigated zones. Our results suggest that in terms of landslides area, zones 2 and 3 are found to be similar with the difference between both zones and zone 1 being statistically significant according to the Tukey post-Hoc test (Table 28). This, along with the above-described results emphasizes the role of tectonic deformation in determining the average size of a landslide. With regards to Aspect ratio, our findings show that the shape of landslides in zones 2 and 3 is more or less similar and that mass movements in zone 1 differ significantly from the bunch. This can be interpreted by the presence of strong expressions of tectonic deformations in both zones 2 and 3, which control the heterogenous landslides dynamics, while their absence in zone 1 promotes plastic deformation styles especially in marly terrains. As for the Kernel density of landslide, it was shown to be significantly different across the three investigated areas, which further supports the above-advanced hypotheses (section 4.3). This is also true for KD values for gullies which seem to suggest a significant difference between zone 1 and the two other investigated zones (Table 29). This statistical result is an expression of the morphotectonic evolution of the region where areas affected by recent (zone 2) or active (zone 1) tectonics are subject to deep water incision processes while the non-deformed marly hills of zone 1 seem to present little to no evidence of active gullying.

The mean slope value discussed above is found to be significantly different between zones 1 and 2, and zones 2 and 3 (Table 28). However, the insignificant difference between zones 1 and 3 is not due to similar geomorphological processes but can be explained by simple statistical chance.

Table 28 ANOVA test results comparing the distribution of landslides morphometric indices across the study area

	ANOVA test		**Tukey difference of significance test**		
Variable	F	P-value	Difference between means		P-value
Area	10,381	< 0,001	1 and 2	5122,40711*****	0,031
			1 and 3	7801,50108*****	< 0,001
			2 and 3	2679,09397	**0,199**
Mean slope	7,154	< 0,001	1 and 2	,03400*****	0,002
			1 and 3	0,00805	**0,621**
			2 and 3	-,02595*****	0,003
Aspect ratio	23,505	< 0,001	1 and 2	-,03330*****	< 0,001
			1 and 3	-,04683*****	< 0,001
			2 and 3	-0,01353	**0,074**
KD	14362,23	< 0,001	1 and 2	-4,71707*****	< 0,001
			1 and 3	-7,86295*****	< 0,001
			2 and 3	-3,14587*****	< 0,001

Table 29 ANOVA test results comparing the Kernel Density of ravines across the study area

	ANNOVA test		**Tukey difference of significance test**		
Variable	F	P-value	Difference between means		P-value
KD	700,24	< 0,001	1 and 2	-180.076	< 0,001
			1 and 3	-182.665	< 0,001
			2 and 3	-2.85	**0.931**

F. Factor of safety for marly slopes

Since marly terrains are the main lithological formations susceptible to slope instability, especially in areas with strong tectonic deformation, they were the subject of a slope analysis that focused on their stability threshold (Fig 139). Two types of marly material are to be distinguished. The first is the grey Tortonian marls (non-weathered) which constitute the bedrock material, and the second is the yellowish weathered marl layers, derived from altering the substratum mentioned above. The geotechnical characteristics of these materials are presented in table 30.

Table 30 Geotechnical investigation results for weathered and sane marls

Soft rocks samples	***Density (10^3. Kg/m^3)***		***c' (Kpa)***		***Φ' (°)***	
	min	max	min	max	min	max
Yellow marls	1.6	2.1	3	21	17	29
Grey Tortonian marls	1.8	2.4	25	37	4	8

As such the results of slope stability analysis are presented for 9 theoretical slopes with varying slope steepness (5, 10 and 15°) and different weathered layers thickness (0, 10, 15m) but with the same height difference (65m) for all scenarios. In the absence of weathered marls (first scenario), the stability analysis showed that a 10° slope slightly exceeded the stability threshold (Fig 139 -A, -B and -C). However, with a 10° slope, the FS is near to 1 suggesting that the material is not fully unstable. With regards to the scenarios involving weathered marly layer, our analysis shows that the presence of a 10m or even 15m thick weathered layer does not change the stability threshold compared to the first scenario.

To interpret these results, the statistical distribution of slope steepness in marly terrain is presented in Fig 5, below slope stability simulation. The histogram shows that zone 1 differs from zones 2 and 3 in terms of statistical mode and frequencies. In fact, 5° to 10° are the most dominant slopes in the former zone, which constitutes the mode of the latter. As for steeper slopes (more than 15°), they are more frequent in zones 2 and 3. Based on the threshold values presented above, a discussion of the stability of marls is presented in section 5.

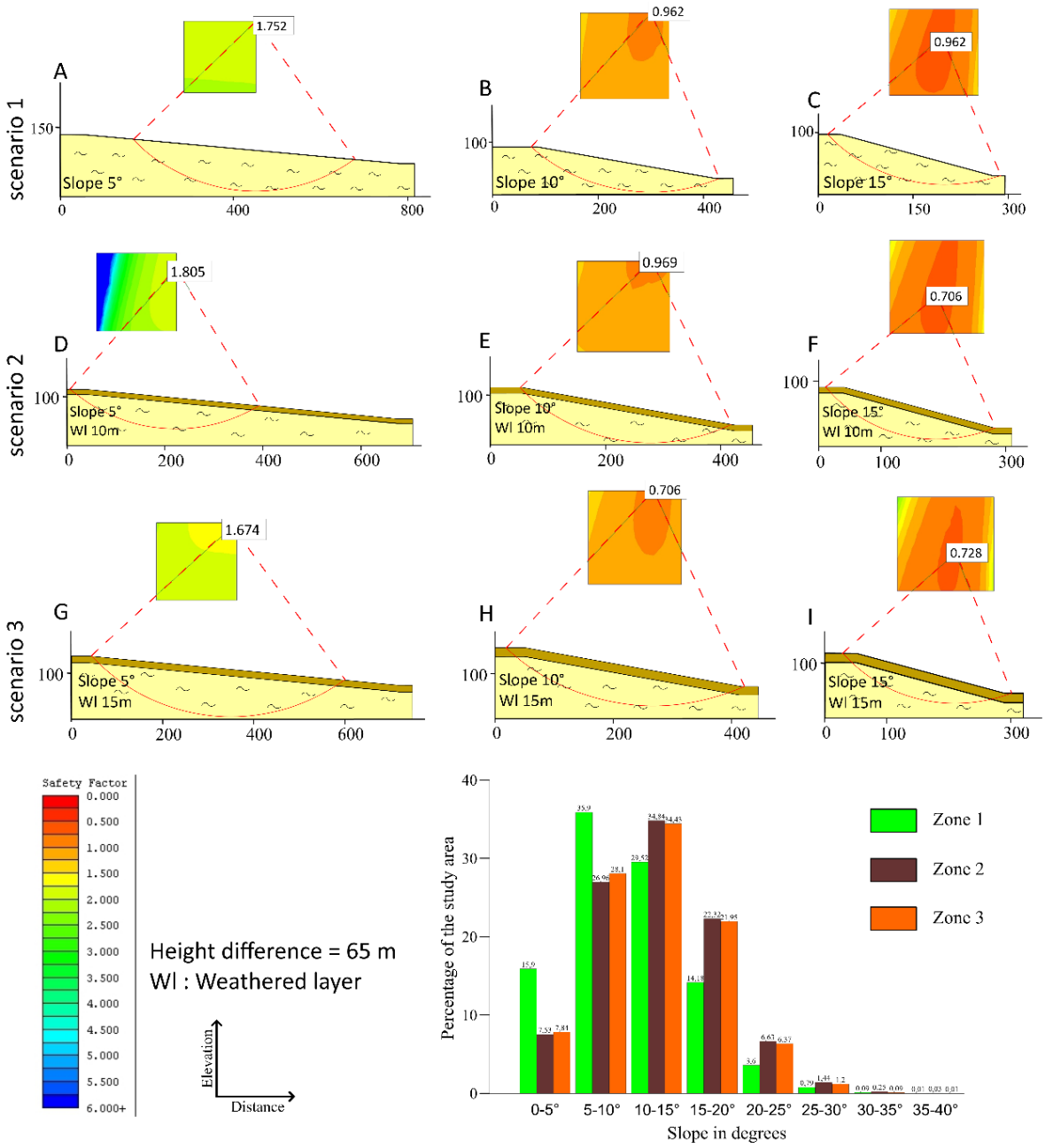

Fig.139 Slope instability analysis for different theoretical scenarios: no weathered marls are present (A, B and C), a 10 m thick weathered layer is present (D, E and F) and a 15 m thick weathered layer is present (G, H and I). The distribution of marly slopes is presented at the bottom.

5. Discussion

A. Stability of marls and their erosional landforms

Our findings show that the areas most affected by tectonic deformation are the ones presenting the highest density of active gullies. In fact, this is proven worldwide in different geological settings where extremely active gullying is linked to elevated zones and steep topography, themselves the product of regional tectonic uplift and/or major climate change events or base level variations

(Menéndez-Duarte et al. 2007; Huang et al. 2012). Other factors such as rainfall erosivity and landcover also contribute to the incisive power of gullies but do not constitute their major control parameters (e.g. Zhao et al., 2016). In the study area, renewed gullies, generated by backward erosion, strongly suggesting a recent uplift activity according to recently published research that uses high-resolution DEM to conduct morphometric analyses (Agharroud et al. 2021). This is supported by Kernel density values presented in this study (Fig 138), which clearly demonstrate that zone 3 is dominated by an active gullying system. An example is shown in Fig 140, where neotectonic topographic growth along a major thrust fault predisposes the terrain to intense hydrographic erosion (a). In addition, it disturbs the flow of ravines in the study area where one can clearly distinguish the presence of micro knickpoints suggesting tectonic uplift (Fig140-d).

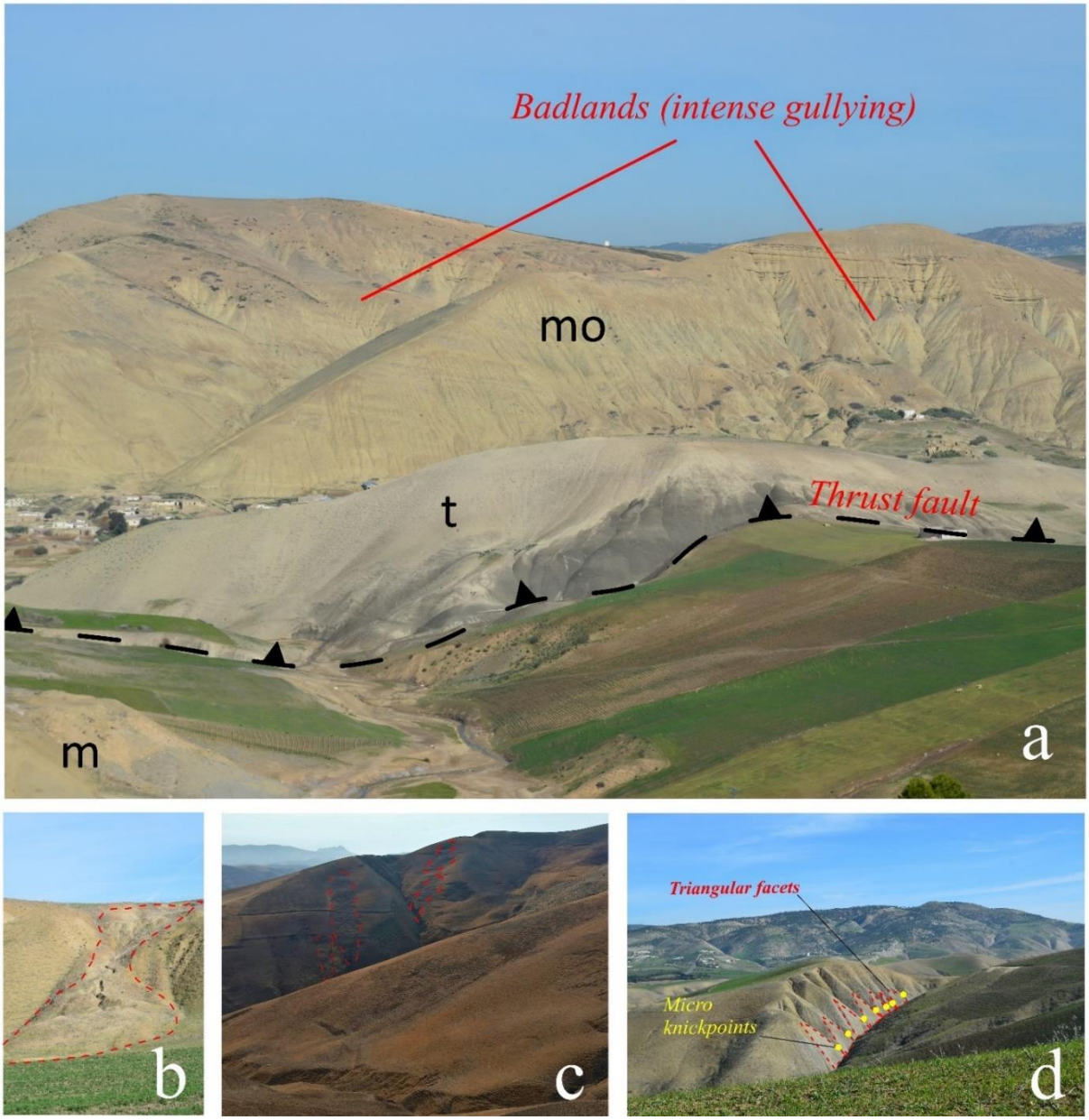

Fig.140 Field photographs of the study area. a Thrust fault photographed in zone 1, mo: marls of Ouazzane unit, m: Pre-Rif marls, t: Triassic clays (zone 3). b slide earthflow sliding down a gully landform in zone 2. c shallow landslides associated with active gullying in zone 3. d Active gullies in zone 3 interrupted momently by another incision phase.

However, gully erosion does not affect all lithological materials equally. In fact, a century of research has proven that soft materials are more easily eroded by hydrological processes in general and active gully systems in particular (Castillo and Gómez 2016). In our study area, such materials are abundantly present in the form of marls and their weathering products (Fig 1). Nevertheless, this situation is not true for zone 1 where the marly terrain is not steep enough to trigger the said gully incision. Consequently, most gullies in this zone are inactive and/or filled by mature alluvial sediments (Fig 141). However, the situation is different in zones 2 and 3 where downcutting processes are more aggressive and thus steepen the otherwise gentle marly hills (Fig 140 d.). Although proof of current or

recent tectonic uplift in zone 2 is not yet presented, evidence for neotectonic deformation since the late Tortonian are already provided by Morel, (1989) and revisited by Capella et al., (2017). This difference in the dip angle of marly slopes is obvious in slope values for each zone (Fig 139) and its overall distribution (Fig 141). While it is obvious that steeper gully-generated slopes promote landslides (Fig 140-c), the role of such landforms can also involve the creation of "established pathways" that facilitate the spread and elongation of earth/debris flows (Fig 140-b), and provides areas where seepage accumulates, thus promoting debris slides (Hungr et al. 2014). In our case study, the Kernel Density values (Table 29) show that the areas with the most gullies are also the ones with the most mass movements. This is more noticeable in marly terrains which have a low stability threshold as shown by stability analysis results (Fig 139). Consequently, the effect of tectonic deformation is indirect in the form of a slow and consistent uplift that intensifies hydro-geomorphological erosion and slope dynamics (Fig 6). Other than the 1755 earthquake estimated to have an intensity of around VIII (El Mrabet 2005), current instrumental data suggest moderate to low magnitude seismicity (less than 4, Fig 135). In fact, the analysis of worldwide landslides historical catalogs proved that an earthquake with a minimum magnitude of 5.5 to 6 is required to trigger large landslides (Keefer 1984; Rodríguez et al. 1999). Consequently, earthquake-induced mass movements are unlikely to occur under the current seismotectonic conditions of the Pre-Rif Ridges. However, the active faults at the region show potential for rapid reactivation, which can trigger more intense earthquake events with magnitudes of up to 6.8 (Agharroud et al. 2021). Such threats are not considerable given the very long return period of such reactivations.

B. The effects of active tectonics on landslide distributions

The Miocene marls found in the study area were deposited in marine channels during the Miocene (Krijgsman et al. 1999). However, in the late Tortonian, this thick marine sedimentation ended because of compressive tectonic deformation. During the early Pliocene, the paleo-Sebou fluvial channels are seen in the sedimentary sequence indicating the passage from a marine sedimentary environment to a terrestrial fluvial regime (Charroud et al. 2007) (Fig 7). During the rest of the Pliocene, the regression continued, and no more marine sedimentation was deposited. Although the exact date of tectonic reactivation of the old inherited structures is not yet given, it is believed that since the Villafranchien, the ridge structures started to form in response to the N-S oriented compressional deformation (Bargach et al. 2004; Chalouan et al. 2006; Sani et al. 2007) (Fig 141). This deformation mainly affected both zones 2 and 3 and is responsible for the tectonic growth and topographic irregularities in these areas. The deformation continued throughout the Quaternary times and affected mainly the frontal area of the thrusted block. In response to this steepening of the topography, hydro-geomorphological processes intensified which explains our empirical analysis results. Consequently, two main domains can be distinguished with respect to slope dynamics. The first is the frontal deformation area which is affected by intense gullying and landslides with both

phenomena being spatially associated (Fig 141). The second is its foreland area which marked by a gentle topography that does not predispose the terrain to landslides (Fig 141). The high LIM completeness in zone 3 indicates that the current significant uplift at the area promotes intense slope dynamics compared to zone 2 where small processes are already eroded. This highlights the role of active tectonics in maintaining surface processes at the region, the intensity of which depends on the oldness of tectonic thrust mechanisms.

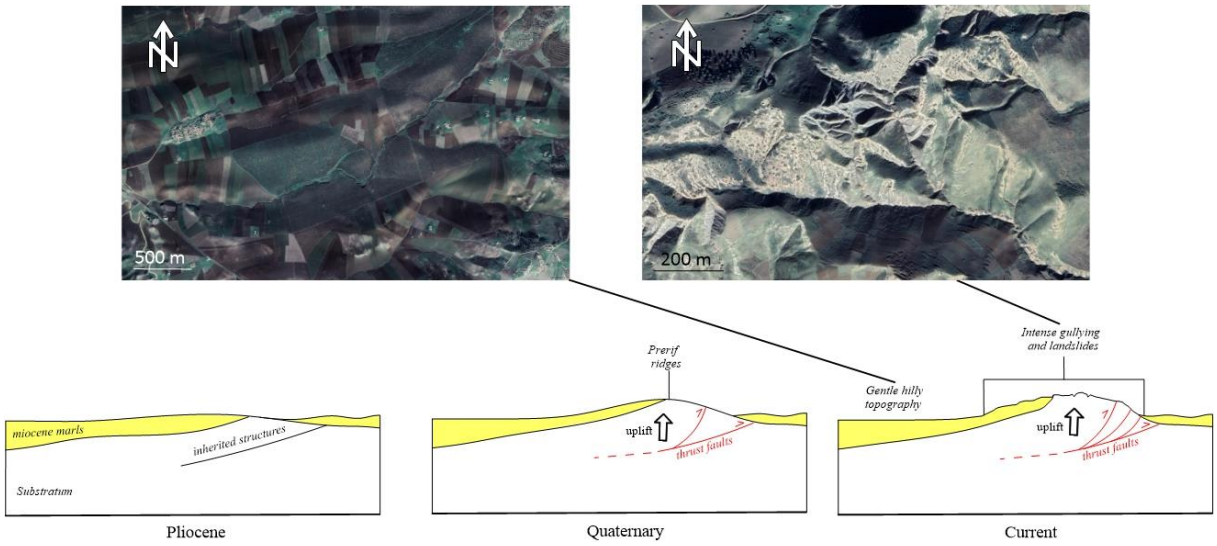

Fig.141 Geomorphological model showing the indirect influence of the tectonic uplift in the Pre-Rif Ridges on surface processes.

6. Conclusion

The tectonic deformation in the Pre-Rif ridges morpho structural unit resembles the deformation patterns observed in frontal car accidents where the front is intensely deformed and folded while the back is relatively unaffected. Such tectonic forces induce large topographic disturbances in the frontal deformation area, which translated into deeper gullies that trigger shallow landslides and steeper marly slopes that predispose the terrain for larger mass movements. Although the above-presented statistical analyses prove to a large extent the validity of this hypothesis for shallow landslides, radiometric dating efforts can be performed in the future to date the large landslides of the study area. This can further enhance our understanding of gravitational processes, especially in relation to major triggering events of the past. In fact, some relict large-scale landslides are also found in the non-deformed area, the triggering conditions of which need further investigation in the light of our findings.

X. General conclusion

The present research project aimed to study mass movements and their conditioning parameters at different spatial scales in the territory of Fes-Moulay Yacoub. This region had never been the subject of such research on this issue, except for few case studies. The originality of this work is based on its thematic framework with strong regional input aimed at a better knowledge and understanding of the functioning of these gravitational processes, the establishment of a typology inventory, then the use of different expert methods, deterministic, probabilistic and statistical for their preventive mapping at different scales. This study is also part of a context in which little database was available on the landslide risk and its predisposing factors. Therefore, it includes different strategies for the acquisition of slope movement variables and other influencing parameters.

Moreover, the interaction between the landslide hazard and the development of socio-economic activities is becoming more and more frequent, as it is observed in several regions worldwide, especially in active mountain belts as the urbanized slopes of the Rif chain. Consequently, developing urban plans, infrastructure or even agricultural projects while neglecting the multi-facets of the landslide risk can have catastrophic and costly consequences, not to mention the complexity of intervention. For this, the development of a strategy of risk approach is necessary to choose suitable investigation methods for each case and scale.

In the first step, the characterization of the study area and its geological, geomorphological, climatic, hydrological, lithological, geotechnical and even socio-economic settings is an essential step in approaching the landslides hazard. It makes it possible to define the study context and to enumerate the predisposing factors, the involvement level of which, to identify the predisposed elements and to quantify the impacts. The chapter "setting of the study area" shows that the territory of Fez - Moulay Yacoub presents a favorable context to the genesis of several mass movements. The active southern part of the Rif chain, dominated by marly and clayey formations outcropping under a sub-arid Mediterranean climate, exhibits the perfect territory for the formation of both superficial and deep slope movements. The analysis of the socio-economic context of inhabited, rural, urban, and peri-urban areas shows that anthropization is strongly involved in increasing the vulnerability of exploited areas, whether for housing or for installation of infrastructure and food production projects. The second step is to establish a complete inventory of slope movements in the study area. Such a database remains fundamental for the implementation of the different approaches used later. Subsequently, we adopted different types of approaches to the landslides hazard, each one adapted to its context and its scale.

Deterministic methods tailored for a detailed scale have proven to be robust and accurate and have enabled us to characterize the risk through its different facets and to identify interacting parameters in

detail, despite the complexity of the measures and surveys in the urban and peri-urban areas investigated. As a result, the lithological and climatic factors were found to be involved in the predisposition of the slopes of the urban extensions to landslides, and where the socio-economic factor exacerbates the problem and interacts in favor of the instability. In fact, the significant increase in the population caused by the succession of rural exodus periods leads to the expansion of these inhabitants towards the lands prone to landslides, which are the least expensive. Consequently, these housing areas do not respect the standards which can resist the sub soil displacements and the shrinkage-swelling phenomena. In addition to this, the sewerage network deteriorates following these displacements and leaks feeding the sliding body. This vicious circle involving different parameters and condemning human activity makes the landslides risk in urban extensions more complex and hinders interventions, mitigation, and reinforcement measures. However, the set of tools used in this deterministic multi-task approach allowed us to understand the kinematics of the movements studied, to define the depth, the displacement velocities, the triggering events as well as the type of the movements. In Moulay Yacoub and Chefchaouen, the slope movements affecting the two towns are slides with a rotational component and are extremely slow with periods of acceleration following major precipitation events. The rupture surfaces tend to exploit weak lithological sequences such as the interface between weathered marls and compact ones in Moulay Yacoub, or that between the scree deposits and pelites in Ain Haouzi in Chefchaouen. Besides, the analysis of damage to constructions in the several neighborhoods surveyed showed that the most affected buildings are those installed near to the main scarps of the slides inventoried, and that the intensity of the damage decreases towards the foot of the slides. Once this information has been acquired, the intervention measures can be extremely precise and effective while avoiding unnecessary costs, which reveals the interest of this approach type in case studies.

As for the heuristic approach, the GIS Matrix method and FR technique allowed us to identify the areas that are most predisposed to slope movements at a broad scale while determining the controlling factors. In addition to lithology and slope, anthropogenic factors, i.e., land use and proximity to the road network, were found to be among the most important predisposing parameters to slope movements in the Moulay Yacoub area studied. Indeed, the conversion of wooded areas and scrublands into cereal growing lands (which dominate the hills of Moulay Yacoub province today) predisposes the latter to shallow gravitational processes (earth flows and solifluctions) by promoting the water retention of the plowed layer. Moreover, the elimination of the root system of the original vegetation (brush) leads to the loss of cohesion of this superficial layer, which facilitates its creep even on gentle slopes.

The interest of this heuristic approach lies in the proactive step to determine the areas at risk and define the pre-requisite norms for any installation of urban plan or other socio-economical goods. The project of elaboration of the maps of the aptitude to urbanization with respect to the natural hazards

and which concerns several provinces of the kingdom adopts this type of approach and underlines its interest in the socio-economic development of the rural and urban extensions.

As for the statistical method, we can say that this type of approach does not have a scale that is necessarily suitable for it. However, in the current study, statistical analysis has served well at both small and large scales. On the other hand, it has been adopted in the determination of the weight of each conditioning factor in the landslide occurrence and in the study and evaluation of the role and impact of topographic growth, generated by the active tectonics, on landslides and gully system in the southern Rif front unit, north of the Sais Fez. The findings showed that in such areas, the size of landslides is significantly larger than in relatively stable areas (the northern foreland). Moreover, the Frequency ratio method used has shown that in such a context, the control of the lithological parameter decreases in favor of the tectonic influence and the topographic growth it generates.

Planned study projects

The logical extension of this work evokes three fundamental points to be investigated further, some of which are already engaged but not yet completed:

- Investigate the control parameters for each type of mass movements at a broad scale while adopting proven susceptibility mapping methods tailored for Mediterranean environments and improve the validation of the results by using recent landslide inventory which characterises the current state of the influencing parameters
- Study and compare the stability of marl slopes between stable zones and other zones with active tectonics in the Fes-MY region.
- To further investigate the alteration process of the shallow marls from a mineralogical point of view
- Compare the degree of control of different influencing factors between the context of the study area and another more heterogeneous context of the Rif chain.
- Assess the impact of climate change on the landslide susceptibility of the slopes and on influencing parameters.

XI. Reference list

Abdulwahid WM, Pradhan B (2017) Landslide vulnerability and risk assessment for multi-hazard scenarios using airborne laser scanning data (LiDAR). Landslides 14:1057–1076

ABHS Agence du Bassin hydraulique de Sebbou

Abidi A, Demehati A, El Qandil M (2019) Landslide Susceptibility Assessment Using Evidence Belief Function and Frequency Ratio Models in Taounate city (North of Morocco). Geotech Geol Eng 37:5457–5471. https://doi.org/10.1007/s10706-019-00992-0

Achalhi M, Münch P, Cornée J-J, et al (2016) The late Miocene Mediterranean-Atlantic connections through the north Rifian corridor: new insights from the Boudinar and Arbaa Taourirt basins (northeastern Rif, Morocco). Palaeogeogr Palaeoclimatol Palaeoecol 459:131–152

Ader F Agence pour la Dédensification et la Réhabilitation de la Médina de Fès

Aditian A, Kubota T, Shinohara Y (2018) Comparison of GIS-based landslide susceptibility models using frequency ratio, logistic regression, and artificial neural network in a tertiary region of Ambon, Indonesia. Geomorphology 318:101–111. https://doi.org/10.1016/J.GEOMORPH.2018.06.006

Agharroud K (2022) Tectonique active du front sud de la chaîne rifaine (Tronçon Fès-Meknès, Nord du Maroc) : Approche morpho-chronologique

Agharroud K, Siame LL, Moussa A Ben, et al (2021) Seismo-tectonic model for the southern pre-rif border (northern morocco): insights from morphochronology. Tectonics 40:. https://doi.org/10.1029/2020TC006633

Akgun A (2012) A comparison of landslide susceptibility maps produced by logistic regression, multi-criteria decision, and likelihood ratio methods: a case study at İzmir, Turkey. Landslides 9:93–106

Alcántara-Ayala I (2002) Geomorphology, natural hazards, vulnerability and prevention of natural disasters in developing countries. Geomorphology 47:107–124

Alexander D (1986) Landslide damage to buildings. Environ Geol Water Sci 8:147–151

Ambroggi PR (1995) Captage du gisement hydrothermal de Moulay Yacoub

Andrieux J (1971) La structure du Rif central: étude des relations entre la tectonique de compression et les nappes de glissement dans un tronçon de la chaîne alpine. Editions du Service géologique du Maroc Rabat, Maroc

ANTONINI G, ARDIZZONE F, CARDINALI M, et al (2002) Surface deposits and landslide inventory map of the area affected by the 1997 Umbria-Marche earthquakes. Boll della Soc Geol Ital 121:843–853

ASTM Committee D-18 on Soil and Rock (2010) Standard test methods for liquid limit, plastic limit, and plasticity index of soils. ASTM international

Ayalew L, Yamagishi H (2004) Slope failures in the Blue Nile basin, as seen from landscape evolution perspective. Geomorphology 57:95–116. https://doi.org/10.1016/S0169-555X(03)00085-0

Ayalew L, Yamagishi H, Ugawa N (2004) Landslide susceptibility mapping using GIS-based weighted

linear combination, the case in Tsugawa area of Agano River, Niigata Prefecture, Japan. Landslides 1:73–81

Bălteanu D, Micu M, Jurchescu M, et al (2020) National-scale landslide susceptibility map of Romania in a European methodological framework. Geomorphology 371:107432

Bao Y, Zhai S, Chen J, et al (2020) The evolution of the Samaoding paleolandslide river blocking event at the upstream reaches of the Jinsha River, Tibetan Plateau. Geomorphology 351:106970

Baratin L-M, Mazzotti S, Chéry J, et al (2016) Incipient mantle delamination, active tectonics and crustal thickening in Northern Morocco: Insights from gravity data and numerical modeling. Earth Planet Sci Lett 454:113–120

Bardi F, Raspini F, Frodella W, et al (2017) Monitoring the rapid-moving reactivation of earth flows by means of GB-InSAR: The April 2013 Capriglio Landslide (Northern Appennines, Italy). Remote Sens 9:165

Bargach K, Ruano P, Chabli A, et al (2004) Recent tectonic deformations and stresses in the frontal part of the Rif Cordillera and the Saïss Basin (Fes and Rabat regions, Morocco). Pure Appl Geophys 161:521–540

Barkaoui A-E, Zarhloule Y, Varbanov PS, Klemes JJ (2017) Geothermal power potential assessment in north eastern morocco. Chem Eng Trans 61:1627–1632

Beguería S (2006) Changes in land cover and shallow landslide activity: A case study in the Spanish Pyrenees. Geomorphology 74:196–206

Belle P, Aunay B, Lachassagne P, et al (2018) Control of tropical landcover and soil properties on landslides' aquifer recharge, piezometry and dynamics. Water 10:1491

Ben Yaïch A, Hervouet Y, Duee G (1991) Les Turbidites calcaires du passage jurassique-cretace du Rif externe occidental (Maroc); processus et controle de depot. Bull la Société géologique Fr 162:841–850

Benaabidate L (2000) Caractérisation du bassin versant de Sebou: Hydrologie, Qualité des eaux et géochimie des sources thermales. Docteur Essciences, Univ S MBA, Fès 228:

Benzougagh B, Gajbhiye S, Baamar B, et al (2020) Relationship between landslide and morpho - structural analysis : a case study in Northeast of Morocco. Appl Water Sci 10:1–10. https://doi.org/10.1007/s13201-020-01258-4

Bernini M, Boccaletti M, Moratti G, Papani G (2000) Structural development of the Taza-Guercif Basin as a constraint for the Middle Atlas Shear Zone tectonic evolution. Mar Pet Geol 17:391–408

Bertolini G, Pizziolo M (2008) Risk assessment strategies for the reactivation of earth flows in the Northern Apennines (Italy). Eng Geol 102:178–192

Bezada MJ, Humphreys ED, Toomey DR, et al (2013) Evidence for slab rollback in westernmost Mediterranean from improved upper mantle imaging. Earth Planet Sci Lett 368:51–60

Booth AM, Roering JJ, Rempel AW (2013) Topographic signatures and a general transport law for deep-seated landslides in a landscape evolution model. J Geophys Res Earth Surf 118:603–624. https://doi.org/10.1002/JGRF.20051

Borrelli L, Ciurleo M, Gullà G (2018) Shallow landslide susceptibility assessment in granitic rocks using

GIS-based statistical methods: the contribution of the weathering grade map. Landslides 15:1127–1142

Boualla O, Mehdi K, Fadili A, et al (2019) GIS-based landslide susceptibility mapping in the Safi region, West Morocco. Bull Eng Geol Environ 78:2009–2026. https://doi.org/10.1007/s10064-017-1217-y

Bouizrou Ismail (2021) Modélisation hydrologique spatialisée pour l'étude de l'impact de de l'urbanisation sur la génération des crues: cas du bassin versant urbain semi-aride de l'Oued Fez, Thèse FST-Fez. University Sidi Mohamed Ben Abdellah

Bounab A (2022) Multi-source analysis for the study of landslides on both sides of the northern Dorsale Calcaire : cartography and modelling. Abdelmaalek Essaadi

Bounab A, Agharroud K, Kharim Y El, et al (2022) The importance of investigating causative factors and training data selection for accurate landslide susceptibility assessment: the case of Ain Lahcen commune (Tetouan, Northern Morocco). https://doi.org/101080/1010604920222028905 1–31. https://doi.org/10.1080/10106049.2022.2028905

Bounab A, El Kharim Y, El Hamdouni R, Hlila R (2021) A multidisciplinary approach to study slope instability in the Alboran Sea shoreline: Study of the Tamegaret deep-seated slow-moving landslide in Northern Morocco. J African Earth Sci 104345. https://doi.org/10.1016/J.JAFREARSCI.2021.104345

Bourenane H, Bouhadad Y, Guettouche MS, Braham M (2015) GIS-based landslide susceptibility zonation using bivariate statistical and expert approaches in the city of Constantine (Northeast Algeria). Bull Eng Geol Environ 74:337–355

Boutakiout M (1990) Les foraminifères du Jurassique des Rides Sud-Rifaines et des régions voisines (Maroc). Trav Doc des Lab Géologie Lyon 112:3–247

Brunet-Moret Y (1971) Etude de l'homogénéité de séries chronologiques de précipitations annuelles par la méthode des doubles masses. Cah ORSTOM, ser Hydrol 8:3–31

Brunetti MT, Guzzetti F, Cardinali M, et al (2014) Analysis of a new geomorphological inventory of landslides in Valles Marineris, Mars. Earth Planet Sci Lett 405:156–168. https://doi.org/10.1016/J.EPSL.2014.08.025

Budetta P, Santo A, Vivenzio F (2008) Landslide hazard mapping along the coastline of the Cilento region (Italy) by means of a GIS-based parameter rating approach. Geomorphology 94:. https://doi.org/10.1016/j.geomorph.2006.10.034

Burbank DW (2002) Rates of erosion and their implications for exhumation. Mineral Mag 66:25–52

Burland JB, Broms BB, De Mello VFB (1978) Behaviour of foundations and structures

Byou T, Obda K, Taous A, Obda I (2020) Susceptibilité aux glissements de terrain dans la ville d'Al Hoceima et sa périphérie : application de la méthode de la théorie de l'évidence. Geomatica 75:1–27. https://doi.org/10.1139/geomat-2019-0025

Cao Y, Wei X, Fan W, et al (2021) Landslide susceptibility assessment using the Weight of Evidence method: A case study in Xunyang area, China. PLoS One 16:e0245668

Capella W, Matenco L, Dmitrieva E, et al (2017) Thick-skinned tectonics closing the Rifian Corridor.

Tectonophysics 710:249–265

Cardinali M, Antonini G, Reichenbach P, Guzzetti F (2001) Photo geological and landslide inventory map for the Upper Tiber River basin. CNR, Grup Naz per la Dif dalle Catastr Idrogeol Publ

Carlini M, Chelli A, Francese R, et al (2017) Landslides types controlled by tectonics-induced evolution of valley slopes (Northern Apennines, Italy). Landslides 2017 152 15:283–296. https://doi.org/10.1007/S10346-017-0871-2

Carlini M, Chelli A, Vescovi P, et al (2016) Tectonic control on the development and distribution of large landslides in the Northern Apennines (Italy). Geomorphology 253:425–437. https://doi.org/10.1016/J.GEOMORPH.2015.10.028

Cascini L (2008) Applicability of landslide susceptibility and hazard zoning at different scales. Eng Geol 102:164–177

Castillo C, Gómez JA (2016) A century of gully erosion research: Urgency, complexity and study approaches. Earth-Science Rev 160:300–319

Catani F, Casagli N, Ermini L, et al (2005) Landslide hazard and risk mapping at catchment scale in the Arno River basin. Landslides 2:329–342

Cendrero A, Dramis F (1996) The contribution of landslides to landscape evolution in Europe. Geomorphology 15:191–211. https://doi.org/10.1016/0169-555X(95)00070-L

Chabok M, Bahrami H, Asakereh A, Jaafarzadeh NA (2019) Landfills site selection in southern cities of Khuzestan province with using fuzzy set and AHP method. J Adv Appl Geol 9:142–155

Chacón J, Irigaray C, Fernandez T, El Hamdouni R (2006) Engineering geology maps: landslides and geographical information systems. Bull Eng Geol Environ 65:341–411

Chalouan A, Galindo-Zaldívar J, Akil M, et al (2006) Tectonic wedge escape in the southwestern front of the Rif Cordillera (Morocco). Geol Soc London, Spec Publ 262:101–118

Chalouan A, Gil AJ, Galindo-Zaldívar J, et al (2014) Active faulting in the frontal Rif Cordillera (Fes region, Morocco): Constraints from GPS data. J Geodyn 77:110–122

Chalouan A, Michard A (2000) evolution of the Mediterrranean contiental margin of northern Morocco. In: CIESM Workshop Serie

Charroud M, Cherai B, Benabdelhadi M, Falguères C (2007) Impact de la néotectonique quaternaire sur la dynamique sédimentaire du Saïs (Maroc): du bassin d'avant fosse pliocène au plateau continental quaternaire. Quat Rev l'Association française pour l'étude du Quat 18:327–334

Chaudhary P, Chhetri SK, Joshi KM, et al (2016) Application of an Analytic Hierarchy Process (AHP) in the GIS interface for suitable fire site selection: A case study from Kathmandu Metropolitan City, Nepal. Socioecon Plann Sci 53:60–71

Chen C-Y, Chang J-M (2016) Landslide dam formation susceptibility analysis based on geomorphic features. Landslides 13:1019–1033. https://doi.org/10.1007/s10346-015-0671-5

Chen C-Y, Yu F-C (2011) Morphometric analysis of debris flows and their source areas using GIS. Geomorphology 129:387–397

Chen Z, Ye F, Fu W, et al (2020) The influence of DEM spatial resolution on landslide susceptibility mapping in the Baxie River basin, NW China. Nat Hazards 2020 1013 101:853–877.

https://doi.org/10.1007/S11069-020-03899-9

Cherai B, Idrissi BEF, Charroud M, El Hnot H (2017) LES MOUVEMENTS DE TERRAIN DANS LE SECTEUR URBAIN DE LA VILLE DE FÈS (MAROC): FACTEURS DE GENÈSE ET CARTOGRAPHIE DES ZONES À RISQUES

Chiocchio C, Iovine G, Parise M (1997) A proposal for surveying and classifying landslide damage to buildings in urban areas. In: Engineering geology and the environment. pp 553–558

Chisty KU (2014) Landslide in Chittagong City: A perspective on hill cutting. J Bangladesh Inst Planners 2075:9363

Chung C-JF, Fabbri AG (1999) Probabilistic prediction models for landslide hazard mapping. Photogramm Eng Remote Sensing 65:1389–1399

Chung C-JF, Fabbri AG (2003) Validation of spatial prediction models for landslide hazard mapping. Nat Hazards 30:451–472

Chung CF, Fabbri AG (2005) Systematic procedures of landslide hazard mapping for risk assessment using spatial prediction models. Landslide hazard risk 139–174

Claessens L, Lowe DJ, Hayward BW, et al (2006) Reconstructing high-magnitude/low-frequency landslide events based on soil redistribution modelling and a Late-Holocene sediment record from New Zealand. Geomorphology 74:29–49

Clarke ML, Rendell HM (2006) Process–form relationships in Southern Italian badlands: erosion rates and implications for landform evolution. Earth Surf Process Landforms J Br Geomorphol Res Gr 31:15–29

Conforti M, Ietto F (2020) Influence of Tectonics and Morphometric Features on the Landslide Distribution: A Case Study from the Mesima Basin (Calabria, South Italy). J Earth Sci 31:393–409. https://doi.org/10.1007/s12583-019-1231-z

Conforti M, Pascale S, Robustelli G, Sdao F (2014) Evaluation of prediction capability of the artificial neural networks for mapping landslide susceptibility in the Turbolo River catchment (northern Calabria, Italy). Catena 113:236–250

Corominas J, Moya J (2008) A review of assessing landslide frequency for hazard zoning purposes. Eng Geol 102:193–213

Costanzo D, Rotigliano E, Irigaray C, et al (2012) Factors selection in landslide susceptibility modelling on large scale following the gis matrix method: application to the river Beiro basin (Spain). Nat Hazards Earth Syst Sci 12:327–340

Crozier MJ (1984) Field assessment of slope instability. Slope Instab 103–142

Cruden D. M., Varnes D. J. (1996) Landslide types and processes , special report , transportation research board , national academy of sciences. United States Geol Surv 247:36–75

Daguin F (1934) Contribution à l'étude géologique de la région prérfiaine (Maroc occidental), par Fernand Daguin. impr. l'Abeille, 14, avenue de Toulouse

Darraz C, Hlila R, El Hajjaji K (2003) Écroulements et mouvements de versants associés au niveau du col de Onsar (Rif, Maroc) dans un contexte géologique de décrochement. Rev française géotechnique 3–11

Dauphiné A, Provitolo D (2001) Risques et catastrophes en Méditerranée

Davis JC (1973) Statistics and Data Analysis in Geology, John Wiley, New York

DeGRAFF J V (1985) Using isopleth maps of landslide deposits as a tool in timber sale planning. Bull Assoc Eng Geol 22:445–453

Degraff J V, Romersburg HC (1980) Regional landslide-susceptibility for wildland management: A matrix approach. Coates and Vitek (eds) 410–414

Del Soldato M, Bianchini S, Calcaterra D, et al (2017) A new approach for landslide-induced damage assessment. Geomatics, Nat Hazards Risk 8:1524–1537

Del Soldato M, Di Martire D, Bianchini S, et al (2019) Assessment of landslide-induced damage to structures: the Agnone landslide case study (southern Italy). Bull Eng Geol Environ 78:2387–2408

Delga MD, Hottinger L, Marçais J, et al (1962) Données actuelles sur la structure du Rif. Livre mém P Fallot 1:399–422

DeMets C, Gordon RG, Argus DF (2010) Geologically current plate motions. Geophys J Int 181:1–80

Demir G, Aytekin M, Akgün A, et al (2013) A comparison of landslide susceptibility mapping of the eastern part of the North Anatolian Fault Zone (Turkey) by likelihood-frequency ratio and analytic hierarchy process methods. Nat hazards 65:1481–1506

DGM Direction Générale de la Météorologie. Fez-Boulemane

DHP Département de l'Habitat et de la Politique de la Ville. Fès-Meknès

Donati L, Turrini MC (2002) An objective method to rank the importance of the factors predisposing to landslides with the GIS methodology: application to an area of the Apennines (Valnerina; Perugia, Italy). Eng Geol 63:277–289

Dubreuil P, Guiscafre J (1971) La planification du réseau hydrométrique minimal. Cah ORSTOM Sér Hydrol 8:3–38

Durand-Delga M, Mattauer M (1960) Sur l'origine ultrarifaine de certaines nappes du Rif septentrional. CK Somm Soc Geol Fr 22:

El Alami S, Lahmid S (2016) Etude géologique d'une mine de sel au prérif. Fez

El Kharim Y (2012) Geological features of the slope instability in Tetouan region (the northern Rif, Morocco). Bol R Soc Esp Hist Nat Sec Geol 106:39–52

El Kharim Y, Bounab A, Ilias O, et al (2021) Landslides in the urban and suburban perimeter of Chefchaouen (Rif, Northern Morocco): inventory and case study. Nat Hazards 107:355–373

El Mrabet T (2005) The great earthquakes in the Maghreb region and their consequences on man and environment. Rabat. ISBN- 9954-0-3777-2

Ermini L, Catani F, Casagli N (2005) Artificial Neural Networks applied to landslide susceptibility assessment. Geomorphology 66:327–343. https://doi.org/10.1016/J.GEOMORPH.2004.09.025

Faccenna C, Piromallo C, Crespo-Blanc A, et al (2004) Lateral slab deformation and the origin of the western Mediterranean arcs. Tectonics 23:

Fadil A, Vernant P, McClusky S, et al (2006) Active tectonics of the western Mediterranean: Geodetic evidence for rollback of a delaminated subcontinental lithospheric slab beneath the Rif Mountains, Morocco. Geology 34:529–532

Faleh A, Sadiki A (2002) Glissement rotationnel de Dhar El Harrag: exemple d'instabilité de terrain dans le Prérif central (Maroc). Bull l'Institut Sci Rabat 41–48

Fassi D (1999) Les Formations superficielles du Saïs de Fès et de Meknès du temps géologique à l'utilisation actuelle des sols. Ed. du Service Géologique du Maroc

Faugeres J-C (1981) Evolution structurale d'un bassin atlantico-mesogeen de la marge africaine; les rides Sud-rifaines (Maroc). Bull la Société géologique Fr 7:229–244

Faugères J-C (1978) Les Rides sud-rifaines: Evolution sédimentaire et structurale d'un bassin atlantico-mesogéen de la marge africaine

Feinberg H (1986) Les séries tertiaires des zones externes du Rif (Maroc): biostratigraphie, paléogéographie et aperçu tectonique. Editions du Service géologique du Maroc

Feizizadeh B, Blaschke T (2013) GIS-multicriteria decision analysis for landslide susceptibility mapping: comparing three methods for the Urmia lake basin, Iran. Nat hazards 65:2105–2128

Feizizadeh B, Jankowski P, Blaschke T (2014) A GIS based spatially-explicit sensitivity and uncertainty analysis approach for multi-criteria decision analysis. Comput Geosci 64:81–95

Fell R, Corominas J, Bonnard C, et al (2008) Guidelines for landslide susceptibility, hazard and risk zoning for land-use planning. Eng Geol 102:99–111

Fernández T, Irigaray C, Chacón J (1996) Inventory and analysis of landslide determinant factors in Los Guajares Mountains, Granada (Southern Spain). In: Landslides. pp 1891–1896

Fernández T, Irigaray C, Hamdouni R El, Chacón J (2003) Methodology for Landslide Susceptibility Mapping by Means of a GIS. Application to the Contraviesa Area (Granada, Spain)

Fisher RA Statistical methods for research workers 1970 14th ed. New York Hafner

Fisher RA (1921) On the'probable error'of a coefficient of correlation deduced from a small sample. Metron 1:1–32

Flinch J (1993) The Gibraltar arc: An orogenic float modified by late transpression. AAPG Bull (American Assoc Pet Geol States) 77:

Frattini P, Crosta GB (2013) The role of material properties and landscape morphology on landslide size distributions. Earth Planet Sci Lett 361:310–319

Fu S, Chen L, Woldai T, et al (2020) Landslide hazard probability and risk assessment at the community level: A case of western Hubei, China. Nat Hazards Earth Syst Sci 20:581–601

G.T.R Classification des sols, Norme NF P 11 300

Gaidzik K, Ramírez-Herrera MT (2021) The importance of input data on landslide susceptibility mapping. Sci Rep 11:1–14

Galli M, Ardizzone F, Cardinali M, et al (2008) Comparing landslide inventory maps. Geomorphology 94:268–289. https://doi.org/10.1016/J.GEOMORPH.2006.09.023

Garcia-Chevesich P, Wei X, Ticona J, et al (2021) The impact of agricultural irrigation on landslide triggering: A review from chinese, english, and Spanish literature. Water (Switzerland) 13

García-Ruiz JM, Beguería S, Alatorre LC, Puigdefábregas J (2010) Land cover changes and shallow landsliding in the flysch sector of the Spanish Pyrenees. Geomorphology 124:250–259

Gartet A (2013) Prevision et prevention des risques des mouvements de terrain dans les agglomerations urbaines: cas de Fes Maroc

Gartet A (2011) Mouvements de terrain et risques environnementaux dans l'agglomération de Fès et son arrière-pays : aménagement, gestion et prévention. Rabat

Gartet A (2008) RISQUES D INST ABILITES ROUTIERES ET PROCEDES D AMENAGEMENT DANS LA PERIPHERIE NORD-EST DE FES

Gartet A (1994) Morphogénèse et hydrologie dans le bassin versant de l'oued Lebène (Rif méridional et Prérif central et oriental, Maroc)

Glade T (2003) Vulnerability assessment in landslide risk analysis. Erde 134:123–146

Goodchild MF (1986) Spatial autocorrelation. Geo Books

Goodman LA, Kruskal WH (1979) Measures of association for cross classifications. Meas Assoc cross Classif 2–34

Guns M, Vanacker V (2013) Forest cover change trajectories and their impact on landslide occurrence in the tropical Andes. Environ Earth Sci 70:2941–2952. https://doi.org/10.1007/s12665-013-2352-9

Guns M, Vanacker V (2014) Shifts in landslide frequency–area distribution after forest conversion in the tropical Andes. Anthropocene 6:75–85. https://doi.org/10.1016/J.ANCENE.2014.08.001

Guzzetti F, Cardinali M, Reichenbach P, Carrara A (2000) Comparing Landslide Maps: A Case Study in the Upper Tiber River Basin, Central Italy. Environ Manage 25:

Guzzetti F, Galli M, Reichenbach P, et al (2006) Landslide hazard assessment in the Collazzone area, Umbria, Central Italy. Nat hazards earth Syst Sci 6:115–131

Guzzetti F, Malamud BD, Turcotte DL, Reichenbach P (2002) Power-law correlations of landslide areas in central Italy. Earth Planet Sci Lett 195:169–183. https://doi.org/10.1016/S0012-821X(01)00589-1

Guzzetti F, Mondini AC, Cardinali M, et al (2012) Landslide inventory maps: New tools for an old problem. Earth-Science Rev 112:42–66. https://doi.org/10.1016/J.EARSCIREV.2012.02.001

Guzzetti F, Reichenbach P, Cardinali M, et al (2005) Probabilistic landslide hazard assessment at the basin scale. Geomorphology 72:272–299

Haddaoui Z (2000) Influence de la geómetrie d'un bassin Jurassique sur la propagation des chevauchements neogenes: Geodynamique meso-Cenozoıque des rides sud-rifaines (Maroc). Model Geom Numer

Haddaoui Z, El Hatimi N, Hervouët Y (1997) Les Rides sud-rifaines (Maroc-septentrional): influence de la géométrie d'un bassin jurassique sur la propagation des chevauchements néogènes. Géologie Méditerranéenne 24:51–71

Hansen A (1984) Landslide hazard analysis. Slope Instab 523–602

Harmouzi H, Dekayir A, Rouai M, Afechkar M (2018) Analyse géomorphologique et géologique du glissement de terrain d'Akchour (Rif, Maroc). Geo Eco Trop 42:19–32

Harmouzi H, Nefeslioglu HA, Rouai M, et al (2019) Landslide susceptibility mapping of the Mediterranean coastal zone of Morocco between Oued Laou and El Jebha using artificial neural networks (ANN). Arab J Geosci 12:. https://doi.org/10.1007/s12517-019-4892-0

Hasekioğulları GD, Ercanoglu M (2012) A new approach to use AHP in landslide susceptibility mapping: a case study at Yenice (Karabuk, NW Turkey). Nat Hazards 63:1157–1179

Hassan T, Benoît D, Abdel-Ali C, et al (2015) Neotectonic and mass movements on the new Fez-Taza highway (Northern Morocco). In: Engineering Geology for Society and Territory-Volume 6. Springer, pp 95–99

Hattanji T, Moriwaki H (2009) Morphometric analysis of relic landslides using detailed landslide distribution maps: Implications for forecasting travel distance of future landslides. Geomorphology 103:447–454. https://doi.org/10.1016/j.geomorph.2008.07.009

Heusch B (1970) L'érosion du pré-Rif. Une étude quantitative de l'érosion hydraulique dans les collines marneuses du pré-Rif occidental

Hölbling D, Friedl B, Eisank C (2015) An object-based approach for semi-automated landslide change detection and attribution of changes to landslide classes in northern Taiwan. Earth Sci Informatics 8:327–335

Holec J, Bednarik M, Šabo M, et al (2013) A small-scale landslide susceptibility assessment for the territory of Western Carpathians. Nat Hazards 69:1081–1107

Hong H, Chen W, Xu C, et al (2017) Rainfall-induced landslide susceptibility assessment at the Chongren area (China) using frequency ratio, certainty factor, and index of entropy. Geocarto Int 32:139–154

Hovius N, Stark CP, Allen PA (1997) Sediment flux from a mountain belt derived by landslide mapping. Geology 25:231–234

Hovius N, Stark CP, Hao-Tsu C, Jiun-Chuan L (2000) Supply and removal of sediment in a landslide-dominated mountain belt: Central Range, Taiwan. J Geol 108:73–89

Howard AD (1994) Badlands in Geomorphology of Desert Environments, A. Abrahams and A. Parsons (eds.), Chapter 9

Howard AD (2009) Badlands and gullying. In: Geomorphology of desert environments. Springer, pp 265–299

Hsieh Y-C, Chan Y-C, Hu J-C, et al (2016) Direct measurements of bedrock incision rates on the surface of a large dip-slope landslide by multi-period airborne laser scanning DEMs. Remote Sens 8:900

Huang CC, Pang J, Zha X, et al (2012) Development of gully systems under the combined impact of monsoonal climatic shift and neo-tectonic uplift over the Chinese Loess Plateau. Quat Int 263:46–54

Huang F, Yao C, Liu W, et al (2018) Landslide susceptibility assessment in the Nantian area of China: a

comparison of frequency ratio model and support vector machine. Geomatics, Nat Hazards Risk 9:919–938

Hungr O, Leroueil S, Picarelli L (2014) The Varnes classification of landslide types, an update. Landslides 11:167–194

Hungr O, McDougall S, Wise M, Cullen M (2008) Magnitude–frequency relationships of debris flows and debris avalanches in relation to slope relief. Geomorphology 96:355–365

Hurrell JW (1995) Decadal trends in the North Atlantic Oscillation: Regional temperatures and precipitation. Science (80-) 269:676–679

Irigaray C (1995) Movimientos de ladera: Inventario, análisis y cartografía de susceptibilidad mediante un sistema de información geográfica (SIG). Aplicación a las zonas de Colmenar (Ma), Rute (Co) y Montefrío (Gr)

Irigaray C, Fernández T, El Hamdouni R, Chacón J (2007) Evaluation and validation of landslide-susceptibility maps obtained by a GIS matrix method: Examples from the Betic Cordillera (southern Spain). Nat Hazards 41:61–79. https://doi.org/10.1007/s11069-006-9027-8

Jafarimanesh A, Mignan A, Danciu L (2018) Origin of the power-law exponent in the landslide frequency-size distribution. Nat Hazards Earth Syst Sci Discuss 1–28. https://doi.org/10.5194/NHESS-2018-167

Jamsawang P, Voottipruex P, Boathong P, et al (2015) Three-dimensional numerical investigation on lateral movement and factor of safety of slopes stabilized with deep cement mixing column rows. Eng Geol 188:159–167

Jeong S, Kassim A, Hong M, Saadatkhah N (2018) Susceptibility assessments of landslides in Hulu Kelang area using a geographic information system-based prediction model. Sustainability 10:2941

Jiang S, Li J, Zhang S, et al (2022) Landslide risk prediction by using GBRT algorithm: Application of artificial intelligence in disaster prevention of energy mining. Process Saf Environ Prot 166:384–392

Jiménez-Perálvarez JD, Irigaray C, El Hamdouni R, Chacón J (2009) Building models for automatic landslide-susceptibility analysis, mapping and validation in ArcGIS. In: Natural Hazards. pp 571–590

Julian M (1989) JC Flageollet: Les mouvements de terrain et leur prévention. Méditerranée 68:90

Kannan M, Saranathan E, Anabalagan R (2013) Landslide vulnerability mapping using frequency ratio model: a geospatial approach in Bodi-Bodimettu Ghat section, Theni district, Tamil Nadu, India. Arab J Geosci 6:2901–2913

Kavzoglu T, Sahin EK, Colkesen I (2014) Landslide susceptibility mapping using GIS-based multi-criteria decision analysis, support vector machines, and logistic regression. Landslides 11:425–439

Keefer DK (1984) Landslides caused by earthquakes | GSA Bulletin | GeoScienceWorld. GSA Bull 95:406–421

Keefer DK, Johnson AM (1983) Earth flows: morphology, mobilization, and movement. US Geological Survey

Komac M (2006) A landslide susceptibility model using the analytical hierarchy process method and multivariate statistics in perialpine Slovenia. Geomorphology 74:17–28

Korup O (2009) Linking landslides, hillslope erosion, and landscape evolution. Earth Surf Process Landforms 34:1315–1317. https://doi.org/10.1002/ESP.1830

Korup O, Densmore AL, Schlunegger F (2010) The role of landslides in mountain range evolution. Geomorphology 120:77–90

Krijgsman W, Hilgen FJ, Raffi I, et al (1999) Chronology, causes and progression of the Messinian salinity crisis. Nature 400:652–655

Krivoguz D, Bespalova L (2017) Spatial analysis of topography of Kerch peninsula using GIS and its impact on landslides. Int J Prof Sci 19–32

Kukemilks K, Saks T (2013) Landslides and gully slope erosion on the banks of the Gauja River between the towns of Sigulda and Līgatne. Est J Earth Sci 62:. https://doi.org/10.3176/earth.2013.17

Lakhdar A, Ntarmouchant A, Ribeiro ML, et al (2006) Nouvelle approche géologique et géodinamique du Complexe Hydrothermal de Moulay Yacoub, bordure septentrionale du Sillon Sud Rifain

Lasri M (2015) Les inondations menaçant l'agglomération de Fès: De l'étude hydrologique et du risque à la cartographie des dangers d'inondation

Lazzari M, Danese M, Gioia D (2012) The contribution of fluvial and mass wasting processes to sedimentary budget in mountain catchments of the southern Apennines, Italy. In: EGU General Assembly Conference Abstracts. p 10740

Le matin (2016) Effondrement d'un immeuble à Fès

Le monde (1988) Le monde. Maroc Glissement terrain à Fès cinquante-deux morts

Leblanc D (1975) Etude géologique du Rif externe oriental au Nord de Taza (Maroc). Notes et Mémoires du Service Géologique du Maroc

Leblanc D (1979) Etude géologique du Rif externe oriental au Nord de Taza (Maroc). Éditions du Service géologique du Maroc Rabat, Morocco

Leblanc M (1977) SYNCHRONISME DES FACIES VOLCANIQUES (PRECAMBRIEN III) ET SEDIMENTAIRES (ADOUDOUNIEN) DANS L'INFRACAMBRIEN D'ALOUS (ANTI-ATLAS, MAROC).

Lee EM, Moore R (1991) Coastal landslip potential assessment: Isle of Wight Undercliff. Vent Rep to Dep Environ

Lee S, Choi J (2004) Landslide susceptibility mapping using GIS and the weight-of-evidence model. Int J Geogr Inf Sci 18:789–814

Lee S, Sambath T (2006) Landslide susceptibility mapping in the Damrei Romel area, Cambodia using frequency ratio and logistic regression models. Environ Geol 50:847–855. https://doi.org/10.1007/s00254-006-0256-7

Lettenmaier DP (1976) Detection of trends in water quality data from records with dependent observations. Water Resour Res 12:1037–1046

Li L, Lan H, Guo C, et al (2017) A modified frequency ratio method for landslide susceptibility

assessment. Landslides 14:727–741. https://doi.org/10.1007/s10346-016-0771-x

Li L, Lan H, Wu Y (2016) How sample size can effect landslide size distribution. Geoenvironmental Disasters 3:1–11. https://doi.org/10.1186/S40677-016-0052-Y/FIGURES/7

Liao Z, Hong Y, Wang J, et al (2010) Prototyping an experimental early warning system for rainfall-induced landslides in Indonesia using satellite remote sensing and geospatial datasets. Landslides 7:317–324

Lomoschitz A, Meco J, Corominas J (2002) The Barranco de Tirajana basin, Gran Canaria (Spain). A major erosive landform caused by large landslides. Geomorphology 42:117–130. https://doi.org/10.1016/S0169-555X(01)00078-2

Malamud BD, Turcotte DL (1999) Self-organized criticality applied to natural hazards. Nat Hazards 20:93–116

Malamud BD, Turcotte DL, Guzzetti F, Reichenbach P (2004) Landslide inventories and their statistical properties. Earth Surf Process Landforms 29:687–711. https://doi.org/10.1002/ESP.1064

Mansour M (1998) Geodynamic processes and cartography of ground movements in the area of Chefchaouen (District of Bouhalla-Amtrass). Application to the stabilization of main road Nb: 39. Western Rif, Morocco

Marcais JSG, Suter G (1952) Description de l'itinéraire Maroc septentional chaine du Rif. Cong géol int Alger 16–24

Marino P, Peres DJ, Cancelliere A, et al (2020) Soil moisture information can improve shallow landslide forecasting using the hydrometeorological threshold approach. Landslides 17:2041–2054

Mastere M (2011) LA SUSCEPTIBILITE AUX MOUVEMENTS DE TERRAIN DANS LA PROVINCE DE CHEFCHAOUEN (Rif Central, Maroc)

Mastere M, Vliet-Lanoë B Van, Brahim LA (2013) Cartographie de l'occupation des sols en relation avec les mouvements gravitaires et le ravinement dans le Rif nord-occidental (Maroc). Géomorphologie Reli Process Environ 19:335–352

Mateos RM, Ezquerro P, Azañón JM, et al (2018) Coastal lateral spreading in the world heritage site of the Tramuntana Range (Majorca, Spain). The use of PSInSAR monitoring to identify vulnerability. Landslides. https://doi.org/10.1007/s10346-018-0949-5

Mathew J, Jha VK, Rawat GS (2009) Landslide susceptibility zonation mapping and its validation in part of Garhwal Lesser Himalaya, India, using binary logistic regression analysis and receiver operating characteristic curve method. Landslides 6:17–26

McKillup S, Dyar MD (2010) Geostatistics explained: an introductory guide for earth scientists. Cambridge University Press

Meghraoui M, Morel J-L, Andrieux J, Dahmani M (1996) Tectonique plio-quaternaire de la chaine tello-rifaine et de la mer d'Alboran; une zone complexe de convergence continent-continent. Bull la Société géologique Fr 167:141–157

Menéndez-Duarte R, Marquínez J, Fernández-Menéndez S, Santos R (2007) Incised channels and gully erosion in Northern Iberian Peninsula: Controls and geomorphic setting. Catena 71:267–278

Meteorology N National Oceanic and Atmospheric Administration

Michard A, Negro F, Saddiqi O, et al (2006) Pressure-temperature-time constraints on the Maghrebide mountain building: Evidence from the Rif-Betic transect (Morocco, Spain), Algerian correlations, and geodynamic implications. Comptes Rendus - Geosci 338:. https://doi.org/10.1016/j.crte.2005.11.011

Millies-Lacroix A (1968) Les glissements de terrains. Présentation d'une carte prévisionnelle des mouvements de masse dans le Rif (Maroc septentrional). Mines et Géologie 27:45–55

Mind'je R, Li L, Nsengiyumva JB, et al (2020) Landslide susceptibility and influencing factors analysis in Rwanda. Environ Dev Sustain 22:7985–8012

Mohammady M, Pourghasemi HR, Pradhan B (2012) Landslide susceptibility mapping at Golestan Province, Iran: A comparison between frequency ratio, Dempster–Shafer, and weights-of-evidence models. J Asian Earth Sci 61:221–236. https://doi.org/10.1016/J.JSEAES.2012.10.005

Monsieurs E, Dewitte O, Demoulin A (2019) A susceptibility-based rainfall threshold approach for landslide occurrence. Nat Hazards Earth Syst Sci 19:775–789

Moratti G, Piccardi L, Vannucci G, et al (2003) The 1755 "Meknes" earthquake (Morocco): field data and geodynamic implications. J Geodyn 36:305–322

Morel JL (1987) Évolution récente de l'orogène rifain et de son avant-pays depuis la fin de la mise en place des nappes (Rif, Maroc). Paris 11

Morel JL (1989) Evolution paleogeographique et tectonique du Rif (Maroc) du Tortonien a l'actuel. Comptes Rendus - Acad des Sci Ser II 309:

Nejjari A, Gille E, François D (2001) Les longues chroniques pluviométriques et la caractérisation de la sécheresse récente au Nord du Moyen Atlas (Maroc). Mosella 25:37–53

Neuhäuser B, Damm B, Terhorst B (2012) GIS-based assessment of landslide susceptibility on the base of the weights-of-evidence model. Landslides 9:511–528

Niculită M (2016) Automatic landslide length and width estimation based on the geometric processing of the bounding box and the geomorphometric analysis of DEMs. Nat Hazards Earth Syst Sci 16:2021–2030. https://doi.org/10.5194/NHESS-16-2021-2016

NiculiţĂ M (2016) Automatic landslide length and width estimation based on the geometric processing of the bounding box and the geomorphometric analysis of DEMs. Nat Hazards Earth Syst Sci 16:2021–2030. https://doi.org/10.5194/NHESS-16-2021-2016

Notti D, Galve JP, Mateos RM, et al (2015) Human-induced coastal landslide reactivation. Monitoring by PSInSAR techniques and urban damage survey (SE Spain). Landslides 12:. https://doi.org/10.1007/s10346-015-0612-3

Nwankwoala HO (2019) Gully Erosion and Landslides in Southeastern Nigeria: Causes, Consequences and Control Measures. Glob J Eng Sci 2:. https://doi.org/10.33552/gjes.2019.02.000541

Obda I (2017) Etude géotechnique des glissements de terrain : cas du village de Moulay Yacoub. Fez

Obda I, El Kharim Y, Bounab A, et al (2022) Multi-criteria assessment approach of slow-moving urban landslide hazard: the case of Moulay Yacoub, Morocco. Can J Earth Sci 99:1–18

Obda I, El Kharim Y, Lahrach A, et al (2018) Risque de mouvement de terrain dans le centre urbain de

Moulay Yacoub, Fès, Maroc. In: Acte du Colloque International sur les risques naturels et l'aménagement du territoire, Université Mohammed Ier, Oujda, Maroc. pp 96–101

Obda K Wavelet Analysis: A Links Between the North Atlantic Oscillation and Winter Drought in the Mediterranean Watersheds of the Western Rif (North Morocco)

Obda K (1991) Etude hydrologique de l'oued Nekor (Rif): précipitations, écoulement et gestion des ressources en eau

OBDA K (2004) Indigences extrêmes des écoulements des oueds méditerranéens: cas des oueds Nekor au Rif et du Haut Sebou au Moyen Atlas

Okeke ACU, Wang F (2016) Critical hydraulic gradients for seepage-induced failure of landslide dams. Geoenvironmental Disasters 3:1–22. https://doi.org/10.1186/S40677-016-0043-Z/FIGURES/19

Osna T, Sezer EA, Akgun A (2014) GeoFIS: an integrated tool for the assessment of landslide susceptibility. Comput Geosci 66:20–30

Othman AA, Gloaguen R, Andreani L, Rahnama M (2018) Improving landslide susceptibility mapping using morphometric features in the Mawat area, Kurdistan Region, NE Iraq: Comparison of different statistical models. Geomorphology 319:147–160. https://doi.org/10.1016/J.GEOMORPH.2018.07.018

Pantelidis L (2011) An innovative landslide risk assessment system: application to highway embankments. In: Geo-Risk 2011: Risk Assessment and Management. pp 1012–1019

Park S, Choi C, Kim B, Kim J (2013) Landslide susceptibility mapping using frequency ratio, analytic hierarchy process, logistic regression, and artificial neural network methods at the Inje area, Korea. Environ earth Sci 68:1443–1464

PCD (2016) Plan Communal de Développement Commune urbaine

Peduto D, Nicodemo G, Maccabiani J, Ferlisi S (2017) Multi-scale analysis of settlement-induced building damage using damage surveys and DInSAR data: A case study in The Netherlands. Eng Geol 218:117–133

Pereira S, Zêzere JL, Bateira C (2012) Technical Note: Assessing predictive capacity and conditional independence of landslide predisposing factors for shallow landslide susceptibility models. Nat Hazards Earth Syst Sci 12:979–988. https://doi.org/10.5194/nhess-12-979-2012

Pérouse E, Vernant P, Chéry J, et al (2010) Active surface deformation and sub-lithospheric processes in the western Mediterranean constrained by numerical models. Geology 38:823–826

Petley DN, Dunning SA, Rosser NJ (2005) The analysis of global landslide risk through the creation of a database of worldwide landslide fatalities. In: Landslide risk management. CRC Press, pp 377–384

Picarelli L, Urciuoli G, Ramondini M, Comegna L (2005) Main features of mudslides in tectonised highly fissured clay shales. Landslides 2:15–30

Pique A, Du Maroc G (1994) Les domaines régionaux et leur évolution structurale. PUMAG Géologie du Maroc

Poujol A, Ritz J-F, Vernant P, et al (2017a) Which fault destroyed Fes city (Morocco) in 1755? A new insight from the Holocene deformations observed along the southern border of Gibraltar arc.

Tectonophysics 712:303–311

Poujol A, Ritz JF, Vernant P, et al (2017b) Which fault destroyed Fes city (Morocco) in 1755? A new insight from the Holocene deformations observed along the southern border of Gibraltar arc. Tectonophysics 712–713:303–311. https://doi.org/10.1016/J.TECTO.2017.05.036

Pourghasemi HR, Pradhan B, Gokceoglu C (2012) Application of fuzzy logic and analytical hierarchy process (AHP) to landslide susceptibility mapping at Haraz watershed, Iran. Nat hazards 63:965–996

Pourghasemi HR, Rahmati O (2018) Prediction of the landslide susceptibility: Which algorithm, which precision? Catena 162:177–192

Pourghasemi HR, Yansari ZT, Panagos P, Pradhan B (2018) Analysis and evaluation of landslide susceptibility: a review on articles published during 2005–2016 (periods of 2005–2012 and 2013–2016). Arab J Geosci 11:1–12

Pradhan B, Lee S (2010) Delineation of landslide hazard areas on Penang Island, Malaysia, by using frequency ratio, logistic regression, and artificial neural network models. Environ Earth Sci 60:1037–1054

Qian B, Corte-Real J, Xu H (2000) Is the North Atlantic Oscillation the most important atmospheric pattern for precipitation in Europe? J Geophys Res Atmos 105:11901–11910

Qin C-Z, Zhu A-X, Pei T, et al (2011) An approach to computing topographic wetness index based on maximum downslope gradient. Precis Agric 12:32–43

Qiu H, Cui P, Regmi AD, et al (2017a) Influence of topography and volume on mobility of loess slides within different slip surfaces. CATENA 157:180–188. https://doi.org/10.1016/J.CATENA.2017.05.026

Qiu H, Hu S, Yang D, et al (2020) Comparing landslide size probability distribution at the landscape scale (Loess Plateau and the Qinba Mountains, Central China) using double Pareto and inverse gamma. Bull Eng Geol Environ. https://doi.org/10.1007/s10064-020-02037-w

Qiu H, Regmi AD, Cui P, et al (2017b) Slope aspect effects of loess slides and its spatial differentiation in different geomorphologic types. Arab J Geosci 2017 1015 10:1–12. https://doi.org/10.1007/S12517-017-3135-5

Ramesh V, Anbazhagan S (2015) Landslide susceptibility mapping along Kolli hills Ghat road section (India) using frequency ratio, relative effect and fuzzy logic models. Environ Earth Sci 73:8009–8021

Razavizadeh S, Solaimani K, Massironi M, Kavian A (2017) Mapping landslide susceptibility with frequency ratio, statistical index, and weights of evidence models: a case study in northern Iran. Environ Earth Sci 76:1–16

Reed M, Kite S (2020) Peripheral gully and landslide erosion on an extreme anthropogenic landscape produced by mountaintop removal coal mining. Earth Surf Process Landforms 45:. https://doi.org/10.1002/esp.4867

Regional inspectorate of Fez-Boulemane (2013) Urban Planning and City Policy. Fez-Boulemane

Revellino P, Grelle G, Donnarumma A, Guadagno FM (2010) Structurally controlled earth flows of the Benevento province (Southern Italy). Bull Eng Geol Environ 69:.

https://doi.org/10.1007/s10064-010-0288-9

RGPH (2014) Morocco Population and Housing Census, High Commission for Planning

RGPH (2004) Morocco Population and Housing Census, High Commission for Planning

Rickli C, Graf F (2000) Effects of forests on shallow landslides-case studies in Switzerland. For Snow Landsc Res 82:33–44

Robert M, Tessier D (1992) Incipient weathering: some new concepts on weathering, clay formation and organization. In: Developments in Earth Surface Processes. Elsevier, pp 71–105

Roche M (1963) Hydrologie de surface

Rodríguez-Peces MJ, García-Mayordomo J, Azañón JM, et al (2011) Constraining pre-instrumental earthquake parameters from slope stability back-analysis: Palaeoseismic reconstruction of the Güevéjar landslide during the 1st November 1755 Lisbon and 25th December 1884 Arenas del Rey earthquakes. Quat Int 242:76–89. https://doi.org/10.1016/J.QUAINT.2010.11.027

Rodríguez CE, Bommer JJ, Chandler RJ (1999) Earthquake-induced landslides: 1980–1997. Soil Dyn Earthq Eng 18:325–346. https://doi.org/10.1016/S0267-7261(99)00012-3

Roering JJ, Kirchner JW, Dietrich WE (2005) Characterizing structural and lithologic controls on deep-seated landsliding: Implications for topographic relief and landscape evolution in the Oregon Coast Range, USA. Bull. Geol. Soc. Am. 117

Roering JJ, Mackey BH, Handwerger AL, et al (2015) Beyond the angle of repose: A review and synthesis of landslide processes in response to rapid uplift, Eel River, Northern California. Geomorphology 236:109–131

Roering JJ, Schmidt KM, Stock JD, et al (2003) Shallow landsliding, root reinforcement, and the spatial distribution of trees in the Oregon Coast Range. Can Geotech J 40:237–253

Rogers NW, Selby MJ (1980) Mechanisms of shallow translational landsliding during summer rainstorms: North Island, New Zealand. Geogr Ann Ser A, Phys Geogr 62:11–21

Roldán Garcia FJ, Galindo-Zaldivar J, Chalouan A, et al (2009) Relaciones entre tectónica y sedimentación asociadas a las Rides Prérifaines en la Cuenca de Volubilis (frente del Rif, Marruecos)

Romer C, Ferentinou M (2016) Shallow landslide susceptibility assessment in a semiarid environment—A Quaternary catchment of KwaZulu-Natal, South Africa. Eng Geol 201:29–44

Rossi M, Cardinali M, Fiorucci F, et al (2012) A tool for the estimation of the distribution of landslide area in R. In: EGU General Assembly Conference Abstracts. p 9438

Rouai M, Jaaidi EB (2003) Scaling properties of landslides in the Rif mountains of Morocco. Eng Geol 68:353–359

Rybar J, Stemberk J, Wagner P (2002) Landslides: Proceedings of the First European Conference on Landslides, Prague, Czech Republic, 24-26 June 2002. CRC Press

S.G.A (1942) Carte géologique de Fès Ouest (1/100 000)

Sabokbar HF, Roodposhti MS, Tazik E (2014) Landslide susceptibility mapping using geographically-weighted principal component analysis. Geomorphology 226:15–24.

https://doi.org/10.1016/J.GEOMORPH.2014.07.026

Sahrane R, Ali B, El Kharim Y Investigating the Effects of Landslides Inventory Completeness on Susceptibility Mapping and Frequency-Area Distributions: Case of Taounate Province, Northern Morocco. North Morocco

Sahrane R, El Kharim Y, Bounab A (2022) Investigating the effects of landscape characteristics on landslide susceptibility and Frequency-area distributions: the case of Taounate province, Northern Morocco. Geocarto Int 1–22

Sani F, Del Ventisette C, Montanari D, et al (2007) Structural evolution of the Rides Prerifaines (Morocco): structural and seismic interpretation and analogue modelling experiments. Int J Earth Sci 96:685–706

Sauvage CH (1963) Le quotient pluviothermique d'Emberger, son utilisation et la representation géographique de ses variations au Maroc. Ann Phys Globe Météorol Inst Sci Chérif 20:11–23

Schicker R, Moon V (2012) Comparison of bivariate and multivariate statistical approaches in landslide susceptibility mapping at a regional scale. Geomorphology 161–162:40–57. https://doi.org/10.1016/J.GEOMORPH.2012.03.036

Schuster RL (1996) Socioeconomic significance of landslides. Landslides Investig Mitigation Washingt Natl Acad Press Transp Res Board Spec Rep 247:12–35

Schuster RL, Highland L (2001) Socioeconomic and environmental impacts of landslides in the western hemisphere. Citeseer

Schuster RL, Highland LM (2007) The Third Hans Cloos Lecture. Urban landslides: socioeconomic impacts and overview of mitigative strategies. Bull Eng Geol Environ 66:1–27

Schuster RL, Varnes DJ, Savage WZ (1996) The Slumgullion earth flow: A large-scale natural laboratory. US Geol Surv Bull 2130:

Schwarz M, Lehmann P, Or D (2010) Quantifying lateral root reinforcement in steep slopes–from a bundle of roots to tree stands. Earth Surf Process Landforms J Br Geomorphol Res Gr 35:354–367

Sendide O (2002) Etude qualitative des eaux de la nappe phréatique du bassin de Fès-Meknés, caractérisation, évaluation, modélisation mathématique et moyen de protection

Shafapour Tehrany M, Kumar L, Neamah Jebur M, Shabani F (2019) Evaluating the application of the statistical index method in flood susceptibility mapping and its comparison with frequency ratio and logistic regression methods. Geomatics, Nat Hazards Risk 10:79–101

Sidle R, Ochiai H (2006) Processes, prediction, and land use. Water Resour Monogr Am Geophys Union, Washingt

Šilhán K (2022) Dendrogeomorphological analysis of landslides on the undercut river terrace bank (a case study in Czech Republic). Landslides 2022 193 19:621–635. https://doi.org/10.1007/S10346-021-01833-Z

Smyth CG, Royle SA (2000) Urban landslide hazards: incidence and causative factors in Niterói, Rio de Janeiro State, Brazil. Appl Geogr 20:95–118

Soeters R, Van Westen CJ (1996) Slope instability recognition, analysis and zonation. Landslides

Investig Mitig 247:129–177

Soini E (2005) Land use change patterns and livelihood dynamics on the slopes of Mt. Kilimanjaro, Tanzania. Agric Syst 85:306–323

Stark CP, Hovius N (2001) The characterization of landslide size distributions. Geophys Res Lett 28:1091–1094. https://doi.org/10.1029/2000GL008527

Student (1908) The probable error of a mean. Biometrika 1–25

Sun D, Xu J, Wen H, Wang D (2021) Assessment of landslide susceptibility mapping based on Bayesian hyperparameter optimization: A comparison between logistic regression and random forest. Eng Geol 281:. https://doi.org/10.1016/j.enggeo.2020.105972

Sun X, Chen J, Bao Y, et al (2018) Landslide susceptibility mapping using logistic regression analysis along the Jinsha river and its tributaries close to Derong and Deqin County, southwestern China. ISPRS Int J Geo-Information 7:438

Suter G (1980a) Carte structurale de la chaîne rifaine au 1/500 000. Notes Mémoires du Serv géologique du Maroc 245b:

Suter G (1986) Carte géologique de la chaîne rifaine au 1/50 000. Notes Mém Serv Géol Maroc 346:

Suter G (1965) La région du Moyen Ouerrha (Rif, Maroc): Étude préliminaire sur la stratigraphie et la tectonique. Not Mém Serv Géol Maroc 24:183

Suter G (1980b) Carte structurale du Rif, 1/500.000. Notes Mém Serv Géol Maroc 245b

Suter G, FIECHTER G-G (1966) Le Rif méridional atlantique (Maroc): aperçu structural sur la région de Zoumi-Ouezzane et le pays du Habt (Larache). Notes Mémoires du Serv Géologique 26:15–20

Swets JA (1988) Measuring the accuracy of diagnostic systems. Science (80-) 240:1285–1293

Tanyaş H, van Westen CJ, Allstadt KE, Jibson RW (2019) Factors controlling landslide frequency–area distributions. Earth Surf Process Landforms 44:900–917. https://doi.org/10.1002/ESP.4543

Taylor FE, Malamud BD (2012) The statistical distributions of landslide length to width ratios. In: EGU General Assembly Conference Abstracts. p 826

Tejera de Leon J (1993) Les bassins néogènes d'avant-pays du Rif externe occidental liés à la transformante Jebha-Arbaoua (Maroc).

Thiery Y, Malet J-P, Sterlacchini S, et al (2007) Landslide susceptibility assessment by bivariate methods at large scales: application to a complex mountainous environment. Geomorphology 92:38–59

Thornberry-Ehrlich TL (2014) Shenandoah National Park: geologic resources inventory report

Tien Bui D, Shirzadi A, Shahabi H, et al (2019) New ensemble models for shallow landslide susceptibility modeling in a semi-arid watershed. Forests 10:743

Tobin G, Montz BE (1997) The cascade of hazards from flooding to environmental contamination: A case study of St. Maries, Idaho. Small T

Tokimatsu K, Mizuno H, Kakurai M (1996) Building damage associated with geotechnical problems. Soils Found 36:219–234

Tribak A (1997) Quelques exemples de mouvements de terrain dans le Prérif oriental (Maroc). Méditerranée 86:61–66

TRIBAK A, EL AMRANI H, ABAHROUR M, et al (2019) Numéro spécial. Geo Eco Trop 43:249–258

Tribak A, El Garouani A, Abahrour M (2009) Evaluation quantitative de l'érosion hydrique sur les terrains marneux du PréRif oriental (Maroc): cas du sous-bassin de l'oued Tlata. Sci Chang planétaires/Sécheresse 20:333–337

Trigo RM, Pozo-Vázquez D, Osborn TJ, et al (2004) North Atlantic Oscillation influence on precipitation, river flow and water resources in the Iberian Peninsula. Int J Climatol A J R Meteorol Soc 24:925–944

Trigo RM, Zêzere JL, Rodrigues ML, Trigo IF (2005) The influence of the North Atlantic Oscillation on rainfall triggering of landslides near Lisbon. Nat Hazards 36:331–354

Tsiampousi A, Zdravković L, Potts DM (2013) Variation with time of the factor of safety of slopes excavated in unsaturated soils. Comput Geotech 48:167–178

Tukey JW (1949) Comparing individual means in the analysis of variance. Biometrics 99–114

UNISDR U (2009) Making Disaster Risk Reduction Gender Sensitive: Policy and Practical Guidelines

Vakhshoori V, Zare M (2016) Landslide susceptibility mapping by comparing weight of evidence, fuzzy logic, and frequency ratio methods. Geomatics, Nat Hazards Risk 7:1731–1752

van Beek LPH (2002) Assessment of the influence of changes in land use and climate on landslide activity in a Mediterranean environment

Van Den Eeckhaut M, Poesen J, Govers G, et al (2007) Characteristics of the size distribution of recent and historical landslides in a populated hilly region. Earth Planet Sci Lett 256:588–603

Van Den Eeckhaut M, Poesen J, Verstraeten G, et al (2005) The effectiveness of hillshade maps and expert knowledge in mapping old deep-seated landslides. Geomorphology 67:351–363

Van Hinsbergen DJ., Vissers RL., Spakman W (2014) Origin and consequences of western Mediterranean subduction, rollback, and slab segmentation. Tectonics 23:393–419

Van Westen CJ (1997) Statistical landslide hazard analysis. Ilwis 2:73–84

Van Westen CJ (2000) The modelling of landslide hazards using GIS. Surv Geophys 21:241–255

Vandaele K, Poesen J, Govers G, van Wesemael B (1996) Geomorphic threshold conditions for ephemeral gully incision. Geomorphology 16:161–173

Vanwalleghem T, Van Den Eeckhaut M, Poesen J, et al (2008) Spatial analysis of factors controlling the presence of closed depressions and gullies under forest: Application of rare event logistic regression. Geomorphology 95:504–517

Varnes DJ (1984) Landslide hazard zonation: a review of principles and practice

Varnes DJ (1978) Slope movement types and processes. Spec Rep 176:11–33

Varnes DJ (1958) Landslide types and processes. Landslides Eng Pract 24:20–47

Varnes DJ, Cruden DM (1996) Landslide types and processes. Landslides Investig mitigation, Transp

Res Board Spec Rep 247:

Velde B (1995) Composition and mineralogy of clay minerals. In: Origin and mineralogy of clays. Springer, pp 8–42

Vernant P, Fadil A, Mourabit T, et al (2010) Geodetic constraints on active tectonics of the Western Mediterranean: Implications for the kinematics and dynamics of the Nubia-Eurasia plate boundary zone. J Geodyn 49:123–129. https://doi.org/10.1016/J.JOG.2009.10.007

Vidal JC (1971) Une interprétation nouvelle des nappes du Prérif central (Maroc) et ses conséquences sur la structure de leur substratum autochtone. Comptes Rendus l'Académie Des Sci Paris 272:24–27

VIDAL JC, FAUGERES JC (1975) RIDES PRERIFAINES (RIFF, MOROCCO) AS EXPLAINED BY WRENCH-FAULTING. COMPTES RENDUS Hebd DES SEANCES L Acad DES Sci Ser D 281:1951–1954

Wang W-D, Guo J, Fang L-G, Chang X-S (2012) A subjective and objective integrated weighting method for landslides susceptibility mapping based on GIS. Environ Earth Sci 65:1705–1714

Wernli R (1988) Micropaléontologie du Néogène post-nappes du Maroc septentrional et description systématique des foraminifères planctoniques. Notes Mémoires du Serv géologique

Wieczorek GF (1984) Preparing a Detailed Landslide-Inventory Map for Hazard Evaluation and Reduction. Environ Eng Geosci xxi:337–342. https://doi.org/10.2113/GSEEGEOSCI.XXI.3.337

Wildi W (1983) La chaîne tello-rifaine (Algérie, Maroc, Tunisie): structure, stratigraphie et évolution du Trias au Miocène. Rev géographie Phys géologie Dyn 24:201–297

Williams RBG (1986) Intermediate statistics for geographers and earth scientists. Macmillan International Higher Education

Winckel A (2002) Etablissement d'une typologie des eaux thermales par une approche hydrochimique, isotopique et tectonique: exemple du Maroc

Wisner B, Gaillard JC, Kelman I (2012) Handbook of hazards and disaster risk reduction and management. Routledge

WP WLI (1995) International Geotechnical Societies' UNESCO Working Party on World Landslide Inventory. Working Group on Rate of Movement (Chairman: Ch Bonnard) A suggested method for describing the rate of movement of a landslide. Bull Eng Geol Env 52:75–78

Xiao T, Segoni S, Chen L, et al (2020) A step beyond landslide susceptibility maps: a simple method to investigate and explain the different outcomes obtained by different approaches. Landslides 17:627–640. https://doi.org/10.1007/S10346-019-01299-0/FIGURES/4

Yalcin A, Reis S, Aydinoglu AC, Yomralioglu T (2011) A GIS-based comparative study of frequency ratio, analytical hierarchy process, bivariate statistics and logistics regression methods for landslide susceptibility mapping in Trabzon, NE Turkey. Catena 85:274–287

Youssef AM, Al-Kathery M, Pradhan B (2015) Landslide susceptibility mapping at Al-Hasher area, Jizan (Saudi Arabia) using GIS-based frequency ratio and index of entropy models. Geosci J 19:113–134. https://doi.org/10.1007/s12303-014-0032-8

Zabell SL (2008) On student's 1908 article ﬠthe probable error of a meanﬠ. J Am Stat Assoc 103:1–7

Zêzere JL, Pereira S, Melo R, et al (2017) Mapping landslide susceptibility using data-driven methods.

Sci Total Environ 589:250–267

Zêzere JL, Trigo RM (2011) Impacts of the North Atlantic Oscillation on landslides. In: Hydrological, Socioeconomic and Ecological Impacts of the North Atlantic Oscillation in the Mediterranean Region. Springer, pp 199–212

Zêzere JL, Trigo RM, Trigo IF (2005) Shallow and deep landslides induced by rainfall in the Lisbon region (Portugal): assessment of relationships with the North Atlantic Oscillation. Nat Hazards Earth Syst Sci 5:331–344

Zhang Y xing, Lan H xing, Li L ping, et al (2020) Optimizing the frequency ratio method for landslide susceptibility assessment: A case study of the Caiyuan Basin in the southeast mountainous area of China. J Mt Sci 17:340–357. https://doi.org/10.1007/s11629-019-5702-6

Zhao J, Vanmaercke M, Chen L, Govers G (2016) Vegetation cover and topography rather than human disturbance control gully density and sediment production on the Chinese Loess Plateau. Geomorphology 274:92–105

Zhou C, Yin K, Cao Y, et al (2018) Landslide susceptibility modeling applying machine learning methods: A case study from Longju in the Three Gorges Reservoir area, China. Comput Geosci 112:23–37

Zhou S, Chen G, Fang L, Nie Y (2016) GIS-based integration of subjective and objective weighting methods for regional landslides susceptibility mapping. Sustainability 8:334

Zieher T, Perzl F, Rössel M, et al (2016) A multi-annual landslide inventory for the assessment of shallow landslide susceptibility–Two test cases in Vorarlberg, Austria. Geomorphology 259:40–54

Zizi M (1996) Triassic-Jurassic extensional systems and their Neogene reactivation in northern Morocco (the Rides prérifaines and Guercif basin)

List of figures

FIGURE 1 A. LOCATION OF THE STUDY AREA AMONG THE NORTHERN PROVINCES; B. COMMUNES OF THE MOULAY YACOUB PROVINCE 9
FIGURE 2 MAIN STRUCTURAL SUB DOMAIN OF THE STUDY AREA 10
FIGURE 3 SYNTHETIC STRATIGRAPHIC LOG OF THE OUEZZANE NAPPE (TEJERA DE LEON 1993) 12
FIGURE 4 WHITE MARL OF THE LOWER MIOCENE (M4OZ, OUAZZANE NAPPE) 13
FIGURE 5 MIDDLE MIOCENE MARL AND LIMESTONE ALTERNATION (OUAZZANE NAPPE) 13
FIGURE 6 MARLS WITH DECIMETRIC INTERCALATIONS OF OLIGOCENE SANDSTONE WITH LIMESTONE CEMENT (OUAZZANE NAPPE) ... 13
FIGURE 7 CRETACEOUS MARL WITH LIMESTONE BANKS (OUAZZANE NAPPE) 14
FIGURE 8 SYNTHETIC STRATIGRAPHIC LOG OF THE PRERIF NAPPES (LEBLANC 1975 AND SUTER 1980A) 15
FIGURE 9 SOFS OF AIN AICHA 15
FIGURE 10 BLOCK DIAGRAM OF THE COMPLEX OF THE PRERIF NAPPE, AS AN ACCRETIONARY PRISM (FLINCH 1993) 16
FIGURE 11 UPPER MIOCENE WHITE MARLS SIDI CHAHED DAM (PRERIF NAPPE) 16
FIGURE 12 UPPER MIOCENE WHITE MARL (PRERIF NAPPE) 17
FIGURE 13 SOME FACIES OF THE PRERIF NAPPE 18
FIGURE 14 STRUCTURAL MAP OF THE EASTERN PART OF THE SOUTH RIF FOREDEEP 19
FIGURE 15 SYNTHETIC STRATIGRAPHIC LOG OF THE SOUTH RIF RIDGES (FAUGÈRES 1978; ZIZI 1996) 21
FIGURE 16 SALIFEROUS TRIASSIC FORMATIONS TO THE NORTH OF JBEL TRHAT 21
FIGURE 17 MARLS AND SANDSTONES OF THE UPPER JURASSIC OF JBEL TRHAT 21
FIGURE 18 MARLS WITH CARBONATE INTERCALATIONS OF THE CRETACEOUS OF JBEL TRHAT 22
FIGURE 19 MIOCENE MOLASSES OF JBEL BOUDRA SIDI KACEM (SOUTH RIF RIDGES) 22
FIGURE 20 GEOLOGICAL MAP OF JBEL TRHAT (ACCORDING TO EL ALAMI & LAHMID, 2016) 23
FIGURE 21 SOME FACIES OF JBEL TRAHT 23
FIGURE 22 PANORAMIC VIEW OF JBEL ZALAGH AND ITS SOUTHERN SLOPES 24
FIGURE 23 STRATIGRAPHIC LOG OF JBEL ZALAGH 24
FIGURE 24 GEOLOGICAL MAP OF JBEL THAT (EL ALAMI & LAHMID, 2016) 25
FIGURE 25 SOME FACIES OF JBEL ZALAGH 25
FIGURE 26 SLOPE MAP OF THE STUDY AREA 26
FIGURE 27 THE SAÏS FEZ FROM THE ROAD LEADING TO MOULAY YACOUB 27
FIGURE 28 RELIEF ANTHROPIZED BY THE EXPLOITATION OF TRAVERTINE LEDGES 27
FIGURE 29 MARLY SLOPES TERRACED AT THEIR SUMMITS IN THE REGION OF SIDI HRAZEM 28
FIGURE 30 THE PRERIF RIPPLE OF JBEL ZALAGH 29
FIGURE 31 LANDSCAPE OF MARLY HILLS IN THE PROVINCE OF MOULAY YACOUB 29
FIGURE 32 LINE OF CRESTS OF THE MIDDLE HILLS (JBELS HALOUT-BEN MANAMA), OVERHANGING THE LOW PRE-RIFAN HILLS (IN THE FOREGROUND) 30
FIGURE 33 THE RAVINE RELIEFS OF WHITE MARL WITH A SKELETON OF CENTIMETRIC INTERCALATIONS OF CLAYEY LIMESTONE (OUAZZANE NAPPE) 30
FIGURE 34 CLAYEY ALLUVIAL CONE FED BY THE LEACHING OF WHITE MARLS, TRIASSIC RED CLAYS AND CRETACEOUS PRE-RIFAN GREY PELITES 31
FIGURE 35 THE CURRENT FLOODPLAIN OF OUED SEBOU AND AN OLD ALLUVIAL TERRACE REINFORCED BY ITS PLIOCENE CONGLOMERATIC CORNICE 31
FIGURE 36 DOUAR KETATBA INSTALLED ON THE MAJOR BED OF OUED MEKKES, JUST BEHIND A TERRACE SHAPED IN MIOCENE YELLOW MARLS AND JBEL SIDI CHAHED IN THE BACKGROUND 32
FIGURE 37 DISTRIBUTION OF MAIN LITHOLOGICAL FORMATIONS IN THE FEZ-MOULAY YACOUB TERRITORY 33
FIGURE 38 CARBONATE ROCKS ON TOP OF AIN SIKH 34
FIGURE 39 SANDSTONE CORNICES OF SIDI CHAHED RIDGE 35
FIGURE 40 SANDSTONE-MARLS ALTERNATION 36
FIGURE 41 LIMESTONE-MARLS ALTERNATION 36
FIGURE 42 MARLY FACIES OF THE MOULAY YACOUB TERRITORY 37

FIGURE 43 CLAYEY COLLUVIUM WITH SANDSTONE PEBBLES IN AIN SIKH.....37
FIGURE 44 EXAMPLES OF ANCIENT ALLUVIUM.....38
FIGURE 45 EXAMPLES OF RECENT ALLUVIAL DEPOSITS.....38
FIGURE 46 BROWN CLAY SOILS IN SAÏS-FEZ.....39
FIGURE 47 LOCATION OF THE MAIN HYDRAULIC STATIONS IN THE EMBERGER CLIMAGRAM (MODIFIED BY SAUVAGE, 1963).....40
FIGURE 48 ANNUAL RAINFALL IN DAR EL ARSA (1976 – 2015).....41
FIGURE 49 VARIABILITY OF ANNUAL RAINFALL AT FEZ-SAÏS STATION (1914/15-2014/15).....41
FIGURE 50 NUMBER OF RAINY DAYS IN DAR EL ARSA (1976 – 2015).....41
FIGURE 51 ISOHYET MAP OF THE STUDY AREA.....42
FIGURE 52 RELATIONSHIP BETWEEN AVERAGE ANNUAL RAINFALL AND THE ALTITUDE OF RAINFALL STATIONS.....43
FIGURE 53 CUSUM OF ANNUAL RAINFALL IN FEZ-SAÏS 1914/15- 2014/15.....44
FIGURE 54 **A.** AVERAGE MONTHLY P SCHEME IN MY YACOUB (2013-2017); **B.** IFRANE, SEFROU, FÈS (1935-2015) AND MY YACOUB (2013-17).....45
FIGURE 55 OMBROTHERMIC DIAGRAM OF FEZ (1980-2010).....46
FIGURE 56 DAILY RAINFALL FROM NOV. 15, 2016, TO FEB. 7, 2017.....47
FIGURE 57 MAXIMUM AND MINIMUM AVERAGE TEMPERATURES IN FEZ-SAÏS AND MOULAY YACOUB.....48
FIGURE 58 DISTRIBUTION OF THE AVERAGE MONTHLY SUNSHINE DURING THE YEAR IN MY YACOUB.....48
FIGURE 59 LOCATION OF THE PROVINCE OF MOULAY YACOUB (IN RED) AND THE PREFECTURE OF FEZ (IN GREEN) IN THE THE MIDDLE PART OF SEBOU WATERSHED (IN GREY).....49
FIGURE 60 WATERSHED OF THE OUEDS CROSSING THE PROVINCE OF MY AND THEIR HYPSOMETRY (ON THE RIGHT).....50
FIGURE 61 HYPSOMETRIC CURVE OF THE WTERSHED OF THE FEZ OUED AND ITS TRIBUTARIES.....53
FIGURE 62 HYPSOMETRIC CURVE OF THE MIKKES OUED WATERSHED.....53
FIGURE 63 HYPSOMETRY OF THE MOULAY YACOUB WATERSHED.....54
FIGURE 64 HYPSOMETRIC CURVE OF THE MOULAY YACOUB OUED WATERSHED.....55
FIGURE 65 WEALTH IN WATER RESOURCES: MAIN SOURCES OF SAÏS-FEZ (OBDA K. ET AL ???).....57
FIGURE 66 PRESENTATION OF FINE SAMPLES IN THE CASAGRANDE ABAQUS.....62
FIGURE 67 POPULATION GROWTH RATE (IN %) OF THE MOULAY YACOUB PROVINCE BETWEEN 2004 AND 2014.....66
FIGURE 68 HISTORICAL MAP OF THE FEZ MEDINA (ADER, FEZ).....67
FIGURE 69 EVOLUTION OF THE POPULATION OF THE FEZ CITY BETWEEN 1912 AND 2014 (RGPH, 2014).....68
FIGURE 70 EVOLUTION OF THE NUMBER OF HOUSEHOLDS BETWEEN 1994 AND 2004 ACCORDING TO THE DISTRICTS (REGIONAL INSPECTORATE OF FEZ-BOULEMANE 2013).....69
FIGURE 71 EVOLUTION OF THE URBAN AREA OF THE FEZ CITY IN A CENTURY (1912 TO 2012), (LASRI 2015).....70
FIGURE 72 : TYPES DE MOUVEMENTS DE VERSANTS (THORNBERRY-EHRLICH TL 2014).....73
FIGURE 73 DISTRIBUTION OF SLOPE MOVEMENTS IN THE FEZ AND MOULAY YACOUB TERRITORY.....75
FIGURE 74 AREA AFFECTED BY LANDSLIDE TYPE (KM²).....76
FIGURE 75 EXTRACT FROM THE PROVISIONAL MAP OF SLOPE MOVEMENTS IN THE RIF AT 1/1,000,000° (MILLIÈS-LACROIX 1968). THE BOUNDARIES OF THE PROVINCES ARE SCHEMATIZED BY DRAWN LINES.....77
FIGURE 76 SUMMARY OF SITES DISTRIBUTION AFFECTED BY LANDSLIDES (CIRCLED IN GREEN) IN THE URBAN PERIMETER OF FEZ CITY (CARTOGRAPHIC SUMMARY FROM THE COLLECTION OF SITES STUDIED BY (A. GARTET, 2008).....77
FIGURE 77 MAP OF AREAS AT RISK OF LANDSLIDES IN THE NORTHERN PART OF THE URBAN PERIMETER OF FEZ CITY (CHERAI ET AL. 2017). 1: AREAS AT RISK OF SLOPE MOVEMENTS, 2: URBAN AGGLOMERATIONS OF FEZ, 3: CLIFFS AND ESCARPMENTS OF QUARRIES, 4: LIMIT OF THE URBAN PLAN OF FEZ, 5: MAIN ROADS, 6: THE RAILWAY.....78
FIGURE 78 VIEW OF THE SAIS PLAIN FROM THE JBEL TRHAT FOOTHILL.....78
FIGURE 79 : VIEW OF FEZ CITY AND ITS CLIFFS FROM THE NORTHEAST.....79
FIGURE 80 ROCK FALLS AT THE TRAVERTINE CLIFF OF BORJ ECHAMAL.....80
FIGURE 81 COLLAPSE OF THE CEMETERY OF THE ZLILIGH DOUAR RESULTING FROM ANCIENT UNDERGROUND CAVITIES CAUSED BY THE EXTRACTION OF PLIOCENE LACUSTRINE SANDS.....80
FIGURE 82 LANDSLIDES UPSTREAM OF THE OUED FEZ DISTRICT.....81
FIGURE 83 LANDSLIDES IN SKHOUNATE EAST OF SIDI HARAZEM (THE ARROWS REPRESENT THE SLIDING DIRECTION).....82

FIGURE 84 LANDSLIDES IN SEHB EL OUERD (ON THE RIGHT) AND IN JNANE EDDAR DISTRICTS (ON THE LEFT) (THE ARROWS REPRESENT THE SLIDING DIRECTION)..... 82
FIGURE 85 LANDSLIDE IN AIN NOKBI DISTRICT (THE ARROWS REPRESENT THE SLIDING DIRECTION)..... 83
FIGURE 86 MAIN AFFECTED URBAN EXTENSIONS IN FEZ CITY..... 84
FIGURE 87 DAMAGED/EVACUATED CONSTRUCTIONS LAYING ON UNSTABLE CLIFFS DUE TO BANK UNDERCUTTING BY OUED FEZ IN JNANATE DISTRICTS..... 84
FIGURE 88 : GAPS BETWEEN CONSTRUCTIONS (LEFT) AND FIXED WALL CRACKS (RIGHT) IN ANNAHDA HOUSING GROUP..... 85
FIGURE 89 : TOPPLES AND ROCK FALLS FROM SANDSTONE LEDGES AT THE ENTRANCE TO SIDI HRAZEM (A) AND ON THE LEFT BANK OF THE OUED SEBOU AT THE EXIT OF FEZ CITY (B AND C)..... 86
FIGURE 90 : PRERIF LANDSCAPE WHERE MIDDLE MARLY HILLS MARLY PREDOMINATE..... 87
FIGURE 91 : SLIDES AND EARTH FLOWS IN THE URBAN PERIMETER OF MY (OBDA ET AL., 2018)..... 88
FIGURE 92 TYPICAL EARTH FLOWS IN THE MY PROVINCE..... 89
FIGURE 93 AERIAL PHOTO OF A SPECTACULAR, ERODED AND RAVINED SLIDE IN THE COMMUNE OF MIKKES..... 89
FIGURE 94 : COMPLEX (SLIDE-FLOW) MOVEMENTS AFFECTING THE SLOPES OF THE SBAA ROUADI COMMUNE IN THE MY PROVINCE..... 89
FIGURE 95 SHALLOW SLOPE MOVEMENTS (EARTHFLOWS AND SOLIFLUCTIONS) AFFECTING MOULAY YACOUB REGION..... 90
FIGURE 96 : JBEL ZALARH (LEFT), JBEL TRHAT (RIGHT) AND OTHER ROCKY CLIFFS WITH SCREE PHENOMENA, SIGNS OF RECURRING ROCK FALLS THREATENING CONSTRUCTIONS DOWNSTREAM..... 90
FIGURE 97 : GULLYING OF MARLY SLOPES IN AERIAL VIEW..... 91
FIGURE 98 : ADVANCED GULLYING IN TRIASSIC SALT CLAYS (LEFT) AND NEOGENE MARLS (RIGHT)..... 91
FIGURE 99 : RAVINES DEEPLY INCISING THE WHITE MARLS OF THE OUAZZANE NAPPE AND REACHING THE UNDERLYING PRERIF CRETACEOUS PELITES..... 92
FIGURE 100 TYPES OF GRAVITATIONAL PROCESSES AFFECTING THE MOULAY YACOUB SECTOR AND ASSOCIATED BUILDING PATHOLOGY (OBDA ET AL., 2018)..... 93
FIGURE 101 **A**. DIAGONAL CRACKING IN THE DISPENSARY OF SBAA ROUADI BUILT ON CLAY ALLUVIUM; **B**. SEVERE STRUCTURAL PATHOLOGY AFFECTING CONSTRUCTIONS OF THE DEPARTMENT OF EQUIPMENT, IN CHARGE OF THE SIDI CHAHID DAM INSTALLED ON A MARLY HILL..... 94
FIGURE 102 : CRACKS AFFECTING MOST CONSTRUCTIONS OF AIN BOUALI COMMUNE (YELLOW ARROWS), BUILT ON FLAT TOPOGRAPHY 94
FIGURE 103 INTENSE CRACKING AFFECTING THE RURAL HOUSES OF SBAÂ ROUADI CENTER..... 95
FIGURE 104 SAMPLE PHOTOS SHOWING DAMAGE CAUSED BY SLOPE MOVEMENTS AND EXPANSIVE SOILS TO ROAD INFRASTRUCTURE IN THE FEZ-MOULAY YACOUB TERRITORY..... 96
FIG. 105 A GEOLOGICAL MAP OF NORTHWEST MOROCCO: (CQ) CONTINENTAL QUATERNARY, (NSR) NEOGENE SOUTH-RIFAN CORRIDOR, (NV) NEOGENE VOLCANISM, (PR) PRÉRIF , (MR) MESORIF , (INR) INTRARIF, (F) FLYSCH UNIT, (IR) INTERNAL RIF, (M) MESOZOIC BLANKET, (CM) CALEDONIAN WESTERN MESETA, (TF) FRONTAL THRUST; B LITHOLOGICAL MAP OF THE MY PROVINCE..... 101
FIG. 106 A. LANDSLIDE INVENTORY MAP AND ITS STATISTICAL ANALYSIS. A. LANDSLIDE INVENTORY MAP; B. OCCURRENCES OF EARTH FLOWS BY AREA OF THE MOVEMENTS; C. OCCURRENCES OF SLIDE BY AREA OF MOVEMENTS; D. DOUBLE PARETO, AND INVERSE GAMMA MODELS WITH FREQUENCY AREA DISTRIBUTION OF THE LANDSLIDE INVENTORY..... 103
FIGURE 107 IMAGE BOARD SHOWING EARTHFLOWS AND THEIR FLOW-LIKE/DUCTILE APPEARANCE IN THE STUDY AREA; A FIELD MISSION PHOTO WHERE THE EARTH FLOW WAS CONCEALED BY CEREAL FARMING (B, C, AND D EARTH FLOWS MAPPED ON GOOGLE EARTH 2018'S IMAGE)..... 104
FIG. 108 LANDSLIDE INFLUENCING PARAMETERS IN THE STUDY AREA..... 105
FIG. 109 DIAGRAMS REVEALING THE LANDSLIDE OCCURRENCES BY SLOPE RANGES (PANEL A), LAND USE SUB-CLASSES (PANEL B) AND BY MATERIAL INVOLVED (C)..... 114
FIG. 110 ACTIVE SHALLOW LANDSLIDES (A) AFFECTING SEVERAL CEREAL FARMING SLOPES..... 117
FIG. 111 DOUBLE PARETO, INVERSE GAMMA, AND FREQUENCY AREA DISTRIBUTION OF LANDSLIDE INVENTORY IN CEREAL FARMING AND OLIVE TREES SLOPES..... 119
FIG. 112 LANDSLIDE SUSCEPTIBILITY MAP DRAWN USING GIS MATRIX METHOD..... 120
FIGURE 113 LANDSLIDE SUSCEPTIBILITY MAP DRAWN BY FR METHOD..... 121

FIG. 114 NOTICEABLE IMPACT OF LAND USE SUB-CLASSES IN MITIGATING LANDSLIDE SUSCEPTIBILITY LEVEL OF BOTH MAPS FR AND GMM; A EFFECT OF BRUSHWOOD, B EFFECT OF ORCHARDS, C EFFECT OF BADLANDS AND BRUSHWOOD 123
FIGURE 115 NOTICEABLE IMPACT OF LITHOLOGY SUB-CLASSES IN MITIGATING LANDSLIDE SUSCEPTIBILITY LEVEL; A. IMPACT OF SANDSTONE-MARL ALTERNATION; B AND C. IMPACT OF SALIFEROUS CLAYS 124
FIG. 116 QUALITY CONTROL RESULTS OF THE TWO SUSCEPTIBILITY MAPS; A DEGREE OF FIT METHOD, B AREA UNDER THE ROC CURVE OF THE LANDSLIDE SUSCEPTIBILITY MAPS GENERATED BY FR AND GMM MODELS 125
FIG. 117 A. STRUCTURAL DOMAINS OF NORTHERN MOROCCO (BASE MAP FROM SUTER G. 1980): (CQ) CONTINENTAL QUATERNARY, (NSR) NEOGENIC SOUTH-RIFIAN CORRIDOR, (NV) NEOGENIC VOLCANISM, (PR) PRERIF, (MR) MESORIF , (INR) INTRARIF, (F) FLYSCH UNIT, (IR) INTERNAL RIF, (M) MESOSOIC BLANKET, (CM) CALEDONIAN WESTERN MESETA; B. LITHOLOGICAL MAP OF THE MY REGION (BASE MAP FROM FÈS-OUEST GEOLOGICAL MAP; SGA, 1942): (1) SOILS AND ALLUVIAL QUATERNARY DEPOSITS; (2) COLLUVIUM; (3) PLIOCENE LACUSTRINE LIMESTONE; (4) MESSINIAN SANDY MARLS; (5) TORTONIAN AND MESSINIAN MARLS; (6) LIMESTONE-MARLS ALTERNATION OF OUAZZANE UNIT (7) CRETACEOUS SHALES; (8) SALTY RED CLAYS OF THE PRERIF UNIT ; C SIMPLIFIED GEOLOGICAL CROSS-SECTION OF MY'S REGION 131
FIG. 118 EXAMPLE OF MODELLED H/V PEAKS USING MASW SURFACE VS, CASE OF THE P28 AND M10 MEASUREMENTS OF THE MASW AND H/V SURVEYS RESPECTIVELY 134
FIG. 119: SLOPE MOVEMENTS, BOREHOLES, MASW AND H/V DISTRIBUTION AND SAMPLING LOCATIONS (ROAD NETWORK, BUILDING BASIC DATA FROM MOULAY YACOUB GOOGLE EARTH IMAGES; TOPOGRAPHIC DATA FROM MOULAY YACOUB TOPOGRAPHIC MAP 1/25 000; ANCFCC 2007) 137
FIG. 120: LITHOLOGICAL CHARACTERISTICS OBTAINED BY CORE DRILLING AND PRESSUREMETER SURVEYS (BASED ON LPEE 2017 BOREHOLE DATA) 139
FIG. 121: X-RAY DIFFRACTION RESULTS ON OF THE CLAY FRACTION OF MY'S MARL SAMPLES; S: SMECTITE, CH: CHLORITE, I/S: IRREGULAR MIXED-LAYER (ILLITE/SMECTITE), I: ILLITES, K: KAOLINITE 141
FIG. 122:SAMPLES OF SLOPE MOVEMENTS IN MY. A ROTATIONAL SLIDE; B ACTIVE HEAD CRACKS; C SOIL CREEP AND CREEPING MASS OF OLD LANDSLIDES (S); D DETAIL VIEW OF A SOIL CREEP 143
FIG. 123: OBSERVED PATHOLOGICAL MANIFESTATIONS AT INSTABLE SLOPES OF THE WESTERN DISTRICT; A RECENT SCARPS OF A NOT YET INDIVIDUALISED LANDSLIDE (I), BACKFILL OUTCROP (II); B SEVERE WALL CRACKING (D5); C RECENT SCARP AFFECTING URBANIZED AREA; D RETAINING WALL WHOSE FOUNDATIONS HAVE BEEN UNCOVERED BY THE HEAD SCARP OF THE LANDSLIDE (I), CRACKS IN THE RETAINING WALL (II), WASTE WATER LEAK DUE TO DAMAGED SEWERAGE NETWORK BY THE LANDSLIDE (III). .. 144
FIG. 124: INCLINOMETER MONITORING (MODIFIED FROM LPEE 2017) 145
FIG. 125: DAILY PRECIPITATIONS OF MY RAINFALL STATION, FROM 06/11/16 TO 28/02/17; I1, I2 AND I3: INCLINOMETER DISPLACEMENTS 146
FIG. 126: AVERAGE ANNUAL VELOCITIES OBTAINED BY PS-INSAR MONITORING IN THE URBAN PERIMETER OF MOULAY YACOUB TOWN 147
FIG. 127: PATHOLOGICAL MANIFESTATIONS INDUCED BY EXPANSIVE SOILS; A: EXPANSION OF THE BUILDING'S JOINTS; B: DIAGONAL CRACKS CONNECTING WINDOWS TO BUILDING STRUCTURE; C: CRACKS AT THE CORNER OF THE BUILDING AFFECTING ITS STRUCTURE; D: DIFFERENTIAL SETTLEMENT AFFECTING STEEL BARS; E: RANDOM CRACKS IN ALL DIRECTIONS INVOLVING EXTERNAL FACADES, WHICH REQUIRES BUILDING EVACUATION, DI: LEVEL OF DAMAGE 148
FIG. 128: BUILDINGS DAMAGE DISTRIBUTION AND INSTABILITY SIGNS (ROAD NETWORK, BUILDING BASIC DATA FROM MOULAY YACOUB GOOGLE EARTH IMAGES; TOPOGRAPHIC DATA FROM MOULAY YACOUB TOPOGRAPHIC MAP 1/25 000; ANCFCC 2007) ... 149
FIGURE 129 CURVES OF THE SEISMIC NOISE MEASUREMENTS 150
FIG. 130: VULNERABILITY OF THE FORMER MY DISTRICT TO THE RISK OF LANDSLIDES; A SHALLOW FOUNDATION, B SHALLOW FOUNDATIONS AND OVERSTORIYING, C EXTENSION OF THE DISTRICT TOWARDS STEEP SLOPES AND ON BACKFILL 158
FIG. 131: HABITATS OF THE JNANATE DISTRICT AT HIGH RISK OF COLLAPSE SLIDING 159
FIG. 132:RRISK OF LANDSLIDES NORTH OF THE TRHAT DISTRICT; A REWORKED MARLY COLLUVIUM TESTIFYING TO THE MULTIGENERATIONAL ACTIVITY OF THE OLD LARGE LANDSLIDES AFFECTING THE TRHAT DISTRICT, B LANDSLIDE ACTIVITY SIGNS: TILTED STREETLAMPS AND DAMAGED ROAD SECTION, C AND D OBVIOUS CRACKS AFFECTING HOUSES DESPITE REPAIR ATTEMPTS159
FIG. 133: LANDSLIDE AFFECTING URBAN AREAS TALLAYOUSSEF AND BOUJIBAR 160
FIG. 134: THE LANDSLIDE SUSCEPTIBILITY MAP OBTAINED BY LOGISTIC REGRESSION ANALYSIS (BYOU ET AL. 2020) 161

FIG.135 GEOLOGICAL MAP OF THE STUDY AREA. A SEISMOLOGICAL AND TECTONIC MAP OF NORTHERN MOROCCO. B GEOLOGICAL MAP OF THE PRE-RIF RIDGES. C 2D CROSS SECTION EXPOSING THE STRUCTURE OF THE PRE-RIF RIDGES MORPHOTECTONIC UNIT.167
FIG.136 LANDSLIDES AND ACTIVE GULLY INVENTORY WITH THE FREQUENCY-TYPE DISTRIBUTION OF LANDSLIDES IN THE RIGHT BOTTOM CORNER 173
FIG.137 FREQUENCY AREA DISTRIBUTION FOR ALL THREE INVESTIGATED ZONES. IG: INVERSE -GAMMA, DP: DOUBLE-PARETO 175
FIG.138 MEAN VALUES OF THE MORPHOMETRIC INDICES USED TO CHARACTERIZE THE LANDSLIDE AFFECTED AREA FOR EACH ZONE (ZONE1 IN BLUE, ZONE 2 IN RED AND ZONE 3 IN GREEN). 176
FIG.139 SLOPE INSTABILITY ANALYSIS FOR DIFFERENT THEORETICAL SCENARIOS: NO WEATHERED MARLS ARE PRESENT (A, B AND C), A 10 M THICK WEATHERED LAYER IS PRESENT (D, E AND F) AND A 15 M THICK WEATHERED LAYER IS PRESENT (G, H AND I). THE DISTRIBUTION OF MARLY SLOPES IS PRESENTED AT THE BOTTOM. 179
FIG.140 FIELD PHOTOGRAPHS OF THE STUDY AREA. A THRUST FAULT PHOTOGRAPHED IN ZONE 1, MO: MARLS OF OUAZZANE UNIT, M: PRE-RIF MARLS, T: TRIASSIC CLAYS (ZONE 3). B SLIDE EARTHFLOW SLIDING DOWN A GULLY LANDFORM IN ZONE 2. C SHALLOW LANDSLIDES ASSOCIATED WITH ACTIVE GULLYING IN ZONE 3. D ACTIVE GULLIES IN ZONE 3 INTERRUPTED MOMENTLY BY ANOTHER INCISION PHASE. 181
FIG.141 GEOMORPHOLOGICAL MODEL SHOWING THE INDIRECT INFLUENCE OF THE TECTONIC UPLIFT IN THE PRE-RIF RIDGES ON SURFACE PROCESSES. 183

List of tables

TABLE 1 AREA OF OUTCROP FOR MAIN LITHOLOGICAL FORMATIONS 33
TABLE 2 MONTHLY AND SEASONAL PRECIPITATION REGIME IN FEZ-SAÏS (1915-2015) 45
TABLE 3 DAILY PRECIPITATION FROM NOV. 15, 2016, TO FEB. 2, 2017 47
TABLE 4 CORRESPONDENCE BETWEEN THE VALUE OF KC AND THE TYPE OF HYDROLOGICAL RESPONSE EXPECTED (ROCHE 1963; OBDA 1991; OBDA 2004) 51
TABLE 5 GEOMETRIC SHAPE OF THE FEZ OUED WATERSHED AND ITS TRIBUTARIES 52
TABLE 6 GEOMETRIC SHAPE AND CHARACTERISTIC ALTITUDES OF THE MIKKES OUED AND ITS TRIBUTARIES 53
TABLE 7 GEOMETRIC SHAPE OF THE MOULAY YACOUB OUED WATERSHED 54
TABLE 8 GEOTECHNICAL PROPERTIES OF HARD/COMPACT ROCKS 59
TABLE 9 GEOTECHNICAL PROPERTIES OF SOFT FORMATIONS 61
TABLE 10 POPULATION OF THE MOULAY YACOUB PROVINCE BY RESIDENCE TYPE AND AVERAGE ANNUAL GROWTH RATE 64
TABLE 11 POPULATION OF THE MOULAY YACOUB PROVINCE ACCORDING TO THE 2014 RGPH 64
TABLE 12 DEMOGRAPHIC EVOLUTION BY 2050 64
TABLE 13 LEGAL POPULATION BY COMMUNES IN 2004 AND 2014 65
TABLE 14 EVOLUTION OF THE POPULATION OF THE CITY OF FEZ BETWEEN 1912 AND 2014 (RGPH, 2014) 67
TABLE 15 A SUMMARY OF VARNES' 1978 CLASSIFICATION SYSTEM 72
TABLE 16 LANDSLIDE VELOCITY SCALE (WP/WLI 1995 AND CRUDEN AND VARNES 1996) 74
TABLE 17 LANDSLIDE-FORMING MATERIAL TYPES (HUNGER, 2014) 74
TABLE 18 G-K AND R VALUES SHOWING THE CORRELATION DEGREE OF THE PRE-SELECTED CONDITIONING FACTORS WITH LANDSLIDE TYPES 107
TABLE 19 SAMPLE OF THE LANDSLIDE-SUSCEPTIBILITY MATRIX CONSIDERING ALL THE SLOPE MOVEMENTS IN THE STUDY AREA: CM: COMBINE NUMBER WHOSE LINE SHOWS THE NUMBERS OF EACH CLASS FACTOR, LITH: LITHOLOGY, ELE: ELEVATION, DS-RI: DISTANCE FROM RIVER, LU: LAND USE, SL: SLOPE, DS-RO: DISTANCE FROM ROADS, TWI, TOPOGRAPHIC WETNESS INDEX, RGH: SLOPE ROUGHNESS, LSM%: PERCENTAGE OF LANDSLIDE SUSCEPTIBILITY MATRIX, LS: LANDSLIDE SUSCEPTIBILITY 108
TABLE 20 CONTINGENCY TABLES SHOWING THE TOTAL SURFACE (CLASS PIXELS), THE AFFECTED SURFACE BY LANDSLIDES (L. PIXELS) AND THE PERCENTAGE OF THE LATTER (% L. PIXELS) OF EACH CLASS FACTOR 110
TABLE 21 COVERING AREA FOR EACH LANDSLIDE SUSCEPTIBILITY CLASS PRESENTED BY THE FR AND GMM MAPS 121
TABLE 22 URBAN POPULATION AND HOUSING TYPE OF MY 131

TABLE 23 DAMAGE SEVERITY LEVELS ALONG WITH THEIR DESCRIPTION 135
TABLE 24 SEISMIC NOISE MEASUREMENTS, PEAK FREQUENCY, INTERFACE DEPTHS (MODELLED) AND VS-VELOCITY OF THE SURFACE LAYER 137
TABLE 25: GEOTECHNICAL CHARACTERISTICS OF MY'S MARLS 140
TABLE 26 COMPARISON OF PARAMETERS RELATING TO THE RISK OF LANDSLIDE BETWEEN THE MY TOWN WITH OTHER INVESTIGATED URBAN EXTENSIONS 163
TABLE 27 FR VALUES FOR EACH LITHOLOGICAL FACIES WITHIN THE STUDY AREA 174
TABLE 28 ANOVA TEST RESULTS COMPARING THE DISTRIBUTION OF LANDSLIDES MORPHOMETRIC INDICES ACROSS THE STUDY AREA 177
TABLE 29 ANOVA TEST RESULTS COMPARING THE KERNEL DENSITY OF RAVINES ACROSS THE STUDY AREA 177
TABLE 30 GEOTECHNICAL INVESTIGATION RESULTS FOR WEATHERED AND SANE MARLS 178